Development and application of a GC system for NMHC analyses of air samples from the CARIBIC aircraft project

Dissertation
zur Erlangung des Grades
„Doktor der Naturwissenschaften"

am Fachbereich Chemie
der Johannes Gutenberg-Universität in Mainz

Bohdan Řanda

geb. in Kutna Hora / Tschechische Republik
Mainz, 2007

Abstract

The subject of this thesis is the development of a Gaschromatography (GC) system for non-methane hydrocarbons (NMHCs) and measurement of samples within the project CARIBIC (**C**ivil **A**ircraft for the **R**egular **I**nvestigation of the atmosphere **B**ased on an **I**nstrument **C**ontainer, www.caribic-atmospheric.com). Air samples collected at cruising altitude from the upper troposphere and lowermost stratosphere contain hydrocarbons at low levels (ppt range), which imposes substantial demands on detection limits. Full automation enabled to maintain constant conditions during the sample processing and analyses. Additionally, automation allows overnight operation thus saving time. A gas chromatography using flame ionization detection (FID) together with the dual column approach enables simultaneous detection with almost equal carbon atom response for all hydrocarbons except for ethyne.

The first part of this thesis presents the technical descriptions of individual parts of the analytical system. Apart from the sample treatment and calibration procedures, the sample collector is described. The second part deals with analytical performance of the GC system by discussing tests that had been made. Finally, results for measurement flight are assessed in terms of quality of the data and two flights are discussed in detail.

Analytical performance is characterized using detection limits for each compound, using uncertainties for each compound, using tests of calibration mixture conditioning and carbon dioxide trap to find out their influence on analyses, and finally by comparing the responses of calibrated substances during period when analyses of the flights were made. Comparison of both systems shows good agreement. However, because of insufficient capacity of the CO_2 trap the signal of one column was suppressed due to breakthroughed carbon dioxide so much that its results appeared to be unreliable.

Plausibility tests for the internal consistency of the given data sets are based on common patterns exhibited by tropospheric NMHCs. All tests show that samples from the first flights do not comply with the expected pattern. Additionally, detected alkene artefacts suggest potential problems with storing or contamination within all measurement flights. Two last flights # 130-133 and # 166-169 comply with the tests therefore their detailed analysis is made. Samples were analyzed in terms of their origin (troposphere vs. stratosphere, backward trajectories), their aging (NMHCs ratios) and detected plumes were compared to chemical signatures of Asian outflows.

In the last chapter a future development of the presented system with focus on separation is drawn. An extensive appendix documents all important aspects of the dissertation from theoretical introduction through illustration of sample treatment to overview diagrams for the measured flights.

Content

List of figures

List of tables

Appendix

Abbreviations

AMOHA	-	Accurate Measurement of Hydrocarbons in Air
CARIBIC	-	Civil Aircraft for the Regular Investigation of the atmosphere Based on an Instrument Container
DL	-	Detection limit
ECMWF	-	European Center for Medium range Weather Forecasting
EPC	-	Electronic pressure controller
ER	-	Enhancement ratio
FID	-	Flame ionization detector
FTIR	-	Fourier Transform Infrared Spectroscopy
GC x GC	-	Two-dimensional gas chromatography
GC-MS	-	Gas chromatography with mass spectrometric detection
IMK	-	Institut für Meteorologie und Klimaforschung, Forschungszentrum Karlsruhe
KNMI	-	Koninklijk Nederlands Meteorologisch Instituut, Netherlands
LS	-	Lower stratosphere
MFC	-	Mass flow controller
MDC	-	Minimum detectable concentration
MPI	-	Max-Planck Institute
NCAR	-	National Center for Atmospheric Research, USA
NH	-	North hemisphere
NIST	-	National Institute of Standards and Technology, USA
NMHCs	-	Nonmethane hydrocarbons
NOMHICE	-	Nonmethane Hydrocarbon Intercomparison Experiment
NPL	-	National Physical Laboratory, UK
PLOT	-	Porous-layer open-tubular column
Ppb	-	nmol/mol (parts per billion)
Ppm	-	µmol/mol (parts per million)
Ppt	-	pmol/mol (parts per trillion)
PTFE	-	Polytetrafluorethene
PTR-MS	-	Proton transfer reaction mass spectrometer
PV	-	Potential vorticity
Sccm	-	Standard cubic centimeter
UEA	-	University of East Anglia
UTC	-	Coordinated universal time
UT	-	Upper troposphere

VOCs	-	Volatile organic compounds
WAS	-	Whole air sampler
WCOT	-	Wall-coated open-tubular column

1. Introduction

1.1 Objective of the work

The objective was to develop an apparatus and measure as many as possible NMHCs at concentrations found in the upper troposphere and lower stratosphere, in other words to enable to do automated measurements within the project CARIBIC. C_2-C_7 compounds including benzene and toluene at few ppb at most must be reliably and accurately measured. Minimum manpower together with low consumption of liquid nitrogen make the measurements easier.

The analyses cannot be done without an application of pre-concentration and sample treatment techniques. Sub-ppb concentrations lay substantial demands on detection limits on the range of a few ppt or less. The aim was to use a GC technique with flame ionization detector. FID instead of a mass spectrometer has the advantage of almost equal carbon atom response for all hydrocarbons except ethyne. Consequently, even not-calibrated compounds can be quantified. The dual column approach enables simultaneous detection on two stationary phases of different polarity thus identification is unequivocal and coelution with unknown substances easier detectable.

1.2 CARIBIC

CARIBIC, **C**ivil **A**ircraft for the **R**egular **I**nvestigation of the atmosphere **B**ased on an **I**nstrument **C**ontainer, is an innovative scientific project to study important chemical and physical processes in upper troposphere and lowermost stratosphere. Commercial flights are used to study the Earth atmosphere on a regular basis with the help of an on board instrumented container. Detailed and extensive measurements are made during long distance flights. NMHCs were already measured during the first phase of CARIBIC with Boeing 767-300 of LTU since April 2000 until April 2002 when the aircraft was decommissioned. An Airbus A340-600 from Lufthansa has been used since December 2004.

Before the aircraft take-off a special air freight container filled with scientific equipment is loaded into the cargo compartment of a passenger aircraft. The container is connected to the outside air through a system of tubes. The purpose of CARIBIC is to carry out research into the quantitative analysis of tropopause region with delivering data in a very economical way. Research aircraft are very expensive, and cannot cover

larger parts of the global atmosphere at a desired frequency and affordable cost. CARIBIC is a European project, many equipment-groups are coming from different parts of Europe.

A total of 20 scientific instruments in the container monitor trace gases and aerosols. The aircraft is equipped with a complete analytical laboratory for measuring water vapor, aerosols and over 50 trace gases in the atmosphere with a high degree of accuracy, see A1 in the appendix. During the flight, all instruments run fully automatically. Several trace gases and aerosols are measured directly in the container on-line. Air samples are collected in 28 glass vessels and analyzed later on the ground. The regular flights have the advantage that they permit changes in atmospheric processes to be observed during all seasons. Flights in South America, across the Andes, provide information about the cleanest air without any industrial pollution.

2. NMHCs in the atmosphere

Volatile organic compounds (VOCs) are organic chemical compounds that have a sufficiently high vapor pressure to exist in atmosphere in gaseous form. In contrast to VOCs, semivolatile substances are found in gaseous form and on particles. Non-methane hydrocarbons (NMHCs) represent a small part of VOCs, consisting of C and H atoms only.

NMHCs include alkanes, alkenes, alkadienes, alkynes and aromatic compounds. Methane obviously is not considered a NMHC compound because of its low reactivity (especially with OH) resulting in a long lifetime (9 years). NMHCs form a significant class of compounds playing a vital role in tropospheric photochemistry. NMHCs compounds in combination with nitrogen oxides are the key components in photochemical reactions, which result in the formation of ozone. NMHCs are thus significant precursors to ozone formation. Their direct impact on stratospheric processes is relatively minor. NMHCs are emitted by natural processes, such as large isoprene emissions from plants, alkenes by sea, all sorts of NMHCs from biomass burning and by anthropogenic processes such as evaporation of gasoline, products of incomplete combustion.

2.1 NMHCs: sources, atmospheric chemistry, abundance of alkenes and alkadienes

Because of their high reactivity, NMHCs are usually found in mixing ratios varying from a few ppt (part per trillion = 1 in 10^{-12} molecules) in the free troposphere to a few ppb (part per billion = 1 in 10^{-9} molecules) in the urban atmosphere. They are removed from the atmosphere mainly during the daytime by reaction with hydroxyl radicals, OH. Because the photochemical lifetimes of NMHC species are short (due to their reactivity with the OH radical the lifetimes are of the order of days in the troposphere with ethane having a lifetime of weeks) the flux of these species into the stratosphere is small. Owing to their reactivity, hydrocarbons are expected to develop larger gradients of mixing ratios between the source regions and the remote troposphere.

Apart from rapid reaction with OH radicals, unsaturated hydrocarbons also react with ozone at rates that make such reactions competitive with OH reactions. NMHCs lifetimes in the troposphere generally are of the order of days. Atmospheric lifetimes

can be obtained by summing the individual rates for dominant reactions and taking the inverse value. A2 in the appendix shows selected hydrocarbons with their rate coefficients for the reactions with OH and O_3. The corresponding atmospheric reaction rates may be estimated on the assumption that typical number densities for OH and O_3 are 8×10^5 and 6.5×10^{11} molecule cm^{-3}, respectively (Warneck, 2000). Because reactive hydrocarbons are removed at a faster rate than less reactive ones, the abundance spectrum in aged polluted air changes in favor of the less reactive species. The longest-lived compounds are ethane and ethyne. They have lifetimes exceeding 1 month, so they are expected to spread around the globe, irrespective of the uneven distribution of their sources. Other lighter alkanes and benzene still can be transported over long distances from their sources and thereby act as a tracer for continental sources (Parrish et al., 1992).

NMHCs are, in terms of emissions, separated into two broad categories of anthropogenic and natural (biogenic) origin. The most important anthropogenic hydrocarbon sources are automobile emissions, anthropogenic burning processes, evaporation of liquid fuels, commercial solvents, natural gas while the sources of biogenic NMHCs are plants and vegetation, oceans, and biomass burning (Hough, 1991; Singh and Zimmerman, 1992; Guenther at al., 1995; Rudolph, 1995; Seinfeld and Pandis, 1997; Warneck, 2000). Industrial and automotive combustion of fossil fuels together with biogenic emissions provide major sources of NMHCs in the troposphere (Friedrich and Obermeier, 1999; Fuentes et al. 2000). The natural and anthropogenic emissions of NMHCs are in a range of hundreds Tg per year (Singh and Zimmerman, 1992; IPCC, 1995). Anthropogenic sources are estimated to account for 100 - 150 Tg/yr (Piccot et al., 1992; Singh and Zimmerman 1992; Prather et al., 1994). Of this total (Singh and Zimmerman, 1992) estimate that 58 Tg/yr are from industrial and fossil fuel sources with the remainder from biomass burning. Piccot et al. (1992) estimate 67 Tg/yr from industrial and fossil fuel sources and 43 Tg/yr from biomass burning. A3 in the appendix provides a breakdown of global emissions of VOCs.

Anthropogenic NMHCs are dominant in urban areas, although they may contribute substantially in less populated locations as well. The major source of ethane is natural gas, either from the leakage during the distribution or from the direct exploitation. Propane derives from natural gas as well as from petrochemical industries. The principal sources of butane and pentane are automotive exhaust and gasoline, although contributions from natural gas and industrial processes are not entirely negligible. The higher alkanes are mostly associated with solvent emissions and fuel evaporation. The alkenes, especially ethene, derive primarily from automotive exhaust. Ethyne is almost exclusively formed in combustion processes. Small amounts of ethyne, however, are produced in burning of agricultural wastes and other plant materials. Three-quarters of

benzene arises from automobile exhaust and the rest from the evaporation and spillage of fuels. Toluene and ethylbenzene originate from both automotive exhaust and solvent emissions. A4 in the appendix gives an overview of sources for individual hydrocarbons according to estimates of (Mayrson and Crabtree, 1976) and (Nelson et al., 1983).

Emissions of reactive NMHCs by natural sources are widely spread and constitute an important part in the global budget of NMHCs. Thousands of biogenic NMHCs and VOCs have been studied and identified (Fall, 1999). The most recognized are ethene, isoprene, and monoterpenes, which are typically emitted from plants. The global annual emission of biogenic NMHCs is estimated to range up to1500 Tg C/yr, and terpenes are thought to constitute the biggest part of this (Guenther, 2003). However, these estimates are uncertain due to the diversity of ecological and climatic variables.

Atmospheric chemistry of NMHCs was discussed in detail by (Atkinson, 1990, 1994 2000) and (Atkinson and Arey, 2003). The most important products of NMHCs oxidation are HO_2 and RO_2 radicals which in reaction with NO are responsible for the photochemical formation of ozone. In the 1960s, it was shown that the oxidation of hydrocarbons and CO over polluted urban regions during summer generates O_3 as a by-product. Tropospheric O_3 photochemical formation is catalyzed by nitrogen oxides (NO_x), involving organic peroxy (RO_2) and oxy (RO) radicals, and the hydroperoxy radical (HO_2). NO_x budget is dominated by fossil fuel combustion. Hence, NO_x emissions are often associated with NMHCs and CO emissions. Emitted NO_x is predominantly in the form of NO, only small fraction is directly released as NO_2. Degradation of NMHCs can be initiated in a number of different ways but the dominant removal process pertaining to all hydrocarbons is reaction with the OH radical. Because the great importance of the photochemical reactions we summarize the main aspect on the next pages.

The formation of OH is governed by the photo-dissociation of O_3 in the presence of water vapor. The photolysis of O_3 in the near ultraviolet band ($\lambda < 330$ nm) generates electronically excited $O(^1D)$ atoms that react with water molecule leading to two OH radicals. This reaction is net loss of tropospheric O_3.

$$O_3 + h\nu \rightarrow O_2 + O\,(^1D) \qquad\qquad (2.1)$$

$$O\,(^1D) + H_2O_{gas} \rightarrow 2OH \qquad\qquad (2.2)$$

In the absence of NO or at sufficiently low NO concentrations, reactions of O_3 with OH and HO_2 radicals are additional loss processes for tropospheric ozone.

$$OH + O_3 \rightarrow HO_2 + O_2 \tag{2.3}$$

$$HO_2 + O_3 \rightarrow OH + 2O_2 \tag{2.4}$$

On the other side, ozone is produced by the photolysis of NO_2.

$$NO_2 + hv \; (< 420 \text{ nm}) \rightarrow NO + O(^3P) \tag{2.5}$$

$$O(^3P) + O_2 \rightarrow O_3 \tag{2.6}$$
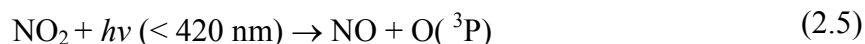
Because ozone reacts with NO back in reaction (2.7) leading to NO_2, the result is a photoequilibrium between NO, NO_2 and O_3 with no net formation or loss of O_3, as shown in Figure 1 (A).

$$NO + O_3 \rightarrow NO_2 + O_2 \tag{2.7}$$

The degradation reactions of VOCs (including NMHCs) lead to the formation of intermediate RO_2 and HO_2 radicals which convert NO to NO_2 without consuming O_3. This process thus leads to the net O_3 production as shown in Figure 1 (B).
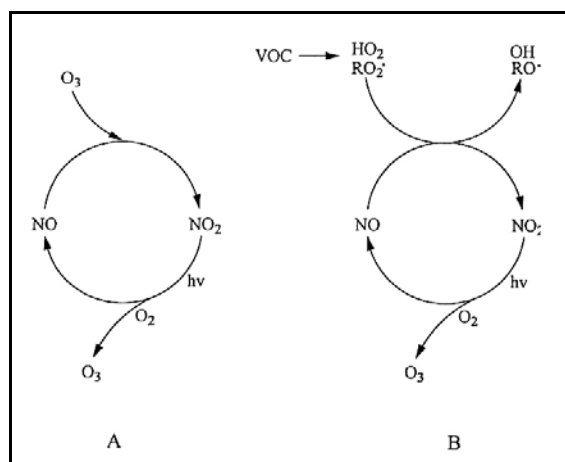
Figure 1: Schema of NO-to-NO$_2$ conversion and O$_3$ formation in (A) NO-NO$_2$-O$_3$ systems in the absence of VOCs, and (B) NO-NO$_2$-O$_3$ systems in the presence of VOCs.

Net photochemical formation of O_3 vs. net photochemical loss of O_3 in the troposphere therefore depends on the NO concentration, and is determined by the rate of the reactions forming reaction cycle. Based on the rate constants and the tropospheric concentrations of HO_2 radicals and NO, the net photochemical O_3 formation occurs for NO mixing ratios $\geq (10\text{-}30) \times 10^{-12}$ while net photochemical O_3 destruction occurs for NO mixing ratios $\leq (10\text{-}30) \times 10^{-12}$ (Logan, 1985). The hydrocarbon degradation sequence with the final net reaction can be written as:

$$RH + OH \rightarrow H_2O + R\cdot \qquad (2.8)$$
$$R\cdot + O_2 + M \rightarrow RO_2\cdot + M \qquad (2.9)$$
$$RO_2\cdot + NO \rightarrow RO\cdot + NO_2 \qquad (2.10)$$
$$RO\cdot + O_2 \rightarrow (\text{aldehyde or ketone}) + HO_2 \qquad (2.11)$$
$$HO_2 + NO \rightarrow OH + NO_2 \qquad (2.12)$$
$$\textit{NET:} \quad RH + OH + 2NO \rightarrow (\text{aldehyde or ketone}) + 2NO_2 + OH \qquad (2.13)$$
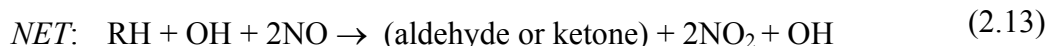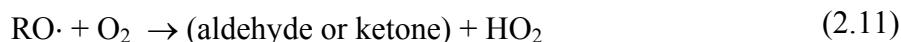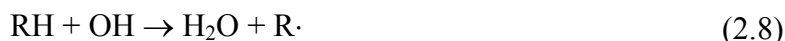
The overall net ozone production from hydrocarbons together with the rate for its production equals the rate for NO_2 production and can be written as:

$$\textit{NET:} \quad RH + h\nu + 3O_2 \rightarrow 2O_3 + H_2O + R \text{ (aldehyde or ketone)} \qquad (2.14)$$
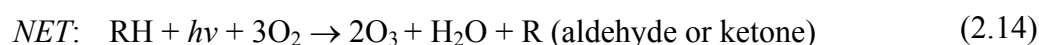
$$r(O_3) = \frac{d[O_3]}{dt} = r(NO_2) = \frac{d[NO_2]}{dt} = k_i \cdot [HO_2] \cdot [NO] + k_j \cdot [RO_2] \cdot [NO] \qquad (2.15)$$

where:

$r()$ is the reaction rate in (molecule.cm^{-3}.s^{-1})

$k_{i,j}$ is the reaction rate coefficient for the ith, jth reaction in

                 ((molecule.cm^{-3})$^{1-n}$.s^{-1}) for „n" as the order of chemical reaction

Since the NO and the OH radical are regenerated, this mechanism forms the important catalytic cycle in Figure 2. Side reactions of the peroxy radicals inhibit O_3 formation by providing an alternative fate, Figure 3.

The competitive reactions shown in both figures are reactions with NO, NO_2, HO_2 and permutation reactions. The relative rates of the side reactions for a given RO_2 radical are dependent on both its structure and the ambient conditions (e.g. NO_x concentration). Oxy radical, RO intermediate, reacts via three pathways: reaction with O_2, decomposition and isomerisation. The relative importance of these depends as in case of RO_2 radical on the structure of the oxy radical and also on ambient conditions, mainly temperature and pressure. Important aspect is additional NO-to-NO_2 conversion during decomposition and the isomerisation processes leading to the generation of altogether three O_3 molecules.

In summary, the general features of O_3 formation from the sunlight-initiated oxidation of VOCs and NOx are well established, with the rates and mechanisms of the oxidation of numerous VOC well characterized and quantified by laboratory study. However, there are certain classes of NMHCs for which the detailed oxidation mechanisms are still uncertain (mainly aromatic NMHCs, terpenes). The contribution of NMHCs to ozone chemistry is related to the amount of tropospheric NMHCs with isoprene having

the largest budget. However, isoprene with very short lifetime is not that relevant for the CARIBIC samples because they are collected in less polluted locations. Apart from ozone chemistry NMHCs are important pollution tracers.
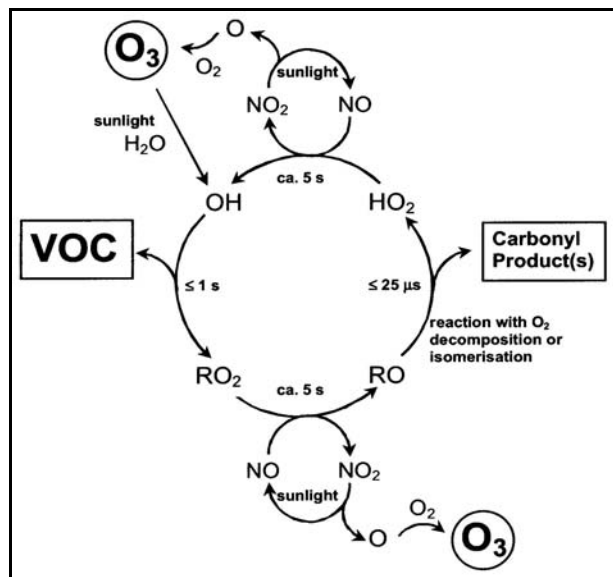
Figure 2: Ozone formation reaction cycle of the free radicals. By regeneration of NO and OH radicals the reaction scheme forms a cycle. Output of the VOCs is generally the carbonyl product. Both intermediates RO_2 and RO undergo several side reactions.
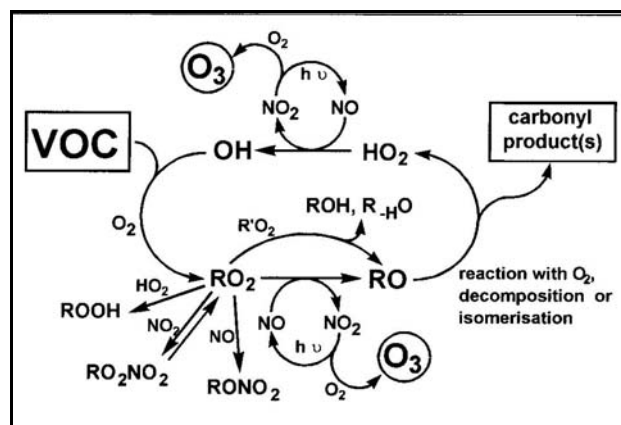
Figure 3: Ozone formation reaction cycle with potentially competitive reactions of the RO_2 radical made by reaction with NO, NO_2, HO_2 and permutation reaction. All inhibit O_3 production. Oxy radical, RO, reacts via three pathways: reaction with O_2, decomposition and isomerisation.

2.2 Measurement techniques for NMHCs

The measurement of NMHCs is challenging because of the variety of compounds and their low concentrations. In addition, other VOCs may cause interferences. The range and limitations of several analytical methods including sampling have been well discussed in (Helmig, 1999; Westberg and Zimmerman, 1993). The two major steps in NMHCs measurements are sampling and analysis. Three types of sampling are usually used: on-line measurements, sampling in suitable canisters and sampling onto suitable adsorbents. The consecutive analysis then uses either a direct technique or an enrichment technique. In on-line measurements the sample is analyzed directly, for instance by proton transfer reaction mass spectrometer (PTR-MS), or the NMHCs are enriched, separated on a GC column and detected by a variety of different detectors.

Most NMHCs measurements are done by taking an air sample in a suitably prepared container and subsequently transferring this sample to a laboratory gas chromatographic analysis. Off-line analyses are generally applied in isolated areas or airborne measurements where in-situ measuring is impossible (Kato et al., 2001; Young et al., 1997; Greenberg et al., 1996). Sample containers have been made from glass, surface treated metal and special plastics. Non-rigid containers such as teflon or tedlar bags are prone to significant wall losses for a range of NMHCs and are thus suitable only for high concentrations (Wang et al., 1996). For many C_1-C_9 NMHCs, passivated clean stainless steel canisters provide better sample stability than aluminium canisters (Gholson et al., 1990) although larger compounds tend to adsorb on the surface of both canister types. When samples of hydrocarbons are analyzed after storage for several days in SS canisters, substantial losses of the heavier hydrocarbons can be expected (Holdren et al., 1979). In addition, for reasons that are not understood, there is a tendency for concentrations of unsaturated NMHCs such as ethyne, ethene, propene and butene to increase in samples collected in canisters (Singh et al., 1988). Changes in concentrations are generally attributed to the reactivity, polarity and water solubility of the NMHCs and water vapor content (Cao and Hewitt, 1999). Water is sometimes introduced to reduce the alkene formation and adsorption losses (Colman et al., 2001). Water is believed to occupy active metal surface sites that would otherwise adsorb NMHCs.

NMHCs in the atmosphere have usually too low concentrations for analysis without pre-concentration. The hydrocarbons are pre-concentrated cryogenically or by using a suitable adsorbent. Several materials are available for use, individually or in combination: organic polymers such as Chromosorb, Porapak and Tenax, inorganic materials including alumina, molecular sieve and silica gel, and finally the most

frequently used carbon-based adsorbents like activated charcoal, Carbotrap and Carbosieve. Selection of the adsorbent depends on the boiling point of the analytes, specific surface area of the adsorbent, its hydrophobicity, breakthrough volume, polarity and desired operating temperature (Camel and Caude, 1995; Cao and Hewitt, 1999; Matisová and Škrabáková, 1995). Carbon-based adsorbents with a large area are useful to trap very volatile compounds, but they pose problems in desorption of less volatile substances. Porous polymers with a comparatively small surface area allow the adsorption and desorption of high-boiling compounds but may not absorb the highly volatile compounds. A wide range of NMHCs of different volatilities and polarities is thus usually pre-concentrated using a combination of 2-3 adsorbents (Helmig and Greenberg, 1994). With a pre-concentration, hydrocarbons with mixing ratios at or below 5 pptv have been measured with good precision by GC-FID systems. However, there are potential problems in using this method because of matrix components which may influence the analysis.

The major components of the matrix are H_2O and CO_2. Although water content in typical CARIBIC sample is small, up to few hundreds ppm, together with 370-380 ppm of carbon dioxide they may block the focusing trap or capillary column (Kurdziel, 1998). Additionally, the effect of water and CO_2 vapor in the air samples on the peak resolution in forms of retention time shifts or a rise of the zero line has been noticed (de Zeeuw et al., 1987). On the PLOT columns CO_2 coelutes with C_2 compounds, particularly ethene, which results in peak deformations (Habram at al., 1998). Ambient air samples have been dried using various drying agents like magnesiumperchlorate (Matuska et al., 1986), potassium carbonate or by using Nafion membrane, a material with very high permeability for water vapor (Gong and Demerjian, 1995). Another way is to freeze the water out (Lai et al., 1993). To get rid of the CO_2 absorption on ascarite (natrium hydroxide on support) and LiOH has been used (Matuska et al., 1986; Mühle, 2002). However, treating with chemical agents has the risk of changing air sample in terms of its composition (Doskey, 1991). Apart from water and carbon dioxide, it is the oxidants contained in the air matrix which may influence analysis, especially analysis of reactive hydrocarbons at low concentrations. Reactions between the hydrocarbons and oxidants, such as residual O_3 or NO_2 that survives the collection procedures, may destroy some hydrocarbons and produce other compounds not originally present (Goldan et al., 1995). Various techniques have been utilized to remove O_3 (Helmig, 1997).

After pre-concentration hydrocarbons are separated at GC column and detected using a suitable detector (Habram et al., 1998). Different pre-concentration/GC systems were designed for different purposes needed for field studies of the tropospheric chemistry (Blake et al., 1994; Gong and Demerjian, 1995; Konrad and Volz-Thomas, 2000; Lewis

et al., 1995, 1996, 1997; Zielinska et al., 1996). Mainly since mid 90s a wide range of automated GC-FID systems that are capable of unattended operation has been developed in (Castello et al., 1995; Dollard et al., 1995; Farmer et al., 1994; Mowrer and Lindskog, 1991; Oliver et al., 1996). Automated on-line GC-FID and GC-MS systems for both long-term and intensive short-term measurements of atmospheric hydrocarbons have been used in (Konrad and Volz-Thomas, 2000; Plass-Dülmer et al., 2002). Higher resolution than by conventional gas chromatography was achieved by the two-dimensional gas chromatography (GCxGC) which is able to separate and classify several hundred chemical species in ambient air when coupled to an appropriate detector. Analysis of all isomers, aromatic compounds C_2-C_5 or higher compounds like terpenes can be made (Lewis et al., 2000; Hamilton and Lewis, 2003; Xu et al., 2003).

After separation, the individual NMHC compounds are usually detected using a flame ionization detector (FID) or a mass spectrometer (MS). The FID is a nonspecific hydrocarbon detector with a response that is nearly linearly proportional to the number of carbon atoms in the hydrocarbon molecule, with a slightly diminished response for aromatic and olefinic carbon atoms (Ackman, 1968). An alternative to the FID is the mass spectrometry technique (MS). Conventional mass spectrometry is a well proven and highly sensitive technique for the identification and detection of organic pollutants. It offers increased sensitivity and can quantify compounds even if they co-elute.

Several direct techniques do not need a pre-concentration step. One such technique is Chemical Ionization Mass Spectrometer (CIMS) which uses ion-molecule reactions producing less fragmentation of molecular ionic species to ionize the analyte. The Proton Transfer Reaction Mass Spectrometer (PTR-MS) is most frequently being used to measure typical VOC compounds (Lindinger et al., 1998). The first PTR-MS instrument was developed at the University of Innsbruck (Hansel et al., 1995). It employs H_3O^+ ions to ionize most VOCs present in gaseous media, usually without fragmenting the parent ion. When H_3O^+ is used as the proton donor, most of the typical VOC components react by forming $VOCH^+$, reaction (2.16).

$$H_3O^+ + VOC \rightarrow VOCH^+ + H_2O \hspace{2cm} (2.16)$$

H_3O^+ is the most suitable primary ion. It does not react with any of the natural components of air, as they have proton affinities lower than that of H_2O molecules. H_2O has a proton affinity of 7.22 eV and common organic molecules have proton affinities in the range from 7 to 9 eV, thus making most of the relevant proton transfer reactions involving H_3O^+ ions slightly exothermic, but keeping the energy low enough, so that breakup of the neutrals to be detected only seldom occurs. Proton transfer occurs on every collision with defined rates. By keeping the density $[H_3O^+]$ high and

using the analyzed air itself as a buffer, the enhanced detection limits can be achieved (Hansel et al., 1998). Nowadays PTR-MS is a method frequently applied in the analysis of air (Williams et al., 2001; Salisbury et al., 2003; Crutzen et al., 2000). The ambient measurements of benzene and toluene using PTR-MS together with investigation of calibration and humidity-dependency, were compared in field with GC-FID (Warnecke et al., 2001). However, distinguishing between two compounds of the same mass like acetone and acetaldehyde is sometimes problematic. The PTR-MS instrument also cannot measure the entire spectrum of NMHCs.

New direct techniques not using GC nor MS are emerging for certain NMHC measurement. A chemiluminiscence reaction of double bond with O_3 is the principle for technique which has been developed to measure isoprene (Guenther and Hills, 1998). The isoprene flux above a forest canopy is measured directly using the combination of an isoprene sensor and sonic anemometer. Isoprene detection is based on chemiluminescence reaction between a primary alkene and ozone. The technique enables long term and continuous measurements but the technique measures only compounds which react with O_3.

An other approach to direct measuring are the optical techniques. They can provide a relatively unambiguous identification of the species present in the atmosphere. Fourier transform infrared spectroscopy, FTIR, can be applied for small compounds such as ethyne or to measure the column densities of selected hydrocarbons. The FTIR technique offers the possibility of continuously measuring levels of many NMHCs which absorb infrared light. Several techniques including FTIR that have been used to speciate NMHC compounds including OVOC were intercompared in well-mixed smoke generated by 47 fires in the U.S. Department of Agriculture Forest Service Fire Sciences Combustion Facility (Christian et al., 2004). At mixing ratios above a few parts per billion, the open-path Fourier transform infrared spectroscopy OPFTIR had advantages for measuring sticky compounds since there is no sampling step in measuring. However, the detection limits in the ppb range make FTIR inadequate for measurements in free troposphere.

In 1975 and 1979, (Noxon, 1975; Noxon et al., 1979) and (Platt et al., 1979) introduced a new method to measure atmospheric trace gas concentrations, Differential Optical Absorption Spectroscopy (DOAS). Since then, DOAS has been applied to measure trace-gas concentrations in the troposphere and stratosphere. Interesting application of the DOAS technique is the measurement of absolute concentrations of aromatic hydrocarbons. Monocyclic aromatic hydrocarbons can be monitored with sub-ppbv sensitivity and time resolution of minute in urban areas (Volkamer et al., 1998). Most aromatic hydrocarbons show a characteristic and well structured absorption in the wavelength range below 300 nm. However, the DOAS detection of aromatic

compounds suffers the spectral overlap from absorptions of atmospheric oxygen where the oxygen absorptions are the dominant spectral structure in the measured spectra (Trost 1997; Volkamer et al. 1998). Since more recently, as far as the wavelength range between 243nm and 290nm concerns, the problems due to interfering oxygen absorption can be overcome thus an interesting spectral range is available for the DOAS detection of a variety of aromatic hydrocarbons. In recent years, the absorption cross-sections of a variety of aromatic compounds like benzene, toluene, o-, m-, p-xylene, TMBs, phenol, cresol-isomers, DMP-isomers, aromatic aldehydes and further aromatic compounds have been determined (Etzkorn et al. 1999) and were applied to the DOAS measurement of aromatic compounds in the atmosphere (Ackermann 2000). The major advantage of the DOAS technique is its ability to measure absolute trace gas concentrations of different isomers. The simultaneous determination of the concentration of several trace gases, by analyzing the sum of their absorptions in one wavelength interval, reduces measurement time and gives well time-resolved insight about the average chemical composition of the observed air mass. However, only a small part of the NMHCs can be measured by DOAS.

Intercomparison of NMHCs measurement systems and sampling canisters has been completed in NOMHICE experiment (Apel et al., 1994, 1999, 2003) and AMOHA experiment (Slemr et. al., 2002) and (Plass-Dülmer et al., 2006). NOMHICE was designed to assess the accuracy and comparability of NMHCs measurements from research groups around the globe. Participants in NOMHICE received canisters containing aliquots of gas samples prepared by NIST or commercial gas suppliers. The experiment had four stages. The first task of the intercomparison was aimed at checking the analytic methods of the participating laboratories and the accuracy of standards. A mixture containing only n-butane and benzene was circulated and the compounds in the mixture were disclosed to the participants. The second task of the intercomparison was aimed at checking the techniques for the identification and quantification of a more complex, gravimetrically prepared, 16-component hydrocarbon mixture to determine whether the analytical methods provided suitable separation, identification and quantification of the individual hydrocarbons. The third task expanded the tests of the second task to a greater range of species that more nearly represents those typically found in the atmosphere. In the last task of the NOMHICE program, participants analyzed a collected ambient air sample. A whole air mixture was distributed and participants were asked to identify and quantify as many NMHC species as possible.

Individual canisters containing the air sample were prepared and analyzed by the NOMHICE group at the National Center for Atmospheric Research NCAR. The samples were collected cryogenically by condensation of ambient air. NCAR analyzed each individual canister before sending them out to participants and after receiving

them back. The canisters were returned to ensure that the content of each canister remained stable. As shown there were often compounds present, such as OVOCs, that could cause problems with the analyses, particularly when a relatively nonselective detector such as FID is used.

The Accurate Measurements of Hydrocarbons in the Atmosphere (AMOHA) project was proposed to evaluate and improve current gas chromatographic methods used across Europe to determine concentrations of C_2-C_9 nonmethane hydrocarbons in ambient air. Four international intercomparisons of increasing complexity were carried out over a period of 4 years. Results from the first three European intercomparisons emphasize the importance of using high-quality NMHC multi-component gas calibration standards. The most frequent causes of problems were interferences by co-elution with other compounds, breakthrough of C_2 compounds during sample pre-concentration and adsorptive losses of C_7–C_9 compounds in the transfer lines before the analytical instrumentation. Calibration with multi-component NMHC standards was demonstrated to provide significantly more accurate results than the frequently used method of calibration with just a single hydrocarbon species, such as n-butane. In the final task of AMOHA, 4th intercomparison, the major objective was to test the overall analysis performance of the participating laboratories which included both the sampling procedure and storage in stainless steel canisters. In phase 1 participants' and referee's canisters were filled by a referee with homogenized air sample of known composition and sent to participants for analyses. The result provided mainly information on the influence of storage and analysis on the uncertainty of the results. In phase 2 all participants sampled air into their own canisters at a DWD (Deutscher Wetterdienst) observatory at Hohenpeißenberg where an on-line instrument was operated. The results were evaluated using a rank-value, characterizing the overall deviation for each participant and task. It was found that better performing laboratories, constituting more than a half of the participants, achieved comparable high rank-values in all tasks. It appears that for these laboratories sampling procedures and canisters have minor effects on the obtained results. On the other hand, laboratories with lower rank values exhibited substantial differences between the phase one and two with substantially worse results in phase two.

Intercomparison of NMHCs measurements made using in-situ GC and off-line analysis of samples collected in canisters and samples collected on adsorption tubes was made in (Volz-Thomas et al., 2002). In this comparison, the German Focus on Tropospheric Research (TFS), the quality assurance procedures were established to obtain estimates on precision, accuracy and comparability of the measurements made with different systems and by different groups and to harmonize the different data by referencing all measurements to a common calibration standard. Stepwise approach during the

intercomparison similar to multi-task projects NOMHICE, AMOHA was choosen. Steps comprised comparisons of synthetic mixtures of increasing complexity and instrument comparisons in ambient air immediately before or after the field campaigns. For evaluation of the ambient measurements one well characterized GC system was chosen as the reference system. All TFS participants used a 70 component standard from NCAR as the reference standard for calibration during the field campaigns. In the first step, n-alkane mixture, an a priori data quality objectives for precision were usually met by most of the participants. For the larger alkanes, most systems progressively underestimate the certified values probably due to adsorption effects of the compounds with high boiling point. The second step, complex mixture, showed few problems with miss-identification which were later corrected. During the first field campaign two *in-situ* GCs were compared with the result that they fulfill the criteria for comparability. At the same time when both instruments operated canister samples were collected and analysed by other system. The same happened with charcoal samples as well. Canister results compared to the first *in-situ* instrument results showed similar combined relative error but larger absolute error which must be due to problems arising from canisters and/or from short term fluctuations in the ambient term. Still, most of the data fulfill the data quality objectives for comparability. In the second field campaign 9 *in-situ* GC systems were compared over a period of 24 hours together with canister sampling. Large differences were found for two instruments that could not reproduce the atmospheric variations at all thus likely caused by excessive blanks and memory effects. Finally, canister results were in reasonable agreement with the reference GC for most of the alkanes and for the aromatic compounds benzene and toluene. The experience in TFS is similar to NOMHICE. The results of experienced groups and proven analytical systems are in much closer agreement than those of newcomers or results obtained with new untested systems.

In summary, the intercomparison exercises demonstrated that reliable NMHCs measurements can be made on a routine basis applying stringent quality assurance procedures by well equipped laboratories with well trained personnel.

3. Experimental

3.1 Analytical system

The instrument developed in this work allows the measurements of non-methane hydrocarbons with acceptable accuracy and reliability within the concentration range of atmospheric samples from upper troposphere and lower stratosphere. Fully automated measurements are possible of either 7 air samples (or 14 in one canister-box TRAC) using the V25 microprocessor system developed at the Max-Planck-Institute for Chemistry in Mainz.

3.1.1 The apparatus description

A schematic overview of the instrument is shown in Figure 4. The detailed description is in Figure 5. The instrument consists of 5 multi-port valves and GC. GC is a model 6890N Agilent with two FIDs. The instrument is controlled by V25 not shown in Figure 4.

The basic functions of the instrument are: to enrich the NMHCs from the sample, to focus the enriched NMHCs and to inject them into the GC column. VA1 serves as a sample selector (lower left side). The sample is stripped of water and carbon dioxide (upper left side) before entering the enriching and focusing traps (PF and KF). The latter parts are pneumatically lowered and lifted into a small Dewar with liquid nitrogen. The focused NMHCs flow directly into the GC oven where they are split onto two different columns, Petrocol and Gas-pro. Flow rates are controlled by mass flow controllers. Multipoint calibration with standard gas mixture requires an additional dilution system (lower central part). The standard gas mixture at low ppb mixing ratios is diluted to sub-ppb mixing ratios found usually in air samples from UT and LS. The sampling volume of the standard and the sample is determined by the flow integration and checked using a pressure increase in a known volume into which the air sample is expanded (upper right corner).

Figure 4 shows description of the instrument, explanation is in Figure 5. VA1 is the first Valco, multi-position 10-way valve. Analogically VA2 is the second 4-port 2-way valve, VA3;VA4;VA5 are the third; the fourth; the fifth, all the 6-port 2-way valves. Multi-position valve means it has 10 inputs and 1 output. Each input can be chosen by the command from electronic remote control. The other 4 valves switch between two

positions. The positions are described using straight lines and curved lines and are titled A,B. CO_2 and SCR are abbreviations for the carbon dioxide trap and the water scrubber respectively. FC means the flow controller. PF, KF are the enrichment and focusing parts respectively. Inside the GC there are 3 columns. Col1 is Petrocol DH, col2 is a restriction capillary and finally col3 is Gas-pro. Columns are connected to two FIDs titled FID A and FID B. H_2 is used as a carrier gas for columns and the valves as well. All lines with H_2 are marked with a thin black line. These are H_2-aux(4) and H_2-aux(3). There are more letters u1,u2,u3 for unions between different columns. The double line is for 1/16" tubing. All samples as well as H_2 run through this tubing in order to flush and carry the sample. Besides Valcos, also CO_2, SCR, PF, KF and GC itself are partly controlled by the V25. On the scheme a single line is ss: 1/16" OD, 1.0mm ID. The double one is ultimetal deactivated 1/16" OD, 1/32" ID. Wave line is ultimetal deactivated 1/32" OD, 0.5mm ID. The line from PF into the port No. 5 on VA4 is PEEK 1/16" OD, 1.0mm ID. u1,u2 – ss 1/16"union, u3 – ss 1/32" union Swagelok. Columns are split with T-piece 1/32" ss.

Figure 4: Scheme of the instrument.

Figure 5: Explanation to the Figure 4 showing instructive description of all parts.

3.1.2 The gas chromatograph

Gas chromatography is a technique for separating volatile substances by percolating a gas stream over a stationary phase. The compounds are separated primarily by the differences in their volatilities and structures. At the end, the compounds leaving the separation process are ordered in elution order. The order of elution is related to the boiling points and polarities of the substances in the mixture.

In combination with sensitive detector, gas chromatography is one of the most important, efficient and sensitive analytical techniques available for the analysis of volatile compounds. For GC analysis, a compound must have sufficient volatility and thermal stability.

Most gas chromatographs consist of several units. The gas supply provides all the necessary gas supplies which may involve a number of different gases. The injector allows to inject a sample onto the column. The column is the most important device that actually achieves the necessary separation. It is followed by chromatographic detector which is a device indicating and measuring the amount of separated components in the carrier gas. A number of different detectors are used to measure the

species separated in the column, each with unique operating parameters and its own performance characteristics.

Capillary gas chromatography uses a capillary as a column. The column resides in an oven whose temperature is accurately controlled. The stationary phase of a column slows the movement of each compound along the column by a different amount, this is called retention. All of the column parameters like length, diameter or the stationary phase affect compound retention.

3.1.2.1 The detector

As solutes elute from the column, they interact with the detector. The detector converts this interaction into an electronic signal that is sent to the data system. The magnitude of the signal is plotted versus time generating a chromatogram. Since chromatographic detectors differ greatly in the principle of which they operate, it is difficult to compare them. Certain characteristics, however, are indicative of the use usefulness of the detector.

Selectivity refers to the extent to which a detector can detect particular analytes in mixtures or matrices without interferences from other components. Detector sensitivity or minimum detectable concentration (MDC) is defined as the minimum concentration of solute passing through the detector that can be unambiguously discriminated from noise. The size of the signal that will make it distinguishable from the noise (the signal–to–noise ratio) is an arbitrary choice. It is generally accepted when the signal to noise ratio is two.

The response of a detector is the quantity of a signal generated by a given amount of the sample. The linear range of a detector may be defined as the ratio of the largest to the smallest concentration within which the detector is linear.

The ideal GC detector should be as sensitive as possible and linear over many orders of magnitude. No existing detector fulfills all these specifications but the FID comes close to this ideal performance. The applicable detectors for GC analyses of volatile organic species are:

Flame ionization detector - FID

Mechanism: Compounds are burned in a hydrogen-air flame. Carbon containing compounds produce ions (e.g. CH_3^+) and electrons, electrons are attracted to the collector. The current produced by electrons is measured and a signal is generated.

Selectivity: Compounds with C-H bonds. A poor response for some non-hydrogen containing organics (e.g., hexachlorobenzene).

Sensitivity: 0.1-10 ng
Linear range: 10^5-10^7

Photoionization detector – PID

Mechanism: Compounds eluting into a cell are ionized by high energy photons emitted from a lamp. Compounds with ionization potentials above the photon energy are not ionized. The electrons are attracted to an electrode, measured, and a signal is generated.

Selectivity: Depends on lamp energy. Usually used for aromatics and olefins (10 eV lamp).

Sensitivity: 25-50 pg (aromatics); 50-200 pg (olefins)
Linear range: 10^5-10^6

Mass spectrometer - MS

Mechanism: Compounds are ionized by impact with electrons (EI) or by reaction with ions (CI). Compounds may fragment into characteristic charged ions or fragments. The resulting ions are focused and accelerated into a mass filter. The mass filter selectively allows all ions of a specific mass to pass through to the electron multiplier. All of the ions of the specific mass are detected. The mass filter then allows the next mass to pass through while excluding all others. The mass filter scans stepwise through the designated range of masses several times per second. The total number of ions are counted for each scan. The abundance or number of ions per scan is plotted versus time to obtain the chromatogram (called the TIC). A mass spectrum is obtained for each scan which plots the various ion masses versus their abundance or number.

Selectivity: Any compound that produces fragments within the selected mass range. May be an inclusive range of masses (full scan) or only select ions (SIM).

Sensitivity: 1-10 ng (full scan); 1-10 pg (SIM)
Linear range: 10^5-10^6

3.1.2.2 The FID

The Flame Ionization Detector – FID, is the most frequently used detector in GC analyses. The FID has a very wide linear dynamic range, a high sensitivity and (with the exception of a few low molecular weight compounds) will detect all substances that contain carbon-hydrogen bonds.

FID consists of a small volume chamber into which the gas chromatograph capillary column is directly connected. Usually the small diameter capillary is fitted directly into the bottom of the detector flame jet. The gaseous eluents from the column are mixed with hydrogen and air and all are burned on the jet tip. The hydrogen-air flame alone creates few ions, but when an organic compound is burned CH^+ ions and corresponding electrons are produced. Surrounding the flame is a cylindrical electrode and a relatively high positive voltage is applied between the jet and the electrode to collect the electrons that are formed in the flame. The resulting current is amplified by a high impedance amplifier and the output fed to a data acquisition system. The current produced is proportional to the amount of sample being burned.

The detector usually requires three separate gas supplies controlled by precision flow regulators. The gases normally used are hydrogen for combustion, helium or nitrogen for the carrier gas and oxygen or air as the oxidation agent. The detector is normally kept at constant temperature. This is not because the response of the FID is particularly temperature sensitive but to ensure that no gases produced by the combustion (mainly water) condense in the detector before leaving the chamber via exhaust.

The body and the cylindrical electrode are usually made of stainless steel and stainless steel fittings connect the detector to the appropriate gas supplies. The jet and the electrodes are insulated from the main body of the sensor with appropriate high temperature insulators. Scheme of the FID is in Figure 6.

The use of high voltages in conjunction with the very small ionic currents require that all connections to the jet or electrode must be well insulated and electrically shielded. In order to accommodate the high temperatures that exist at the jet-tip, the jet is usually constructed of a metal that is not easily oxidized such as stainless steel, platinum or platinum/rhodium. The background current (ions and electrons from the hydrogen flame alone) is very small ($1 - 2$ x 10^{-12} amperes) and consequently, the noise level is also commensurably small, about 10^{-14} amperes.

The flame plasma contains both positive ions and electrons which are collected on either the jet or the plate depending on the polarity of the applied voltage. Initially, the current increases with applied voltage, the magnitude of which depend on the electrode spacing. The current continues to increase with the applied voltage and eventually reaches a plateau at which the current remains nearly constant. Once electron/ion pair production is initiated the recombination starts to take place. The longer the ions take to reach the electrode the more recombination takes place. Thus, the greater the distance between the electrodes and/or the lower the voltage, the greater the recombination. The plateau is reached at a lower voltage when the electrodes are closer together. The plateau level is the same for both electrode conditions and it is assumed that on the plateau, all electrons being produced in the flame are collected. In practice the applied

voltage would be adjusted to suit the electrode distance to ensure that the detector operates under conditions where all electrons and small fraction of the ions are collected.
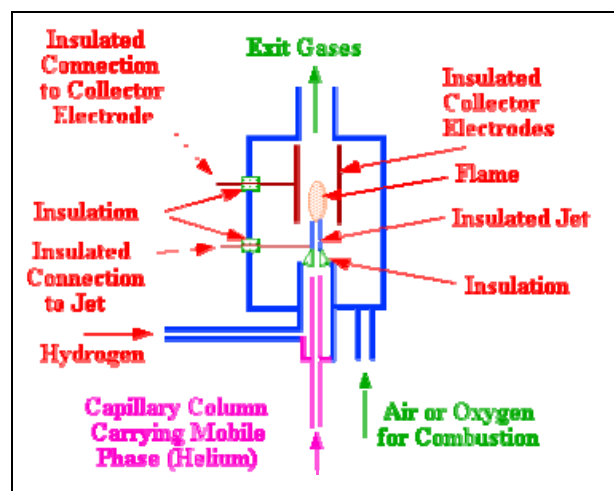
Figure 6: Scheme of the FID detector.

The general response of the FID to substances of different type varies significantly. For a given homologous series the response appears to increase linearly with carbon number but there is a large difference in response between a homologous series of hydrocarbons and a series of alcohols. The signal is approximately proportional to the carbon content, giving rise to the so-called equal per carbon rule. Thus, all hydrocarbons should exhibit the same response, per carbon atom. Molecules that contain only carbon and hydrogen respond best but the presence of heteroatoms in a molecule, such as oxygen, decreases the detector response comparing to the relative response as the carbon rule says. Relative response values are often tabulated as effective carbon numbers *ECN*. Therefore, highly oxygenated molecules, sulfides or halocarbons might best be detected using another detector instead of the FID.

The detector responds to mass per unit time entering it. This is particularly advantageous and allows it to be used very effectively with capillary columns. Although the column eluent is mixed with the hydrogen prior to entering the detector, as it is mass sensitive and not concentration sensitive, the diluting effect has no impact on the sensitivity. The total volume of gas in the FID that yields the most sensitive and widest linear response is not the same volume of gas when the column effluent flow and hydrogen and air flows are flowing. To maintain the best analytical conditions, a makeup gas must be added. Generally, conditioning is needed to reach the optimum operating parameters of FID. In Figure 7 is FID sensitivity as a function of the burning

gas and the make up gas. The maximum is relatively flat but e.g. 10% different flows may cause change in sensitivity by 5-10%.

The linear dynamic range of the FID covers at least four to five orders of magnitude for 0.98<r<1.02 which is a remarkably wide range. One of the major areas of application for the FID is in the analysis of hydrocarbons although it is also employed extensively for pharmaceutical analysis, pesticide analysis, forensic chemistry and essential oil analysis Nevertheless, its major area of application is in the analytical laboratories of the hydrocarbon industry.
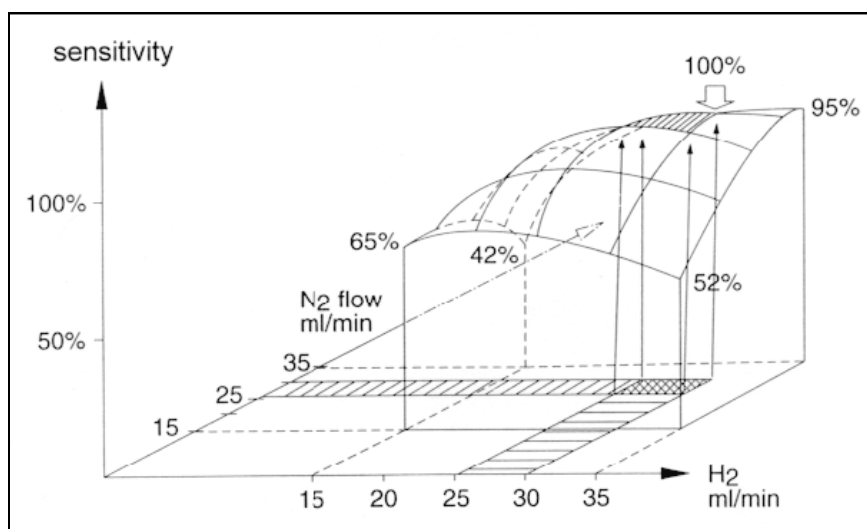
Figure 7: Dependence of the sensitivity of the FID on the flow rates of H_2 (burning) and N_2 (make-up) respectively.

3.1.2.3 The used GC

The used gas chromatograph is the 6890N model from Agilent. This GC system is equipped with full electronic pneumatics control (EPC) that keeps pressure and flow setpoints constant from run to run which leads to retention time repeatability less than 0.008%. It controls electronically all the gas flows and pressures in the instrument. Each EPC unit is optimized for its intended use with a specific inlet and detector option.

The GC provides three additional auxiliary pressure control channels. They are controlled by the Aux 3, Aux 4, and Aux 5 outputs. The first one supplies columns inside the oven, the second supplies all valves and the third one is free. The second Aux 4 defines the pressure on all the Valco Vici valves. During most of the analyses pressure between 150 and 160 kPa (relative) was used.

Gas chromatograph has two FID detectors optimized for use with capillary columns, see Table 1. The standard 6890/6850 FID with grounded jet eliminating the need for a jet insulator has minimum detectable level (for Tridecane) less than 1.8 pg C/s. Data rates up to 200 Hz accommodate peaks as narrow as 25 ms at half height. The software used for continuous monitoring and updating on the display was the Agilent ChemStation version A.10.01 from September 2003. Execution of multi-method sequences, entering all GC parameters electronically, and an advanced reporting capabilities all belong to the advantages which distinguish this version from the older ones. Using grouped post-run commands, i.e. macros, the customized reporting was used to form uniform *.xls* table with information about calibrated peaks, unknown peaks, their retention times and finally the mixing ratios based on calibration. The uniform structure provides basis to apply SQL queries thus is enabling to gain the requested information.

Using the enhanced integration algorithm a user-friendly integrator-settings are possible. A definition of integration events for each of multiple signals allows easier tuning for the better integration performance. Chromatograms requiring human interpretation can be stored with the method separately, the corrections-events are recorded in the method and used as a part of interpretation.

FID	
Flows	**ml/min**
H_2	column$+N_2$
N_2	25
Air	400
Temperature	300 ^{o}C
sampling frequency	50 Hz

Table 1: Settings table of the used FID.

3.1.3 The columns

Column is the heart of the chromatographic system. Here is where the separations take place. Capillary, open tubular, columns are open tubes with 0.1 to 0.5 mm I.D. and 5 to 100 m lengths. They consist of three distinct layers: the fused silica tube, the protective coating and the stationary phase. Fused silica is a synthetic quartz-like glass. Untreated fused silica is a very active due to the presence of silanol groups. The deactivation process eliminates the silanols by converting them into relatively

nonpolar and nonreactive groups. The deactivation process creates a suitable surface for the stationary phase.

The stationary phase is usually a thin layer (with 0.1 to 5 μm film thickness) on the inner wall of the column. Modern column technology enables cross-linking of the polymer molecules of the liquid and attachment of the phase at the silica surface due to chemical bonding. Interestingly, these cross-linked phases thermodynamically behave very similar to the initial liquid.

The structure of the stationary phase influences the separation of the compounds. Column dimensions primarily affects the resolution. A column with very high resolution is not useful if the stationary phase can not separate the desired compounds. There are only about 15-20 distinct stationary phases available.

Two types of the stationary phases are used: the wall coated open tubular columns, *WCOT*, and the porous layer open tubes, *PLOT*. The *PLOT* columns are mostly used for gas analysis and the separation of low molecular weight hydrocarbons. The external diameter of *PLOT* columns range from 320 to 530 μm with a porous layer that can be 5 to 50 μm thick. Both column types are compared in the Figure 8.
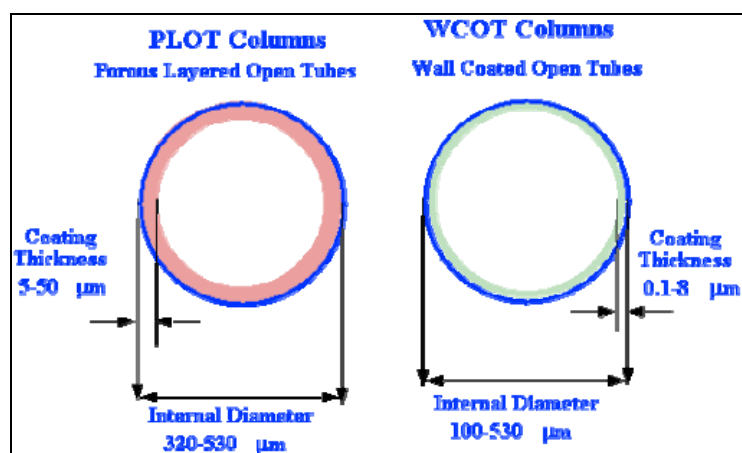
Figure 8: Basic characteristics of PLOT, WCOT columns.

The predominant polymers used as a stationary phases in *WCOT* columns are substituted polysiloxanes. Another common stationary phase is polyethylene glycol (*PEG*). Polymers have unique separation characteristics but high low-temperature limit and are sensitive to oxygen. Porous polymers make small particles coated onto the inner wall. Stationary phases of aluminium oxide or molecular sieves occur in typical *PLOT*. They are more retentive than liquid phases.

The single most important characteristic of the phase is polarity, because it controls selectivity, or the ability of the column to separate sample components. A nonpolar column is best for analyses of nonpolar compounds. Polar columns most effectively

separate polar compounds. The polarity of stationary phase is directly related to the amount and polarity of each functional group. The polarity of a stationary phase increases as with the polarity of the substituted groups and their relative amounts. Non-polar stationary phase columns can be used over a wider temperature range.

3.1.3.1 The separation

Separation is best described as a series of absorption-desorption processes which are continuous from the time the sample is injected into the distribution system until the time the solutes exit from it. Equilibrium occurs between the mobile phase and the stationary phase. The probability of a solute molecule entering the stationary phase is the same as the probability of a solute molecule randomly acquiring sufficient kinetic energy to leave the stationary phase and enter the other phase.

The efficiency of the column separation can be described in terms of retention time t_r, partition ratio k, separation factor α, resolution R, and trennzahl TZ.

$$t_r = time\ of\ elution \tag{3.1}$$

$$k = \frac{t_r - t_m}{t_m} \tag{3.2}$$

$$\alpha = \frac{k_2}{k_1} \tag{3.3}$$

$$R = 1.18 \cdot \left(\frac{t_{r2} - t_{r1}}{W_{h1} + W_{h2}} \right) \tag{3.4}$$

$$TZ = \left(\frac{t_{r2} - t_{r1}}{W_{h1} + W_{h2}} \right) - 1 \tag{3.5}$$

where:

t_m is t_r of non-retained peak

$k_1(k_2)$ is the partition ratio of earlier (later) eluting peak

W_{h1-2} is the peak width at half height of peak 1,2

Retention time is one of the most fundamental parameter in GC. Retention time is a measure of how long it takes a compound to travel down the column. It is a sum of the time the compound spends in the stationary and mobile phases. Partition ratio is a dimensionless measure of how long a compound spends in the stationary phase compared to another compound. It is a more direct measure of the actual magnitude of compound retention than its retention time. Separation factor is a measure of the

amount of peak separation. $\alpha = 1$ represents the same retention, thus complete coelution. It is just the distance between two peaks. Resolution is the measure of the amount of separation between two peaks taking the width of peaks into account. $R = 1.5$ represents fully resolved peaks without baseline between. Values below 1.5 mean only partial peak-resolution. The separation factor means little if peak resolution is not considered. If resolution is achieved, separation automatically occurs. Two broad peaks can have equal separation than two narrow peaks, but the narrow peaks are better resolved. Trennzahl takes the peak widths into an account as well but is defined as a resolution of two consecutive members of a homologous series.

Another measure of the column separation is the number of a theoretical plate N and its height equivalent H.

$$N = 5.545 \cdot \left(\frac{t_r}{W_h} \right)^2 \tag{3.6}$$

$$H = \frac{L}{N} \tag{3.7}$$

where:

L is the column length in mm

A higher number of theoretical plates results in thinner peaks at their respective retention times. Height equivalent to a theoretical plate is a column length per plate.

The number of theoretical plates is directly proportional to column length. Increasing the number of theoretical plates results in better resolution, but the resolution increase is not directly proportional to the increase in the number of theoretical plates. The resolution is proportional to the square root of the number of theoretical plates thus to the column length. As defined, the number of theoretical plates is inversely proportional to column diameter. In other words, theoretical plates per meter increases as column diameter decreases. Increasing the film thickness generally increases peak width (reduces column efficiency), increases analyte retention times (may also increase resolution) and reduces sample interaction with the tubing wall which helps to prevent overloading.

Thick film columns increase retention of highly volatile compounds. A longer column will provide greater resolution than a shorter column but doubles the analysis time and increases the pressure required to move the sample through the column. Longer columns also reduce the optimum linear velocity for an analysis.

Apart from temperature programming or column parameters it is the carrier gas that influences the separation as well. Peak broadening is a consequence of dispersion. It is described by the model of the theoretical plate height.

The first comprehensive approach to dispersion in chromatographic columns was taken by Van Deemter who developed the dispersion equation for a packed GC column. Van Deemter et al. assumed that four processes are responsible for peak dispersion. The total plate height is the sum of the four contributions:

H_{diff} term describing the contribution from longitudinal diffusion,

H_{conv} term for convective mixing,

$H_{ex,m}$ term describing the kinetics of mass exchange from the mobile phase to the interface between mobile and stationary phase,

$H_{ex,s}$ term describing the kinetics of mass exchange from the stationary phase,

Due to the compressibility of the gaseous mobile phase in GC, neither the linear velocity nor the pressure is constant along the column. These two effects are taken into an account in the Golay version of the Van Deemter equation. Figure 9 shows the plate height as a function of the mobile phase velocity according to the Golay equation (the green curve) which is calculated as a sum of the two major dispersion processes. The first is a longitudinal diffusion (the black curve) and the second is a combination of the both terms describing mass transfer for the mobile and the stationary phase (the red curve). The function has a minimum, i.e. for the given gas velocity the plate height exhibits a minimum value thus peak broadening is the smallest.

This optimal gas linear velocity gives the maximum separation efficiency. Carrier gas linear velocity is not uniform throughout the column. The particular velocity depends on the pressure drop along the column. Van Deemter and similar curves show that using too high or too low average linear velocities results in a loss of efficiency.
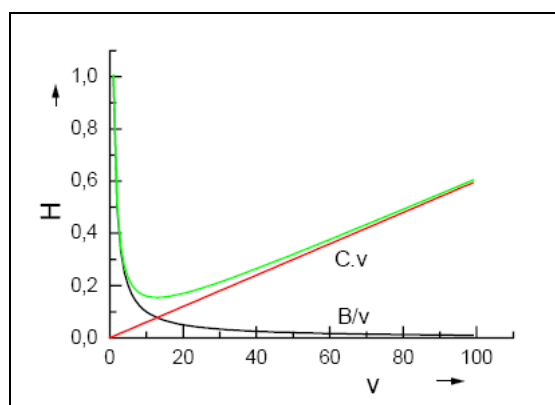
Figure 9: Plot of the plate height as a function of the mobile phase velocity. (Golay equation)

In reality the used velocity should be above the optimum at least 1.25 times to shorten the retention times and by this enhance the analyses frequency. The price for substantial

reduction in retention time is worth of to sacrifice a small amount of efficiency. Decrease in linear velocity due to temperature programming has to be taken into account as well. Velocities below the minimum cause lowering the separation efficiency because of the much steeper curve.

The choice of the medium as a carrier gas is also important. A plot of carrier gas versus column efficiency according to the Golay equation clearly shows a different optimum of flowrate for different gases. In Figure 10 are the plate curves for nitrogen and hydrogen as a carrier gas.
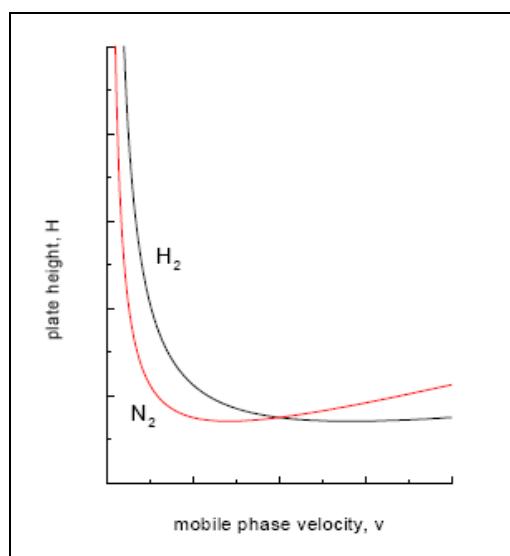
Figure 10: Plot of the plate height vs. mobile phase velocity for hydrogen and nitrogen as a carrier gas.

There are several benefits to using hydrogen as a carrier gas. The optimum average linear velocity H_2 is higher than for N_2 or even for He. This means an analysis can be carried out in less time with no loss in column efficiency. The H_2 curve is much flatter thus the velocity can be increased above the optimum without a substantial losses in efficiency.

3.1.3.2   The used columns

The system has undergone several changes in the course of its development. The current setup uses two columns: Petrocol DH and Gas-pro.

Petrocol column from Supelco is a typical *WCOT* used for hydrocarbons analysis. Petrocol has bonded, poly(dimethylsiloxane) stationary phase. Polysiloxanes are characterized by the repeating siloxane backbone, Figure 11. Polysiloxanes are

thermally stable, their viscosity is affected only slightly by temperature. The major limitation of the dimethyl silicone phase is its lack of functionality. CH_3 groups as a functional group give the lowest polarity, resulting in a polymer that is nearly as polar as a hydrocarbon. The interactions between solutes and a dimethyl silicone phase is limited largely to dispersion forces. The solute elution order is based on solute vapor pressure thus solute elutions occur in the order of solute boiling points.

The GS-GasPro Column from Agilent/JW is a Porous Layer Open Tubular column with proprietary bonded silica based stationary phase for the separation of low molecular weight hydrocarbons. The GasPro column is not adversely affected by H_2O, CO_2 or sulfur gases. It also appears to be more inert than aluminum oxide columns since it does not cause the decomposition of most reactive analytes.

Disadvantage is its bleeding which results from the elution of stationary phase degradation. Larger quantities of stationary phase generate correspondingly larger quantities of degradation products. Although it is more inert than Al_2O_3 columns, for an analysis at detection limits any affection implies certain risks. The problem arose with CO_2. Carbon dioxide had an influence on ethane, ethane peak shape and generally lowered the sensitivity. A CO_2 trap partly eliminated this problem.

After the injection the stream was split. The restriction column in front of the GasPro was adjusted to create 1:1.2 flow ratio of Gas-pro:Petrocol DH because higher concentrations of low boiling compounds needed to be measured on Gas-pro.

Originally, a CP-Wax column was installed instead of Gas-pro column, but it did not resolve the C_2 hydrocarbons. The CP-Wax 52 CB from Varian has polyethylene Glycol PEG stationary phase, Figure 11. With the given length of CP-Wax and its high low-temperature limit, the resolution of C_2 hydrocarbons was not achieved. Columns parameters are in Table 2.
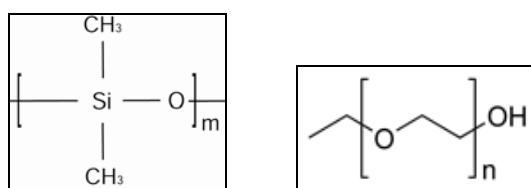
Figure 11: Petrocol DH (left) and CP-Wax (right) stationary phase.

The length, diameter, and film thickness of the columns were entered into the GC software. With this information, the instrument can calculate the flow through the column. Flow rates are corrected to normal temperature and pressure, i.e. 25°C and 1 atmosphere. Electronic pressure control (EPC) maintains a constant mass flow rate of carrier gas in the column throughout the run.

columns					
column	length (m)	ID (mm)	stationary ph. (mm)	flows (25 °C) (ml/min)	baseline (100 °C) (pA)
Petrocol DH 150	100	0.25	1	3.7	4.5
GS-GasPro	30	0.32	-	4.2	4.4
Restriction capillary	4	0.1	-	-	-
(CP-Wax 52 CB) + (Petrocol DH)	(30+50)	-	(0.5+1)	-	-

Table 2: Columns parameters and dimensions.

During the development of a temperature program the initial temperature was decreased to improve the resolution. The used temperature program was:

-10 °C (2.5 min)--- 20 °C/min up to 8 °C---5 °C/min up to 70 °C---10 °C/min up to 200 °C (2 min)

Initial temperature of -10 °C was kept constant for 2.5 min. The GC oven with column was then heated with the rate of 20 °C/min up to 8 °C where the rate changed to 5 °C/min up to 70 °C and finally with the rate 10 °C/min up to 200 °C and kept there for 2 minutes. A lower initial temperature has negligible effect upon the resolution for high boiling compounds since they are essentially frozen. The resolution of the later eluting peaks was thus affected minimally but a complete resolution of C_3 and partial resolution of C_2 were improved. The initial temperature hold time was chosen long enough to ensure sufficient resolution. Before the temperature program was initiated, the starting temperature had to be maintained at least for two minutes in order to stabilize baseline for the GasPro. As a coolant for GC-oven was used liquid nitrogen from isolated 100L Dewar. The heating rate was a compromise between resolution and analysis speed.

The final temperature and hold time were chosen large enough to ensure elution of the heaviest compounds to be sure that all solutes elute from the column for every run.

Under these operating conditions the Gas-pro shows more resolution than is needed simply because *PLOT* columns are more retentive than *WCOT*. Coelution of heavier compounds on Gas-pro aggravates integration of all compounds beyond C_4 thus they cannot be measured properly.

3.1.4 The gas supply

N_2 is supplied from a pressurized cylinder, H_2 and air are supplied from generators. Stainless steel diaphragm pressure regulators on the cylinders and generator

control the amount of gas delivered to the gas chromatograph. All metal plumbing manifold are made of pre-cleaned 1/8" stainless steel tubing and Swagelok fittings.

The whole GC system works with hydrogen serving as a carrier gas and a fuel gas for FID, and also supplies all tubings between Valco valves. Its purity is thus essential. At the beginning the system worked with hydrogen from cylinder but its purity 99.999% was not sufficient and the lack of a restricting unit meant an unacceptable risk of explosion. The cylinder was thus replaced by the Packard Hydrogen Generator model 9150 which generates by electrolysis of pure deionised water. The electrolysis unit uses a solid polymer electrolyte rather than caustic liquid electrolytes to produce ultra pure hydrogen on demand. Only 100mL of gaseous hydrogen is stored in the system at any time and at low pressure. A built-in sensing circuit shuts the generator down if a hydrogen leak is detected. According to the specification the generator produces up to 160ml/min of 99.9995% pure hydrogen. The 9150 model is up to 160 ml/minute. Water from cartridge unit with 18 MΩ/cm had been used to supply the generator with deionizer water. Although the 9150 model is complemented with a scrubber the residual moisture contained in the stream caused interferences in PLOT column chromatogram. Another problem was contamination by high concentrations of light hydrocarbons $C_2 \sim C_3$ causing offsets on calibration curves.

For these reasons the 9150 model has been replaced with the H2-300 Parker Balston Hydrogen generator. Its principle is similar, but hydrogen is purified by diffusion through a palladium membrane. As only hydrogen can penetrate the membrane, the purity of the output gas is two orders of magnitude higher than that of solid polymer electrolysis, i.e. 99.99999+%. As the electrolyte a caustic metallic ion free 22% sodium hydroxide solution is used.

The air maintains the burning process in FID and is used to dilute standard. Air from an oil free compressor in the institute was purified using CAP 60 model from Headline Filters. The cleaning process consists of filtration, adsorption and catalytic burning. A Pt/Pd catalyst at 380 ^{o}C provides total oxidation of all hydrocarbons including methane producing CO_2 and H_2O. Also H_2 and CO are quantitatively converted into the mentioned products. Such air quality is generally higher than of synthetic air from gas cylinders with 99.999%. As the purified air did not meet expected demands, an additional Pt catalyst was installed to reach below-ppt concentrations. As a final step in purification Supelcarb HC NMHCs trap was added downstream the produced air.

For the flame ionization detector the best make up gas is nitrogen. The purity of nitrogen used was 99.999%.

3.1.5 The description of instrument components

3.1.5.1 The CO_2 and H_2O traps

Although CARIBIC samples are usually dry, every air sample does contain some traces of moisture. A H_2O scrubber is filled with white crystalline powder magnesium perchlorate $Mg(ClO_4)_2$, Fluka Chemie, 98%. Controlled by V25, the scrubber is regenerated after each analysis by heating it up to 120 ^{o}C.

The CO_2 trap was built up in the same way as the scrubber. It is filled with sodium hydroxide Na(OH) from Sigma-Aldrich, PA hydroxide on a carrier. Controlled by V25, the trap is heated and its temperature kept at 60 ^{o}C.

The same dimensions, the same principle of heating regulation and temperature sensing (details in Figure 12) were used. Both constructions are interchangeable. Traps were prepared as a glass tube (1/4" OD) filled with chemicals held by glass wool from both sides. The part of the tube filled with the compound is inserted into a metal fitting profile which ensures the heat conduction from a heater. The heater is a simple heating foil. The foil is wound round the tube and tightened with a metal profile. This geometry warrants a uniform temperature profile along the tube. The thermometer must be small enough so it can be in direct contact with the foil. A small platinum (100 Ω) sensor, Pt-100, has been used. These temperature sensors offers accuracy over a wide temperature range. A 2 x 1 mm thermometer was fixed between glass and foil. The traps are connected to the tubing using Swagelok reduction unions 1/4-1/16 inches, tightened by elastic ferrule from Supelco which is normally used for packed chromatographic columns.

A critical point in trace analysis is the purity. Both tubes were pre-conditioned by evacuating and heating to 120 ^{o}C. After the high vacuum was reached both glass tubes were flushed with N_2 (purity 5.0) and closed. The used sodium hydroxide was granulated on support with 0.8-1.6 mm diameter, 14-25 mesh. Its density is ca. 70g/100ml which is about 0.5 g per trap. Molar weight is 40g/mol what makes 12.5 mmol. The absorbing capacity was at least 50% thus 6 mmol NaOH can react with 3 mmol CO_2, see reaction (3.8). Each analysis consumed around 1.5 l of air sample at standard conditions which is ca. 70 mmol. Given the CO_2 concentration between 370-380 ppm the packing should last for ca. 100 analyses.

$$2\,NaOH + CO_2 \rightarrow Na_2CO_3 + H_2O \qquad\qquad (3.8)$$

The used magnesium perchlorate consisted of larger granules. Although its density is 260g/100ml there was only 0.5-1 g per trap.

An important aspect is the sequence of the H_2O and CO_2 traps. The air must contain a small amount of humidity for reaction of CO_2 with natrium hydroxide, the CO_2 should be upstream of the H_2O trap.
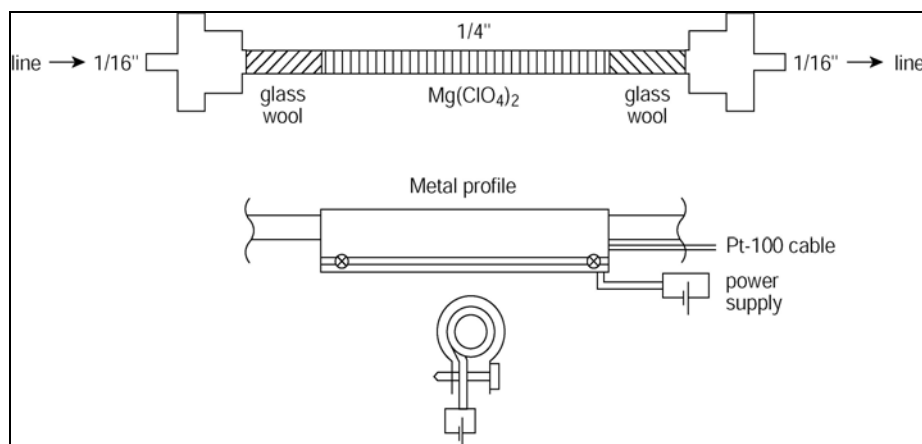
Figure 12: Scheme of the CO_2/H_2O trap. Upper part represents the trap profile, middle part shows the metal fitting and on the lower part stands for a front view along the tube.

There are temperature controllers #6 and #8 for the H_2O, CO_2 traps respectively. H_2O-controller called *Heater2* takes the variable from procedure file. CO_2-controller gets the setvalue directly, i.e. manually in the *Param* option because the temperature is constant irrespective of the procedure.

3.1.5.2 The enrichment trap (PF)

The PF, enriching trap, is made as a "U" profile from ss-1/8" tubing 16 cm long with 2.1mm ID. It is filled with Carbopack BHT, mesh 60-80, from Supelco. BHT is like Carbopack B but HT represents for additional *Hydrogen treatment* which makes it more suitable for ultra pure analyses. Carbopack is held in position using a glass wool. Almost all of the tube is heated. Thermocoax 800 x 0.5 mm long, 40 Ω resistance, is wrapped around it. Thermocouple, type K 250 x 0.5 mm long, fastened by a teflon tape to the tube, measures temperature during analysis, Figure 13.

Carbopack B belongs to a class of graphitized carbon blacks (GCBs) adsorbents. GCBs are generally non-porous materials with a homogeneous surface whose entire surface is available for interactions that depend solely on dispersion (London) forces. Compounds are adsorbed on the external surfaces based on their molecular size and shape. The majority of the surface sites are nonpolar and correspond to a graphite-like array of

carbon atoms without any preference to functional groups. Polar adsorption sites are few in number but they can still establish specific interactions with polar compounds.
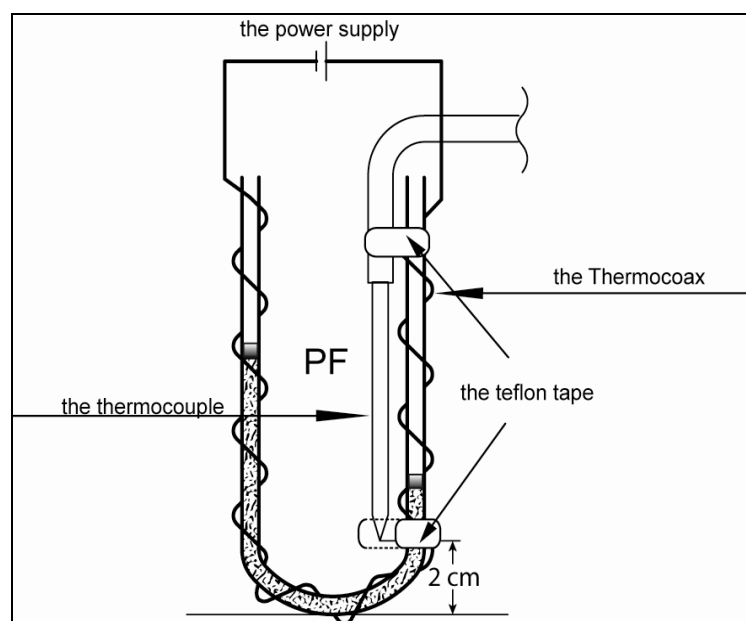
Figure 13: Scheme of the enrichment trap (PF). The heating cable, Thermocoax, is wounded around U-shape 1/8" tube. The thermocouple is fixed using teflon tape.

The term *graphitized carbon* generally means that a particular carbon has been heated to a temperature in the region of 3000 °C in a graphitizing furnace. These adsorbents offer excellent thermal stability and high chemical inertness. The coarse 60-80 mesh particle size prevents high pressure drop across the tube. Their hydrophobic properties minimize sample displacement by water, enabling efficient sampling even at high humidity. Trapped compounds can be desorbed by solvent or thermal desorption, with virtually 100% desorption efficiency. The chemical inertness of Carbopack B permits the determination of organic compounds in antropogenic emissions, where large amounts of NO_2, water, ozone and strong acids are present.

Adsorption runs at -100 ^{o}C with the flow 50 ml/min. PF is lowered pneumatically into a LN_2 dewar to cool it. Desorption is made by controlled power heating with position out of the dewar at 120 ^{o}C. When the tube is heated to desorb the sample, the heat energy required for volatilisation raises gradually since each molecular mass range is trapped on an appropriate location inside the sorbent material from which it is easily released and helps to focus them later in KF.

Carbopack bed ends at the height of 7.5 cm on adsorption side and at the height of 3.0 cm on desorption side; the PF geometry is in Figure 14. Longer adsorption path arrangement is due to the trapping gradient established in front of secure zone with the

lowest temperature close to the bottom. The secure zone is basically the part of tubing behind temperature sensor. All NMHCs are expected to be adsorbed before they leave the secure zone. Packing behind the zone implies unnecessary resistant, see Table 3. The table presents maximum air flows allowed by the packing under the given pressures matching operational ones. *Flow-1* is a flow without any restriction like *Flow-2* which results from *Flow-1* by adding a restriction in a form of needle valve into the stream behind the PF as it is seen in Figure 4 of the instrument scheme.
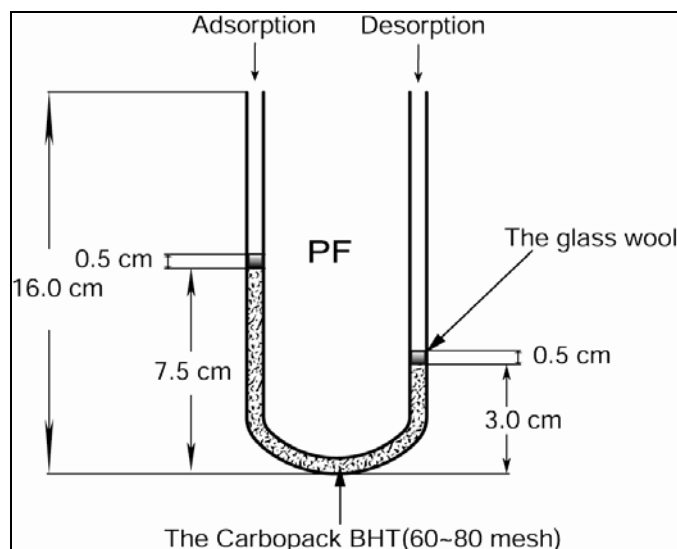
Figure 14: Scheme of the enrichment trap (PF). Geometry of the bed corresponds to the adsorption vs. desorption stream. The bed is held using glass wool plugs.

Pressure (Bar)	Flow-1 (sccm)	Flow-2 (sccm)
1	170	90
2	380	215
2.5	490	255

Table 3: Operational resistance of the enrichment trap. The table presents maximum air-flows allowed by the bed under the given pressures. Flow-1 is a flow without any restriction. Flow-2 results from Flow-1 by adding a restriction in a form of needle valve into the stream behind the PF as it is seen in Figure 4.

Thermocouple position is at the height of 2 cm from bottom of the tubing. Location above the bottom of the U-tubing is essential because it defines a zone with the the lowest temperature behind which no adsorption processes should occur. As the Thermocoax is wounded along the tubing it heats everything including the coolest zone. The ambient temperature drops downwards. The information from the temperature sensor is representative the level 2 cm above the bottom which means the

tubing from this site down to the tip will have, after stabilizing, slightly lower temperature than the controlled one. Placing the thermocouple in this way can help to determine required characteristics of the trap.

3.1.5.3 The cryo-focusing trap (KF)

The KF, cryo-focusing column in "U" shape, is made of ultimetal *WCOT* CP7120 from Varian Chrompack with CP-Sil 5 CB stationary phase, 0.53mm ID, 0.8mm OD, 1.0 μm film. Its length is 175 cm. The KF is heated directly by sending current through a 110 cm long section of it. Resistance of those 110 cm is about 3.5 ohms. V25 controls the power input to achieve a fast temperature rise. The piston system is the same as for PF. KF is lowered pneumatically into a LN_2 Dewar to cool it. KF is immersed in LN_2 during the focusing. To be sure that the temperature gradient is always the same and also to have the information of position KF in N_2 the same thermocouple as for PF was installed, see Figure 15.
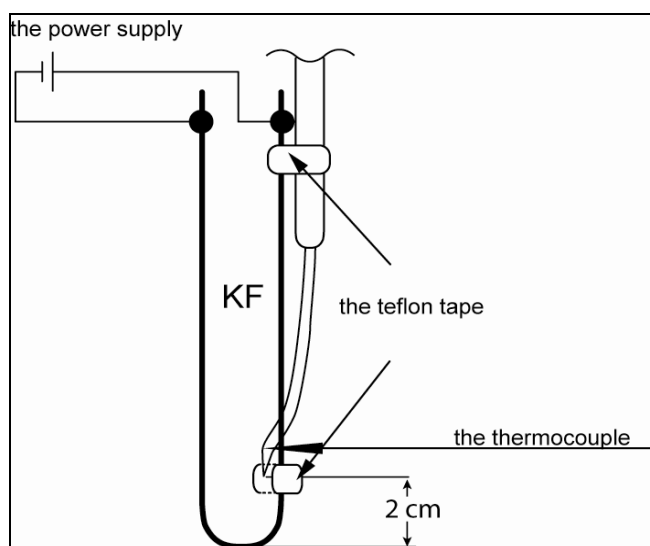
Figure 15: Scheme of the cryo-focusing trap (KF). The thermocouple is placed 2 cm above the tip. The KF, metal capillary, is heated via current because of its conductivity.

The trapped analytes are released during heating up to 140 ^{o}C with flow given by the sum of column-flows (Gas-pro + Petrocol), i.e. ca. 7 ml/min. The heating of KF starts when the piston rises the KF from Dewar and is fast enough to evaporate the trapped compounds in short time to ensure they move in narrow zones.

During lifting the KF the whole U-shape column vibrates which could potentially cause the thermocouple to fall off. Falling or breaking off brings a risk that KF get overheated

because the information for regulator is then distorted. This would lead to uncontrolled heating of KF followed by its destruction.

A controller #11, named *Heater3*, controls the power sent through the KF. 160 Watt is a maximum power which is being used to desorb all the hydrocarbons in as short time as possible. The temperature is set to 140 $^\circ$C above which the regulator reduces power to prevent the damage of it. KF is a metal capillary. Both contacts making the electrical circuit are not placed at the capillary ends. One is connected near the Valco valve where the capillary is fixed inside a port. The used ferrule is isolating that the metal body does not touch stator or any other metal parts of the valve. The other is formed by the holder by which the capillary is mounted to piston.

High power and rapid heating require some mechanism to prevent overheating. Variable *TmpKFMod* represents the model, the theoretical temperature describing the process of heating. Variable *TmpKF* is the temperature measured by thermocouple. At the moment when theoretical *TmpKFMod* exceed the real measured *TmpKF* by 50 $^\circ$C the heating is switched off and the just running procedure as well. The theoretical *TmpKFMod* follows the real *TmpKF* temperature according to incoming energy which is directly proportional to the temperature:

$$\Delta Q = m \cdot c \cdot \Delta T \qquad (3.9)$$

where:

Q is the incoming energy (J)

m is the KF mass (kg)

c is the KF heat capacity (J.kg^{-1}.K^{-1})

T is the KF thermodynamic temperature (K)

The thermocouple is in thermal and electrical contact with the metal body of KF. Since thermocouple is a source of voltage, the signal must be transmitted without a galvanic connection. This was achieved by transformer-coupled isolation amplifier AD202. This is the reason why *TmpKF* shows continuously lower temperature of about -192 $^\circ$C when KF is immersed in LN$_2$.

An idea of focusing is in this arrangement valid for compounds C$_2$~C$_4$. Compounds from C$_5$ higher are refocused in the gas chromatographic column at -10 $^\circ$C. Already slight changes in gradient during heating may cause substantial shift in retention times. Steep gradient ensures minimization of side effects like ambient temperature fluctuations etc. Evaporation under fast heating cannot be influenced that much. As the *Data-record* shows, see chapter 3.2.1.2, + 140 $^\circ$C is reached within 5 seconds from starting -192 $^\circ$C.

3.1.5.4 The dewars

Two Dewar vessels are used for measurements, a small one to cool the PF and the KF and a big one which provides cooling of the GC-oven. The latter one is a commercial 100L Dewar.

The small Dewar is a spherical flask, type 21 AL, custom-made by Cryotherm with volume of about 1 L. Filling up the certain level, 8-10 cm inside the vessel, with liquid nitrogen ensures the required temperature profile, in Figure 16.

Temperature profiles inside the dewar
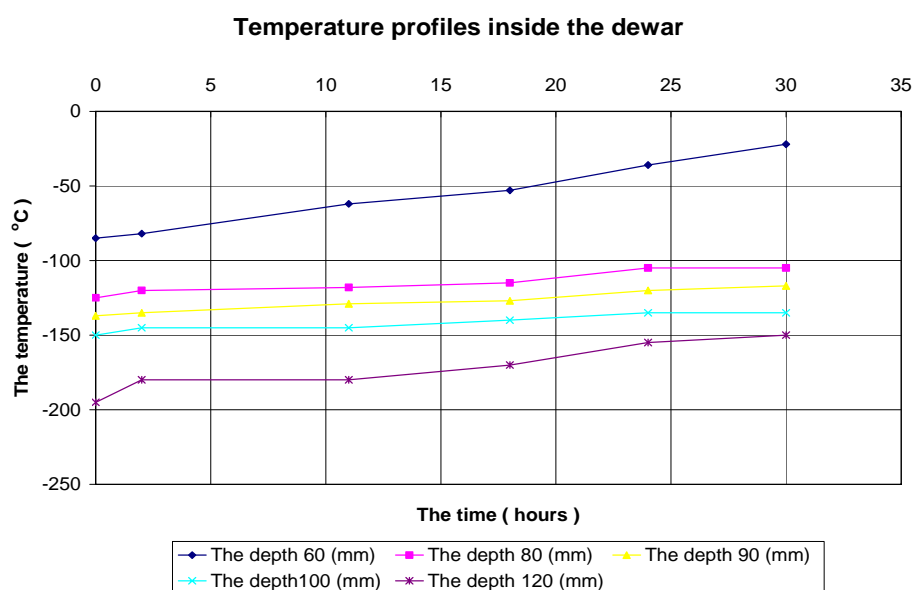
Figure 16: The temperature profiles in the Dewar as a function of the depth of temperature sensor for the 9cm of LN$_2$ and of the time. Curves in the middle (100mm~80mm) present constant cooling gradient, i.e. they are flat in time.

All three curves for depths 8, 9 and 10 cm (where the temperature sensor was placed) from the Dewar neck show how temperature changes within time if LN$_2$ is at height 9 cm. Flat characteristic for temperature decrease of PF lies between the yellow and light-blue curve. Too high LN$_2$ level would cause too fast drop which may imply problems to reach stabilized temperature inside the PF (the PF tip is in touch with LN$_2$). Too low LN$_2$ level would cause insufficient cooling gradient thus prevent the PF from reaching desired -100 ^{o}C within 3 minutes as the procedure defines.

The position of the PF is always above the level of liquid. With controlled heating, the temperature inside PF during the enriching process is kept constant. This situation is described in Figure 17. The sphere is placed inside a small aluminium container, see Figure 18. This outer vessel was vertically adjustable. Its position against PF and KF was exactly fixed, see Figure 19.
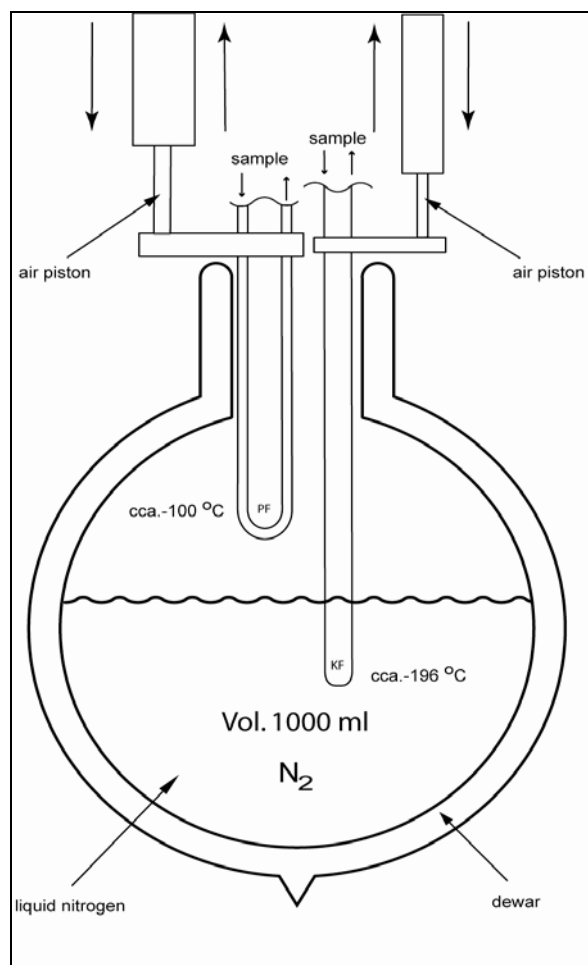
Figure 17: Positioning of PF and KF in the Dewar. The enrichment trap is always above the level of LN₂. The cryo-focusing trap is immersed in LN2.
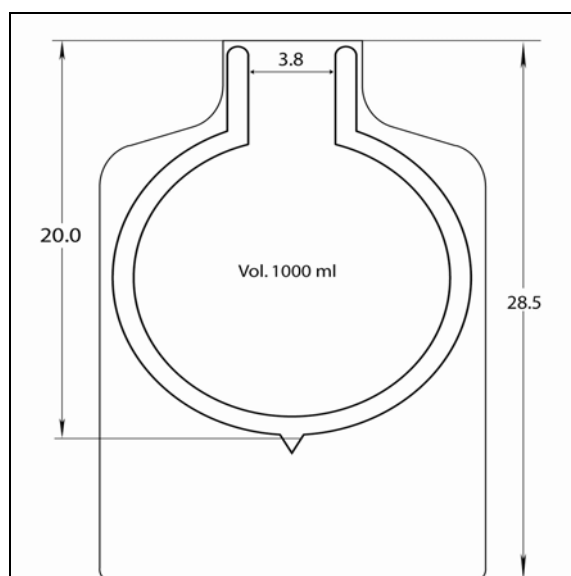
Figure 18: Dimensions of the aluminium container containing the 1L Dewar. Dimensions are in centimeters.
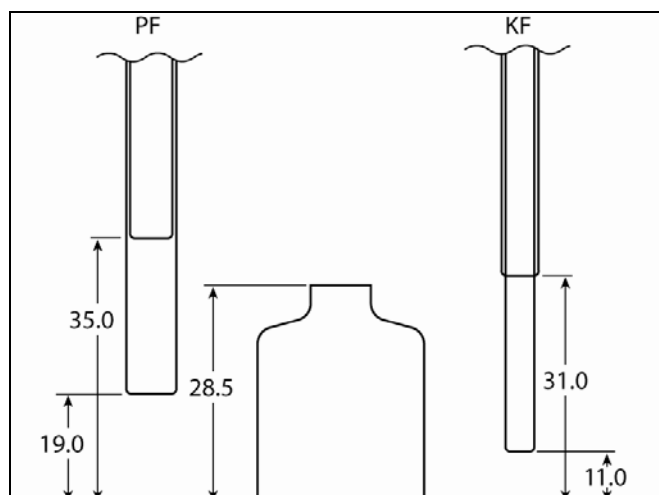
Figure 19: Positioning of the enrichment trap and the focusing trap towards the aluminium container placed on a liftable plain. Both traps differ in their depth of immersion relative to the vessel. Dimensions are in centimeters.

The big Dewar for cooling purposes is a low-pressure Dewar with a safety relief valve to prevent a pressure build-up. The relief valve is set by the supplier at 20 to 25 psi. The most of commercial available Dewar tanks work with this pressure. If liquid nitrogen were trapped between a closed tank valve and the cryo-valve on the GC, pressure would be develop which may cause an explosion.

Agilent N_2 GC-valve operates with low-pressure coolant, i.e. 1.5 ~ 2.0 bar absolute which has to be stabilized. Fluctuation in the pressure valve influences the baseline. The working pressure is reached by heating the LN_2. Pt-100 thermosensor, pressure sensor, and the heating element Thermocoax were added. The pressure is controlled by the V25 system.

Dewar is normally filled from a storage tank under an atmospheric pressure. Liquid nitrogen is stored at a lower temperature than it would be after conditioning. In this case the Pt-100 showed temperature around -201 ^{o}C for the fresh nitrogen and around -196 ^{o}C for the conditioned nitrogen which corresponds to a liquid nitrogen under the standard conditions.

Inlet/outlet pipes were made of PTFE. Vapor inlet/outlet pipe ends above LN_2 level and the longer one for liquids ends at the bottom. The heating element was placed on tip of the longer pipe. A Thermocoax coil wound on a metal belt had to have at least 200 watts otherwise heating up would take too long. Its length was determined from voltage 42V from 6A transformer added on V25 output. With 7 Ω Thermocoax corresponding to over 250 watts the pressure of 1.6 bar is achieved within 2 hours. Pressure of 1.6 bars was chosen because the pressure relief valve did not open and the cooling of the oven was sufficiently rapid.

Position of the Pt-100 sensor was one centimeter above the Thermocoax. Desired pressure was monitored by pressure sensor from SensorTechnics placed at a top of the valve-head. There were Swagelok T-piece and cross-piece which allowed to connect besides mentioned sensor also the pressure relief valve, Pt-100 cabling and power cabling.

3.1.5.5 The pistons

The pistons moving both traps are twin rod pressurized-air cylinders from Hoerbiger, RDV 5025/0200 for KF, AZV 5032/0160 for PF. Air with 3 bar is supplied from an external compressor and brought through polyurethane tubes from Legris. Both cylinders are equipped with pressure brakes which enable to adjust lifting-speed. Twin rod arrangement ensures stable position of an aluminium socket in which the traps are mounted. The air is split in T-piece to supply two solenoid valve for each cylinder, see Figure 20. The valve is 3/2 way VQ 381RF-1/8-NG, 12 VDC, from Hoerbiger. Each valve open/close air supply to move downward or upward.
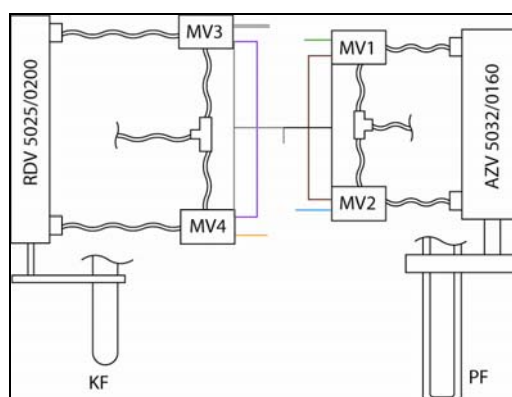
Figure 20: Pneumatic pistons lifting both traps fixed in an aluminum socket. Solenoid valve MV1 lowers the PF, valve MV2 lifts the PF, valve MV3 lowers the KF and MV4 lifts the KF.

3.1.5.6 The mass flow controllers

The instrument employs 4 mass flow controllers (FCs) from MKS, all controlled by V25. They are a general purpose, elastomer-sealed mass flow controllers. The first and the second controller, FC0 and FC1, are type 1179A with a range of 500 ml/min and 10 ml/min respectively. FC2 and FC3 are 1179B with the range of 100

ml/min and 200 ml/min respectively, a second generation mass flow controllers with a digital electronics which enhances accuracy and reaction time.

Type 1179A has an accuracy (including non-linearity, hysteresis and non-repeatability) of $\pm$ 1% of the full scale. Repeatability is 0.2% of the full scale and resolution 0.1% of the full scale. Digital 1179B has an accuracy which, apart from the scale, depends on reading as well, $\pm$ 0.5% of reading $\pm$ 0.2% of the full scale. Resolution for the 1179B is 16 bit.

The FC measures a mass flow, i.e. volume flow at standard conditions of 0 °C and 1 atmosphere, mostly standard cubic centimeters per minute (sccm). When other gases than air, nitrogen or oxygen are used the correction factors must be implemented before calculating the flow.

As mentioned above an accuracy refers to the difference between the actual physical flow of FC and that of a theoretical given by the setvalue at any set point. Every flow controller has its own characteristic which is basically a functionality of the applied voltage against the real physical flow. In an ideal case the curve is linear. In the zero point is shifting due to aging of various electrical components as well as of the thermal sensor. Consequently, the FCs have to be calibrated from time to time.

The V25 enables the use of non-linear calibration curves. Calculations like flow integration for an overall volume determination or an automatic flow corrections like in case FC0 and FC2 were made with the already corrected real physical flow. The real physical flow has been measured using an external flow metering standard mercury-sealed piston which serves here as a primary method.

FC0 and FC1 have been used only for the dilution of the standard calibration gas. Their flow-ratios defined points on calibration curve. The third controller FC2 is the crucial flow controller for overall volume determination. Its signal is integrated and, after reaching the pre-selected sample volume, valves stop the enrichment. The last FC3 restricts the flow through tubing before analysis starts in order not to waste the sample.

3.1.5.7 The V25

The V25 system has been designed for automatic acquisition and/or control of common physical variables of typical processes run in a physical-chemical laboratory or in the field. Its main parts are an industry standard x86 compatible NEC V25 Microcontroller, a ECB Bus standard interface backplane and various 3U sized extension boards, which interface the process controller to the outside world. Because of its high modularity, the system is easily scaleable and, therefore, adaptable to very different demands without changing the basic modules it consists of.

The software built into the ROM consists of a multitasking, multiprocessing real-time operating system with a very small UNIX-type API, a command line interpreter for communication to a host and a Pascal compiler with real-time multitasking extensions. Its high potential lies in its capabilities from communication with PC, data collection, adjustable regulators to power supplies.

3.2 Analytical procedure

Analytical procedure is a stepwise process from sample introduction to sample injection. To handle all system-parts as needed the platform of procedures and sequences had to be developed, everything fully implemented in V25.

Analytical procedure is given by the valve design. Valve design defines how the sample stream is switched. The most important aspect as far as design is concerned are the flows of hydrogen between valves as these flush all traps or transport compounds into the KF. Regeneration of H_2O trap is made in opposite direction (back flush) from sampling with 10 ml/min at 100 ^{o}C. Desorption of PF is made in opposite direction from enriching with 10 ml/min while PF is continuously heated. Regeneration of PF is in the opposite direction as well with 15-20 ml/min. Regenerating and desorpting flows are given by the needle valves on VA3, VA5 and behind the PF on VA4. Changing their positions adjusts all three flows, Table 4. Table shows two valve positions: ABAB as a flushing of the H_2O trap, AAAB as a flushing of the PF. All three needle valves on Valco valves VA3, VA4, VA5 are marked as I, II, III respectively. Pressure on H_2-aux(4) was raised from 120 kPa up to 160 kPa and hydrogen flows were measured. Outlets flows named as B were measuerd after the needle valve II was constricted, i.e. flow IIB is smaller comparing to IIA. Flow IIB was reduced on behalf of the other two flows IB, IIIB, i.e. both are bigger but not with the same extent. IB is proportionally bigger which shows that the resistance of PF (VA4) lies above resistance on outlet IB. In the position AAAB the resistance of H_2O trap is not included into the hydrogen stream thus IB is bigger than IIIB even more.

Flow profiles on instrument outlets						
Flushing SCR ABAB	Outlet\Pressure	120 (kPa)	130 (kPa)	140 (kPa)	150 (kPa)	160 (kPa)
	IA	4.95	5.6	6.38	7.16	8
	IIA	18.85	20.7	22.5	24.4	26.3
	IIIA	6.1	6.7	7.2	7.8	8.5
	IB	7.83	8.85	9.92	11	12.2
	IIB	15.57	17.05	18.55	20	21.55
	IIIB	7	7.6	8.3	9	9.7
Flushing PF AAAB	Outlet\Pressure	120 (kPa)	130 (kPa)	140 (kPa)	150 (kPa)	160 (kPa)
	IA	5.13	5.86	6.62	7.43	8.3
	IIA	18.4	20.19	21.96	23.86	25.8
	IIIA	6.2	6.8	7.3	8	8.6
	IB	8.34	9.38	10.5	11.7	12.9
	IIB	15.03	16.4	17.75	19.35	20.85
	IIIB	7.1	7.7	8.4	9.1	9.9

Table 4: Flow profiles on instrument outlets as a function of pressure on H_2-aux(4). Outlets I-II-III are needle valves on Valco valves VA3, VA4 and VA5 respectively. A vs. B means flows before and after constricting the needle valve II.

3.2.1 The automation

The source code are instructions „how to operate" the entire system. The microprocessor inside is programmed in Turbo Pascal thus automates the sequences and procedures. The source code orders the controllers what they should do with the read variables, for instance: signal processing, counting of value-thresholds, the secondary data evaluation etc.

Next to it there are instructions for: the interval timing, integration of volume, flow adjustments, process-data storing or the execution of procedure-commands. Each of above will be discussed furthermore.

3.2.1.1 Building the menu

The visual interface for communication with PC shows 3 options. The option *Data* is an on-line display of all the, for procedure, important values of process-parameters, otherwise called variables. Next option *Param* are adjustable parameters mainly for the controllers or temperature sensors. The third option is the *Control*. There are information about procedure, like status of the heaters, location of the procedure and sequence-files, positions of the valves or power outputs. These three options, technically *MENU,* make interface between the operator and the process.

3.2.1.2 The *Data*-option

The option *Data* is the most important. Everything what is shown there is stored on a flash memory card. The result is so called *Data-record* of the sequence. With a pre-selected frequency the all variables are stored in a simple ASCII file. *Data-record* consists of two files, *PrsFile* and *LogFile*. *LogFile* is the main file named as the time when recording started, *hour_minute_second.log*. *PrsFile* is a smaller side file named in the same way but with the *prs* extension in order to point out its purpose. Only the periods of the process are stored. Periods which help to record the most important moments. In this case it stores *Data* option only when the pressure on expansion volume is measured. To gain an accurate pressure difference between start of enriching and its end the two values had to be calculated. Values which are means from 10 pressure readings where these readings are made at an exact moment before and after enriching. The increase in pressure gives then an overall volume. This is happening only two times per one process-run thus two numbers per procedure. For the moment recording into the main *LogFile* stops and just one scan of *Data* option is recorded into the *PrsFile*.

In the appendix, A5, there are the first 14 seconds of the calibration procedure stored in the main *LogFile*. The *Data-record* was taken with 2.5 Hz which means 2 and 3 values per second alternately. Each process variable is sampled through multiplex with the shortest step 25 ms so maximal accuracy for one means lower accuracy for the others. This is reason why variables sampled with the frequency below 3 Hz appear to have the same values although, considering their dynamic behavior, they should not. In Figure 21 is an example of *Data-record* showing all the temperature-sensing variables as they change in a course of the procedure. Variables are described later.

In Figure 22 is the temperature increase on KF during injection. The model temperature, *TmpKFMod*, increases at the beginning slightly faster but then the real *TmpKF* takes it over. Once the real temperature reach 140 $^{\circ}$C the model one is put equal *TmpKF* and protecting mechanism stops. *TmpKFMod* is delayed in following the *TmpKF* by few seconds.

The *Data* option has 5 groups of variables. The first is the datum plus the time, the second group deals with temperatures, the third displays the flows, the fourth corresponds to the quantification of passed volume and the last one measures the pressures. The first variable from the first group *TimeDate* displays the real datum together with the time of computer clock, both in two columns in a format *day:months:year* and *hh:mm:ss*. *ProcTime* is the time of procedure in a format *hh:mm:ss*. *TmpSCR* is the temperature of scrubber in ($^{\circ}$C). *TmpDWR* is the temperature inside the dewar with LN_2 in ($^{\circ}$C).
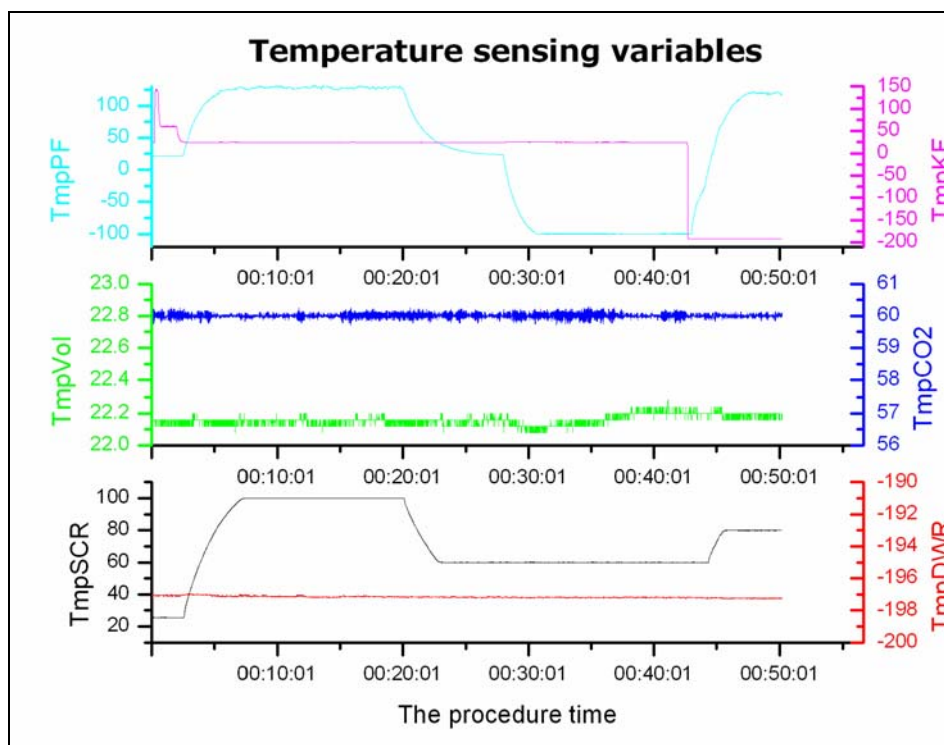
Figure 21: Temperature-sensing variables are plot as a function of procedure time. TmpPF, TmpKF, TmpVol, TmpCO2, TmpSCR, TmpDWR stand for temperature of enriching trap, cryo-focusing trap, expansion volume, CO_2 trap, H_2O trap and liquid nitrogen respectively.
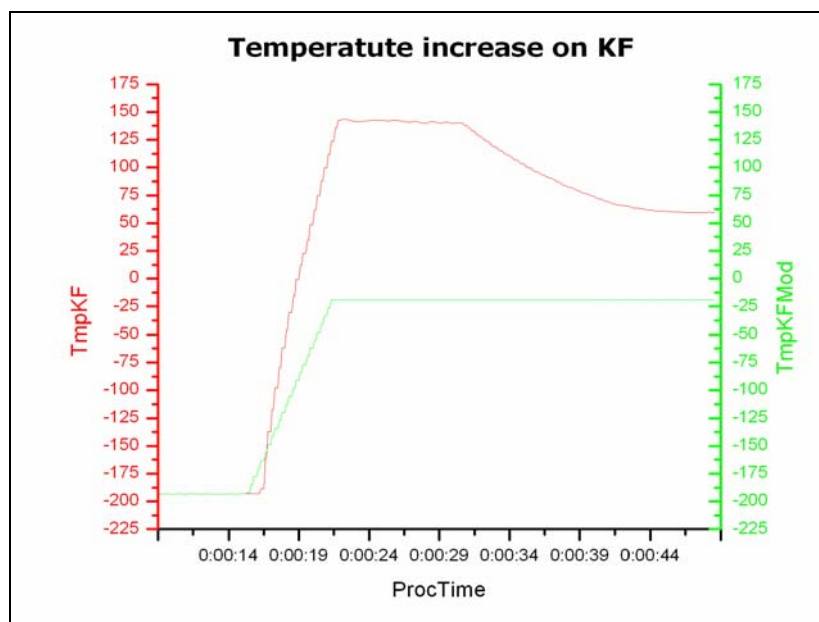
Figure 22: Heating of the cryo-focusing trap. KF reaches 140 ^{o}C in a ca. 5 seconds. Temperature gradient was sampled with 4 Hz. Data record was being saved with 10 Hz. TmpKFMod follows TmpKF with a certain delay.

TmpVol is the temperature measured on the expansion volume in (^{o}C). *TmpCO2* is the temperature on the carbon dioxide trap in (^{o}C). *TmpPF* is the temperature of the enriching trap in (^{o}C). Analogically *TmpKF* is the temperature measured on the cryo-focusing trap in (^{o}C). *TmpKFMod* is the model temperature of KF as it was explained in the section about KF. Next group of variables belongs to all the flow controllers. Each of them has two values, *FlowN* displays the actual flow of controller number *N* in (ml/min) and *RawFlowN* displays the out-coming signal in (mV) of the controller number *N*. The actual flow is already interpolated thus it shows the real physical flow. The last section of variables corresponds mainly to the determination of the passed volume. *Vol* is the integrated volume in (ml). It shows how the overall volume is rising as the signal is being integrated. *mol* is the absolute amount in (mol) which is presently contained inside the expansion volume. *Volth* is the theoretical volume under the standard conditions in (ml). *Pressure* is the measured pressure inside the dewar with LN$_2$ in (mBar). *PressVol* is the present value given by the gauge in (Pa). *PressVol1* is the value in (Pa) before and after the enrichment.

3.2.1.3 The *Param*-option

Option *Param* contains parameters for the procedure. Technically most of the parameters can be adjusted manually by overwriting the old value. Some of them admit second possibility of calling from procedure directly. This is useful for those variables which need to be changed often during the sequence or when they have an implicit value which is called after the procedure eventually the process is off.

SetPresure sets the pressure in Dewar in (mBar). It does not need to be adjusted from procedure. It is easier to do it manually because the pressure is demanded for longer time regardless the procedure. *SetTmpCO2* is the setvalue for the temperature on the carbon dioxide trap. *SetFlow0* up to *SetFlow3* are the setvalues for the flows of particular controllers. *SetLdFlow* up to *SetLdFlow3* are the auxiliary variables for setting the flows. It is useful to store the original flow called from the procedure because some later calculations need the information about it. Variable *SetVol* stores the value for overall volume. *RangePress* is the range for the pressure sensor on Dewar with LN$_2$. *OffsetPress* is the offset for the same sensor. *Rgpressvol* is the range for pressure gauge on the expansion volume. Analogicaly *Offpressvol* is the offset for the same gauge. Following are the range together with offset settings for all the Pt-100 temperature sensors. *Pta* is for the scrubber, *Ptb* is for the dewar, *Ptc* is for the carbon dioxide trap and finaly *Ptd* is for the expansion volume. *RangeTC* is the range for both used thermocouples. Analogically *OffsetTC* is the offset for both sensors. They are

used to compensate slight changes caused mainly by imperfection in welding or cabling. *RangeFL0* up to *RangeFL3* is the range for particular flow controller 0 up to 3. *KFHeatCap* is the heat capacity of KF as it was already explained. *KFPwrLoss* is the heat loss of KF. *MaxTimeLd* is the half time needed to make flow corrections on FC0 and FC2. If the corrections have not been successful within doubled *MaxTimeLd* the flow is set to half of each controller range. *MuPo1Addr* is the address for communication with the VA1. *LogPeriod* is the inverse recording frequency of the *Data* option.

Following are the constants of control for each controller that has been used. *RegPF*, *RegKF*, *RegSCR* and *RegCO2* are the submenus for enriching trap, focusing trap, scrubber and CO_2 trap, respectively. In each submenu there are other parameters of controlling like proportional band etc.

3.2.1.4   The *Control*-option

Option *Control* consists of parameters which control the process directly. They switch on/off each of the controller for particular process variable. Some display files where the *Data-record* is stored, where the procedure file with the sequence file are stored or simply variable status like on/off for power supplies is adjusted.

Process is the main variable telling whether the process is running. By switching it on/off the process is started. *Proctest* is auxiliary variable which starts imaginary process to test the stepwise calling of commands from procedure. *Logger* trigger the *Data-record*. When it is on, all the data from *Data* option are being stored in *LogFile* in directory *LogDir*. A coincidence between starting process and recording of data was programmed. Whenever the process starts, all data starts to be recorded as well. But it is also possible to record data without running process. *Sheater1* is a switch for the PF controller. Switching it on means heating of the enriching trap. *Sheater2* is switch for the H_2O trap. *Sheater3* is switch for the KF trap.

ParamSave enables to save all the parameters from *Param* option into a separate file with *ini* extension which is define in *ParamFile*. *CtrlFile* is the name of procedure file with its path. *RFNFile* is the name of sequence file with its path. *PrsFile* is part of the *Data-record*. *MuPo1Pos* is the position of first valve. VA1 is multi-position 10-way valve, its position tells which canister in TRAC is measured. *MuPo1Addr* is address of the VA1. Defining the address is essential because it enables to address the specific valves. *MuPoExt* is a variable which helps system to recognize which VA1 is going to be used. It admits two values, *int* or *ext*. *Int* tells the system that it is its own VA1 which is going to be used. *Ext* is for „external" thus any multi-position valve outside the

system can be used, in this case TRAC. *IOWago* is a switch for magnet valves. Four values, each on/off, actuate MV1~MV4. *IOD50* is a switch for Valco-Vici valves. Four values, each on/off, switch VA2~VA5 between A/B positions. *Pow220-0 ~ Pow220-7* display power supply 220 V for different outputs with their power. As mentioned, power can be controlled in 8 bit system of V25 in range from 0 up to 255. *Pow24_0 ~ Pow24_7* display power supply 24 V for different outputs with their power. Range from 0 up to 255 is the same as for *Pow220-0*.

There are other submenus *Com2File*, *Com2Str*, *Position*, *Work*, *ReadRec*, *RFNRec* which detailed description is not necessary. They help to debug new process.

3.2.2 The system procedure

Let us define „procedure" as how the sample is treated before it is analyzed. A „sequence" is then a series of such procedures. Procedure is a simple ASCII file. V25 reads the ASCII file with a list of commands and then, according to it, actuates each part: valves, flow controllers, heating elements, pneumatic pistons or pressure gauge. Every procedure has its own timing, thus every command is executed at the same moment from beginning of the procedure. This configuration provides high reproducibility. Changes in the procedure are done simply by rewriting of the ASCII file. Every part which needs to be controlled has its own controller inside V25, altogether 12. Data coming from controllers can be sampled with a different sampling frequency. The shortest step for sampling is 25 ms. The maximal accuracy for one means lower accuracy for the others. E.g. flow controller FC2 is the crucial one for the determination of the sample volume. This controller is sampled with 10 Hz in order to integrate properly.

From the beginning of reading of the ASCII file time is measured. Every row in ASCII begins with the time parameter. Next to it there is an command for operation. For instance, HeaterX implies START HEATING THE ELEMENT X, next in the row there is a parameter for that action. (0:02:30   Heater1   130*)* implies „START HEATING THE ELEMENT 1 (PF) UP TO TEMPERATURE 130 ^{o}C AND CONTROL". In A6 in the appendix is an example of one procedure with the list of commands, see appendix. This particular procedure has been used to calibrate the system. It represents one point on the calibration curve.

As it may be seen the whole procedure takes 1 hour and 5 seconds. It depends on an amount of air which is being concentrated in PF. Flushing, temperature gradient on PF, cooling time of the scrubber etc., all determine the length of procedure. After the last

command is red, GC analysis starts and a new procedure too. The whole idea is to unify everything so the next procedure can begin.

Next procedure must be called according to the schedule, the sequence. The sequence is technically a sequence of procedures. Next procedure may differ from the previous one. This is the principle how to switch connected samples via a multi-position valve. Table 5 shows an example of calibration sequence. There are 2 different procedures called: *pr1* and *pr2*. They both are carried alternately several times. Each represents one calibration point, together measured three times. The analysis time, meaning how long it takes to run the chromatogram, depends on temperature program and cooling time. With the used program it takes around 45 minutes. The important thing is that it must be shorter than the procedure length.

time	procedure name
0:00:00	pr1
1:00:06	pr2
2:00:12	pr1
3:00:18	pr2
4:00:24	pr1
5:00:30	pr2

Table 5: Timing of the calibration sequence. Two procedures pr1 and pr2 are carried alternately. Each represents treatment of calibration mixture to measure one point on the calibration curve.

An exact description of each step in the procedure is not simple. ASCII file is every file with standardized table of bit-translation, Notepad is sufficient. The first row is only description of following commands arranged in columns. The first column is the timing. The time is in format: HOURS:MINUTES:SECONDS. The second column is a name of the procedure-variable. The next column is its status, variable can be either set to a new value thus be ON or to be switched OFF thus the default value is set or eventually the latest set value stays. The last column contains the set values. These are positions, flows, temperatures, volume or power.

The procedure starts with switching of the multi-port valve. Up to 7 canister-samples can be connected to the apparatus and switched by internal multi-port valve. An external device with stored samples can be connected and samples switched using the external multiport-valve inside provided that the system of communication is the same. This is the case of samples-box with glass cylinders called TRAC used for the CARIBIC project. The starting position for each valve is implemented in the source code. When the process is off, all valves are always switched into their start-up positions thus switching on/off is ensured to be the same regardless the procedure or sequence.

At the 5th second the multi-port valve called MuPo1 is switched to the requested position and as a new setting it must be switched ON. Next commands are new settings for the flow controllers Flow3, Flow0 and Flow1. Setvalues are already in ml/min. Their location in time-schedule is not strict. At the beginning of schedule, there is enough time to flush the tubing. FC0 is additionally controlled so every new setvalue starts a loop of new commands. The flow precision of setvalue is within one decimal.

At the 10th second the valve number 5 is switched to the position B. The valves 2, 3, 4, and 5 are all two-way valves. The first way is titled A. The second is B. Considering that procedures are running in a loop the ending status of previous procedure is starting point for the next one. Shortly before the injection the sample had to be focused in KF. This happens at the end of schedule which ends with a command for chromatogram run. The injection is done during the already running chromatogram. In other words the procedure is completely finished at the beginning of the following one and this is the sense of looping. As the temperature on KF rises, the frozen compounds evaporate and carrier-gas takes them along into the capillary. The focusing takes place in a direction A. The A direction changes into B direction 5 seconds before it is heated. At the 15th second the magnet valve 4 let the pressurized air into the piston which moves with KF upward and V25 starts heating. The source code makes reading of multiple-commands of the same time possible.

Heater3 is the controller belonging to KF. Status ON together with setvalue 140 means the upper threshold from which the maximum power of V25 will become controlled so that the thermocouple on KF would measure 140 ^{o}C. The first 15 seconds of 140 ^{o}C are enough to evaporate everything inside. From the 30th second the temperature drops to 60 ^{o}C. Immediate temperature fall through switching OFF could cause contraction of the carrier-gas few seconds after the injection. All these operations were done with lowered piston. The 35th second is releasing the air from the piston. The second minute switches the Heater3 off.

As a next step in procedure the PF is regenerated. It means PF gets rid of all the compound-traces and the medium, Carbopack, gets ready for the enrichment. The position on the valve 4 must be A which is the position from previous procedure. The reason for the command at 02:20 is the very first procedure where the valve 4 is still in starting position B. Temperature of PF heating can be chosen up to ca. 130~140 ^{o}C where the Heater1 does not generate enough energy. The heat emission as a result of the temperature gradient between the ambient and the chosen temperature is then equal to the heat development, to the incoming energy. At 02:30 the temperature is adjusted to 130 ^{o}C. During the regeneration Carbopack is flushed with hydrogen at ca. 10 ml/min. This „regeneration" lasts 20 minutes after which it is switched off and cooled down to ambient temperature where it stays 5~10min before lowering into the Dewar.

The same system of adjustment in case of H_2O scrubber, Heater2, is executed five seconds after. Its temperature was chosen 100 ^{o}C. And again, the position of valve 3 must be now B as it stays from previous procedure. H_2O trap regenerates under the flushing of 10 ml/min too. The power is so limited to reach 100 ^{o}C slower than PF reaches its 130 ^{o}C. Heater1 is switched off at 20:00. Five seconds after the controller from Heater2 gets new command to drop with temperature to 60 ^{o}C. The sample is opened to ambient through restricting outlet on the valve 2. Before a sample enters the PF it must fill all the small volumes outside the PF trap. At 25:00 the valve 2 is switched to position B. Air sample goes directly into the lines and through the flow controller 3 out of the instrument. The flow 40 ml/min is given by the FC3. The volume of H_2O scrubber is bypassed thus not included. At 28:00 the magnet valve MV1 pressurized the piston and lower the PF. Ten seconds later the air is released but piston stays in lowered position. At 29:00 the valve 3 includes the H_2O-trap volume into the sample-stream. Reactions with NaOH and $Mg(ClO_4)_2$ needs to be „stabilized". CO_2 removal is already running because the trap is located right behind the valve 2 but H_2O removal needs some time till enriching starts. Two minutes should be sufficient. Since the PF went down it has been cooled by the N_2 vapors. As the analyses proceed, the LN_2 evaporates and its level sinks. Temperature on PF is dropping slowly to its minimum given by the level of LN_2. This process is relatively slow with a small gradient. The gradient depends on the level, whether it is right under the PF without a real air layer between or more below isolated by the air layer. In optimal position the layer is so thin that it takes over 2 minutes to reach -100 ^{o}C. If a command for the controlled temperature comes earlier within those 2 minutes then the PF-controller has enough time to act properly. So, at 29:30 the Heater1 is set to -100 ^{o}C.

At 29:31 the outlet on expansion volume is opened so that the pressure inside equalizes the ambient. Its process-variable is called p24_5 as the 5th location of the 24-AC voltage output of V25. From the 8-bit system the maximum power is given by the value 255. The first 30s after the opening are adequate for such a simple vessel to equalize its pressure with ambient. During the second 30s the first pressure before trapping is determined.

At 30:00 the overall volume is set. One second later the FC2 gets command for setting the flow. According to experience this extra step does not take more than 20s so at the moment when next command is executed the proper flow is already running. At 30:29 the 3-way valve directs the sample-stream into the FC2. The same valve on 4th position has process-variable p24_4. After this command the flow controller starts immediately acting and is additionally controlled from v25 until the exact setvalue from 30:01 is reached.

The integration starts at 31:00 by switching the valve 4 into the position B. At the same moment the outlet on expansion volume must be closed with the valve p24_5 which is set to 0 thus actually OFF. With the real flow close to the theoretical one, the overall time needed to enrich the set-volume is calculated as *volume / flow*. A time-gap between when the integration is enough and the theoretical time is minimalised to zero. The intention has always been to use the same time, 10-20 minutes, with the same flow of 50 ml/min for every procedure. With that settings the integration is finished at 51:00. The sample-stream is cut from a line 5 seconds later at 51:05 by switching the valve 2 into the position A. By switching the valve 2 at the same moment as valve 4, the sample line and the hydrogen line would be connected simultaneously which leads to a pressure transient inside the PF. Hydrogen line (black single line in Figure 4) represents hydrogen at ca. 150-160 kPa while the sample line (black double line in Figure 4) represents sample at ca. 2 Bar. 5 seconds delay makes the pressure transient smaller because the sample line is already open to an ambient at that time thus higher pressure from the rest of a sample goes rather out through 3-way valve and FC3.

The reason for using volume integration lies in its dynamic behavior. It is stopped by the source code. When the condition for overall volume is fulfilled the valve 4 and p24_4 are switched at once. Any effect which is rather dynamic is handled better directly from the source code. Static commanding from the procedure would not be that accurate. Problems can occur when the flow does not correspond to the setflow, for instance it is smaller. Then the integration needs more time and would not switch the valve 4 back to A according to schedule. That is why the valve 4 returns to ON at 51:06. Basically this command is redundant and serves as a safety precaution in case of empty samples in TRAC. The second pressure after the trapping is determined within 10 seconds from the 10th second till the 20th second. At 52:40 the magnet valve MV3 pressurizes the piston and lowers the KF into LN_2. Five second thereafter the air is released. The temperature on PF was stabilized using its heating during the enrichment. When it is lifted from the Dewar it should not be heated any more. At 52:59 the Heater1 is OFF and immediately one second afterward the trap moves up. At that moment warmer ambient causes increase of the temperature which is important for the flushing. Other compounds which might disturb the FID signal were trapped too together with NMHCs. These are mainly CO_2 and N_2O. Rests of it can be taken away by the flushing stream at the lower temperature but not too low because then the lighter NMHCs might be lost as well. Important is the valve 4. After it had been switched from one position to the other, the hydrogen-stream replaced the sample-stream. Only these two gases can flow through, either A position or B position. It is obvious that flushing from PF into the KF would make no sense. Valve 5 must be in position B so that the oxides go out to ambient. The difference in temperature between the enrichment and

the end of flushing is given by the time when valve 5 is switched into position A, in this case 15 minutes later at 53:15. Position A means the valve-input and ambient are connected together through the KF which is immersed in LN_2. In other words, everything what is leaving the PF is going to be trapped in KF from that moment. Now it is clear all the compounds would be trapped quantitatively in KF. The transfer can be speeded up, PF is heated at 120 ^{o}C at 54:05.

At 54:10 valve 3 is switched into position B. Ten seconds thereafter, the Heater2 starts heating with the setvalue 80 ^{o}C. The H_2O scrubber is regenerated with a flushing stream in an opposite direction. This regeneration lasts till it is OFF in the following procedure or as long as the main process is running. At 1:00:00 the V25 sends signal CTRL2 for a remote control of the chromatogram-start. When GC receives this signal which is basically voltage puls at 5 volts the GC-software starts chromatogram together with temperature program. The pulse takes 5 seconds so that its end is at 1:00:05.

In the appendix, A7-A11, there are time space diagrams describing Valco-Vici valves switching, magnet valves switching, 3-way valves switching, all the flows and finally all temperature during procedure. All these diagrams were made for the shorter version of procedure, i.e. overall trapped volume of 500 ml. Procedure ends then at 50:05 because with 50 ml/min the integration of 500 ml takes 10 minutes. In the valves diagram there is described how Mupo1 position is not implemented in starting positions. Its status stays regardless the process. Other valve-positions stay although the actual procedure is finished but only in case that the process is still running. At 41:00 the valve 4 is switched according to integration which is a dynamical command. The magnet valves diagram shows the time when pistons are actuated. Next diagram shows timing of the 3-way valves. The p24_4 switching is a dynamical command thus the exact moment is given by the side information coming from integration. The flow diagram shows timing at which time the flow controllers get their commands with which value. Except for the flow2, the flows stay regardless the main process. Because procedure takes now only 50:05 it implies 500 ml overall volume thus flow0 is only 57.5 ml/min and flow1 is 5 ml/min, see calibration section. The last diagram shows temperatures timing and their values of the sensed apparatus-parts. The CO_2 temperature is not handled from the procedure and consequently is constant. The KF temperature is controlled only during the heating phase and not during the focusing, that is why it is not showed in the diagram.

3.3 Calibration

The system has to be calibrated by injection of exact amounts of standard gas mixture. Values of the peak areas are then plotted in a graph against the known amounts. The analysis consists of several steps. Errors that occur in any step can invalidate the chromatographic analysis, so attention must be paid to all steps. The calibration has to be made in the same way as analysis to account for changes in all analytical steps. The system must be able to make calibration run as often as it is needed.

Method of external standard was used and included in the Chemstation. Known amounts of the analyte of interest were chromatographed, the areas measured, and calibration curve plotted.

3.3.1 The calibration curves

A calibration curve represents the functionality between the amount of injected standard and the calibrated variable which stands for the response. The response is technically percentage ratio to the calibrated variable which is being used. The height, width or areas all may be variables. The area is usually used. The functionality is expressed as:

$$\% = \frac{Area \cdot \dfrac{Amount_{st}}{Area_{st}}}{Amount_{injected}} \cdot 100 \tag{3.10}$$

$Amount_{st}$ and $Area_{st}$ are independent and dependent variables corresponding to the standard. In denominator there is an absolute amount of injected sample. The second multiplier in nominator is the reciprocal response factor. The response factor is constant if the calibration curve is linear.

Despite of the FID linearity the multipoint calibration had to be made. Calibration curves were constructed for each compound by using calibration levels to define the curve. The algorithm used to generate the calibration curve was a simple linear regression with forced origin.

For regular analyses the two-point calibration was made. Individual calibration point weighting was specified as equal. Both calibration points were considered of equal importance in drawing the calibration curve. In practice, the first(second) calibration point corresponded to enriched 40(20)ml NPL standard gas mixture that was used. Standard was diluted in ratio which corresponds to the overall trapped volume 1000 ml, i.e. 960 ml diluting air for the first calibration point and 980 ml for the second point. It

is obvious that impurities from diluting air have to individually subtracted. The diluting air was purified in three steps to avoid this.

3.3.2 The peak identification

If the column and all operating conditions are kept the same, a given compound always travels through the column at the same rate. Thus, a compound can be identified by the time required for it to travel through the column, by the retention time. Compound identification was enabled by defining individual retention time window parameters. Only compounds lying inside the predefined window are identified. The calibration table was defined by entering compounds and locating their retention time windows. New calibration run provided recalibration, i.e. new location of each retention window and a new response factor. All new events were recorded in the method and used in an automatic evaluation of an unknown sample.

The definition of calibration table in first step was done by injection of approximate amounts of diluted standard gas mixtures N18, N19 from Messer Griesheim. N18 contained $CH_4/C_2H_6/C_3H_8/n-C_4H_{10}/i-C_4H_{10}/n-C_5H_{12}/n-C_6H_{14}$, all at 1000 ppm mixing ratios. N19 contained $C_2H_2/C_2H_4/C_3H_6/i-C_4H_8/cis-C_4H_8/trans-C_4H_8$, all at 100 ppm mixing ratios. Because of high concentrations both gas mixtures had to be diluted to 1-10 ppb which is by 4-5 orders of magnitude. Diluting line with vacuum pump and accurate pressure sensors was used.

In the second step of identification the NCAR standard gas mixture from National Center for Atmospheric Research as a primary standard was used. Compounds with different carbon-content were safely identified. In the course of development the new NPL standard gas mixture, cylinder APE 289347, from National physical laboratory was bought and has been used. In the appendix, A12, there is a table of all the compounds contained in NPL with their uncertainties.

3.3.3 The dilution

The high concentrations of the new NPL standard were diluted to concentrations comparable to mixing ratios occurring in CARIBIC samples. As a diluting gas the ultra pure air was used. Pressurized ambient air was purified in CAP 60 unit from Headline Filters. Purified air contained still small impurities of ethane, propane and iso-butane thus additional purification unit was installed. SiO_2 wool with deposited Pt was placed in 20 cm long stainless steel tube, fixed with a filter and

welded with 1/8 inch tubing together. The unit was located in CARBOLITE MTF12/25 furnace, kept at 600 ^{o}C. CARBOLITE MTF furnace is a vertical ceramic work-tube with wire heating elements which are wound directly onto an impervious ceramic tube. As the last step in purification the Supelcarb HC NMHCs trap was installed downstream the produced diluting air, between the instrument and the furnace. Supelcarb HC from Supelco gets rid of C_3 and higher compounds at the room temperature. According to specification, Supelcarb HC activated carbon adsorbent has twice the trapping ability of activated charcoal.

The NPL calibration gas was diluted by the device shown in Figure 23. The FC1 and FC2 are mass flow controllers with 0-10 ml/min and 0-500 ml/min range, respectively. Both controllers were calibrated. The excess of resulting mixture, is vented by a back pressure regulator from Tescom. 2 Bar pressure has been used to have similar conditions as during sample analysis.
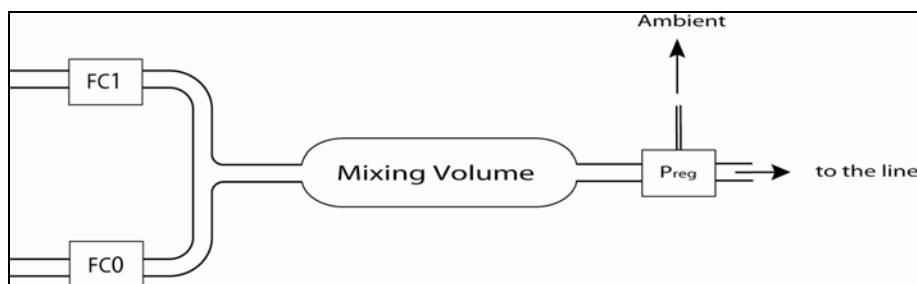
Figure 23: Dynamic dilution used for calibration. FC1, FC0 are mass flow controllers for NPL and diluting air respectively. P$_{reg}$ is a back pressure regulator which releases the excess of calibrating mixture.

The flows of FC0 and FC1 were chosen in order to have the same overall flow (*flow0+flow1*) and still to enrich 40ml resp. 20ml of NPL with the *flow2* equal 50 ml/min. The combination (96ml/min + 4ml/min) resp. (98ml/min + 2ml/min) was used. The flows were calculated based on the time of enrichment 20min as:

$$\frac{flow2}{flow0 + flow1} \cdot flow1 = 20 \Rightarrow for\ 40\,ml \tag{3.11}$$

$$\frac{flow2}{flow0 + flow1} \cdot flow1 = 10 \Rightarrow for\ 20\,ml \tag{3.12}$$

3.3.4 The determination of the sample volume

The volume can be calculated from flow by multiplying it with time. The flow must be accurate and constant during enrichment otherwise the overall volume would have a large uncertainty since error in volume is a cumulative feature.

$$V = t \cdot \dot{V} \tag{3.13}$$

Integration is basically a sum of read actual flow values multiplied by time for which the one value lasted. The summing is made by *for-loop* with variable *Vol* displaying volume that has already passed. The time step is given by sampling frequency.

$$V = \int_0^t \dot{V}(t) \cdot dt = \sum_{i=1}^t \dot{V}_i \cdot \Delta t \tag{3.14}$$

This means, of course, that the multiplex-reading must be symmetrical which demands even-numbered frequency. The flow of FC2 was sampled with 10 Hz frequency. Variable *Flow2* is in ml/min thus there were 600 readings per minute. One reading took 1/600 of minute. In the source code the time was rounded up to 0.0016667.

The flow integration method was compared to a method using a pressure increase in an expansion-vessel. A volume measurement based on the pressure gauging is ca. 1-2 orders of magnitude more accurate therefore enables to have a physical prove. If a passed amount is added to a defined volume the pressure inside rise. From its difference it can be count how much it was added. The defined volume is presented by a stainless steel canister. The canister was calibrated using two-step method where pressure was passed to two other vessels. One of them V_3 was calibrated by filling it with water and weighting it. The volume is then calculated from the weight of the water, its temperature and the water density. The canister could not be calibrated in the same way just because of too many dead volumes like volume of pressure gauge itself, volume of the connecting line or the releasing valve.

The metal canister has two outlets. The first was connected to the releasing valve and closed. The second, 1/16" Swagelok, was connected together with pressure transducer using of T-piece KF-16 vacuum fitting coupling with O-rings rubber gasket. The unit was forming volume V_1 as described in Figure 24.

V_1 ended where the valve was detaching it from rest of the line. Volume number two V_2 resulted from the lines between V_1, the pump and V_3. V_2 and V_3 were detached by glass valves inside the glass line. V_3 was a glass vessel of spherical shape with closing valve which was precisely opening and closing the volume number three. Its shape helped during the filling and empting.
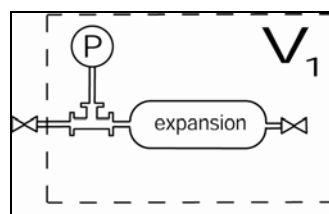
Figure 24: Volume V_1 formed by canister and the pressure gauge.

Stepwise opening the valves of V_1, V_2 and V_3 respectively led to two pressure steps, see Figure 25. At the beginning the V_1 was pressurized up to P_1 with pure nitrogen and closed. The rest of the line was evacuated by the turbo molecular pump to 0.1 Pa. In the first step we get the second pressure P_2 and the second volume V_B which consists of V_1 and V_2. The last step expanded P_2 into V_3 so we get P_3 in the overall volume V_C which consists of V_1, V_2 and V_3.
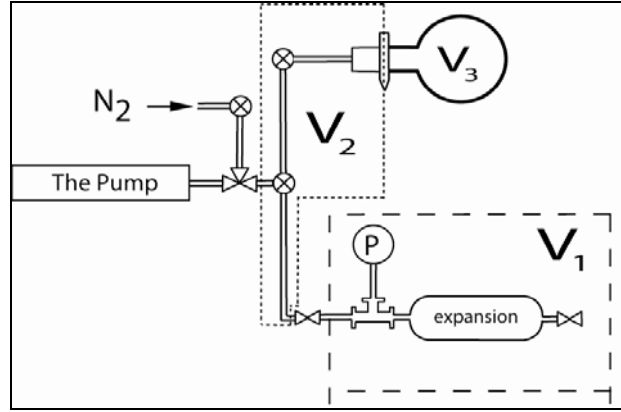
Figure 25: Two-step expansion to determine V_1. Stepwise opening the valves of V_1, V_2 and V_3 respectively expanse V_1 into known volumes so that V_1 can be determined.

All the steps carried out at the same temperature can be described in equations as:
It is true that:

$$V_A < V_B < V_C \tag{3.15}$$

From ideal gas equation we get :

$$P_A \cdot V_A = P_B \cdot V_B = P_C \cdot V_C \tag{3.16}$$

The pressure can be denoted as:

$$(P_A = P_1) \wedge (P_B = P_2) \wedge (P_C = P_3) \tag{3.17}$$

Analogically for the volumes holds:

$$(V_A = V_1) \wedge (V_B = V_1 + V_2) \wedge (V_C = V_1 + V_2 + V_3) \tag{3.18}$$

By substitution of (3.18) and (3.17) into (3.16) we get:

$$P_1 \cdot V_1 = P_2 \cdot V_1 + P_2 \cdot V_2 = P_3 \cdot V_1 + P_3 \cdot V_2 + P_3 \cdot V_3 \tag{3.19}$$

Equation (3.19) is formed by 2 sub-equations. From the first we express V_2:

$$V_2 = \frac{P_1 \cdot V_1 - P_2 \cdot V_1}{P_2} \tag{3.20}$$

And following by its substitution into the second equation we get:

$$P_1 \cdot V_1 = P_3 \cdot V_1 + \frac{P_3 \cdot V_1}{P_2}(P_1 - P_2) + P_3 \cdot V_3 \tag{3.21}$$

The requested volume V_1 is expressed then as:

$$V_1 = P_3 \cdot V_3 \cdot (P_1 - P_3 - \frac{P_3}{P_2}(P_1 - P_2))^{-1} \qquad (3.22)$$

Connecting V_1 directly to the flow controller with the same Swagelok connections as it was during calibration the dead volume is diminished and pressure sensor shows exact passed volume.

The used pressure gauge was baratron capacitance manometer type 222BA 0100DD, 1000 Torr from MKS with resolution 10^{-5} of the full scale. Pressure is determined by measuring the change in capacitance between the metal diaphragm and an adjacent electrode. It is an absolute transducer, the reference side of the diaphragm is evacuated. Its accuracy is expressed as a percent of reading and not full scale, i.e. an absolute error increases with increasing readings. The accuracy includes non-linearity, hysteresis and non-repeatability. The last „D" marking means an extra accuracy of 15% of the reading. The temperature coefficient for span is 0,04% of reading /°C and 0,05% of reading /°C for the zero. Temperature was sensed with a Pt-100 sensor fastened on the outer wall of the canister. which was in touch with an outer wall of the canister. The whole vessel was wrapped in an insulating foam to minimize effect of fluctuating ambient temperature.

To avoid errors due to dynamical pressure drop, the pressures are measured before and after the flow of FC2 was switched off. Variable *PressVol1* displays the pressure before and after the enrichment. 3-way valves Pow24_5 and Pow24_4 define when to calculate the average, see Figure 26. Pow24_5 is the outlet valve. It takes 20 seconds to release 1l sample and equal the pressure to ambient. Within next 10 second the first value before enrichment is counted. The second value after the enrichment is counted within 10 second measured 10 second after the Pow24_4 is switched thus no more flow goes through. The outlet was programmed to be coincident with Pow24_4.
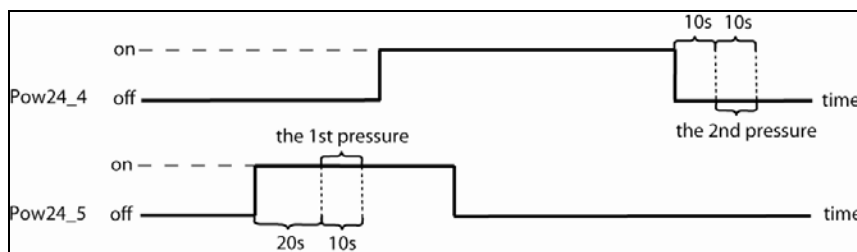
Figure 26: Calculating the pressure before and after the enrichment. A mean of pressure readings during 10s period was calculated.

3.4 Air sampling

Stainless steel canisters are known to suffer from alkene artefacts (Mühle, 2002) and losses of aromatic compounds. To reduce these artefacts, the new whole air sampler, TRAC was built with glass vessels instead of stainless steel canisters. TRAC, **T**riggered **R**etrospective **A**ir **C**ollector, was developed at the Max-Planck-Institute in Mainz. It consists of 14 glass cylinders each, and a pump system. Four of the units were available with two being in the measurement container.

The glass cylinders are made of borosilicate glass manufactured by Louwers Hapert Ltd, Netherlands. The cylinders are certified for 7 bar absolute. Each glass cylinder is covered with a heat shrinkable tubing. Cylinder dimensions are: outer diameter 100 mm, length 450 mm, volume 2670 cm^3, see Figure 27.
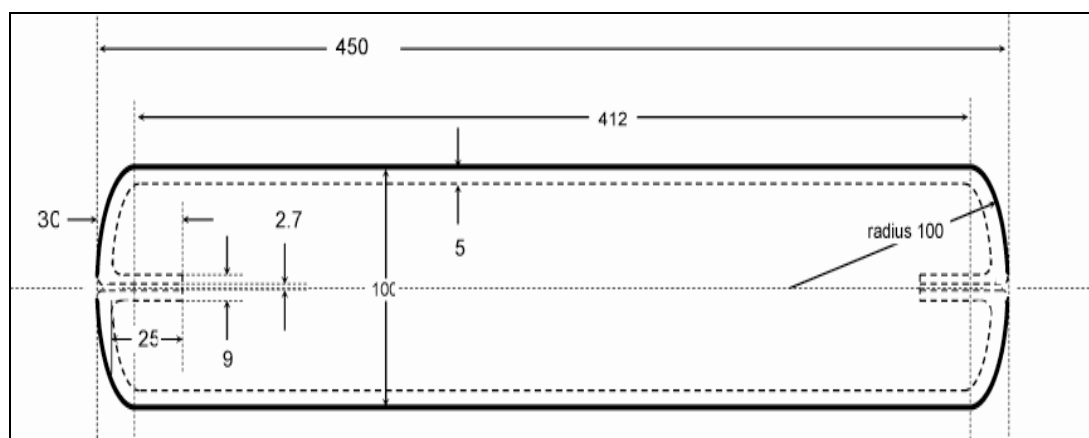
Figure 27: Glass cylinder of TRAC collector. Vessel made of borosilicate glass is wrapped in a heat shrinkable tubing. Each cylinder has two open points, inlet and outlet, where the stainless steel tubing is connected to. All linear dimensions are given in (mm).

Two stainless steel tubes (outer diameter 2.5 mm, wall thickness 0.4 mm) were bonded to each point using a two component epoxy glue ARALDITE 2020. Cylinders are switched using two multi-position 16-way valves from Valco-Vici. The free ends of the stainless tubing were connected to corresponding multi-position valves, i.e. all inlets were connected with the first valve while all outlet were connected with the second valve, Figure 28.

Upstream of the multi-position valve inlet a 2 μm stainless steel filter from Swagelok was installed to protect the valves and the cylinders from particle contamination. Detailed scheme of the input-output connections is in the appendix, A13.

All 4 cassettes of 14 sample bottles each are identical in construction. Instrument housing was made from lightweight aluminium sandwich panels (thickness 5.2 mm)

from Metawell. The housing consists of corpus subdivided into 15 "pigeon" holes (110 x 110 x 460 mm) arranged as five times three matrix to encase, fix and protect the glass cylinders.
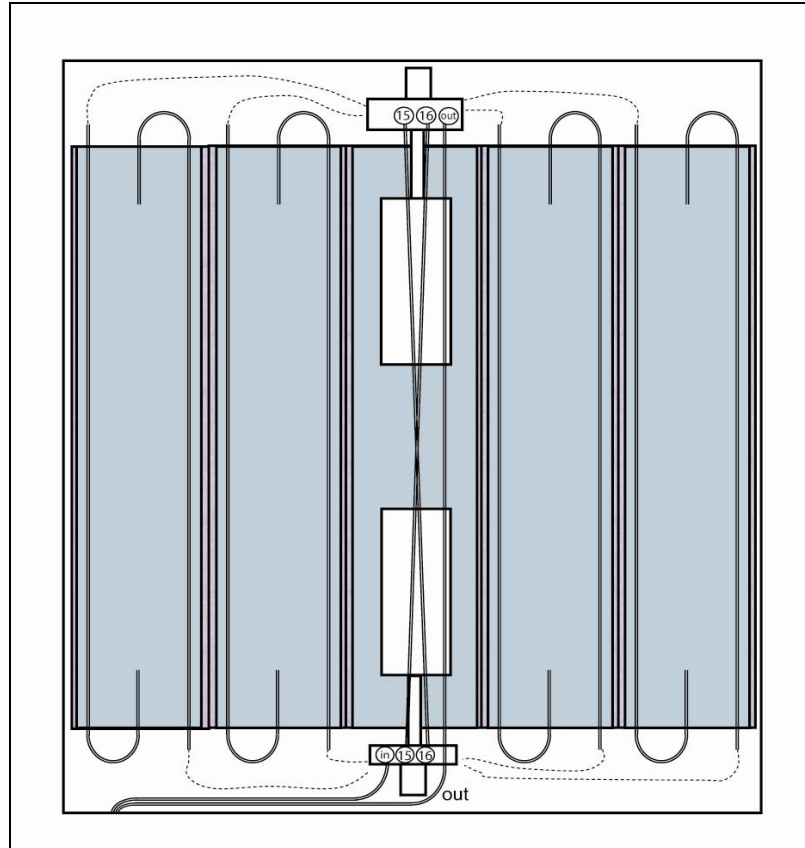
Figure 28: Top view of TRAC collector. The section is made above the multi-position valves. The shown vessels present the lowest compartment plane. The first multi-position valve controls all inlets while the second multi-position valve controls all cylinder outlets. The internal size of TRAC housing is 565 x 583 x 340 cm. The external size is 580 x 600 x 360 mm.

The pigeon hole in the middle of the corpus is occupied by two multi-position valves. This cage structure, combined with the outer instrument housing, prevents glass particles in case of a cylinder burst.

The pump module consists of two metal bellow pumps from Senior Aerospace (Metal Bellows Division). Each pump has two metal bellows connected parallel in pump 1 and in series in pump 2. Pump 1 is connected via 3/8" stainless steel tubing with the CARIBIC air-inlet system of the aircraft. The inlet pressure of pump 1 during the flight-phase at aircraft altitude of about 10 000 meter is ca. 200 mbar absolute. The pressure increases to ca. 1 bar absolute at the outlet of the first stage. Pump 2 fills the glass cylinders to a final pressure of ca. 4 bar. The flow rate of entire pump system is ca. 13 liter per minute. The filling time for one sample at cruising altitude is ~ 45s. The

outlet of pump 2 is connected via ¼" stainless steel tubes with the inlets of both TRACs. Two valves from Clippard are located after the pump 1 and after the pump 2 to avoid a pump start against pressure left from a prior pump run.

The sampling can be made according to preprogrammed schedule or can be triggered by measurements made by the selected instruments in the CARIBIC container. Before filling, the next (in the row) coming vessel is flushed with 1.5 bar until the filling starts. Both collectors are filled during the outward flight alternately, first, cylinder one of the TRAC1 followed by cylinder one of the TRAC2. Second, cylinder two of the TRAC1 followed by cylinder two of the TRAC2. Filling proceeds so long till both TRACs are full. During the return flight, cylinders TRAC2 are refilled sequentially. In this way all canisters are filled even if malfunction during the return flight occurs.

After connecting TRAC to the NMHCs apparatus using the *MuPoExt* switch from *Param* option the 16-way valve on output stands for to the system own VA1.

4. Results and discussion

4.1 Analytical performance

Measurement procedure consisted of:

a)   calibration function obtained using diluted gas standard

b)   analysis of sample

c)   calculation algorithm (executed automatically by Chemstation (Agilent))

Choice of calibration function with or without forced origin is discussed in 4.1.1. Conditioning of calibration mixture is discussed in section 4.1.2. In section 4.1.3 the uncertainty of an individual measurement is estimated using propagation of uncertainties of individual parameters. The detection limit is calculated in section 4.1.4. Accuracy of the NMHCs measurements was determined by an intercomparison with an independent technique described in section 4.1.5. Influence of carbon dioxide and humidity is discussed in section 4.1.6. Finally, the system stability is shown in section 4.1.7.

4.1.1 Calibration function

The calibration function was measured using known mixing ratios of the standard gas mixture NPL. Peak areas were determined and concentrations calculated by the Chemstation software after each chromatogram was checked and manually reintegrated. The independent variable was the ppt-concentration of particular hydrocarbon. The dependent variable was the peak area in pAs. The sampled volume of diluted standard was in the later phase the same as the volume of normal sample. The calibration function is then:

$$A_{HSGM} = a_H \cdot x_{HSGM} + b_H \qquad (4.1)$$

where:

A_{HSGM} is the peak area for the particular hydrocarbon from standard gas mixture

a_H is the slope of calibration curve for the particular hydrocarbon

x_{HSGM} is the calibration mixing ratio for the particular hydrocarbon

b_H is the offset on calibration curve for the particular hydrocarbon

With the forced origin modus in Chemstation the offset b_H becomes zero. The ppt-concentration as an independent variable was linked to the standard gas mixture through its volume that was enriched. The first, most concentrated, point on the calibration curve had ppt-concentration of standard gas mixture as declared whereas the other point had gradually lower mixing ratios related to the smaller quatity that had been enriched. Provided that slope has unit (pAs.ppt^{-1}) as stated the final mixing ratio, calculated from the measured peak area, must be multiplied by a factor which defines the ratio between an injected amount of NPL and the injected amount of sample. In other words, hydrocarbon from sample produces certain response from which the calculated ppt-concentration has to be multiplied by this factor.

$$x_{HS} = x_{MES} \cdot factor \tag{4.2}$$

where:

x_{MES} is the mixing ratio calculated directly from peak area

x_{HS} is the mixing ratio for the particular hydrocarbon from sample

The produced response is caused by the absolute amount of hydrocarbon. Response is peak area, absolute amount of substance is mol. The ratio of two responses is equal to the ratio of amounts which made the response (provided that there is no offset).

$$\frac{n_x}{n_y} \approx \frac{Area_x}{Area_x} \tag{4.3}$$

x_{HSGM} is defined as a mol of pure hydrocarbon from calibration mixture (n_{HSGM}) divided by the mol of NPL standard gas mixture (n_{SGM}) which was enriched no matter its dilution. Analogically, x_{HS} is a mol of pure hydrocarbon from sample (n_{HS}) divided by the mol of sample (n_S) which was enriched. After modifications we get the final relation for both molar ratios (4.6).

$$x_{HSGM} = \frac{n_{HSGM}}{n_{SGM}} \tag{4.4}$$

$$x_{HSGM} \cdot x_{HS} = \frac{n_{HSGM}}{n_{SGM}} \cdot x_{HS} \Rightarrow x_{HSGM} \cdot \frac{n_{HS}}{n_S} = \frac{n_{HSGM}}{n_{SGM}} \cdot x_{HS} \tag{4.5}$$

$$x_{HSGM} \cdot \frac{n_{SGM}}{n_S} \cdot \frac{n_{HS}}{n_{HSGM}} = x_{HS} \tag{4.6}$$

Considering an ideal gas and constant conditions, n_{SGM} can be expressed via its volume (V_{SGM}) at the defined conditions, the same holds to the n_S and its V_S. After substitution in (4.6) and replacement of mol with response we get the final relationship (4.7) which clearly shows how to calculate the final ppt-concentration.

$$x_{HS} = x_{MES} \cdot factor = x_{HSGM} \cdot \frac{Area_{HS}}{Area_{HSGM}} \cdot \frac{V_{SGM}}{V_S} \qquad (4.7)$$

Because of the dynamic dilution, the factor can be written in form including participating flows (4.8).

$$factor = \frac{V_{SGM}}{V_S} = \frac{\dfrac{f_2 \cdot f_1}{f_0 + f_1} \cdot t_{CAL}}{f_2 \cdot t_{MES}} = \frac{f_1 \cdot t_{CAL}}{(f_0 + f_1) \cdot t_{MES}} \qquad (4.8)$$

where:

f_i is the flow in ml/min

$t_{CAL,MES}$ is the time for which the calibration, measurement lasted

As mentioned, in later phase the sampled volume of diluted standard was the same as the volume of normal sample during measurement. The final mixing ratio is calculated then:

$$x_{HS} = x_{MES} \cdot \frac{f_1}{(f_0 + f_1)} = \frac{A_{HS} - b_H}{a_H} \cdot \frac{V_{SGM}}{V_S} \qquad (4.9)$$

Calibration should ideally be made with concentrations within the measurement range. With calibration gas containing 30 compounds of which some are found at concentrations near to or below the detection limit in air samples from lower stratosphere or upper troposphere – the above optimal calibration could not be realized for all compounds. As mentioned, for regular measurements a two-point calibration was made. Test of system linearity from November 2004 showed that calibration was linear in the range from 10ml of enriched NPL to 40ml thus two-point calibration was satisfactory. Both calibration points were measured alternatively in order to simulate the conditions at which samples were measured.

During calibration, almost all calibrated compounds appeared to have a positive offset. Chemstation offers two different algorithms: one with the calibration curve forced through origin and one with ignored origin. Ignored origin may fit better to description of how compound behaves, but on the other hand, it exaggerates the uncertainty due to the disproportionality of relative errors of area vs. ppt. Detector response in counts recalculated into area-unit corresponding to the mixing ratio is always smaller in relative value no matter the concentration. Thus $\delta A_{HS}/A_{HS}$ would always be smaller than $\delta x_{HS}/x_{HS}$ as a consequence of existing positive non-zero offset. Forced origin does not produce this disproportionality but it may overestimate the final concentration. To investigate which of these two algorithms provides more consistent results the following steps were done:

a)   slopes of calibration curves with forced and ignored origin, together with offsets, were calculated in counts/ppt and normalized to carbon response in counts/pptC, see Tables 6, 7

b)   ideally the slopes in counts/pptC should be the same for all compounds - the slopes of the data sets with forced and ignored origin were averaged and tested for outliers (separately for Gas-pro and Petrocol)

c)   the consistency of the slopes was compared in terms of: I – number of identified outliers, II – STD of the resulting average values of slopes

From measurements of zero air used to dilute the NPL gas mixture it is clear that all offsets are not caused by impurities contained in zero air. In Figure 29 there are the slope ratios between the forced origin curve and the ignored origin curve, each with normalized slope.
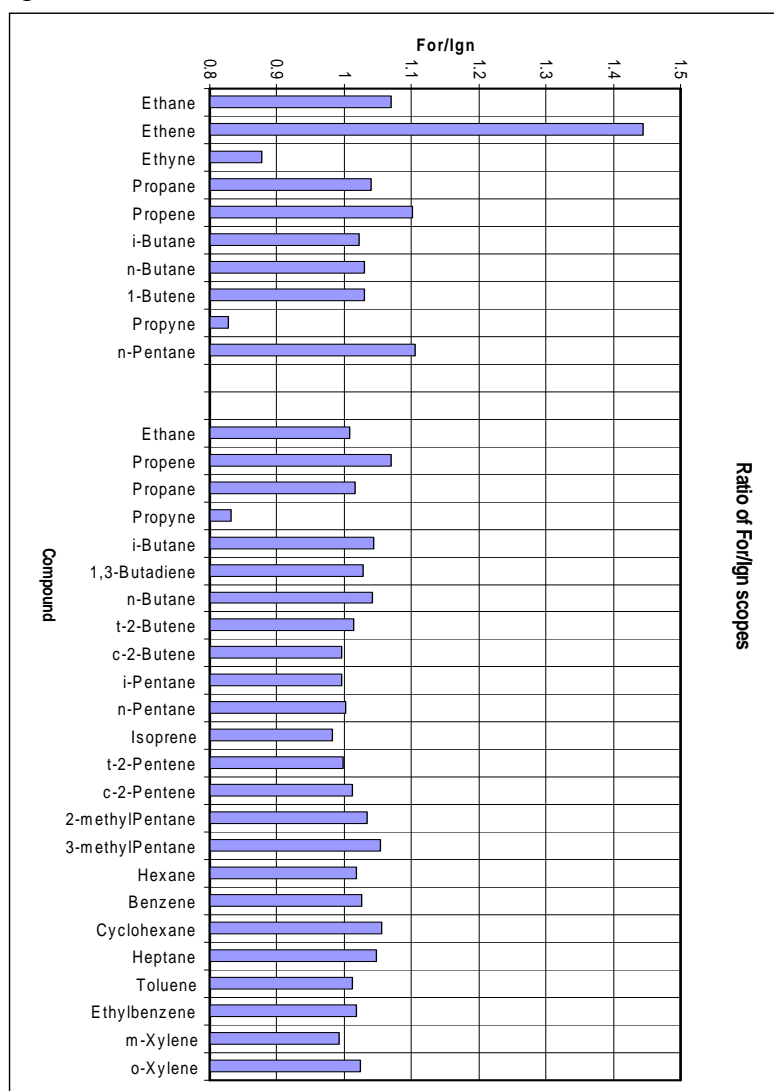
Figure 29: Ratio of standardized slopes as they are calculated by forced origin and ignored origin algorithm. Each column was calculated separately, i.e. first set of compounds belong to Gas-pro column.

Ratios were calculated separately for each column. The first set of compounds up to n-pentane stands for Gas-pro column, the second for Petrocol. It is obvious that with mostly positive offsets the ratio is above 1. Extreme deviations from 1 appear to have ethene, ethyne, propyne on Gas-pro while on the Petrocol it is only propyne.

In Figures 30, 31 are chromatograms of zero air. The first shows retention times from 5.5 till 10 minutes where most of the important compounds elute on Petrocol. As it can be seen there is only rest of propene together with i-butene which is not used for calculation anyway. Two other peaks are not calibrated unknown peaks. Propene elutes on Gas-pro later at 17.5th minute. The second chromatogram shows propene which apparently lies even below the limit of detection. Impurities would produce offsets on both columns with the same extent which is not the case thus losses eventually reactive stationary phase on Gas-pro are probably the reason.

Comparison of two data sets with ignored and forced origin was made. The *t*-test is an objective method to examine whether two mean values belong to the same set. In the *t*-test for dependent means, it is being compared the mean difference (mean$_1$-mean$_2$) calculated on linked data to an expectation that there is no difference in the population (μ_1-μ_2 = 0). According to (Kaiser and Gottschalk, 1972) calculated *TAU* value is the main criteria provided that the processing data set contains no outliers. Before testing the outlier test was done (Kaiser and Gottschalk, 1972). The *TAU* value is calculated as:

$$TAU = \left| \frac{\bar{x}_1 - \bar{x}_2}{s_d} \right| \cdot \sqrt{\frac{n_1 \cdot n_2}{n_1 + n_2}} \tag{4.10}$$

$$s_d = \sqrt{\frac{(n_1 - 1) \cdot s_1^2 + (n_2 - 1) \cdot s_2^2}{n_1 + n_2 - 2}} \tag{4.11}$$

where:

$\bar{x}_i$ is the mean of *i*-data set

n_i is the number of data in the *i*-set

s_i is the standard deviation of *i*-data set

By comparing the *TAU* value with *t*-test critical value for 95%, we decide whether both data sets differ from each other. In Tables 6, 7 are the slopes for each hydrocarbon and its normalized value to pptC for Gas-pro and the Petrocol. Slopes were calculated for the forced and ignored origin. Additionally to ignored origin an offset value is shown too. Offset value, put in the equation with forced origin, shows ppt threshold concentration which would not be included into the calibration function. This value is shown next to the offset. Standardized slopes in the second column for forced and ignored origin should exhibit the same value. The outlier-slopes are marked as a grey field.
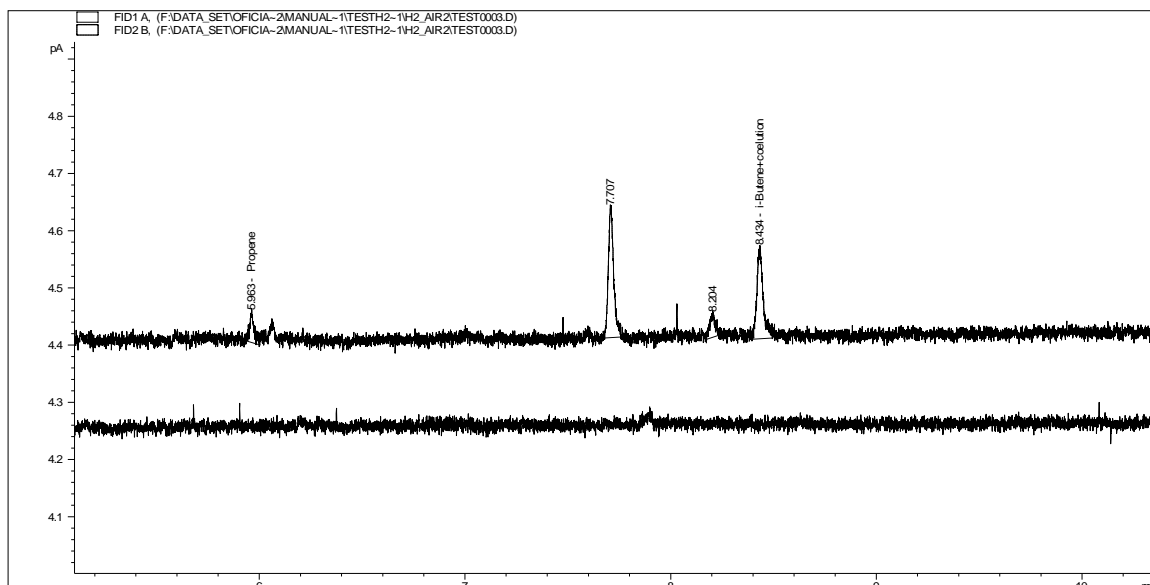
Figure 30: Chromatogram of diluting air showing both signals. The upper signal (Petrocol), apart from the rest of propene, shows three other peaks (two unknown plus i-butene) which are not used for calculation. All the other calibrated compounds, eluting between 5th and 11th minute, are missing in contradiction to what the offsets suggest.
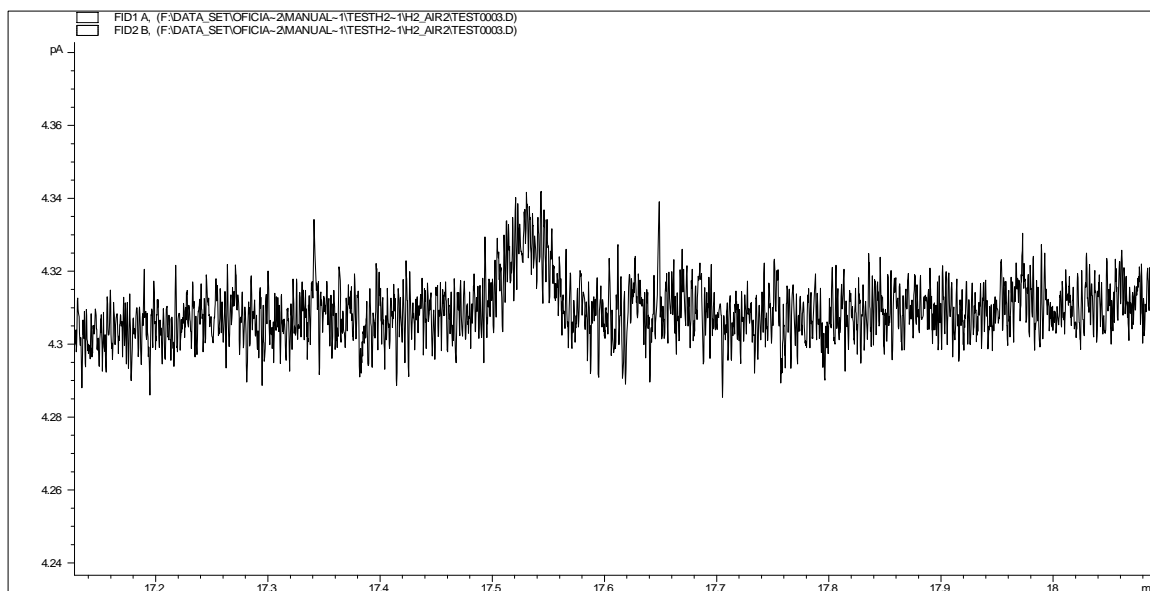
Figure 31: Chromatogram of diluting air with expanded scale for propene showing only Gas-pro signal, again with rest of propene. Propene elutes on Gas-pro later at 17.5th minute. Shown hardly detected peak would have to have area at least of 0.391 as its offset suggest.

Gas-pro					
Compounds\Slopes	**Forced origin**		**Ignored origin**			
	Slope (counts/ppt)	Slope (counts/pptC)	Slope (counts/ppt)	Slope (counts/pptC)	offset (counts)	concentration (ppt)
Ethane	0.000501	0.000250	0.000468	0.000234	0.224	17.9
Ethene	0.000674	0.000337	0.000467	0.000233	0.737	43.7
Ethyne	0.000556	0.000278	0.000633	0.000317	-0.587	-42.3
Propane	0.000969	0.000323	0.000932	0.000311	0.112	4.6
Propene	0.001239	0.000413	0.001124	0.000375	0.391	12.6
i-Butane	0.001307	0.000327	0.001278	0.000320	0.029	0.9
n-Butane	0.001243	0.000311	0.001207	0.000302	0.058	1.9
1-Butene	0.001286	0.000321	0.001247	0.000312	0.129	4.0
Propyne	0.000249	0.000083	0.000301	0.000100	-0.110	-17.6
n-Pentane	0.001515	0.000303	0.001370	0.000274	0.134	3.5

Table 6: Gas-pro slopes for both forced and ignored origin algorithms. Concentrations in the last column correspond to the offset of the ignored origin algorithm. Grey are the outliers identified by the Nalimov outlier test (Kaiser and Gottschalk, 1972).

Petrocol					
Compounds\Slopes	**Forced origin**		**Ignored origin**			
	Slope (counts/ppt)	Slope (counts/pptC)	Slope (counts/ppt)	Slope (counts/pptC)	offset (counts)	concentration (ppt)
Ethane	0.000439	0.000219	0.000435	0.000217	0.027	2.4
Propene	0.001105	0.000368	0.001034	0.000345	0.244	8.8
Propane	0.000887	0.000296	0.000873	0.000291	0.042	1.9
Propyne	0.000318	0.000106	0.000382	0.000127	-0.136	-17.1
i-Butane	0.001301	0.000325	0.001247	0.000312	0.055	1.7
1,3-Butadiene	0.001045	0.000261	0.001016	0.000254	0.129	5.0
n-Butane	0.001204	0.000301	0.001155	0.000289	0.078	2.6
t-2-Butene	0.001340	0.000335	0.001322	0.000331	0.020	0.6
c-2-Butene	0.001176	0.000294	0.001180	0.000295	-0.010	-0.3
i-Pentane	0.001510	0.000302	0.001516	0.000303	-0.007	-0.2
n-Pentane	0.001486	0.000297	0.001483	0.000297	0.002	0.1
Isoprene	0.001366	0.000273	0.001391	0.000278	-0.062	-1.8
t-2-Pentene	0.001400	0.000280	0.001403	0.000281	-0.011	-0.3
c-2-Pentene	0.001397	0.000279	0.001381	0.000276	0.032	0.9
2-methylPentane	0.001766	0.000294	0.001707	0.000285	0.088	2.0
3-methylPentane	0.001935	0.000322	0.001835	0.000306	0.231	4.8
Hexane	0.001828	0.000305	0.001796	0.000299	0.086	1.9
Benzene	0.001871	0.000312	0.001822	0.000304	0.221	4.7
Cyclohexane	0.001867	0.000311	0.001767	0.000295	0.396	8.5
Heptane	0.002187	0.000312	0.002086	0.000298	0.202	3.7
Toluene	0.002196	0.000314	0.002170	0.000310	0.088	1.6
Ethylbenzene	0.002438	0.000348	0.002395	0.000342	0.059	1.0
m-Xylene	0.002386	0.000341	0.002403	0.000343	-0.030	-0.5
o-Xylene	0.002448	0.000350	0.002393	0.000342	0.064	1.1

Table 7: Petrocol slopes for both forced and ignored origin algorithms. Concentrations in the last column correspond to the offset of the ignored origin algorithm. Grey are the outliers identified by the Nalimov outlier test (Kaiser and Gottschalk, 1972).

The forced origin algorithm has more outliers than the ignored origin for both columns. Some of these can be explained by well known deviations from FID response (acetylene), problem with calibration gas (propyne) or incomplete enrichment as for ethene. Generally are 4 to 1 outliers for Gas-pro on behalf of ignored origin which

suggests possible losses on stationary phase of this column. On Petrocol there are 4 to 3 outliers on behalf of ignored origin again but already at first look the differences are more similar. For both data sets the *TAU* value was calculated and compared to t-value with results much below t-value. Gas-pro has 1.22 while Petrocol has even only 0.57 which implicates quite homogeneous sets thus they belong to the same selection.

According to Tables 6,7 the physical offsets as blanks would have to been largely above detection limit. For instance in pictures 30, 31 shown propene has an offset 0.244 on Petrocol and 0.391 on Gas-pro. The hardly detected peak on Petrocol has an area cca. 0.05 pAs. Next example is ethene. This compound cannot be detected on Gas-pro in zero air at all but its offset is 0.737. On Petrocol it has coelution with ethyne but the peak is again at the limit of detection, i.e. much below 0.1 pAs.

In Table 8 are the standard deviations of standardized slopes for both algorithms and both columns. Deviations were calculated separately, with included outliers and without them. Ignored origin algorithm produces higher value for Gas-pro column and set without outliers which suggests to work with forced origin algorithm although according to number of outliers the ignored algorithm would be preferred. However, there is no significant difference between counts/pptC of forced and ignored algorithm.

Slope-standard deviation STD				
Column\STD	Forced origin		Ignored origin	
	with outliers (counts/pptC)	without outliers (counts/pptC)	with outliers (counts/pptC)	without outliers (counts/pptC)
Gas-pro	0.000085	0.000012	0.000075	0.000045
Petrocol	0.000052	0.000022	0.000046	0.000022

Table 8: Standard deviations of standardized slopes for both forced and ignored origin algorithms, separately for Gas-pro and Petrocol column and for each algorithm calculated with and without outliers.

In summary, the offsets from the calibration curve differ from blank much more than the measurement implies. Explanation of mentioned effects must involve non-linear behavior of hydrocarbons on the from injection to detection. These are: losses connected with preconditioning (adsorption isotherms are not linear with concentration), not quantitative enrichment, losses on the stationary phase of the Gas-pro column and lower sensitivity on the same column due to rests of CO_2. The forced origin algorithm is preferable because it alleviates problems with virtual offsets but on the other side overestimate the real mixing ratio.

4.1.2 Conditioning of the calibration mixture

As mentioned above, the calibration runs differed in CO_2 trapping and in the overall volume of calibration gas mixture that was enriched. To find out to which extent the possible effects like adsorption losses, memory effect etc. influence the system stability, the LiOH test was made.

During this test LiOH was compared to NaOH. Both traps were newly conditioned without being exposed to vacuum but flushed with N_2 at ca. 70 ^{o}C (with the same conditioning of H_2O trap). Both calibration points 40ml and 20ml of NPL were measured with NaOH and LiOH via 500ml and 1000ml of sample volume alternately with a series (500(40ml)-500(20ml)-1000(40ml)-1000(20ml)). The measurement series repeated three times thus each calibration point was measured six times (three times with sample volume 500ml and three times with sample volume 1000ml). The calibration run with NaOH was measured on 15th August 2006, the run with LiOH was measured one day later, on 16th August 2006. After NaOH runs were made, the CO_2 trap was replaced for LiOH (as well as H_2O trap) and the measurements repeated. Responses in the form of peak area ratio between 1000ml and 500ml are shown in Figures 32, 33. Responses were calculated as a mean from three runs with sample volume 1000ml and three runs with 500ml. The first figure shows responses of light hydrocarbons from ethyne to propyne (as mentioned ethyne and ethene were measured on Gas-pro). The second figure shows responses of hydrocarbons from i-butane to o-xylene. Both calibration points were considered separately, i.e. two different fillings plus two points make altogether four data series. In an ideal case the area responses should be 1 for all compounds and series lying over each other. Generally, the peak ratios tend to larger values with decreasing volatility of the compound. Additionally, the peak ratios for 20ml are almost always larger than the same ratio for 40ml.

Light hydrocarbons show generally lower response what implies underestimation of the less concentrated gas mixture corresponding to 1000ml of calibration gas mixture. Reason for this is probable not quantitative enrichment. The more diluted gas mixture gets enriched the less effective trapping occurs. This effect is visible the most in case of ethane. Its response ratio of 0.75 is independent from data series. In other words, no matter the filling, no matter the calibration point, the overestimation of more concentrated calibration mixture is obvious.

In case of compounds with double and triple bonds other side effects connected with chemical effects may play a role. The most apparent is situation with ethyne and ethene. LiOH and NaOH series of 40ml for ethyne lie below 1 while the same series of 20ml lie above.
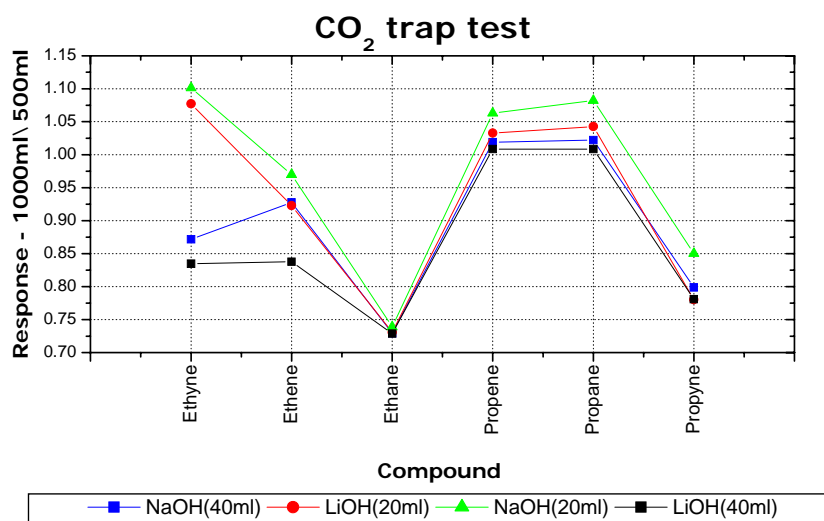
Figure 32: Test of the carbon dioxide trap. LiOH was compared to NaOH as a function of the overall volume of calibration gas mixture. Responses of lighter compounds were calculated as a ratio of peak area of more diluted (1000ml) and less diluted (500ml) calibration gas mixture.
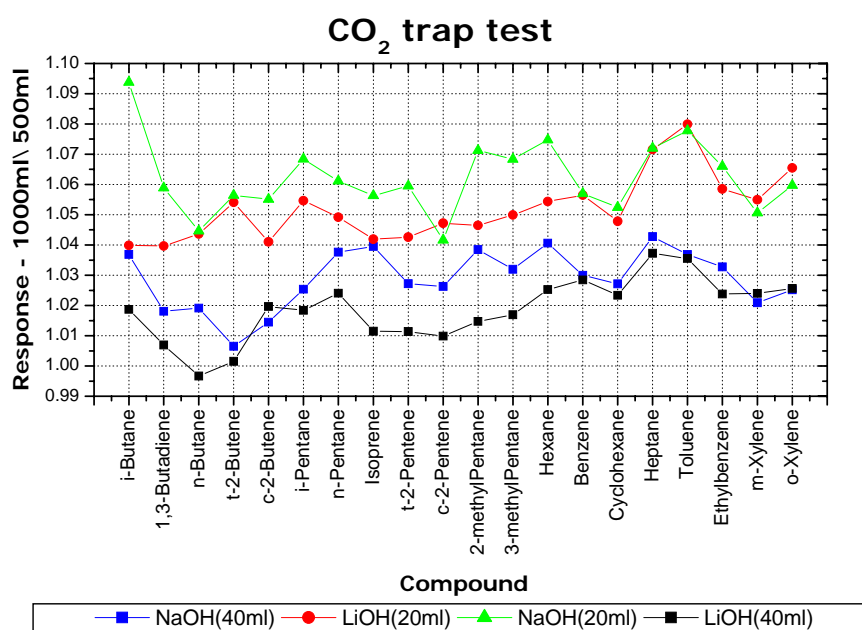
Figure 33: Test of the carbon dioxide trap. LiOH was compared to NaOH as a function of the overall volume of calibration gas mixture. Responses of compounds from i-butane to o-xylene were calculated as a ratio of peak area of more diluted (1000ml) and less diluted (500ml) calibration gas mixture.

This suggests other effect overbeating general underestimation of the less concentrated gas mixture. Ethene responses lie all below 1 but variations in data series support the idea of side effects. Underestimation of the less concentrated gas mixture holds most likely only up to propene. Propene and propane lie both already slightly above 1 although propane is very volatile as well and does not react that much. The second lowest response for propyne ratio is probably caused by chemical effects again.

In contradiction to lighter substances, response ratios of compounds with higher boiling points lie all except for one (79 points) above 1. It simply shows exactly opposite finding, i.e. overestimation of the less concentrated gas mixture relative to more concentrated gas mixture. Contrary to the lighter hydrocarbons this effect cannot be referred to difference in quantitative enrichment, already n-butane can be said to be enriched quantitatively (shown later). Possible reasons are memory effect, adsorption losses together with chemism or losses due to a pressure transient which occurs when the valve VA4 is switched. Memory effect should put on an extent with the heavier compounds, especially aromates. The effect occurs with diluted gas mixture more intensively. Toluene exhibits indeed local maximum in the given data series but on the other side benzene does not. Adsorption losses, provided linear adsorption isotherms, should occur with an extent proportional to the concentration thus only chemical effects or substantially not linear isotherms would overestimate the less concentrated gas mixture. Pressure transient on VA4 may blow compounds trapped at the front zone of the Carbopack away. If the less concentrated gas mixture is trapped deeper in the filling then the more concentrated gas mixture would suffer from these losses more. However, all data series in Figure 33 have very similar pattern. The origin for the overestimation of less concentrated gas mixture lies most likely in combination of mentioned effects.

In order to assess an absolute change in substance response, each run was analyzed in detail using an intercept on the calibration curve and using the carbon response for each substance. Table 9 summarize offsets on calibration curves which were calculated as an average from mentioned three runs with the same weight.

All intercepts were expressed via ppt concentration when the curve function is considered without offsets and the slope is constant. Concentrations associated with the sample volume 500ml were considered as mixing ratios coming from a mixture with the overall volume 1000ml. This enables comparison to the concentrations associated with the sample volume 1000ml on one side but on the other side, it quasi underestimates the mixing ratio because this calculation makes the concentration half. A striking feature is an obvious difference in offsets not only between sample volumes, but also the trap itself plays a role. Offsets of both traps for sample volume 1000ml (for all compounds except for ethyne and propyne) are only positive. Interestingly LiOH with sample volume 500ml exhibited almost only negative offsets. This applies to

NaOH only from a part. However, the tendency to increase an intercept irrespective the trap is apparent when the sample volume is doubled.

Compounds	Intercept$_{500ml}$ (pA.s)		Intercept$_{1000ml}$ (pA.s)		concentration$_{500ml}$ (ppt)		concentration$_{1000ml}$ (ppt)	
	LiOH	NaOH	LiOH	NaOH	LiOH	NaOH	LiOH	NaOH
Ethyne	-1.0649	-1.1953	0.0280	-0.2350	-65.29	-73.37	2.53	-19.63
Ethene	0.0722	0.0633	0.3037	0.1774	4.54	4.03	25.54	12.78
Ethane	0.0137	-0.0052	0.0185	0.0410	0.95	-0.36	1.77	3.93
Propene	0.0624	0.0608	0.1520	0.2230	2.87	2.82	7.11	10.62
Propane	0.0024	0.0021	0.1082	0.1880	0.11	0.10	5.21	9.18
Propyne	-0.0316	0.0009	-0.0254	0.0516	-3.01	0.09	-3.09	7.09
i-Butane	0.0066	0.0114	0.0360	0.0899	0.23	0.41	1.26	3.27
1,3-Butadiene	-0.0164	0.0226	0.1657	0.2511	-0.64	0.89	6.62	10.10
n-Butane	-0.0251	0.0403	0.0767	0.0974	-0.86	1.44	2.77	3.51
t-2-Butene	-0.0198	-0.0050	0.0600	0.0719	-0.69	-0.18	2.21	2.63
c-2-Butene	0.0121	0.0070	0.0757	0.1290	0.44	0.25	2.77	4.78
i-Pentane	-0.0010	0.0450	0.0707	0.1335	-0.03	1.29	2.02	3.90
n-Pentane	0.0107	0.0426	0.0509	0.0824	0.30	1.23	1.44	2.35
Isoprene	-0.0254	0.0988	0.0916	0.1689	-0.76	3.09	2.80	5.16
t-2-Pentene	-0.0623	0.0285	0.1369	0.2380	-1.78	0.83	4.00	6.97
c-2-Pentene	-0.0243	0.0822	0.0980	0.1362	-0.70	2.46	2.91	4.04
2-methylPentane	0.0069	0.0388	0.1050	0.1424	0.19	1.10	2.99	4.02
3-methylPentane	-0.0188	-0.0001	0.1394	0.1745	-0.52	0.00	3.89	4.86
Hexane	-0.0265	-0.0116	0.1291	0.1716	-0.62	-0.27	3.01	3.98
Benzene	-0.0392	0.0158	0.2236	0.2726	-0.89	0.36	5.07	6.21
Cyclohexane	-0.0386	-0.0068	0.1701	0.2089	-0.85	-0.15	3.76	4.64
Heptane	-0.0137	0.0036	0.1548	0.1480	-0.27	0.07	3.02	2.87
Toluene	-0.0967	-0.0392	0.2742	0.3064	-1.87	-0.76	5.34	5.98
Ethylbenzene	-0.0355	-0.0200	0.1017	0.1117	-0.60	-0.34	1.73	1.89
m-Xylene	-0.1098	-0.0851	0.0356	0.0558	-1.85	-1.44	0.60	0.95
o-Xylene	-0.0633	-0.0124	0.0620	0.0984	-1.06	-0.21	1.06	1.70

Table 9: Offsets of calibration curves as they were calculated during the LiOH test. Concentrations in last four columns correspond to the intercepts of curves for LiOH (NaOH) and sample volume 500ml (1000ml) respectively.

In order to identify an influence of individual calibration runs the carbon responses were calculated and analyzed. Figures 34, 35 show carbon responses in (pAs. ppbC^{-1}) as a function of compounds from i-butane to o-xylene. Each figure represents two graphs standing for volume 40ml and 20ml of enriched NPL. There are six data series per substance. First three series are responses measured via 500ml sample volume, series are called 500ml-run1(run2, run3). Analogically, series called 1000ml-run1(run2, run3) were measured via 1000 sample volume. Responses are shown in the same scale from 0.25 up to 0.32. The first Figure 34 shows results of LiOH trap. Second Figure 35 shows results of NaOH trap. Already at the first look, all responses copy similar pattern with lower values for 1,3-butadiene, isoprene, t-2-pentene and c-2-pentene. This is neither affected by LiOH vs. NaOH packing nor sample volume.

**Carbon response of sample volumes 500 ml and 1000 ml for LiOH
40ml of NPL**

**Carbon response of sample volumes 500 ml and 1000 ml for LiOH
20ml of NPL**
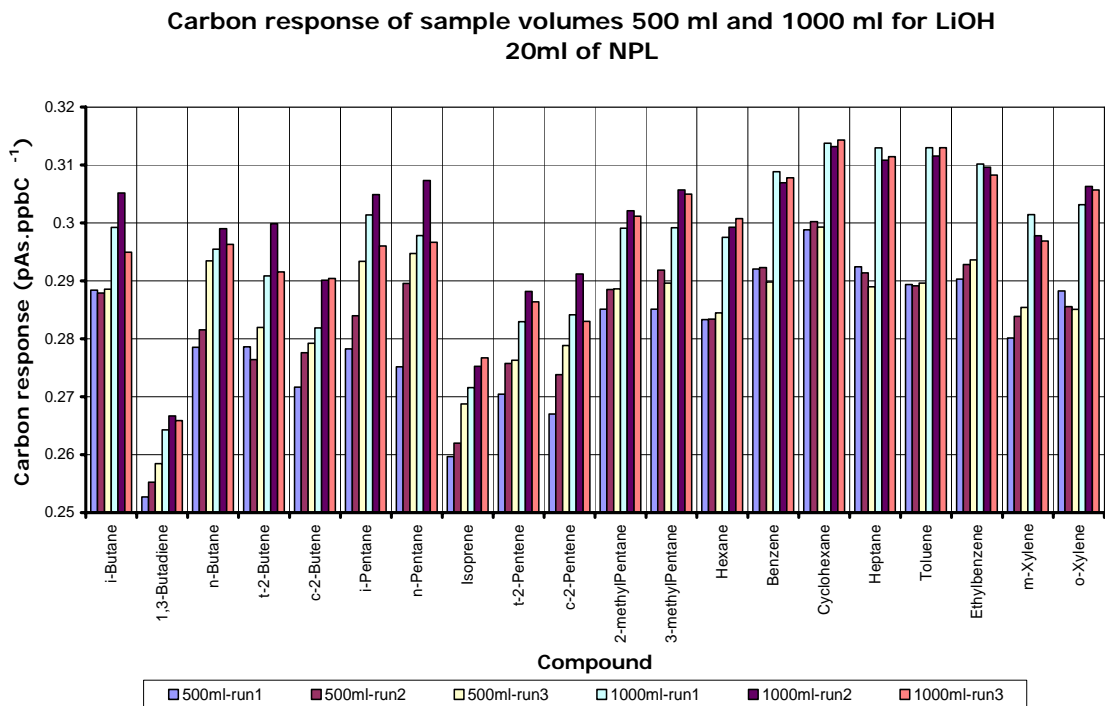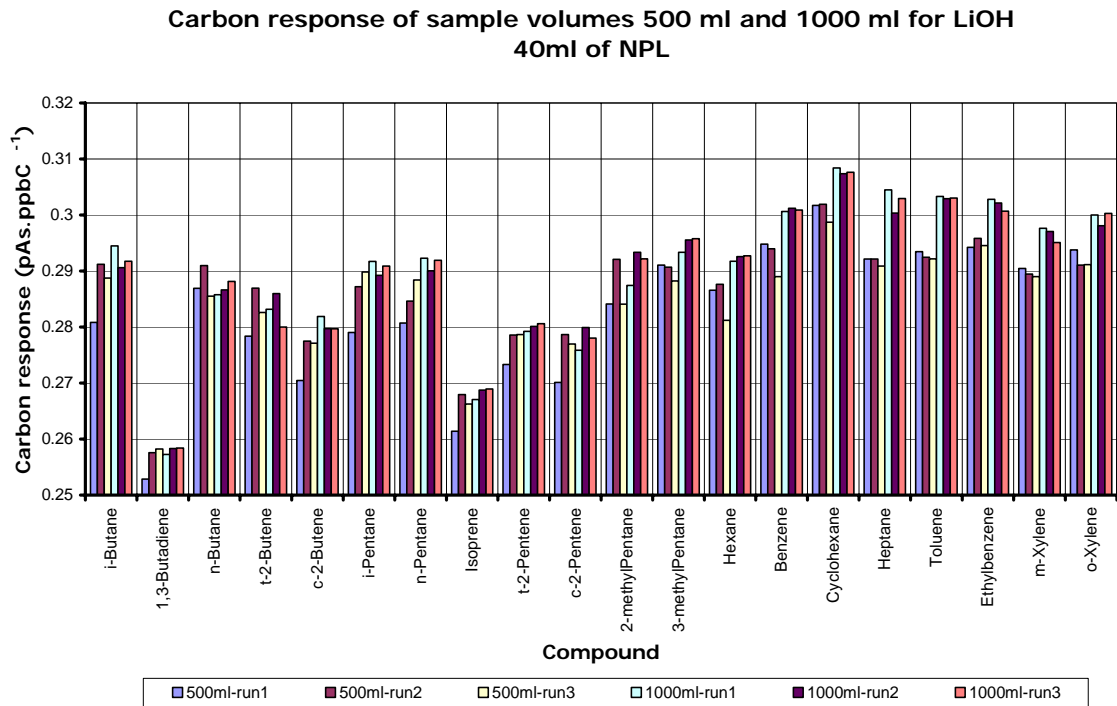
Figure 34: Carbon responses in (pAs.ppbC^{1}) as a function of compounds from i-butane to o-xylene as they were calculated with installed LiOH trap. Upper graph represents sample volume 40ml, lower graph is 20ml.

Carbon response of sample volumes 500 ml and 1000 ml for NaOH
40ml of NPL

Carbon response of sample volumes 500 ml and 1000 ml for NaOH
20ml of NPL
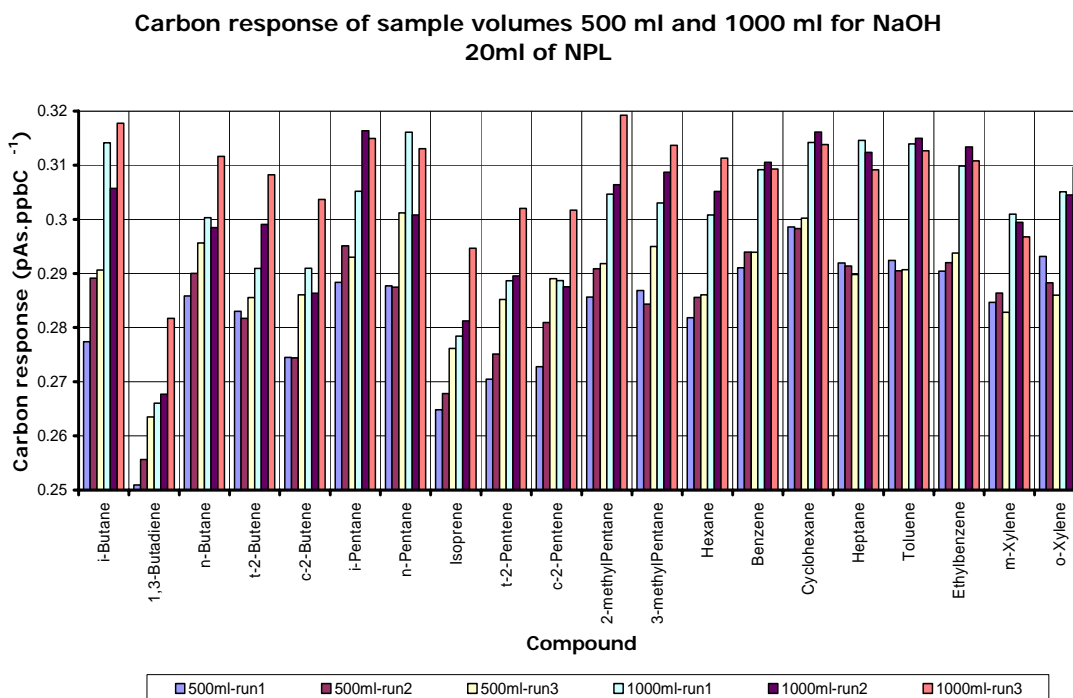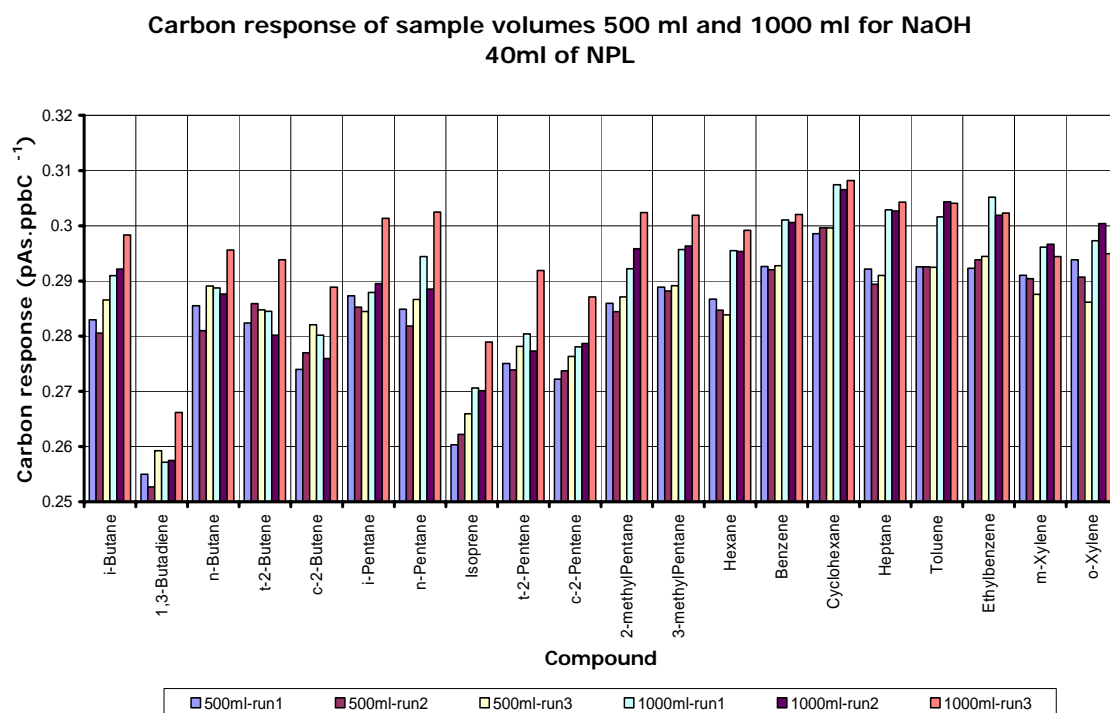
Figure 35: Carbon responses in (pAs.ppbC^{-1}) as a function of compounds from i-butane to o-xylene as they were calculated with installed NaOH trap. Upper graph represents sample volume 40ml, lower graph is 20ml.

Generally, LiOH shows more unified data while NaOH appear to have larger variance in data what suggests differences related to chemical composition of the trap. Runs measured in series do not exhibit trend thus it cannot be said that later runs produce larger responses.

Responses in each graph tend slightly to larger values with less volatile compounds. Deviation of results obtained with 1000ml sample volume from expected pattern (equal to 500ml) is representative for all substances from i-butane to o-xylene irrespective the trap or enriched volume of NPL. Larger deviations for substances from 2-methylpentane to o-xylene in case of enriched 20ml of NPL represent a difference of 0.02 pAs.ppbC^{-1} for both traps, compared to 40ml of NPL it concerns twofold difference. For substances from i-butane to c-2-pentene the effect is not that strong. Remarkable feature is the last data series in case of NaOH trap for both calibration points 40ml, 20ml of NPL. Its response exhibits larger values from i-butane to hexane. Considering the measurement sequence, those two runs represent last two measurements with 1000ml sample volume. After ca. 14 calibration runs (included the very first calibration, i.e. calibration for calibration) it can happen the trap becomes saturated and start releasing NMHCs. Thus from that moment all later runs would produce overestimated responses. Other explanation is simply instrument malfunction. However, important fact is that also the second calibration point (20ml of NPL) exhibited larger values thus en error arosing from using the arithmetic average from all three runs is minimized.

Volatile compounds were analyzed separately. Figure 36 shows carbon responses in (pAs.ppbC^{-1}) as a function of compounds from ethene to propane. Ethyne together with propyne were not considered because they deviate from common response. Ethyne exhibits variations too while propyne deviates so much that its values lay out of the range of the figure. The response range in both graphs was purposely chosen to be equal the range shown in the graphs related to less volatile compounds from i-butane to o-xylene. Graphs stand for calibration runs with LiOH and NaOH. Each of them shows four compounds where each of the compound has 12 data series. Data series represent six runs of the first calibration point 40ml of NPL with 500ml, 1000ml respectively and six runs of the second calibration point 20ml of NPL with 500ml, 1000ml respectively. It is the same situation as with previous figures with less volatile compounds only the series are not split, two calibration points are shown together.

Ethene response exceeds the given range. Propyne response was around 0.1 which is not even a half of the lower range limit. Ethane response lays below the value 0.25, around 0.21, when the sample volume is 1000ml what corresponds to finding in Figure 32.

**Carbon response of sample volumes 500 ml and 1000 ml for LiOH
20ml + 40ml of NPL**

**Carbon response of sample volumes 500 ml and 1000 ml for NaOH
20ml + 40ml of NPL**
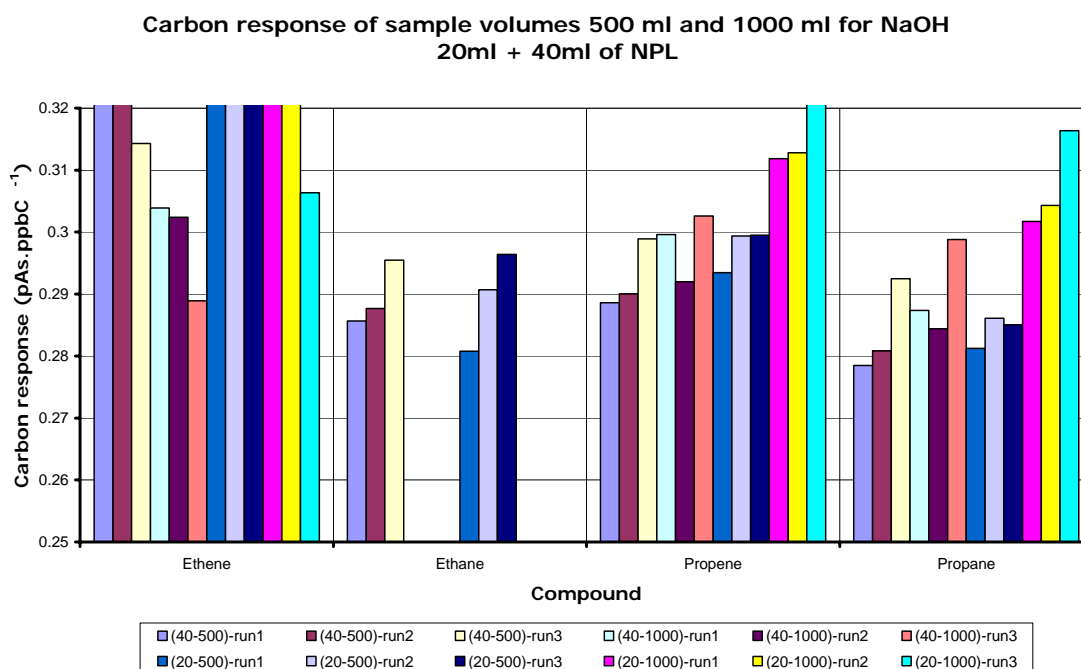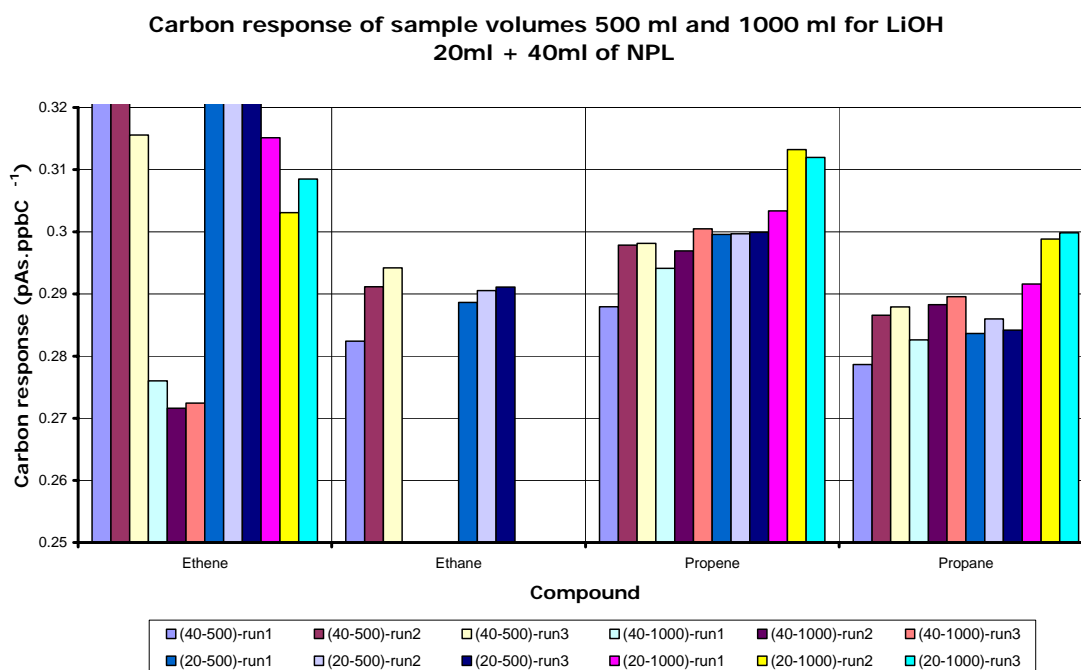
Figure 36: Carbon responses in (pAs.ppbC^{-1}) as a function of compounds from ethene to propane as they were calculated with installed LiOH, NaOH trap. Upper (lower) graph represents volume 40ml, 20ml of enriched NPL via 500, 1000ml sample volume for LiOH (NaOH) trap.

The interesting feature is that the general pattern of overestimation connected to less diluted calibration gas mixture is much less obvious. This effect occurs basically only at the second calibration point 20ml of NPL thus volatility must play role.

To assess the variability in offsets in relation to dilution of calibration gas mixture a difference between intercepts was calculated for each compound. Table 10 shows the differences expressed in carbon response in (pAs.ppbC^{-1}). The intercepts of calibration curves measured via sample volume 500ml were subtracted from intercepts of calibration curves measured via sample volume 1000ml, all separately for LiOH and NaOH trap. All shown differences are positive which demonstrates that the effect of larger offsets for the less diluted gas mixture (1000ml sample volume) is apparent.

Compounds	Intercept$_{1000ml-500ml}$ (pAs)		Carbon response (pAs.ppbC^{-1})	
	LiOH	NaOH	LiOH	NaOH
Ethyne	1.0929	0.9603	0.06031	0.05300
Ethene	0.2315	0.1141	0.02710	0.01336
Ethane	0.0049	0.0462	0.00030	0.00283
Propene	0.0896	0.1622	0.00728	0.01319
Propane	0.1058	0.1859	0.00971	0.01707
Propyne	0.0062	0.0508	0.00081	0.00669
i-Butane	0.0294	0.0785	0.00613	0.01636
1,3-Butadiene	0.1821	0.2285	0.00837	0.01050
n-Butane	0.1017	0.0571	0.01338	0.00751
t-2-Butene	0.0798	0.0769	0.01466	0.01414
c-2-Butene	0.0637	0.1219	0.00592	0.01133
i-Pentane	0.0717	0.0885	0.01032	0.01274
n-Pentane	0.0402	0.0398	0.00725	0.00717
Isoprene	0.1169	0.0701	0.00801	0.00480
t-2-Pentene	0.1992	0.2095	0.00853	0.00897
c-2-Pentene	0.1223	0.0540	0.01019	0.00450
2-methylPentane	0.0980	0.1035	0.00913	0.00964
3-methylPentane	0.1582	0.1746	0.00952	0.01051
Hexane	0.1556	0.1831	0.00823	0.00969
Benzene	0.2628	0.2568	0.00813	0.00794
Cyclohexane	0.2087	0.2158	0.00731	0.00755
Heptane	0.1686	0.1444	0.00995	0.00852
Toluene	0.3710	0.3456	0.01274	0.01187
Ethylbenzene	0.1372	0.1316	0.01009	0.00968
m-Xylene	0.1454	0.1409	0.00861	0.00835
o-Xylene	0.1254	0.1108	0.01127	0.00997

Table 10: Differences in offsets on calibration curves. The differences between offsets (1000ml-500ml) are shown as a carbon response (pAs. ppbC^{-1}).

Variability in the offset-difference may point out the mechanism of the intercept generation. Two mechanisms have not been discussed yet: wrong calibration of flow controllers and not quantitative mixing due to a laminar flow in the dilution device. Both effects, if occurred, would affect the offset difference in the same way irrespective of compound. Thus variances of up to 10 percent (including NPL uncertainties) would be expected. But this is not the case, the differences vary between 20 and 30 percent. Toluene, for instance, has a difference larger by 50 percent than benzene.

In summary, the LiOH test demonstrates how important the concentration of calibration gas mixture compared to expected concentration in sample is. Dilution factor for the calibration does play role as well as the CO_2 trap. A striking feature are negative offsets in case of LiOH for 500ml sample volume. Bearing in mind the traps were not exposed to vacuum their conditioning does play role as well. As the most probable reason for generally positive offsets, as they were observed during made measurements, appear to be combination of memory effects with adsorption losses, eventually pressure transient on VA4.

4.1.3 Uncertainty

Uncertainty of similar systems has two parts, the statistically defined uncertainty and the systematic error. The systematic uncertainty can be estimated only by intercomparing with a proven independent system. In practice, the uncertainty on the measurement result y may arise from many possible sources which may need to be treated separately to obtain the uncertainty contribution alias component from each source. Uncertainty component expressed as a standard deviation is known as the standard uncertainty. Combined standard uncertainty $u_c(y)$, can be obtained by combining all the standard uncertainty components and evaluated using the law of propagation of uncertainty (Taylor, 1997). If there is correlation between any components then this has to be taken into account by determining the covariance (EURACHEM / CITAC Guide CG 4, 2000).

$$u_c(y(x_{i,j\ldots})) = \sqrt{\sum_{i=1,n} c_i^2 \cdot u(x_i)^2 + \sum_{\substack{i,k=1,n \\ i \neq k}} c_i \cdot c_k \cdot u(x_i, x_k)} \qquad (4.12)$$

$$c_i = \frac{\partial y}{\partial x_i} \qquad (4.13)$$

where:

$y(x_1, x_2,\ldots)$ is a function of several parameters

$u(x_i, x_k)$ is the covariance between x_i and x_k

c_i, c_k are the sensitivity coefficients

Combining standard uncertainty components is simplified for models involving only a sum (difference) or product (quotient) quantities like $y = (p+q/r+\ldots)$. The combined standard uncertainty $u_c(y)$ is expressed then as:

$$u_c(y) = y \cdot \sqrt{u(p)^2 + \left(\frac{u(q)}{q}\right)^2 + \left(\frac{u(r)}{r}\right)^2 + \dots} \qquad (4.14)$$

For most purposes an expanded uncertainty U should be used. The expanded uncertainty provides an interval within which the value of the measured variable is believed to lie with a higher level of confidence. U is obtained by multiplying $u_c(y)$ by a coverage factor k which is chosen based on the level of confidence desired. Where the combined standard uncertainty is dominated by a single contribution with fewer degrees of freedom, it is recommended that k be set equal to the two-tailed value of Student's t-statistic for the number of degrees of freedom associated with that contribution. For an approximate level of confidence of 95%, k equals 2.

Uncertainties from linear least squares calibration are calculated according to (4.15), (4.16) (Miller and Miller, 1984). System response y (A_{HSGM}) is calibrated by observing its value as a function of different levels of the analyte x (x_{HSGM}). The most significant for normal practice are random variations in observed value y.

$$u(x_{HS}) = \frac{S_{A/x}}{a_H} \cdot \left(\frac{1}{m} + \frac{1}{n} + \frac{(A_{HS} - \overline{A}_{HSGM})^2}{a_H^{\ 2} \cdot \sum_i \left((x_{HSGM})_i - \overline{x}_{HSGM} \right)^2} \right)^{\frac{1}{2}} \qquad (4.15)$$

$$S_{A/x} = \left(\frac{\sum_i \left((A_{HSGM})_i - \hat{A}_{HSGM} \right)^2}{n} \right)^{\frac{1}{2}} \qquad (4.16)$$

where:

$\overline{A}_{HSGM}$	is the observed response for the centroid
$\hat{A}_{HSGM}$	is the predicted response by calculated regression line
$\overline{x}_{HSGM}$	is the analyte level for the centroid
n	is the number of calibration points on regression line
m	is the number of reading of A_{HS}

Equation (4.15) holds only for regression line where the constants a_{HS} and b_{HS} were determined by un-weighted least squares regression on a set of n pairs values $(A_{HSGM})_i$, $(x_{HSGM})_i$. Such a uncertainty calculation procedure reflect constant uncertainty in y-value and not the uncertainty of the standard gas mixture, nor the inevitable correlations induced by successive dilution from the same NPL standard. The reference values $(x_{HSGM})_i$ may each have uncertainties which propagate through to the final result. Proper regression line in this case would be bilinear regression.

In the first step the uncertainty components were considered as being independent because with the forced origin there is no intercept. The $u_c(y)$ was calculated according to (Mühle, 2002) in order to enable mutual comparison. The combined standard overall uncertainty δx_{Hov} involves already $u_c(y)$ together with the uncertainty of the NPL. It is considered to have two sub-parts coming from measurement and calibration (ISO/IEC, 1999). Uncertainty from calibration δx_{CAL} has two sub-parts again, these are the systematic error of NMHCs mixing ratios in NPL δx_{HSGM} and the uncertainty of calibration function δx_{FUN}. The latter is given basically by the uncertainty of slope defining used calibration function and it already involves uncertainty of dilution factor etc. The combined standard overall uncertainty is expressed then as:

$$\delta x_{Hov} = x_{Hov} \cdot \sqrt{\left(\frac{\delta x_{MES}}{x_{MES}}\right)^2 + \left(\frac{\delta x_{CAL}}{x_{CAL}}\right)^2} = \left(\frac{\delta x_{MES}}{x_{MES}}\right)^2 + \left(\frac{\delta x_{HSGM}}{x_{HSGM}}\right)^2 + \left(\frac{\delta x_{FUN}}{x_{FUN}}\right)^2 \qquad (4.17)$$

where:

δx_{Hov}	is the combined standard overall uncertainty
δx_{MES}	is the uncertainty from measurement
δx_{CAL}	is the uncertainty from calibration
δx_{HSGM}	is the uncertainty of the concentration given by NPL
δx_{FUN}	is the uncertainty from calibration function

Uncertainty of calculated mixing ratio, estimated from equation (4.17), already involves δx_{MES} and δx_{FUN}. The deviation δx_{HS} is mathematically a differential dx_{HS} formed by a sum of partial differentials for each variable (4.18).

$$dx_{HS} = \left[\frac{\partial x_{HS}}{\partial a_H}\right] \cdot da_H + \left[\frac{\partial x_{HS}}{\partial A_{HS}}\right] \cdot dA_{HS} + \left[\frac{\partial x_{HS}}{\partial V_{SGM}}\right] \cdot dV_{SGM} + \left[\frac{\partial x_{HS}}{\partial V_S}\right] \cdot dV_S \qquad (4.18)$$

After substitution we get (4.19).

$$\left(\frac{\delta x_{HS}}{x_{HS}}\right)^2 = \left(\frac{\delta A_{HS}}{A_{HS}}\right)^2 + \left(\frac{\delta a_H}{a_H}\right)^2 + \left(\frac{\delta V_{SGM}}{V_{SGM}}\right)^2 + \left(\frac{\delta V_S}{V_S}\right)^2 \qquad (4.19)$$

where:

δA_{HS}	is the uncertainty of peak area from sample
δa_H	is the uncertainty of slope, offset of calibration curve
δV_{SGM}	is the uncertainty of NPL volume
δV_S	is the uncertainty of sample voume

As mentioned V_{SGM}/V_S is a dilution factor where δV_{SGM} has already been quantified in uncertainty of the slope. In equation (4.18) it is treated as a constant with no

uncertainty. The uncertainty of sample volume cannot be expressed accurately but it can be showed that δV_S is negligible comparing to the above mentioned errors. The expansion volume V_E was determined to be (2558 ± 1.7) ml. Calibration of each FC enhanced the accuracy significantly. The automated flow corrections enhanced the precision of FC0 significantly as well. δV_S is given mainly by the signal integration. δV_S can be calculated as a standard deviation of overall volume measured by the pressure gauge. Even this approach is technically not correct because from the Figure 4 it is clear that it is FC2 what closes the V_E. Consequently, although FC2 reaction time is very short, some small amount of volume gets lost as the pressurized medium tries to escape from V_E when outlet valve is closed. This causes constantly lower values of overall volume and partly makes the standard deviation of repeated values bigger. However, already from measured pressure it can be seen the systematic deviation is in order of permil. For 500 ml overall volume the average was 498.97 which makes 0.087%. For 1000 ml overall volume the average was 994.7 which is 0.1% comparable to error of pressure gauge itself. Considering squaring of this uncertainty and the additional error 1.7 ml of V_E, the V_S uncertainty can be neglected.

The slope uncertainty can be calculated from the calibration linear function which was made using the least squares method in Chemstation (Bhattacharyya and Johnson, 1977).

$$\delta a_H = \delta Area \cdot \sqrt{\frac{N}{N \cdot \sum_{i=1}^{N}\left(x_{HSGM}\right)_i^2 - \left(\sum_{i=1}^{N}\left(x_{HSGM}\right)_i\right)^2}} \qquad (4.20)$$

where:

N is the number of measured value-couples of $(x_{HSGM})_i$ and $(A_{HSGM})_i$

$\delta Area$ is the standard error for the A_{HS} estimate from regression

$$\delta Area = \sqrt{\frac{1}{N-2}\sum_{i=1}^{N}\left(\left(A_{HSGM}\right)_i - a_H - b_H \cdot \left(x_{HSGM}\right)_i\right)^2} \qquad (4.21)$$

The uncertainty of peak area δA_{HS} can be estimated from the calibration curve using a $\delta Area$ and confidence interval along the calibration curve (Mitchell et al., 1977) or δA_{HS} can be calculated as a standard deviation of replicate measurements of typical CARIBIC sample. In an ideal case the uncertainty should be plotted with each calibration curve and for each ppt concentration calculated individually. As this is time demanding, duplicate measurements of the flight # 114-117, TRAC 2, were made. The combined standard overall uncertainty δx_{Hov} is finally calculated as:

$$\delta x_{Hov} = x_{Hov} \cdot \sqrt{\left(\frac{\delta A_{HS}^2}{A_{HS}}\right)^2 + \left(\frac{\delta a_H}{a_H}\right)^2 + \left(\frac{\delta V_S}{V_S}\right)^2 + \left(\frac{\delta x_{HSGM}}{x_{HSGM}}\right)^2} \qquad (4.22)$$

In the appendix A14, A15 are the ppt concentrations of detected compounds for the flight # 114-117. Signal-1 was the Gas-pro column, signal-2 was the Petrocol column. The first table shows absolute differences in duplicate measurements. In A15 are the relative errors of ppt concentrations for all detected compounds. As it can be seen the concentrations of C_2-C_3 are in range of 10-100 ppt except for ethane with much higher concentrations. Even comparing to later CARIBIC samples this set was quite low in all mixing ratios which makes the uncertainties too large. Additionally for this flight the overall enriched volume was only 500 ml what unfortunately enlarges the error as well. 114-117 was the last flight with 500 ml, after that 1000 ml have been used. The uncertainties were calculated as an arithmetic average from canisters 2-13. In A16 is the uncertainty overview for the detected compounds split into three groups of uncertainties: (δx_{MES} + δx_{FUN}), δx_{HSGM} and δx_{Hov}. The individual uncertainties were calculated separately for both columns. The relative uncertainty of NPL standard is in square between one and two orders of magnitude lower than the relative error calculated from calibration equation. The overall relative uncertainty of ppt-concentration lie mostly up to 10%. Mostly the uncertainty for C_2-C_3 is up to (5-7)% which means the peaks are well resolved, well defined and above the detection limit with no considerable uncertainty in integration. From the column x_{HS} (average of measured concentrations) it can be seen how different results it gets from Gas-pro comparing to Petrocol column. Gas-pro produces constantly smaller values which is due to the rest of CO_2.

In the second step the uncertainty was calculated as a confidence interval along the calibration curve using equations (4.15), (4.16) (EURACHEM / CITAC Guide CG 4, 2000). The 6 point calibration was used. The most diluted calibration point represented 10 ml of NPL standard. The most concentrated point was 60 ml of enriched NPL standard. Two calibration points differed from each other by 10 ml of NPL. A17 in the appendix shows measured peak areas (pA.s) and corresponding slopes with their uncertainties. $u_c(y)$ is the combined standard uncertainty. As the A_{HS} the duplicate measurements of the flight #114-117 were used again as in the case of uncertainty calculation in the first step. The combined standard uncertainty $u_c(y)$ corresponds to the combined standard overall uncertainty dx_{Hov} quite well although uncertainty of NPL standard was not included yet, see A16. The Mühle (2002) procedure for the uncertainty calculation takes uncertainty of NPL into account by adding its relative uncertainty in square. The last column dx_{Hov} stands for the combined standard overall uncertainty δx_{Hov} as mentioned above. Only compounds with relatively high concentrations (ethane, propane) deviate in $u_c(y)$ and dx_{Hov} substantially. Substances with low concentrations have minimal difference in both estimates what indicates error

in the calculating procedure thus simple adding of uncertainty of NPL standard alternatively bilinear regression would reflect the uncertainty estimation better.

4.1.4 Detection limit

Detection limit is the smallest concentration of analyte that can be reliably discerned from background measurement noise. One definition by (Skogerboe and Grant, 1970) uses standard deviation of replicate measurements at low concentrations. Detection limit (DL) is defined as follows:

$$DL = \frac{t(n-1,1-\alpha)}{\psi} \qquad (4.23)$$

where:

t(n-1,1-α)   is the student t-statistic for *n* replicates at the given confidence level

ψ is the sensitivity defined as:

$$\psi = \frac{slope}{std(Area)} \qquad (4.24)$$

Sensitivity has the ability to diagnose small variations in the measured property. Slope is determined around the measured range of interest while standard deviation describes variation in the property (peak area). Replicate analyses at a very low concentration can provide the *std(A$_{HS}$)* needed for the estimation of the detection limit. In Table 11 detection limits for the flight 114-117, TRAC2, are calculated. Standard deviations duplicate measurements of area for cylinders 2-13 were used as a *std(A$_{HS}$)*. As the samples had concentrations varying by a factor of 3-4, *std(A$_{HS}$)* were normalized using variation coefficients instead of standard deviations. The mean standard deviation was calculated from mean variation coefficient and the mean concentration. The used relations are below:

$$std(A_{HS}) = \frac{dA_{HS}}{\sqrt{2}} \qquad (4.25)$$

$$VC_{HSi} = \frac{std(A_{HSi})}{Area_{HSi}} \qquad (4.26)$$

$$\overline{VC}_{HS} = \frac{\sum\limits_{i-1}^{n} VC_{HSi}}{n} \qquad (4.27)$$

$$\overline{std}(A_{HS}) = \overline{A}_{HS} \cdot \overline{VC}_{HS} \qquad (4.28)$$

where:

VC_{HSi} is the variation coefficient of hydrocarbon for the i_{th} canister

dA_{HS} is the difference of peak areas for duplicate measurement of the given substance

Because the slope used in sensitivity has an unit of A_{HS}/x_{MES}, it must be multiplied by the factor which has been used to get the final ppt-concentration x_{HS}. Detection limit can be then calculated as:

$$\psi = \frac{slope}{std(Area)} \Rightarrow \psi_{HS} = \frac{\dfrac{A_{HS}}{x_{MES}} \cdot \dfrac{1}{factor}}{std(A_{HS})} = \psi_{MES} \cdot \frac{1}{factor} \qquad (4.29)$$

$$DL_{HS} = \frac{t(n-1,1-\alpha)}{\psi_{HS}} = \frac{t(n-1,1-\alpha) \cdot \overline{std}(A_{HS})}{slope} \cdot factor \qquad (4.30)$$

After the normalization, number of levels of freedom for the *t*-statistic is not 1 as the duplicate measurement suggests anymore but *n*-1 where *n* is a number of canisters in which the hydrocarbon was detected.

Table 11 shows final detection limits with related slopes, overall normalized standard deviations of measured area, overall variations coefficients and the sensitivities from measurement (ψ_{MES}). Not all compounds were detected in every canister thus *t*-statistic column for a confidence interval of 95% (what corresponds to 3 times signal-to-noise ratio) shows tabulated values. Heptane and m-xylene have only 1 level of freedom because they were detected only in two samples which can be seen in the *n*-replicates column. Final detection limits in the last column lie mostly around few ppt with exception of ethane, heptane and m-xylene. The first has much higher concentration far above the detection limit what conflicts with the assumptions of the detected peaks close to DL. The other two compounds suffer from overestimated detection limit due to the small number of measurements. Both were detected only in 2 samples which results in a *t*-statistic of 12.71. In addition, these peaks exhibit asymmetrical peaks suggesting coelution.

Alternatively, the detection limits were estimated using a signal-to-noise (S-N) ratio. With the pre-defined macro in Chemstation, the S-N ratio was calculated for each peak. In Table 12 are the detection limits which were measured based on the individual S-N for each peak. As an example two canisters 2 and 8 are shown. Detection limits can be calculated from the measured signal-to-noise ratio and from concentration in ppt as:

$$DL = \frac{ppt}{\dfrac{1}{3} \cdot (S-N_{ratio})} \qquad (4.31)$$

Detection limits

signal	Name	slope (pA.min/ppt)	std (A_{HS}) (pA.min)	VC_{HS}	sensitivity (ppt)	t-statistic t(n-1,95%)	n-replicates	DL (ppt)
1	Ethane	0.000700	0.1067	0.0247	0.0066	2.20	12	26.8
1	Ethene	0.000612	0.0148	0.0423	0.0413	2.20	12	4.3
1	Ethyne	0.000724	0.0133	0.0618	0.0544	2.20	12	3.2
1	Propane	0.000940	0.0304	0.0295	0.0309	2.20	12	5.7
1	Propene	0.001057	0.0324	0.0585	0.0326	2.20	12	5.4
1	i-Butane	0.001169	0.0289	0.1102	0.0405	4.30	3	8.5
1	n-Butane	0.001175	0.0252	0.0899	0.0466	2.20	12	3.8
1	1-Butene	0.001181	0.0308	0.0931	0.0383	2.23	11	4.7
1	n-Pentane	0.001414	0.0195	0.0635	0.0724	2.20	12	2.4
2	Ethane	0.000552	0.0876	0.0218	0.0063	2.20	12	28.0
2	Propene	0.000830	0.0215	0.0254	0.0386	2.20	12	4.6
2	Propane	0.000758	0.0097	0.0105	0.0778	2.20	12	2.3
2	i-Butane	0.001027	0.0152	0.0325	0.0675	4.30	3	5.1
2	n-Butane	0.001018	0.0162	0.0490	0.0629	2.20	12	2.8
2	n-Pentane	0.001272	0.0204	0.0662	0.0624	2.20	12	2.8
2	Hexane	0.001547	0.0697	0.1105	0.0222	2.37	8	8.5
2	Benzene	0.001612	0.0104	0.0280	0.1550	2.20	12	1.1
2	Heptane	0.001839	0.0428	0.0879	0.0430	12.71	2	23.7
2	Toluene	0.001758	0.0086	0.0388	0.2033	2.37	8	0.9
2	Ethylbenzene	0.001731	0.0469	0.1247	0.0369	4.30	3	9.3
2	m-Xylene	0.001300	0.1313	0.1556	0.0099	12.71	2	102.7
2	o-Xylene	0.001234	0.0323	0.0783	0.0383	2.78	5	5.8

Table 11: Detection limits calculated from the standard deviations of peak area for duplicate measurements of the flight 114-117, TRAC2. Values were calculated separately for both columns, signal 1 stands for the Gas-pro, signal 2 stands for the Petrocol capillary column. Std(A_{HS}) and VC_{HS} are overall averaged standard deviations of peak area and variation coefficients. Detection limit (DL) was calculated from related sensitivities, all for n-replicates alias number of canisters with detected hydrocarbon and corresponding t-statistic.

Detection limits

signal	Name	canister - 2			canister - 8		
		S-N	ppt	$DL_{N=3}$	S-N	ppt	$DL_{N=3}$
1	Ethane	117.3	384.98	9.8	145.1	431.76	8.9
1	Ethene	18.4	60.15	9.8	15	47.49	9.5
1	Ethyne	5.4	19.64	10.9	5.8	29.01	15.0
1	Propane	11.2	46.4	12.4	17.3	64.66	11.2
1	Propene	23.3	41.76	5.4	11.2	25.53	6.8
1	i-Butane				2.4	6.85	8.6
1	n-Butane	6.6	8.76	4.0	7.5	8.8	3.5
1	1-Butene	7	12.41	5.3	4.7	7.25	4.6
1	n-Pentane	3.2	5.02	4.7	7.8	13.12	5.0
2	Ethane	674.1	426.91	1.9	1339.1	518.3	1.2
2	Propene	191.6	81.88	1.3	139.1	67.67	1.5
2	Propane	76.9	48.52	1.9	83.8	76.2	2.7
2	i-Butane				N	5.52	
2	n-Butane	15	10.68	2.1	13.3	11.57	2.6
2	n-Pentane	10.8	6.26	1.7	18.2	15.18	2.5
2	Hexane	13	6.3	1.5	9.9	3.7	1.1
2	Benzene	41.9	16.65	1.2	26.4	22.84	2.6
2	Heptane	6.3	4.53	2.2			
2	Toluene	17.5	6.37	1.1	10.6	6.44	1.8
2	Ethylbenzene	15.9	7.01	1.3	8.7	3.94	1.4
2	m-Xylene	N	5.73				
2	o-Xylene	9.4	7.54	2.4	7.7	5.22	2.0

Table 12: Measured detection limits (DLs) at two canisters 2 and 8 of the flight # 114-117, TRAC2. S-N values were measured separately for both columns, signal 1 stands for the Gas-pro, signal 2 stands for the Petrocol capillary column, ppt is calculated concentration. $DL_{N=3}$ is detection limit for ratio S-N= 3. N stands for detected peak but its asymmetry disabled to measure S-N.

All peaks found in canister 2 and 8 were well detected although their S-N is sometimes smaller than 10. Comparing of DLs from Table 11 with those in 12 show mostly comparable values with Table 12 tending to smaller values. We believe the latter ones, obtained from the directly measured S-N ratios, to be more realistic ones. Comparison of DL from Gas-pro and Petrocol columns in both tables also suggests that better DLs are achieved for Petrocol column. This is caused probably by three reasons. The first is simply 2-3 larger noise at Gas-pro, than at the Petrocol column. In addition, Gas-pro peaks tend to tail. At last, the FID response at Gas-pro seems to be suppressed by the presence of CO_2.

4.1.5 Intercomparison

Accuracy of a system can be assessed by comparison with independent measurements. The developed system was compared to other one which employed similar technique of enrichment, GC separation but detected the NMHCs by MS. Two intercomparisons were made: a) an informal one in October 2003 and b) a blind one in March 2006. In both cases the intercomparisons were made using CARIBIC whole air samples.

Compared systems, presented GC-FID and GC-MS (Mühle, 2002), differenced mainly in detection. GC-MS system was HP 6890 with quadrupole mass-spectrometer HP 6973. The principle of enrichment was similar, as an enriching fill the glass beads in LN_2 were used.

This system did not use focusing of the sample; the enriching trap was used as a focusing trap at the same time. The GC separation was made only on one PLOT Al_2O_3/KCl Chrompack column. Amount of sample that was enriched was 600 ml. Calibration of GC-MS system was made using 1ml loop which served as a measure of volume. Calibration function was linear curve made of 5 points with different standard gas mixture. The samples in stainless steel canisters were analyzed immediately after the sampling using a GC-MS technique described by (Mühle, 2002) and the rest was stored at -20 °C.

Intercomparison in October 2003 was made at an early stage of the technique development of the GC-FID system. Calibration was made only with one point and the standard gas mixture, NCAR, was injected directly without any dilution. FID detector used different flows of all gases, temperature during enrichment was not controlled and integration of volume was not implemented. 2 CARIBIC whole air samples were selected: WAS 37-5 and 38-5, from flights #37 in July 2001 and #38 in August 2001. Additionally to immediate post-flight analysis the samples were measured after storage

in October 2003 by GC-MS, and independently by the here described GC-FID system at about the same time. Contrary to the second comparison in March 2006, alkenes were measured in addition to alkanes. Alkenes were not normally reported for GC-MS analyses because they did not pass the plausibility tests. Alkenes are too high for CARIBIC samples because of storage artefacts (Mühle, 2002). However, for this comparison it is meaningful because analyses were made at the same time. The results are summarized in Tables 13, 14. Alkenes are shown separately. Analyses made by GC-MS-A were made immediately after the flight, GC-MS-B were made during the comparison. The enriched amount of sample was 600 ml for both systems. Concentrations of system GC-FID were averaged for both signals of Gas-pro and Petrocol. STD(GC-MS) stands for the standard deviation of the GC-MS system as it was determined before this comparison (on repeated measurements) while STD(GC-FID) stands for standard deviation of duplicate measurements of the GC-FID during this comparison.

Results show generally good agreement in most alkanes and alkenes. The exceptions are propane, benzene, ethyne, i-butene, trans-2-butene and cis-2-pentene. Although propane measured by GC-FID in the WAS 37-5 sample has ca. 20% higher concentrations, ethane is on the other side in perfect agreement for which there is no reasonable explanation. 2-methylbutane and cyclohexane are overestimated by GC-FID system which suggests problems with either coelution or misidentification, especially considering early stage of development. There has not been determined detection limit for 2-methylbutane. Based on the detection limit of pentane (ca 2.5 ppt) on GC-FID with Petrocol column the measured concentration of 2-methylbutane was just above, especially considering lower limit of detection due to enriched 600 ml only, so probable integration error overestimated its concentration. Difference in benzene concentration might be explained by large uncertainty in measurements by GC-MS. From alkenes it is i-butene which has much higher concentrations at GC-MS which was attributed to contamination for the GC-MS system.

Higher concentration of c-2-penetene suggests contamination at GC-FID on the other side. STD(GC-FID) of t-2-butene shows problem with identification which does not occur in the second sample WAS 38-5. Sample WAS 38-5 shows even better agreement for most of the compounds. Propane at GC-FID has ca. 15% higher concentrations again. As expected 2-methylbutane was not with GC-FID detected at all. Benzene is in agreement to the first measurement GC-MS-A. t-2-butene and c-2-pentene is overestimated again.

WAS 37-5

Compounds	concentration GC-MS-A (ppt)	concentration GC-MS-B (ppt)	STD (GC-MS) (ppt)	concentration GC-FID (ppt)	STD (GC-FID) (ppt)
Ethane	415.32	390.0	13.75	393.29	19.59
Propane	34.57	41.1	0.85	51.89	3.06
n-Butane	5.72	14.5	0.45	13.86	1.06
n-Pentane	3.32	10.9	0.43	9.18	0.38
n-Hexane	5.22	8.2	0.61	8.89	0.45
2-Methylbutane	1.29	2.2	0.23	6.42	0.93
Cyclohexane	0.00	0.6	0.41	6.87	0.15
Acetylene	28.20	25.7	0.75	34.20	3.46
Benzene	39.88	34.5	3.95	19.19	0.12
Ethene		441.6		454.24	36.74
Propene		272.1		257.46	7.16
trans-2-Butene		6.1		17.62	15.00
1-Butene		80.8		66.29	0.59
i-Butene		198.6		14.18	1.87
cis-2-Butene		5.1		3.42	0.02
trans-2-Pentene		1.7		1.49	0.03
cis-2-Pentene		1.2		27.61	0.09

Table 13: Comparison of the presented system GC-FID and the other GC-MS (Mühle, 2002) made at WAS 37-5 CARIBIC sample of the flight #37 in July 2001. Alkenes are shown separately. GC-MS-A, GC-MS-B stands for immediate post flight analysis and comparison in October 2003 respectively. The enriched amount of sample was 600 ml for both systems (GC-FID + GC-MS).

WAS 38-5

Compounds	concentration GC-MS-A (ppt)	concentration GC-MS-B (ppt)	STD (GC-MS) (ppt)	concentration GC-FID (ppt)	STD (GC-FID) (ppt)
Ethane	542.85	514.01	13.75	516.33	27.24
Propane	80.46	83.12	0.85	93.02	3.89
n-Butane	9.56	11.48	0.45	11.74	1.19
n-Pentane	3.32	4.44	0.43	4.89	1.23
n-Hexane	2.62	2.68	0.61	3.96	1.01
2-Methylbutane	1.58	1.94	0.23		
Cyclohexane	0.00		0.41	10.80	0.63
Acetylene	70.88	80.92	0.75	79.33	4.39
Benzene	31.77	57.92	3.95	27.50	2.90
Ethene		249.19		224.40	11.86
Propene		124.05		125.04	8.08
trans-2-Butene		4.18		16.87	1.37
1-Butene		44.96		46.42	2.65
i-Butene				11.29	2.09
cis-2-Butene		1.36		3.07	0.83
trans-2-Pentene		1.62		1.60	0.30
cis-2-Pentene		0.71		13.50	0.75

Table 14: Comparison of the presented system GC-FID and the other GC-MS (Mühle, 2002) made at WAS 38-5 CARIBIC sample of the flight #38 in August 2001. Alkenes are shown separately. GC-MS-A, GC-MS-B stands for immediate post flight analysis and comparison in October 2003 respectively. The enriched amount of sample was 600 ml for both systems (GC-FID + GC-MS).

For the formal blind intercomparison in March 2006, 8 whole air samples from flights # 43 in February 2002 and # 47 in April 2002 were selected, WAS 47-4, 47-5, 47-6, 47-7, 47-8, 47-11, 47-12, and WAS 43-5, 43-10. Samples were analyzed immediately after the sampling by technique of (Mühle, 2002) - only alkane, ethyne and benzene data reported. Rest of the samples was stored at -20 °C.

The samples for the intercomparison were selected by an independent person to cover the concentration range usually encountered in CARIBIC samples. The identity of the samples was disclosed only after the delivery of the analyses results. The results are summarized in Table 15. GC-FID system measured some of detected compounds simultaneously on two columns, Gas-pro and Petrocol. For each canister two signals standing for Gas-pro and Petrocol columns are shown as 1 and 2 respectively. The values marked grey stand for apparent outliers. Four obvious discrepancies in ethane, propane, benzene and hexane are coming from one sample WAS 47-11. The respective chromatograms were inspected and no irregular features were found. The reasons are not know, possible reason may be too high temperature of enrichment.

Comparison		Was 47-4 (ppt)		Was 43-10 (ppt)		Was 43-5 (ppt)		Was 47-11 (ppt)		Was 47-12 (ppt)		Was 47-6 (ppt)		Was 47-7 (ppt)		Was 47-8 (ppt)	
Compounds	System\Signal	1	2	1	2	1	2	1	2	1	2	1	2	1	2	1	2
Ethane	GC-FID	909.3	919.5	774.6	821.1	960.9	962.5	174.8	182.5	153.9	162.8	1174.4	1205.1	1171.0	1194.1	872.9	918.8
	GC-MS	833.9		721.6		893.7		867.6		131.8		1009.0		1038.8		769.7	
Ethyne	GC-FID	96.7		11.0		9.7						70.7		81.6		69.3	
	GC-MS	208.8		92.0		114.4		257.4				200.1		177.1		162.7	
Propane	GC-FID	80.4	81.1	95.4	99.2	188.0	185.6	25.3	26.1	19.2	22.5	203.1	210.3	207.6	207.8	81.5	84.5
	GC-MS	82.8		103.6		197.6		94.7		21.8		206.6		208.9		85.6	
i-Butane	GC-FID	5.9	6.1	7.8	6.7	18.7	17.6	4.8				17.1	17.7	19.4	18.6	6.0	6.3
	GC-MS	4.9		6.1		18.5		5.1				20.2		19.2		5.7	
n-Butane	GC-FID	11.5	12.7	11.5	12.3	32.3	33.5	10.9	10.1	8.5	8.6	40.6	43.0	40.2	42.2	11.3	11.6
	GC-MS	11.2		11.7		32.8		12.5		8.0		45.0		41.9		13.7	
i-Pentane	GC-FID		2.4				6.9						8.9		8.5		2.4
	GC-MS	1.7				6.2						9.0		9.0		2.9	
n-Pentane	GC-FID			3.1	3.8	7.4	7.8			6.4	6.1	9.6	10.5	9.3	9.6	4.3	4.4
	GC-MS			3.7		7.3				5.8		10.7		9.3		4.8	
Benzene	GC-FID		54.6		30.0		50.5		28.7		31.4		60.3		57.3		52.9
	GC-MS	61.0		35.9		49.2		63.6		22.2		59.4		57.8		52.5	
Hexane	GC-FID		3.1				3.5		8.7		5.5		3.4		3.5		3.3
	GC-MS	2.8				3.6		2.4		5.6		4.0		3.2		4.7	

Table 15: Comparison of the presented system GC-FID and the other GC-MS made at 8 CARIBIC WAS- samples. Simultaneous detection with the GC-FID stands for Gas-pro (1) column and Petrocol (2) column. Outliers are grey shaded. The enriched amount of sample was 600 ml (GC-MS) and 1000 ml (GC-FID).

Rest of the data was compared using orthogonal regression (York, 1966). Opposite to the ordinary least square fit, the orthogonal regression takes into account uncertainties of both, dependent (GC-FID) and independent (GC-MS) variable. Each variable (ppt-concentration) is equally subject to the random error. The error is measured perpendicular to the regression plane which is invariant under a change of slope. Uncertainties of the GC-FID system used here were calculated in chapter 4.1.3. Uncertainties of the GC-MS measurements were calculated individually for each compound. An arithmetic average from the given uncertainties was used during this

comparison. Because there was not any uncertainty determined for i-pentane in case of GC-FID the uncertainty of GC-MS measurement was used. Result of orthogonal linear regression is calculated slope, offset and correlation coefficient, first two with its uncertainties. The results of this technique are presented in Table 16. In an ideal case of identical measurements by both systems the slope would be 1 and the offset 0. Slope larger than one means that the GC-FID system provides systematically higher concentrations than the GC-MS system, i.e. the higher concentration the more overestimated value. Offsets differing from 0 mean that the systems vary constantly from each other no matter the measured value.

Comparison									
Compounds	Signal	Uncertainty GC-FID (ppt)	Uncertainty GC-MS (ppt)	Slope (counts/ppt)	Offset (ppt)	Corelation coefficient R^2	Number of pairs N	Significance	
								slope %	offset %
Ethane	1	18.47	34.4	1.134±0.044	-14.67±36.09	0.9962	7	≥ 99.9	< 95
	2	22.59		1.149±0.057	-2.28±46.78	0.9938	7	≥ 99.9	< 95
Ethyne	1	1.81	15.6	0.834±0.135	-76.12±22.24	0.9461	6	95 ∼ 99	≥ 99.9
	2								
Propane	1	2.77	4	0.994±0.044	-3.77±2.73	0.9991	7	< 95	95 ∼ 99
	2	2.49		0.990±0.029	-0.94±4.29	0.9978	7	< 95	< 95
i-Butane	1	1.44	1.1	0.892±0.075	1.23±1.00	0.9823	7	99 ∼ 99.9	95 ∼ 99
	2	0.54		0.846±0.039	1.64±0.55	0.9958	6	≥ 99.9	≥ 99.9
n-Butane	1	1.06	1.3	0.935±0.034	0.18±0.89	0.9961	8	99 ∼ 99.9	< 95
	2	0.68		0.994±0.042	-0.23±1.10	0.9947	8	< 95	< 95
i-Pentane	1	0.5	0.5						
	2			0.948±0.096	0.38±0.62	0.9848	5	< 95	< 95
n-Pentane	1	0.48	1.4	1.005±0.109	-0.28±0.80	0.9763	6	< 95	< 95
	2	0.54		0.994±0.065	-0.06±0.48	0.9919	6	< 95	< 95
Benzene	1		3.2						
	2	0.82		0.914±0.146	4.03±7.29	0.9344	7	< 95	< 95
Hexane	1		0.5						
	2	0.13		1.076±0.338	-0.55±1.38	0.7784	6	< 95	< 95

Table 16: Comparison of the GC-FID and the GC-MS system using orthogonal regression. Regression parameters are shown separately for both signals of Gas-pro (1) and Petrocol (2).

Generally, there is a good agreement between the GC-MS and the GC-FID measurements. Slopes are not significantly different from 1 for five components. Offsets are not significantly different from 0 for 6 components. In addition, slope for n-butane on Petrocol column is not significantly different from 1 as well as offset for propane on Petrocol column is not significantly different from 0. Both systems are well correlated with R^2 mostly above 0.97. Number of pairs of measurements is the same for both signals except for i-butane which was not detected on both columns in canister WAS 47-11. The significance of deviation of slopes from 1 and offsets from 0 was tested using a modification of general *t*-test for dependent means, for significance of difference between an average and a fixed value (Kaiser and Gottschalk, 1972). Both regression parameters were calculated from pairs of values where each pair had principally the same weight. It means that the slope, respectively offset, are already

means. Calculated uncertainty then becomes a standard deviation used in the test. The significance of the differences is given in the two last columns.

Most of the slopes are below 1. Significant differences in slope have: ethane, ethyne, i-butane and n-butane where only ethane exhibits difference on both columns. Slopes for ethane are above 1. Problems with dilution are not possible because it would affect other gases to the same extent. The most probable is non-quantitative enrichment. Calibration still differs from measurement thus it does not cancel this effect. Ethyne and n-butane have different slopes only on Gas-pro which suggests problems with CO_2 and suppressed signal of FIDA. In case of ethyne its reactivity may play role too. On the other side i-butane has significantly different slope on Petrocol column and partly on Gas-pro as well. Both slopes are one of the smallest. Possible reason may be contaminants or memory effects although the latter effect would be detectable for large compounds as well. In this case it is possible that GC-MS system did not measured well.

Significant differences in offset have ethyne, i-butane and propane. Offset is biggest for ethyne, -76.12. Already at the first look, all ethyne concentrations are several times lower. Considering their absolute value the offset makes over 100% difference which is caused by systematic error connected to Gas-pro column. The only reasoning can be a serious difference between ethyne calibration and ethyne measurements. Propane has slight negative significant offset only on Gas-pro column thus signal suppression via CO_2 is believed to be the reason. i-butane has problems with offset on both columns, the offsets are positive thus contamination is possible. Another reason may be underestimated uncertainty of i-butane concentration which consequently underestimate uncertainties of both parameters, slope and offset.

Except for hexane all compounds are well correlated. R^2 equals 0.78 together with hexane concentrations suggest problem with the detection limit. Looking at the hexane detection limit and the measured concentration clearly shows that hexane was hardly detected.

In conclusion, majority of slopes and offsets do not vary from the expected values. Both intercomparisons demonstrate that almost all NMHCs on Petrocol column can be reliably measured by the newly developed technique. Generally, it is Gas-pro column which produce worse results.

4.1.6 Influence of CO₂ and humidity

As mentioned in above chapters, presence of CO_2 in the sample results in suppression of the FIDA signal relatively to the calibration gas mixture which does not

normally contain CO_2. During the measurements of CARIBIC samples it was observed that the concentration of more volatile compounds measured on the Gas-pro column was lower by few percents up to tens of percents than that measured on the Petrocol column. Both columns detect ethane, propane, propene, i-butane, n-butane, propyne and n-pentane. To demonstrate how this effect influence the results in relation to CO_2 trap, the calibration before CARIBIC measurements and afterwards was repeated. First symptom of CO_2 presence is negative peak on Petrocol appearing before the very first peak of coeluted ethene and ethyne as shown in Figure 37 with four calibration chromatograms.
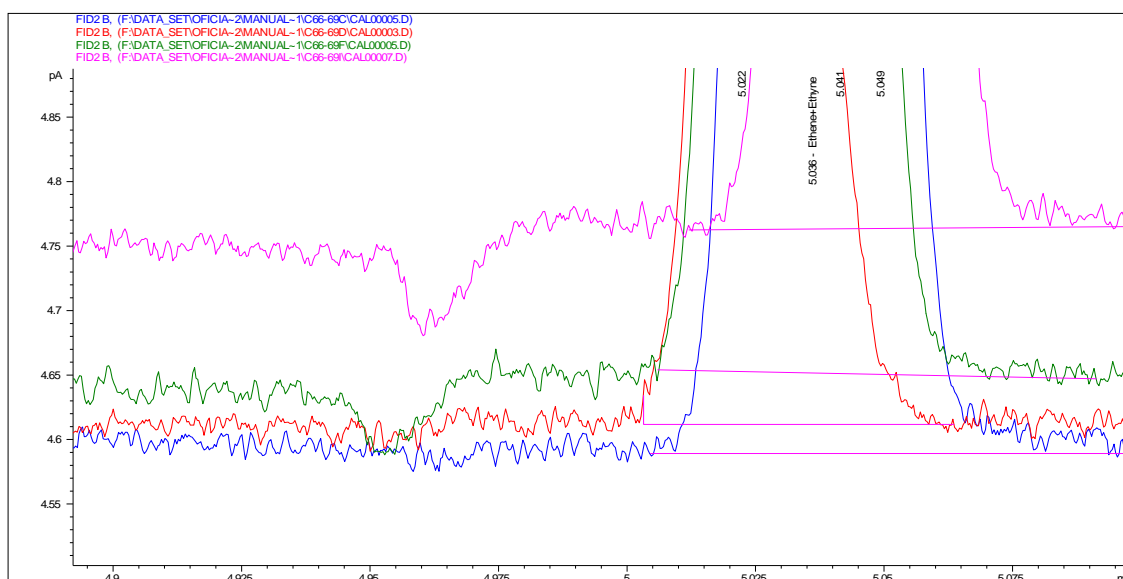
Figure 37: Four calibration runs demonstrate the appearance of the negative peak due to breakthrough of CO_2 through the CO_2 trap. Calibration runs before (blue) and after (red) the analyses of 28 CARIBIC samples do not suffer from these symptoms. Next two runs (green, purple) were made at the same conditions after 7L of diluting air were blown through the trap between the first after-calibration (red) run and the second after-calibration (green) run. Before the last, third, after-calibration (purple) run 7L of diluting air passed the CO_2 trap again.

Calibration runs made before (blue) and after (red) the measurements of 28 CARIBIC samples have no negative peak while during the runs made even later (green, purple), after another 7L of diluting air passed through the CO_2 trap, the negative peak appears and increases. The dip in baseline negative peak is deeper for the later run suggesting that it increases with the amount of carbon dioxide which passed the trap. The latest run (purple) exhibits the deepest dip in the baseline.

The degree of the suppression is shown in Figure 38. Both graphs show common substances detected in CARIBIC samples. Propyne is hardly detectable and coelute slightly with 1-butene on Gas-pro which makes the quantification inaccurate.
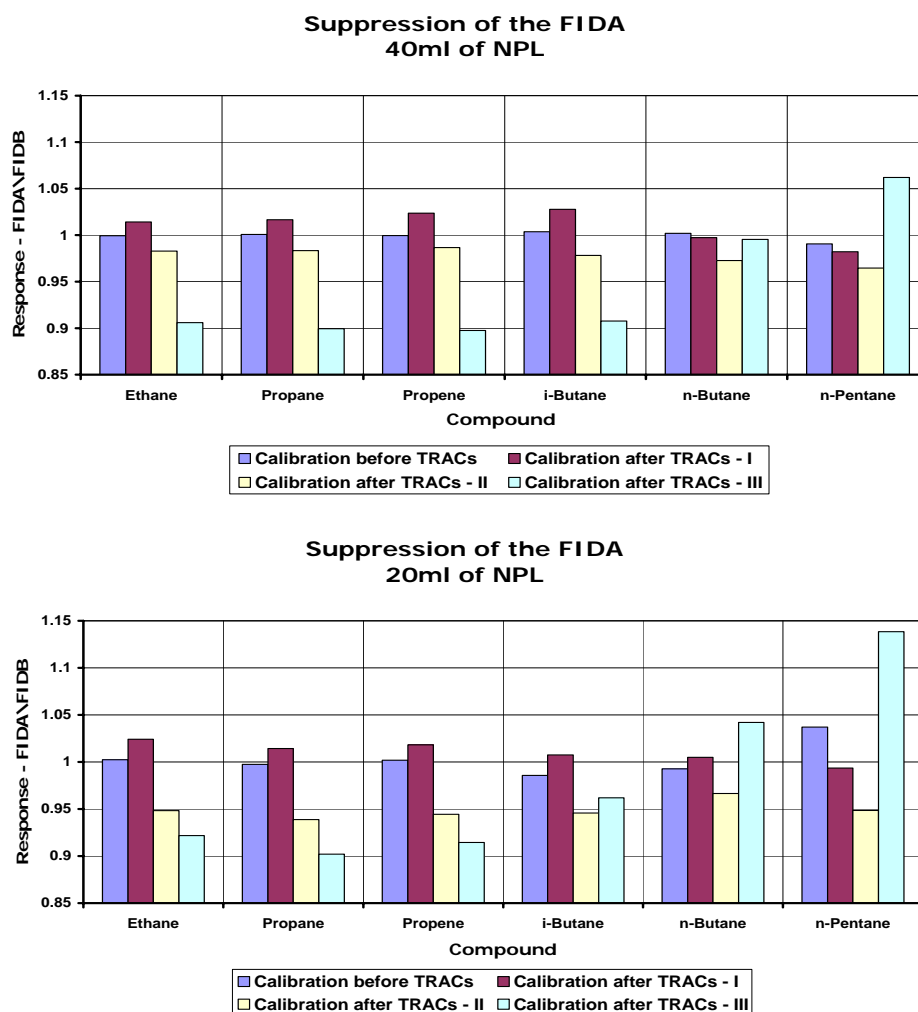
Figure 38: Quantification of the suppression effect for the 40ml (upper graph) and 20ml (lower graph) of NPL. Response was calculated as a ratio of ppt-concentration for FIDA\FIDB. Between each of the three after-calibration runs (I, II, III) 7L of diluting air passed the CO_2 trap.

Both graphs are showing response calculated as a ratio of ppt concentration for Gas-pro and Petrocol, FIDA\FIDB, as a function of calibration run for ethane, propane, propene, i-butane, n-butane and n-pentane. Responses were calculated for each calibration point corresponding to injection of 40ml, 20ml of NPL. Altogether four calibration runs were made. The first calibration (blue bar) was made just before the flight #166-169 from October 2006, the flight was evaluated according to this run. The next three calibration runs (red, yellow, sky-blue), named as I, II, III, were made after the measurements of CARIBIC samples, i.e. after passing of 28L of air. Between runs I and II, another 7L of diluting air passed the CO_2 trap as well as between runs II and III.

The first calibration (blue bar), follows the expected ratio of unity for both calibration points very well. The first calibration after analyses of CARIBIC samples, I (red bar), is

slightly above unity for all compounds and for both calibration points. The difference from unity is relatively small (1-2)% thus potential trend is inconclusive. The second calibration after analyses of CARIBIC samples II (yellow bar), exhibits losses in response particularly for the second calibration point (20ml). These runs were accompanied with the negative peak syndrome as the first, see the chromatogram in Figure 37. The response is smaller by (2-3)% for 40ml point and by 6% for 20ml point. It means the suppression of FIDA is not only dependent on amount of carbon dioxide and the given substance but also on the substance concentration. Provided that suppression effect occurs already during the analysis of CARIBIC sample, the difference in concentration produced by both columns will not be equal for the given compound but will deviate with varying concentration. Before the third calibration after analyses of CARIBIC samples, III (sky-blue bar), source of hydrogen had to be changed several times because of malfunction of the H_2 generator what led to contamination of system. This is probable reason for opposite behavior of n-butane and n-pentane. However, the suppression for ethane, propane, propene and i-butane by about 10% is apparent.

Analyses of the samples from flight #166-169 demonstrate that chromatograms of the TRAC1, which were measured after the TRAC2, tend to have negative peak in baseline within time as the amount of passing air was increasing. Figure 39 shows this trend. Three chromatograms represent canister 1 (blue), 7 (red) and 14 (green) of the TRAC1.
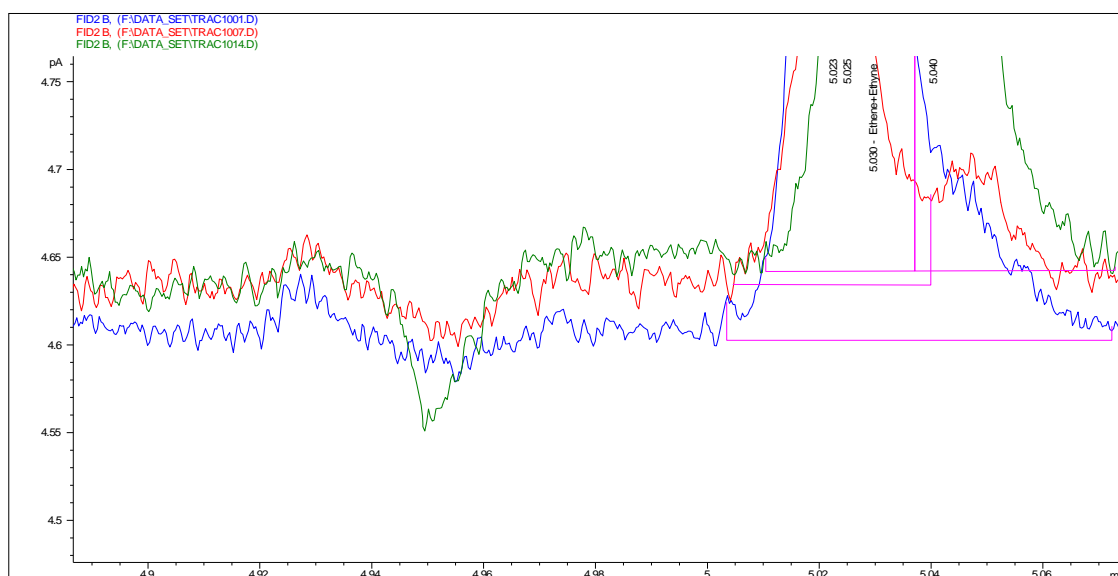
Figure 39: Three chromatograms representing canisters 1(blue), 7(red) and 14(green) of the TRAC1, flight #166-169. The dip in baseline is deeper for later analyzed canisters.

The 14th canister has negative peak comparable to calibration run III. Although the first calibration I does not suffer from these symptoms, the effect is obvious during the

TRAC1 analysis. It suggests other effect participating in absorption of carbon dioxide. Most probable is the moisture. CARIBIC samples are very dry comparing to the diluted calibration mixture thus lower moisture implies less effective removing of CO_2. Moisture in the calibration mixture comes from the diluting air using to dilute the NPL standard gas mixture.

Development of the suppression of ethane is documented in Figure 40. From the 7th canister the trend is obvious. Constantly lowered response reach a difference of almost 15% for the canister 14.

Suppression of ethane during the TRAC1 analysis, flight #166-169
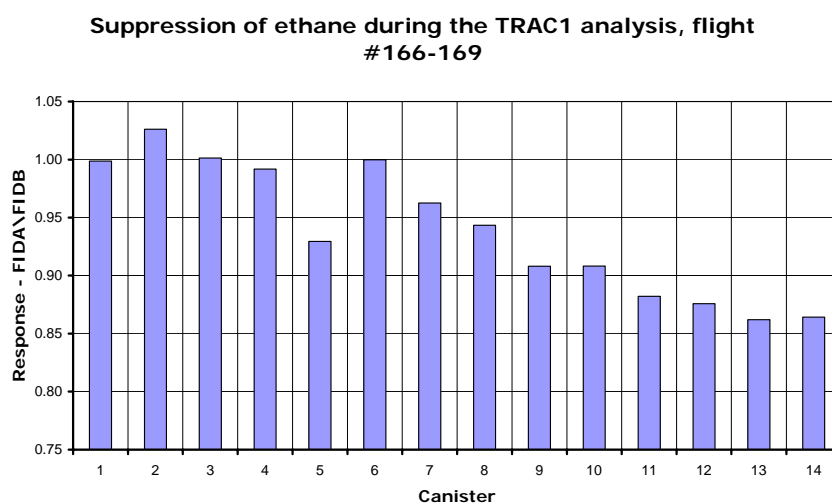
Figure 40: Development of the suppression for ethane. Response was calculated for each canister analysis. From the 7th canister the tendency to lower responses is obvious.

In summary, signal suppression of the FID at the outlet of the Gas-pro column makes the measurements with the Gas-pro column unreliable. Reduced response was observed for almost all compounds detected on Gas-pro. Apart from its dependency on amount of breakthroughed CO_2, the extent of this effect seems to be dependent on amount of detected substances as well. In the course of the instrument development the NaOH trap was replaced with LiOH trap. The capacity of the LiOH trap was estimated to be at least twice as larger than NaOH. The analyses of samples from the flights #166-169 show the absorption of CO_2 is not quantitative even with the LiOH trap although its capacity exceeds consumption of sample several times. Probable reason of the breakthrough of CO_2 is lack of water in CARIBIC samples. Considering short period during which the sample reacts with the packing of the trap, the kinetics may be influenced by the water content.

In further CARIBIC data processing the Gas-pro results, except for ethyne and ethene, have not been taken into an account.

4.1.7 System stability

Stability of the system over longer periods was checked using carbon responses for the calibration runs and, independently, by repeated analyses of the working standard. The calibration runs were successful for the flights # 114-117, 130-133, 166-169, and run during the comparison, linearity and the LiOH tests. The consecution of the tests was: linearity test in November 2004, flight # 114-117 in June 2005, flight # 130-133 in December 2005, comparison test in March 2006, LiOH test in August 2006 and flight # 166-169 in November 2006.

Response of each compound in the NPL standard was recalculated into the carbon response for pptC ($pAs.pptC^{-1}$). Figure 41 shows carbon response factors for each calibration point separately. Altogether 26 substances are shown. Ethyne and ethene are results from Gas-pro column while the rest is from the Petrocol column. Table 17 lists identification numbers of all substances presented in Figure 41.

Carbon responses of the second calibration point (20 ml of NPL) were multiplied by factor of 2 to have the same scale as those of the first one. Both calibration points show very uniform carbon responses of larger compounds with a tendency to overestimate the 20 ml of NPL point by 2-3%. Responses of lighter compounds with double and triple bonds differ more. Ethyne (substance 1) for the 20 ml of NPL exhibits generally smaller response than for 40 ml of NPL. Substances with double bond on the other side, ethene (substance 2) and propene (substance 4), exhibit for the 20 ml of NPL larger response than for 40 ml of NPL. Ethane (substance 3) and propane (substance 5) agree very well for both points, 20 ml and 40 ml of NPL. Propyne (substance 6) shows good agreement as well although its constant loss in response is obvious.

Carbon responses of the linearity test are generally smaller than all others. At that time (November 2004), the FIDs worked with lower flow rates of H_2, air and make up gas which led to a lower sensitivity by ca. 20%. The second smaller responses exhibit the series of the flight # 114-117 which is ca. by 10% smaller comparing to runs made later. These two data series differ significantly from later runs in decreasing response starting from heptane (compound 22). This effect is probably due to higher losses of less volatile compounds on the two-stage pressure regulator (Air liquide) used with NPL cylinder (Slemr et al., 2002). Later calibrations were all made using one-stage pressure regulator (Scott specialty gases).

The best agreement exists among data series of comparison test, LiOH test and the flight # 166-169, their responses vary within 3-5%. Reason for generally lower response of the flight # 114-117 is not clear. The most probable are losses during flushing of the enrichment trap.
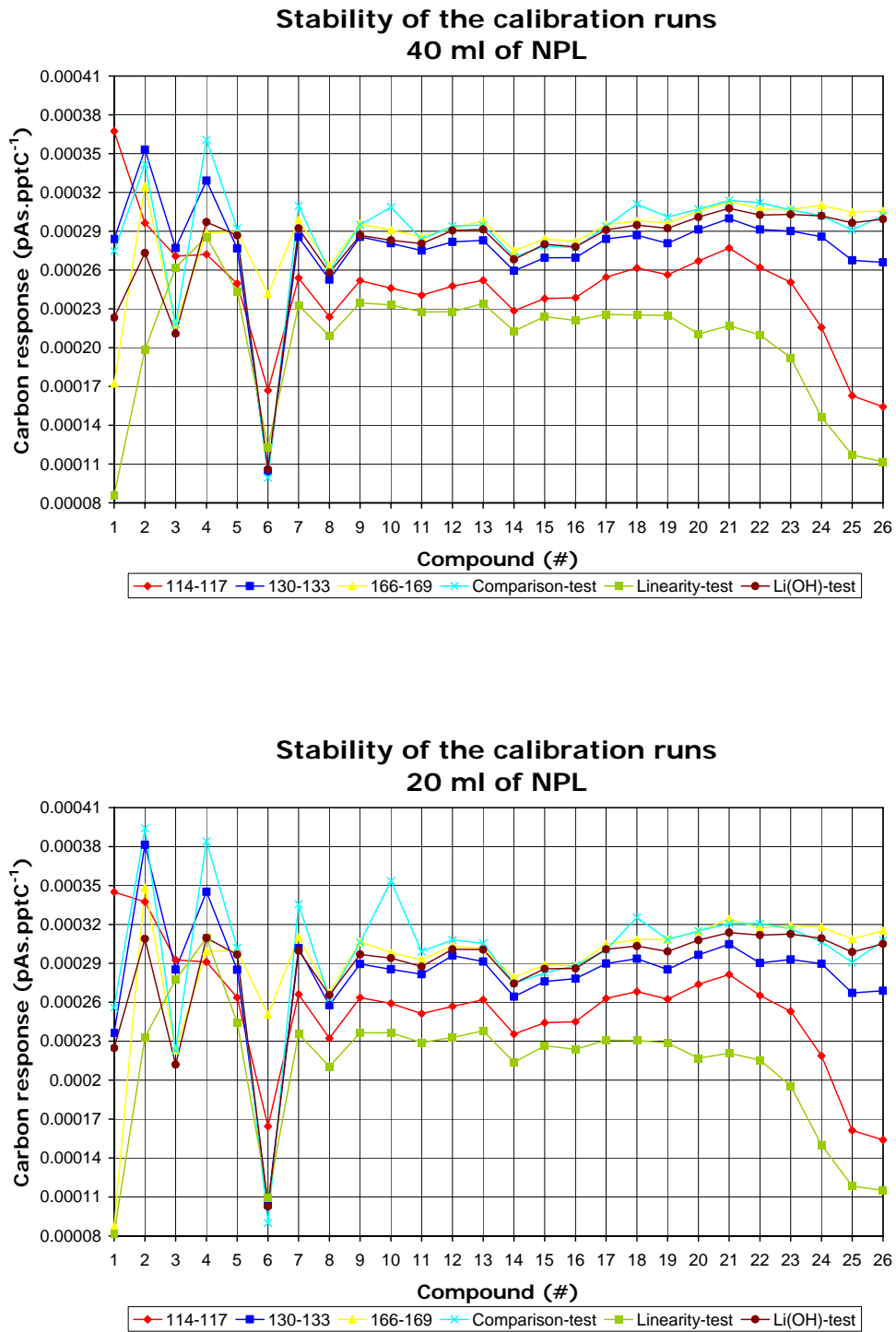
Figure 41: Comparison of the made calibration runs for each calibration point separately. Upper graph shows 40 ml of NPL, lower graph shows 20 ml of NPL. Substances from NPL are identified via ID number #. Responses were calculated as carbon response (pAs.pptC⁻¹). Both calibration points are shown with the same scale.

compound	ID (#)	compound	ID (#)
Ethyne	1	Isoprene	14
Ethene	2	t-2-Pentene	15
Ethane	3	c-2-Pentene	16
Propene	4	2-methylPentane	17
Propane	5	3-methylPentane	18
Propyne	6	Hexane	19
i-Butane	7	Benzene	20
1,3-Butadiene	8	Cyclohexane	21
n-Butane	9	Heptane	22
t-2-Butene	10	Toluene	23
c-2-Butene	11	Ethylbenzene	24
i-Pentane	12	m-Xylene	25
n-Pentane	13	o-Xylene	26

Table 17: Identification key, ID number #, of 26 substances. Ethyne and ethene are responses of the Gas-pro column, the rest are results of Petrocol column.

Losses on NaOH trap are not probable because calibration of the flight # 130-133 does not have such low responses (although they are still lower comparing to runs made later). As mentioned in chapter 4.1.5, during analyses the NaOH trap was replaced with LiOH trap. The first calibration with LiOH trap was the comparison test. Additionally, the same test was calibrated using 1000ml overall volume of calibration gas mixture. The tests made before (linearity test, # 114-117, # 130-133) were using 500ml overall volume.

In addition to calibration runs, the working standard has been measured repeatedly. It was air sampled from firn drilling (ice core air) at Berkner Island in Antarctica in January 2003 and its mixing ratios of NMHCs correspond roughly to concentrations found in CARIBIC samples. Analyses were made for the flights # 114-117, # 122-125 and # 130-133. Table 18 lists all detected substances and their concentrations. Only ethyne is missing in one measurement, in flight # 130-133. Considering ethyne detection limit of ca. 10 ppt, it is clear the peaks in # 114-117 and # 122-125 were hardly detected.

Generally, the results are well reproducible with standard deviation mostly below 10%. Largely above 10% deviate i-butane (22%), i-pentane (18%) and 2-methylpentane (13%). Concentrations of all three substances are overestimated only in the flight # 114-117 which is in accord with the finding that calibration run for # 114-117 exhibited constantly lower carbon response. Substances overestimation may be connected with memory effects or not standard conditions during the flight # 114-117. Interestingly, also ethane concentration in core air analysis for this flight exhibits larger deviation of 10% to lower mixing ratio of 144 ppt although considering its absolute value it should not. Thus a real difference in operational conditions of the mentioned flight could be present. Of course, stability of the core air have to be assumed.

Stability of the CORE air runs				
Compound	# 114-117	# 122-125	# 130-133	average concentration (ppt±std)
	concentration (ppt)	concentration (ppt)	concentration (ppt)	
Ethene	22.70	19.83	21.92	21.48 ± 1.48
Ethyne	6.44	7.26		6.85 ± 0.57
Ethane	144.47	168.74	171.95	161.72 ± 15.03
Propene	15.26	17.13	14.23	15.54 ± 1.47
Propane	31.07	28.42	25.66	28.38 ± 2.70
i-Butane	14.99	10.77	10.10	11.95 ± 2.65
n-Butane	7.69	8.71	7.78	8.06 ± 0.57
i-Pentane	8.62	6.90	6.08	7.20 ± 1.30
n-Pentane	10.30	10.52	10.42	10.41 ± 0.11
2-methylPentane	3.76	2.88	3.15	3.26 ± 0.45
3-methylPentane	4.43	3.66	4.34	4.14 ± 0.43
Hexane	3.71	3.75	4.13	3.86 ± 0.23
Benzene	7.74	7.75	7.71	7.74 ± 0.02
Cyclohexane	2.50	2.88	2.36	2.58 ± 0.27
Heptane	2.29	2.25	2.26	2.26 ± 0.02
Toluene	18.96	19.10	17.90	18.65 ± 0.66

Table 18: Detected substances and their concentrations. All substances were detected during the analyses of CORE air connected to the flights # 114-117, # 122-125 and # 130-133. Concentrations are in ppt.

In summary, the carbon response was demonstrated to be stable for most of the compound over a period 2005-2006. Calibration runs made later on with the same CO_2 trap (LiOH) vary by few percent. CORE air analyses with the same CO_2 trap (NaOH) are repeatable within 10 percent for most compounds.

4.2 CARIBIC

Atmospheric monitoring using civil aircraft is one of several components in global observation system. The civil aircraft based projects offer the advantage of regular, long-distance, and long-term coverage of dynamic processes at 10 to 12 km altitude. The cruising altitude of usually 10-12 km is providing information about UT/LS at mid-latitudes and information about free troposphere in the tropics.

CARIBIC is one of several projects involving civil aircrafts. The MOZAIC project (Measurement of Ozone and Water Vapor by Airbus In-Service Aircraft) provides measurements of ozone and water vapor (since 1991) and of CO and NOy (since 2001), (Marenko et al. 1998). Measurements of nitrogen oxides and ozone were measured on a board of Boeing 747 of Swissair in 1996/1997 (Brunner et al., 2001). The summarized observation results for CO_2, CH_4 and CO in the upper troposphere observed using a commercial airliner from 1993 to 1996 are presented in (Matsueda and Inoue, 1996). The sampling system was operated regularly using a JAL airliner between Australia and Japan for 3 years from April 1993 to April 1996. CARIBIC started regular flights

in November 1997 (www.caribic-atmospheric.com). Since December 2004 the newly certified long range Airbus A340-600 has been used. Figure 42 shows the CARIBIC flight patterns with a base in Frankfurt. Because there is some spread in actual trajectories, the coverage is not limited to narrow flight corridors.
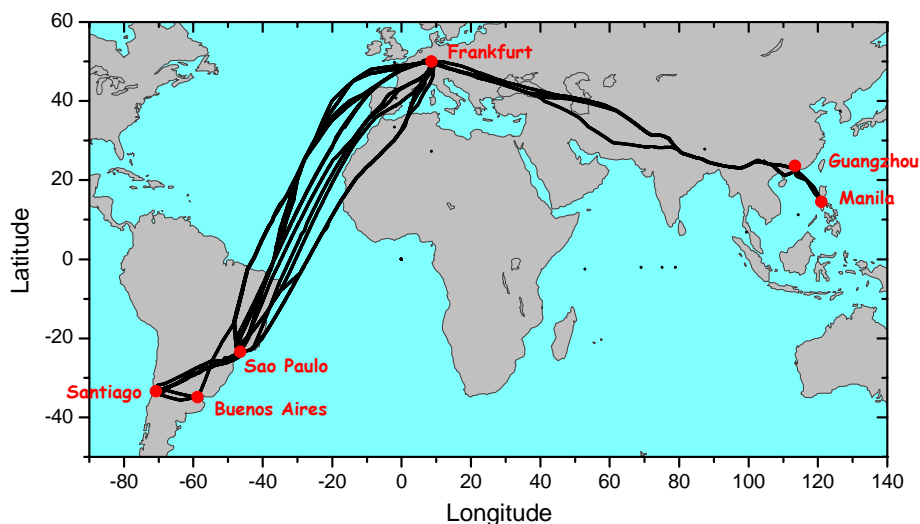
Figure 42: Examples of flight routes to South America and Manila. The variations in the exact route and altitude mean that generally other air traffic has no influence on the intercepted air. For the flight levels of long-range aircraft and typical routes, about 40 % of the intercepted air is stratospheric.

A1 in the appendix lists all the scientific equipment involved in the CARIBIC container. The CARIBIC system and its operation is described in detail by (Brenninkmeijer et al., 2007). Table 19 shows the discussed flights with dates since the commissioning of the system in December 2004 and the coordinated universal time UTC. Dates of landing and take-off are the same for short flights, table shows exact take-off and landing times. Measurement flights started and landed at different locations. In a flight set #114-117 four flights took place where the samples were taken only in three last flights: #114 from Frankfurt (50° N, 9° E) to São Paulo (24° S, 47° W) on 20th June 2005, #115 from São Paulo to Santiago(33° S, 71° W) on 21st June 2005; #116-117 were back flights, #116 from Santiago to São Paulo on 21st June 2005 and #117 from São Paulo to Frankfurt on 22nd June 2005. In a flight set #166-169 four flights took place: #166 from Frankfurt to Guangzhou (23° N, 113° W) on 19th October 2006; #167 from Guangzhou to Manila (15° N, 121° W) on 20th October 2006; #168 is back flight from Manila to Guangzhou and #169 is from Guangzhou to Frankfurt, both on 20th October 2006.

Flight-No. CARIBIC notation	Lufthansa Flight schedule No.	Form Tracking Number	Destination	Date of take-off	Schedule UTC	Off Block UTC	Airborn UTC	Date of landing	Schedule UTC	Touch-down UTC	On Block UTC	Legend
114	LH526		FRA - GRU	20/06/2005	20:45	20:45	21:05	21/06/2005	9:00	8:53	9:15	GRU = Sao Paulo / Brasilien
115	LH526	2005/HE03	GRU - SCL	21/06/2005	10:00	10:08	10:21	21/06/2005	14:05	14:00	14:07	SCL = Santiago / Chile
116	LH527		SCL - GRU	21/06/2005	16:10	16:11	16:25	21/06/2005	19:50	19:35	19:41	
117	LH527		GRU - FRA	21/06/2005	21:05	20:54	21:09	22/06/2005	8:45	8:27	8:32	
118	LH526		FRA - GRU	27/07/2005	20:45	20:57	21:20	28/07/2005	9:00	9:08	9:20	GRU = Sao Paulo / Brasilien
119	LH526	2005/HE04	GRU - SCL	28/07/2005	10:00	10:14	10:25	28/07/2005	14:05	13:50	13:57	SCL = Santiago / Chile
120	LH527		SCL - GRU	28/07/2005	16:10	16:02	16:15	28/07/2005	19:50	19:31	19:38	
121	LH527		GRU - FRA	28/07/2005	21:05	21:02	21:13	29/07/2005	8:45	8:32	8:44	
122	LH526		FRA - GRU	30/08/2005	20:45	20:48	21:17	31/08/2005	9:00	8:52	9:00	GRU = Sao Paulo / Brasilien
123	LH526	2005/HE05	GRU - SCL	31/08/2005	10:00	10:01	10:14	31/08/2005	14:05	13:43	13:51	SCL = Santiago / Chile
124	LH527		SCL - GRU	31/08/2005	16:10	15:57	16:12	31/08/2005	19:50	19:35	19:42	
125	LH527		GRU - FRA	31/08/2005	21:05	20:57	21:13	01/09/2005	8:45	8:31	8:40	
130	LH788		FRA - CAN	14/11/2005	20:40	20:54	21:15	15/11/2005	8:25	8:21	8:27	CAN = Kanton/Guangzhou, China
131	LH788	2005/HE07	CAN - MNL	15/11/2005	9:25	9:25	9:42	15/11/2005	11:35	11:29	11:36	MNL = Manila, Philippines
132	LH789		MNL - CAN	15/11/2005	12:55	13:01	13:12	15/11/2005	15:10	15:06	15:13	
133	LH789		CAN - FRA	15/11/2005	16:30	16:23	16:38	16/11/2005	5:20	6:00	6:09	
166	LH788		FRA - CAN	19/10/2006	20:10	20:31	20:46	20/10/2006	7:10	7:03	7:11	CAN = Kanton/Guangzhou, China
167	LH788	2006/HE08	CAN - MNL	20/10/2006	8:10	8:12	8:31	20/10/2006	10:25	10:36	10:45	MNL = Manila, Philippines
168	LH789		MNL - CAN	20/10/2006	11:50	11:50	12:05	20/10/2006	14:00	13:51	13:59	
169	LH789		CAN - FRA	20/10/2006	15:20	15:30	15:40	21/10/2006	3:35	3:25	3:33	

Table 19: Schedule of the measurement flights. All times are presented as the coordinated universal time UTC.

Usually there are 14 samples taken during the first leg, 3 samples each during the second and third leg, and 8 samples during the fourth leg. Samples are usually analyzed for greenhouse gases and NMHCs at MPI and halocarbons at UEA. In addition to the analyses results, O_3 and CO concentrations for the sampling intervals are calculated from the continuous measurements. 8-day backward trajectories are calculated for each sample. Within this work samples from mentioned flights #114-117, #118-121, #122-125, #130-133 and #166-169 were analyzed. The results are presented and discussed here.

4.2.1 Plausibility of the NMHCs data

Comparison with the GC-MS system (Mühle, 2002) showed good agreement of the results – this agreement is related only to analytical performance but it excludes sampling (sampling artefacts such as contaminants during the sampling and storage, possible reactions with O_3, long term stability of the NMHCs in the sample). In addition, the analytical procedure has been modified in the course of the measurements described here. Consequently, the analytical performance does not remain constant – therefore, the plausibility of the data is discussed first.

From literature and comparisons it is known that substantial discrepancies occur in measured concentrations of more reactive NMHCs like ethene or aromates made by different investigators (eg. Parrish et al., 1998; Slemr et al., 2002; Apel et al., 1994,

1999, 2003). Independently of analytical technique the NMHCs concentrations must comply with tests on internal consistency. Plausibility tests for the internal consistency of the given data set are based on common patterns exhibited by tropospheric NMHCs as shown in (Parrish et al., 1998). Anthropogenic NMHCs are emitted with known fingerprints, diluted and removed by known chemical reactions. Consequently, the absolute and relative concentrations of NMHCs have to comply with ranges and fingerprints resulting from the above mentioned processes. If these patterns are not present in reported data, the measurement problems should be suspected in a first place. The test of the plausibility of ethane data is based on ethane lifetime on the order of several weeks which is large enough to establish minimum concentration of ca. 300 ppt in the troposphere of the NH (Parrish et al., 1998). Figure 43 shows ethane tropospheric concentrations as they are distributed from -60 ^{o}N to 60 ^{o}N in respect to individual flights. Classification between troposphere and stratosphere was based on the dynamic definition of the tropopause where values of potential vorticity above 2 indicate stratospheric air (Bluestein, 1993) and (Smith, 1993). Suspicious measurements were additionally tested via O_3 concentrations. At the tropopause the potential vorticity may take an incorrect value. Chemical definition of the tropopause is then more reliable. (Zahn and Brenninkmeijer, 2003) showed how the ozone mixing ratio undergoes a well defined seasonal variation at the chemical tropopause: $O_3 = 97 + 26 \cdot \sin(2\pi \cdot$ (day of the year - 30) / 365). The functionality is valid only for NH. Samples with the measured ozone concentration below this limit are classified as tropospheric, mixing ratios above are from stratosphere. For SH the limit concentrations of below 80 ppt are considered as troposphere while concentrations above 120 ppt stand for stratosphere.

As expected, the majority of the sampled air comes from the troposphere. Stratospheric air comes mainly from latitudes above 30° as the altitude of the tropopause decreases poleward. From both pictures, it is clear how ethane mixing ratios decrease in direction from northern latitudes to southern latitudes. The troposphere in contrast to the stratosphere has sources of ethane (Warneck, 2000). Most of the mixing ratios for troposphere air lie above 300 ppt. At a first look, it is the flight sets #115-125 that lie below the limit concentrations. In troposphere in the NH these are #118, #125 and #122. In the SH ethane concentrations may be detected below 300 ppt which is the case of flights #119, #120 and #121. Generally, there is an accord with expected pattern in ethane concentrations but earlier flight sets #118-125 seem to be too diluted.

Absolute concentration limits cannot be set for other NMHCs because of their much shorter lifetime and the correspondingly much larger gradients. But the ratios of NMHCs with almost identical reactivity should remain constant. When working with ratios the geometric mean should be used.
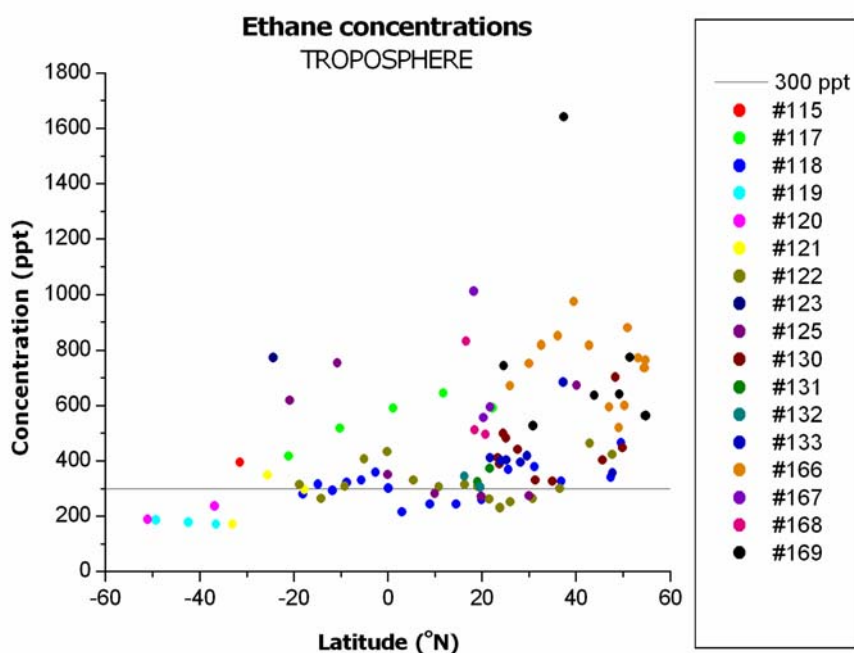
Figure 43: Ethane concentrations in troposphere as a function of latitude. The expected limit minimum concentration in the NH is 300 ppt (grey horizontal line). Individual flights are marked with different colors.

Generally, observed concentrations of primary pollutants like NMHCs tend to be distributed log-normally. The ratio of two NMHCs is approximately log-normally distributed as well. Thus using a geometric mean approximates the median of the ratios data set.

The photochemical lifetimes of i-butane and n-butane are nearly equal (summer ca. 4 days, winter ca. 50 days). Although sources of both isomers vary both in space and in their ratios, data sets of an ambient i-butane/n-butane measurements show relatively constant ratio of ca. 0.5 in the troposphere (Parrish et al., 1998). The reason for this observation is that the emitted butanes from different sources mix rapidly in comparison to the lifetime of butanes and to average transport times of air parcels on route to the measurement sites. Parrish et al., (1998) showed that butane isomer ratios vary only between 0.40 and 0.57 irrespective of its origin, e.g. urban data set 71 U.S. cities has a geometric mean ratio of 0.40. Arithmetic average of all the analyzed data set was 0.47 which is compared to measured ones.

Figure 44 shows a correlation between the butane isomers, separated according to tropospheric and stratospheric based on the dynamic definition of the tropopause. Both axes are in log-scale because most of the measured values were below 10 ppt. The grey line represents the ratio of 0.47 (Parrish et al., 1998) for i-butane to n-butane. In the graphs i-butane is displayed on the x-axis. Troposphere exhibits generally larger scatter from the ideal ratio on the one hand but on the other hand this is related to only five

flights. Stratospheric ratios indicate a very good conformity what is in an agreement that stratospheric NMHCs are better mixed. The variations do not follow a trend of larger scatter at the region of detection limit which implies that even small concentrations are reliable and that few outliers at the detection limit deviate from expected ratio more due to an experimental problem caused not by random effects. Interestingly, five flights with differences from expected ratio in troposphere are in an accord with the finding that the 300 ppt limit concentration of ethane was exceeded by the earlier flights.
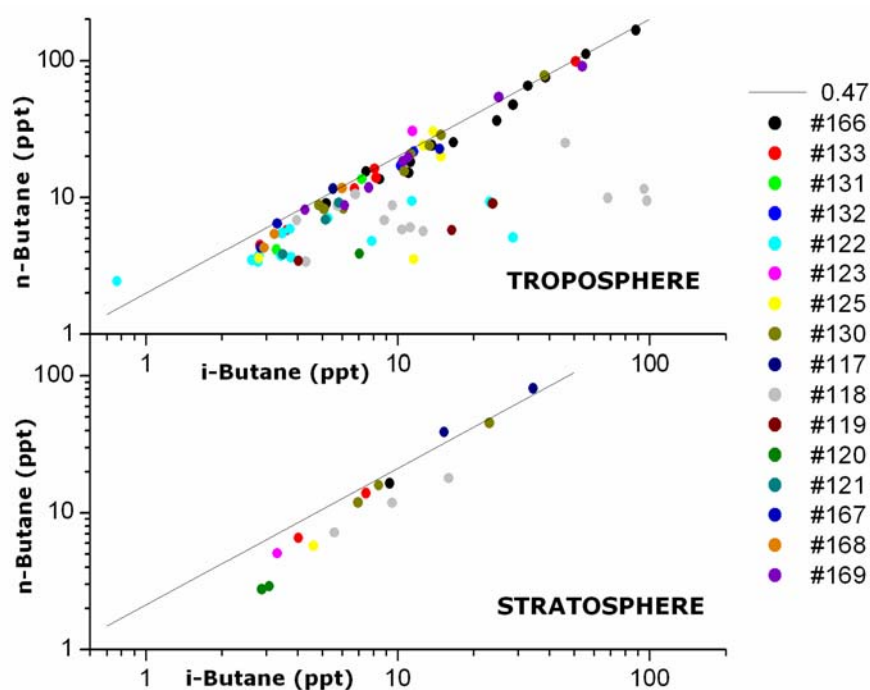
Figure 44: Tropospheric and stratospheric butane isomer ratios. The grey line stands for expected ratio of i-butane/n-butane = 0.47 in the tropospheric NH (Parrish et al., 1998). Both axes representing ppt concentrations are in log-scale. Individual flights are marked with different colors.

Ratios of the flights #118, #119, #120, #122 and #125 lie below the value 0.47 which means, considering i-butane on the x-axis, the i-butane had higher concentrations. The worst deviations has the flight #118 where almost all i-butane concentrations exceeded those of n-butane. This indicates analytical problems during analysis of samples from early flights. In 14 samples from flights #115-117 i-butane was not detected in 11 samples and the i/n-butane ratio of the remaining three samples was 0.39, 0.42 and 0.48.

When the results for flights # 115-125 are neglected, the i-butane to n-butane ratio as a geometric average was 0.58 with the deviation σ of 14%. The deviation σ is calculated

as the root mean square of the fractional uncertainty in the measurement of each NMHC of the ratio. Geometric mean ratio of stratospheric values is 0.55 with σ 9%, geometric mean ratio of tropospheric values is 0.58 with σ 22%. Although there are only six ratios in stratosphere, half deviation suggests better conformity thus well mixed air.

Linear regression between i-butane and n-butane (stratosphere together with troposphere) is defined by *i-butane=(0.517 ± 0.008)n-butane+(0.90 ± 0.33)* with a squared correlation coefficient of 0.99. Comparing this equation to (Mühle, 2002) whose regression was *i-butane=(0.457 ± 0.007)n-butane+(0.68 ± 0.26)* (without outliers WAS-28-1,2,3) with a squared correlation coefficient of 0.96 we get a good agreement. Variance of the presented data set is better (R^2=0.9895) but on the other side in the second data set (Mühle, 2002), an inconsiderable part of data was above 50 ppt and tended to lower slope. Overall geometric mean ratio of (Mühle, 2002) is 0.47 with σ 33%. (Parrish et al., 1998) states the i-/n-butane geometric mean ratio should be in the range of 0.4 to 0.6 with a standard deviation below 20% unless very different source regions are sampled. Secondly, the butanes should be above detection limits when other NMHCs are quantifiable.

Standard deviation of the presented data is smaller than (Mühle, 2002) thus smaller variability in butane isomers sources can be expected. n-butane was detected in all samples from #115-177, #130-133 and #166-169. i-butane was detected in all samples from #166-169, in 23 samples from 26 of #130-133 and only in 25% samples of #115-117. In terms of butane isomers ratio, the later flight sets are more homogeneous and correspond to (Mühle, 2002) data set well.

The ratio of pentane isomers behaves similarly to those of butanes. The reactivity of i-pentane and n-pentane is very nearly equal. They remain in the atmosphere for equal period of time (ca. 4 days). Although variation in pentanes sources is smaller compared to butanes, i-pentane is a marker for gasoline evaporation whereas combustion contributes more to n-pentane. Measured concentrations of pentanes in our samples are smaller than those of butanes because of their shorter lifetime. There were only few detected pentanes in the stratosphere thus they were not considered separately. The geometric mean of (Mühle, 2002) data set with no respect to stratosphere vs. troposphere was 0.61 with σ 51%. Figure 45 shows a correlation between i-pentane (x-axis) and n-pentane (y-axis). Both axes are in log-scale. The grey line represents geometric mean of (Mühle, 2002). As in case of ethane limit concentrations and in case of butane isomers, the values from early flights #121, #123 together with one sample of #125 and with two samples of #130 deviate from apparent linear structure. The structure results mainly from the samples of the flights #169, #166 and from the flight

#132. In the first set #115-117 n-pentane was detected almost in each cylinder but i-pentane in none. (Mühle, 2002) line lies almost everywhere above the measured dependence which implies constantly overestimated n-pentane concentrations.
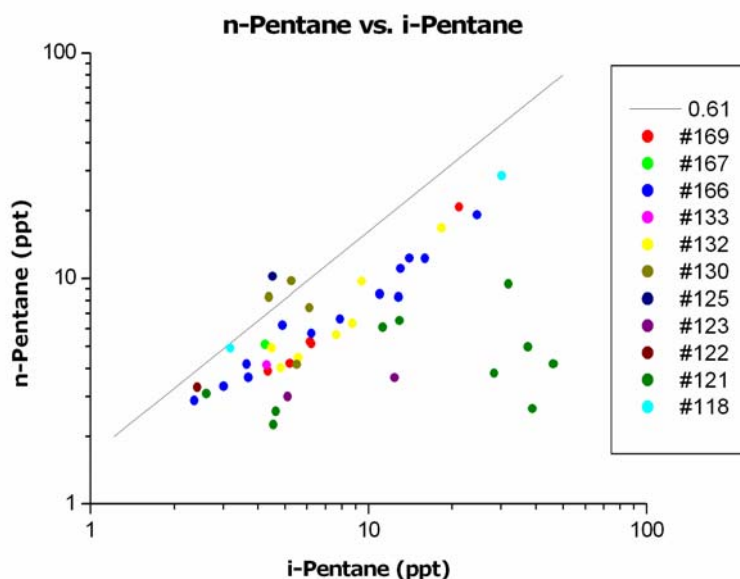
Figure 45: n-Pentane vs. i-Pentane concentrations. The grey line stays for the geometric mean found by (Mühle, 2002) no matter stratosphere or troposphere. Both axes representing ppt concentrations are in log-scale. Individual flights are marked with different colors.

This finding corresponds to a difference in geometric means. After releasing the early flight sets, the i-pentane to n-pentane ratio was determined from the flights #130-#169 as 1.08 with σ 13%. From linear regression between i-pentane and n-pentane we get *i-pentane=(1.12 ± 0.05)n-pentane+(0.47 ± 0.02)* with a squared correlation coefficient of 0.9560. Mühle (2002) linear regression was calculated as *i-pentane=(1.01 ± 0.02)n-pentane-(1.76 ± 0.26)*. Its squared correlation coefficient was 0.91. Already from σ it is clear that variance in the presented data set is substantially smaller which comply with the difference in correlation coefficients. The slope of the (Mühle, 2002) regression is almost twice as big as the geometric mean. Slope of the presented data set is almost equal to the geometric mean which indicates ratios in higher concentration range agree with the ratios of the less concentrated values. Because the constructed regression is unweighted, the regression line must go through a centroid defined by coordinates $(\bar{x}, \bar{y})$ where each is an arithmetic average from x,y-coordinates for the measured values. Thus, considering the log-normal distribution of concentration ratios, ratios of more concentrated values influence the slope of regression with larger extent than the geometric mean. According to regression parameters and their uncertainties it can be said that measured ratios of samples of the presented data set are more evenly distributed (larger slope uncertainty) along the fitted line with stronger linear

relationship (larger correlation coefficient) while (Mühle, 2002) data set appear to have overestimated concentration of i-pentane when the absolute concentration lies in a higher range.

Aging of NMHCs with very short lifetime results in very low mixing ratios. Lifetimes of alkenes are ca. one order of magnitude shorter than the lifetimes of their correspondent alkanes. Alkenes concentration should decrease substantially as the air sample age. On the flight routes, at higher altitudes, more aged air is expected. This expectation is not met in CARIBIC data set since majority of the samples (including samples from stratosphere) contained well detectable alkenes at relatively high levels. A typical example is the last sample No. 28 from the flight #169. PV with a value of 7.16 and O_3 concentration of 206.7 ppb indicate with no doubt stratospheric air masses. The alkanes ethane and propane have indeed lower concentrations as expected, i/n-butane, n-pentane together with aromates (toluene, benzene) were not detected at all, but the alkenes ethene and propene were determined at 10 and 20 ppt respectively. It is most unlikely the sample from stratosphere with aromates mixing ratios below the detection limit could contain alkenes. There are two possible reasons: contamination during sampling or problems associated with storing of the sample.

Greenberg et al., (1996); Parrish et al., (1998); Young et al., (1997) compared canister-based measurements with in situ GC system. They found substantially higher alkene levels in the canisters. Colman et al. (2001) used water added into the whole air sample to maintain sample stability without hydrocarbon losses or artefacts building. Although TRAC sample collector for the CARIBIC project employs glass canisters, alkene artefacts present in the samples suggest potential problems with storing as during the first CARIBIC phase (Mühle, 2002) or simple sampling contamination.

4.2.2 Flight #130-133: detailed analysis

An overview of the flights # 130-133 is shown in A18-A21 in the appendix. Each diagram represents one flight leg within the flight set. In the upper part the flight track is denoted as a thick black line between starting and landing location (black squares). Sampling intervals during the flight are marked as grey circles. There are five sections below the diagram name, each with its own y-axis and common x-axis standing for the time (alternatively sample). Y-axes present NMHCs (other chemical species) concentrations or certain flight parameters. The latter are shown in the first section: latitude, altitude, potential vorticity, pressure and temperature. The second section shows in-situ measurements of ozone, CO and particle number concentrations. The other three sections show the mixing ratios of measured NMHCs. The flight legs

were assessed in terms of sample origin (troposphere vs. stratosphere) in a first step and after that the NMHCs levels in relation to samples backward trajectories were analyzed. The classification of troposphere, stratosphere is based on PV and ozone mixing ratios in a first step and alternatively on the chemical fingerprints. PV is derived from an ECMWF (European Center for Medium range Weather Forecasting) model and is given in potential vorticity units (PVU). Backward trajectories together with meteorological information were prepared by Peter van Velthoven at KNMI (Koninklijk Nederlands Meteorologisch Instituut). The trajectories denoting the "origin" of air masses (http://www.knmi.nl/samenw/campaign_support/CARIBIC) were calculated 8 days back using the horizontal and vertical wind components from the ECMWF model. The trajectories have been calculated with the KNMI trajectory model TRAJKS (Scheele et al., 1996). The wind fields were given with time intervals of 6 hours. Sample subsets of trajectories corresponding to the time interval for each sampling event have been made. The CARIBIC air samples are taken within 46 ± 5 second which means a horizontal distance of about 12 km only, so the backtrajectories for the samples usually stick very close to each other. In order to get an impression of uncertainty of trajectories 15 additional trajectories in a cube centered around the sample were calculated too. The additional trajectories end in the corners and the centre of 3 squares located at the average pressure of the sample, and at pressures of 97 and 103 percent of the average sample pressure. The sides of the squares are 0.8 degrees in longitude and latitude.

The first flight leg # 130 started from Frankfurt and ended in Guangzhou. 14 samples were taken during this leg. 8 samples No. (1, 2, 3, 10, 11, 12, 13, 14) can be classified as tropospheric while only 2 samples No. (4, 7) were beyond doubt sampled in the stratosphere. Samples No. (5, 6) and No. (8, 9) cannot be classified as purely tropospheric or stratospheric air. According to PV levels and ozone concentration samples No. (5, 6) correspond more to the stratosphere (although PV had local minimum with ozone having a local maximum), but their similar pattern indicates that both are similar and that they are rather mixed samples partially from stratosphere and troposphere. Almost all measured NMHCs were concentrated similarly including i/n-butanes and n-pentane, sample No. 5 contained toluene at the level resembling tropospheric values of this flight leg, which excludes sampling had taken place in the stratosphere. PV of sample No. 7 had the highest value of 5.5 of the whole flight leg. The ozone concentration was the third largest (104 ppb). Concentration of ethane and propane was the lowest and second lowest, respectively, i/n-pentanes were not detected at all. Samples No. (8, 9) were very similar to each other.

Generally polluted samples of the flight # 130 were: No. (2, 4, 11, 12, 13). From the first three samples No. 2 had the highest concentrations of ethane (702 ppt) and almost

all hydrocarbons were enhanced in their concentrations. Although the concentration of CO has a small maximum, its value of ca. 100 ppb does not clearly indicate anthropogenic pollution. Together with sample No. 4, both air masses were relatively young as their propane/ethane ratios are the highest at 0.34. To find out possible sources of elevated hydrocarbons levels the backtrajectories were analyzed. Figure 46 shows the 8-day backtrajectories calculated for the sample No. 2. Its origin was in mid Atlantic where one path of the split trajectories had contact with boundary layer. That part of backtrajectory which was above the continent is colored in blue and green thus surface contact is not probable because air masses with pressures below 300 hPa remain in the free troposphere. In Figure 47 are the same backtrajectories with the additional 15 trajectories emanating from the sampling location according to cube centered round the sample.
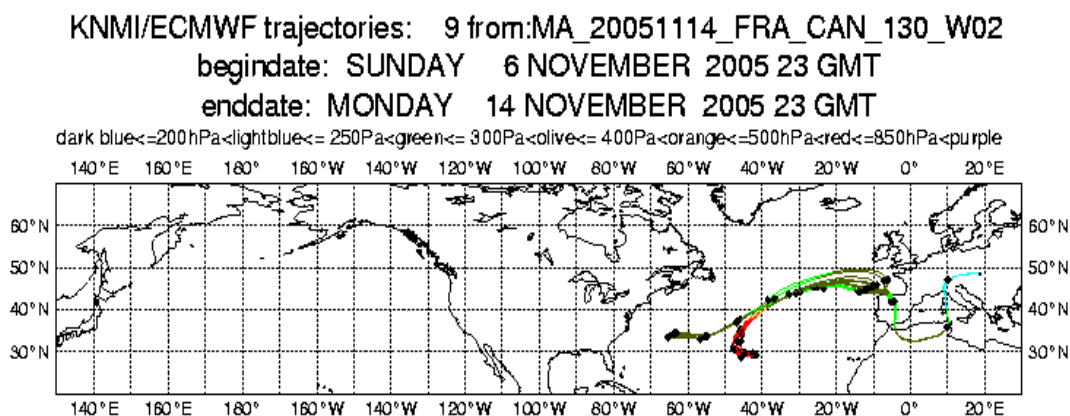
Figure 46: 8-day backtrajectories of the sample No. 2 during the flight leg # 130. Origin of the air mass was in mid Atlantic with two clearly split main paths. Coloring indicates the instantaneous trajectory pressure. Pressures above 400-500 hPa represent the air mass was in touch with boundary layer.
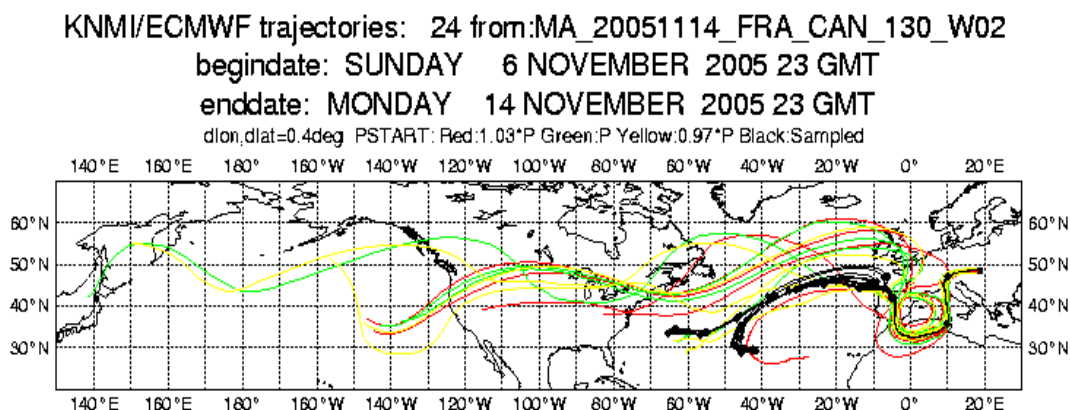
Figure 47: 15 additional 8-day backtrajectories coming out off a cube centered round the sample. The green, yellow and red trajectories stand for air mass located at pressures of 97, 100 and 103 percent, respectively, of the average sample pressure. Black trajectories represent the sample trajectories. An obvious scatter among particular pathways indicates large uncertainty in origin of the sample.

Apparently, there exists a real difference in trajectories pathways. Additional and sample trajectories disperse after the second day back in time. Sample trajectories are substantially shorter in terms of their length which implicates slow moving of air masses. On the contrary, air masses originating at lower or same altitudes (97 and 100 % of the average sample pressure, i.e. green and yellow lines) were carried away much faster (some traveled from eastern Pacific). The "dispersion" of the backtrajectories means that they do not reliably indicate the origin of the air masses sampled. The meteorological condition along the pattern of air parcel must have been complex.

Sample No. 4, on the other side, is the opposite as far as backtrajectories are concerned. Very good agreement between sample and additional trajectories means low uncertainty. The sample trajectories showed the air mass drifted from the eastern coast of the United States at altitudes above 7 km (blue lines with pressures below 200-250 hPa). Thus, possible reasons for elevated mixing ratios in samples No. (2, 4) are convective activities over the continent. Sample No. 2 had twice as high number concentrations of ultra-fine particles (4-12 nm, blue line below the red line) than fine particles, which indicates fresh air masses as ultra fine particles have very short lifetimes of the order of hours (Jaenicke, 1993). The rest of the polluted samples, No. (11, 12, 13), are aged masses according to their propane/ethane ratios of 0.17-0.18. Depressed ozone for these samples indicates photochemically strongly processed air. At the same time enhanced CO levels indicate pollution. Samples No. 11 and 13 exhibited almost identical chemical fingerprints thus similar backtrajectories are expected. Indeed, although the distance along the surface between both samples is ca. 1500 km, the distance between locations where the air masses had the first and only contact with boundary layer is ca. 1 ^{o}N, i.e. 110 km (at 99 ^{o}E) at the north-eastern cost of Thailand. Sample No. 11 was collected in the south from Nepal Mountains, southeasterly from city of Bhagalpur (25.09 ^{o}N, 87.15 ^{o}E). Sample No. 13 was collected in the Yunnan province of the People's Republic of China south from the city of Chuxiong (24.52 ^{o}N, 101.68 ^{o}E). Both backtrajectories followed the same path. Over the north of India they turned down and back to Thailand forming an elbow across the Indian Ocean. After 8 days (8.5 days No. 13) both air masses No. 11, 13 had contact with cost of Burma and Thailand. Sample No. 12 was slightly less polluted but anyway, analysis of its backtrajectories does not show any direct surface contact thus convective activity most likely must have been responsible. Note that in November, convection can well occur in the tropics. The trajectories of samples No. (11, 13) went more to the north over northern Thailand up to Laos. Samples No. (1, 3, 5, 6, 10, 14) were moderately polluted thus closer analysis was not made.

Pairs of samples No. (15, 16 and 17, 18) belong to two short flight legs # 131 and # 132 from Guangzhou to Manila and back to Guangzhou. All four samples were from the

free troposphere with PV slightly above zero. The meteorological analysis shows a tropopause height of 13-14 km. Three backtrajectories of the flight legs # 131 and # 132 related to samples No. (16, 17, 18) resemble each other quite well thus similar chemical fingerprints are expected. All had contact with ocean boundary layer for several days easterly from Philippines from 150 ^{o}E to 180 ^{o}E at ca. 10 ^{o}N. The air mass of sample No. 15 followed a path from Sri Lanka (where it had surface contact) over north of India and north of Thailand. Both samples No. (15, 17) were taken in an ascending phase of the flight. All four samples were aged air masses according to propane/ethane ratio. A remarkable feature is, however, ratio of short lived species with different lifetimes, toluene/benzene ratio. Samples No. (17, 18) have high values of 0.44, 0.40 respectively, while samples No. (15, 16) have lower values of 0.14, 0.27 respectively thus extra emissions of aromates are suspected. Interestingly, samples No. (17, 18) had higher numbers of ultra-fine particles compared to No. (15, 16) which suggests mixing of air masses.

The last flight leg # 133 started in Guangzhou and landed in Frankfurt. 8 samples were collected and analyzed, No. (19-26). From these the first 6 samples were sampled in the troposphere (note that the cruising altitude after leaving Guangzhou was only 9 km) and last two No. (25, 26) seem to be mixed from the troposphere and stratosphere (note the large variations in ozone). They are very similar in chemical composition but because of almost twice as concentrated ozone and high PV level, sample No. 25 is rather from the stratosphere. At a first look, flight parameters follow expected trends. During the flight the temperature dropped constantly as the cruising altitude was approaching the tropopause. At the locations of samples No. (25, 26) the ozone concentration was well correlated with NOy and it was almost an exact mirror copy of humidity. Every maximum of ozone had minimum in humidity because the stratosphere is extremely dry in an absolute and relative sense. The aerosol results do not show any elevated levels of ultra-fine particles, although particles above 12 nm changed in number very fast between two last samples. The cleanest samples were No. (22, 23). Both had the lowest concentrations of ozone, propane as well as benzene. The lowest propane/ethane ratio indicates highly processed air masses. In contrast, toluene/benzene ratio is the highest for both samples. Both backtrajectories originated over America (No. 22 south of Florida) alike with very fast transport at high altitudes with no surface contact which is in agreement with the low level of pollution, Figures 48, 49.

Moderately polluted samples were No. (19, 20, 21). These samples had almost identical NMHCs patterns. Only the air represented by sample No. 20 had the surface contact at the eastern coast of India on the 8th day. Moderately polluted samples were No. (24, 25, 26). Sample No. 24 was the most polluted, and was collected in a plume of CO. All NMHCs were elevated in their concentrations. Propane with 306 ppt represents a

fivefold over other propane mixing ratios. n-Butane and n/i-pentanes were even ca. ten times more concentrated. Both NMHCs ratios of propane/ethane and toluene/benzene correspond to fresh air masses. Analysis of the sample backtrajectory shows surface contact earliest after 5 days thus convective activities are suspected.

Indeed, satellite global infrared cloud composite image of SSEC (space science and engineering centre) at University of Wisconsin-Madison's Graduate School shows presence of clouds between the Caspian see and Arabic peninsula on 15th November 2005 at 21:00 UTC. Sample No. 24 was collected at 37.25 ^{o}N, 41.9 ^{o}E south westerly from the Caspian see where the oil fields are thus petrochemical influence is suggested. Samples No. (25, 26) were collected over Europe. Sample No. 25 was collected in the stratosphere. Interestingly, the sample No. 26 appeared to be less polluted. Samples backtrajectories show fast transport not below 300 hPa over the USA with split pathways.
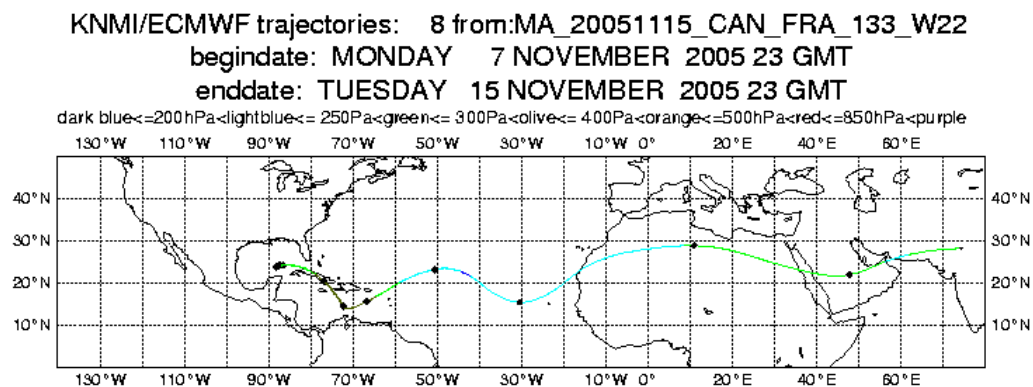
Figure 48: 8-day backtrajectories of sample No. 22 during the flight leg # 133. Origin of the air mass was in the Gulf of Mexico, south of Florida. Fast transport took place at high altitudes.
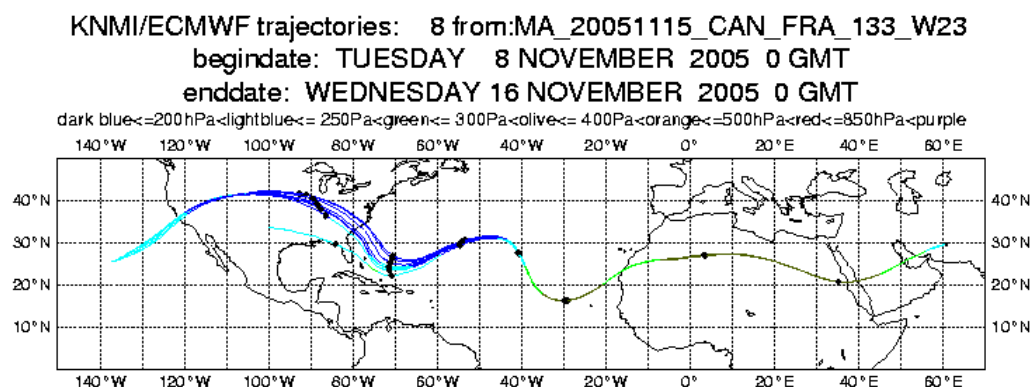
Figure 49: 8-day backtrajectories of sample No. 23 during the flight leg # 133. Origin of the air mass was over the United States of America, north of Florida. Fast transport took place at high altitudes.

4.2.3 Flight #166-169: detailed analysis

An overview of the flights # 166-169 is shown in A22-A25 in the appendix. Destinations were the same as for the set # 130-133, namely Frankfurt-Guangzhou-Manila-Guangzhou-Frankfurt. However the first and the second flight leg (# 166 and # 169) took place with flight routes north of the Caspian sea flying over Tibet. This new route saves 1 hour because its length is ca. 1000 km shorter. Flight legs are assessed in terms of sample origin (troposphere vs. stratosphere) in a first step and after that the samples backward trajectories in relation to NMHCs levels are analyzed. Detected plumes were compared to chemical signatures of Asian outflows (plumes of the leg # 166 and of the back flight # 169 were analyzed together in case they were related to similar location).

Contrary to set # 130-133, the flight set # 166-169 contained samples with clearer troposphere vs. stratosphere patterns. Figure 50 shows vertical profiles of PV (red contours) for the flight # 166 with values between 1 and 5 PVU, shaded from yellow to red.

Figure 50: Vertical profiles of PV (red contours) for the flight # 166 with values between 1 and 5 PVU, shaded from yellow to red. Cruising altitude (purple thick line) denotes heights and times where the samples were collected (black points). The 400 K isentrope is plotted in purple(top).

All samples from the flight leg # 166 except for sample No. 5 were sampled in the troposphere. Furthermore, 4 plumes (plume 1, 2, 3, 4, 5) were detected by samples No. (9, 10, 11, 12, 13, 14). With samples No. (1, 2, 3, 4, 5) the CO concentration followed a decreasing trend while ozone mixing ratio increased constantly as the plane was approaching the tropopause.

Samples No. (2, 3, 4) contained NMHCs at similar concentration levels. This is consistent with very similar backtrajectories of the samples No. (2, 3, 4) compared to No. 1 with surface contact over Philadelphia. A reason for elevated concentrations of toluene in sample No. 3 is not clear, and a measurement error is suspected. Samples No. (6, 8) were moderately polluted with very fast backtrajectories reaching to the United States of America over Greenland. Sample No. 7 was slightly more polluted with slower backtrajectories coming from the United States of America more or less straight over the Atlantic Ocean. The backtrajectories belonging to samples No. (9, 10) are quite similar. Both paths went over the Caspian see. Backtrajectories of samples No. (11, 12) were relatively similar as well, the latter backtrajectory was much faster starting at the western coast of the United States of America. Backtrajectory of the sample No. 11 started in Atlantic Ocean close to western coast of Africa. Both trajectories went over the north of Africa and Arabic Peninsula without apparent surface contact. The backtrajectory of sample No. 13 originated at the eastern coast of Africa, went over Arabic Peninsula to the south of India where it turned north to China. The trajectory did not have any contact with the surface. In case of sample No. 14, the air mass had surface contact only in the Indian Ocean east from Sri Lanka where basically no pollution occurs. The sample backtrajectory went at high altitudes near Kunming industrial centre in Yunnan province to southwest over Wuliang Shan Mountains.

The plume 1 of the flight # 166 is presented by the sample No. 9 which exhibits a clear step in almost all NMHCs concentrations. Sample No. 8 seems to be at the beginning of the same plume but its NMHCs concentration pattern does not appear to fit in the later plume. Ozone increases constantly from sample No. 8 up to the sample No. 12, but PV remains low. This indicates polluted tropospheric air. CO had a local maxima, i.e. between samples No. (8, 9), at the sample No. 10, between samples No. (11, 12) and at samples No. (13, 14). Except for the plume 1, the other plumes are typical in decreasing concentration of ethane as well as i/n-butanes and propane from the plume 2 (sample No. 10) to the end of the last plume 4 (sample No. 14). Except for samples No. (9, 10), the propane/ethane ratio does not show remarkably fresh air masses. Backtrajectory analyses did not show noticeably low trajectories with surface contact. Toluene was not detected in any of the polluted samples but a noticeable feature is the toluene/benzene ratio just in case of samples No. (9, 10) which, in contradiction, does not indicate fresh

air. From what was mentioned above, there is a difference in the origin of those plumes. The plumes 1, 2 do not present as fresh air masses as plumes 3, 4. High and strongly fluctuating number concentrations of ultra-fine particles in the range of 4–12 nm point to recent particle nucleation because lifetimes of ultra-fine particles are of a few hours to 1 day (Jaenicke, 1993). Within the 46 second period of sample collection, around 6500 particles/cm^3 on average were detected in case of No. 12, 700 particles for No. 13 and around 7300 particles for No. 14. All plumes were detected by NOy as well which concentration raised from ca. 0.5 to 3 ppb. Methane did not show enhanced values, only last two measurements (samples No. 13, 14) contained about 0.05-0.1 ppm CH$_4$ more. SF6 was not correlated with plumes at all. Interestingly, the amount of TGM (total gaseous mercury) was consistent with plumes 1, 3 and 4. Generally, the plumes 1, 2 exhibit chemical fingerprints typical for petrochemical industry without additional sources of aromatic compounds.

To quantify plumes 1-4, the relation of a trace species X to CO was calculated. Enhancement ratios (ERs) are obtained by dividing the excess of trace species X concentration measured in the plume versus background by the excess concentration of a simultaneously measured reference gas like CO versus background (Andreae and Merlet, 2001), i.e.:

$$\frac{\Delta X}{\Delta CO} = \frac{X_{plume} - X_{background}}{CO_{plume} - CO_{background}} \tag{4.32}$$

CO is an attractive reference because it correlates well with other partially oxidized and reduced compounds emitted during combustion processes. Additionally, CO is not taken up by vegetation. To characterize the plume, enhancement ratios were inferred using samples No. (6, 7, 8) and compared with published values of fresh and recent biomass burning plumes, see Table 20.

Emission ratios made on the basis of sample No. 6 resemble ratios calculated using sample No. 8 as a background more than ratios inferred from sample No. 7 as a background. Generally samples No. (12, 13) fall in the range of previous observations. Sample No. 14 for all NMHCs except for i-butane has slightly lower ERs. ERs for samples No. (9, 10, 11) are larger than reported results, particularly samples No. (9, 10), which exceed literature ratios several times. This observation points to emissions of ethane, propane, i-butane and n-butane by processes other than biomass burning.

Plumes were assessed in relation to other trace gases: TGM (total gaseous mercury) and CH$_3$CN. TGM is measured using dual channel, single amalgamation, cold vapor atomic fluorescence analyzer (Tekran-Analyzer Model 2537 A). CH$_3$CN is measured using PTR-MS developed at IMK (Institut für Meteorologie und Klimaforschung), Forschungszentrum Karlsruhe.

Samples		Ethane	Propane	i-Butane	n-Butane	Benzene
bck.[a]	canister					
6	9	22.33	13.57	4.88	10.09	1.63
	10	26.78	15.91	5.70	10.92	2.36
	11	12.60	3.53	0.82	1.14	1.94
	12	5.62	0.82	0.21	0.30	1.18
	13	3.71	0.19	0.07	0.11	0.77
	14	1.61	-0.25	0.06	0.03	0.71
7	9	25.30	14.48	4.33	8.76	1.47
	10	28.40	16.29	5.19	9.85	2.15
	11	15.08	4.93	0.89	1.25	1.83
	12	7.30	1.71	0.28	0.40	1.16
	13	5.39	1.07	0.14	0.21	0.77
	14	3.24	0.57	0.13	0.13	0.71
8	9	18.04	11.93	3.93	7.81	1.32
	10	22.90	14.33	4.87	9.10	2.02
	11	11.38	3.79	0.77	0.93	1.73
	12	5.40	1.14	0.22	0.24	1.12
	13	3.61	0.53	0.09	0.06	0.74
	14	1.63	0.08	0.08	-0.01	0.68
Literature[b]		4-9	0.8-3.2	0.04-0.08	0.1-0.4	0.8-1.7

Table 20: Enhancement ratios (ERs) of five NMHCs in (pptv/ppbv) calculated for canisters No. 9-14. As a background concentration levels of NMHCs in canisters No. (6, 7, 8) were taken. The ratios are compared to previous results reported for fresh and recent plumes of biomass burning.
[a]Canisters No. 6, 7, 8 (separately) stand for background mixing ratios.
[b]Reported results: Mauzerall et al. (1998), Andreae and Merlet (2001).

Jaffe et al. (2005) derived that the enhancement ratio above the background for Hg^0/CO appears to be a good indicative of Asian industrial outflow. The ratio was found to be 0.0056 ± 0.0016 ng/m^3/ppbv. In the remote atmosphere the total gaseous mercury (TGM) fraction consists of gaseous elemental mercury (GEM) and the reactive gaseous mercury (RGM) which is present in much lower concentrations. Thus Hg^0 can be associated with TGM.

The plumes 3 and 4 of the flight #166 were detected in TGM measurements during the return flight # 169 as well (plumes 5, 6). Samples corresponding to these plumes were No. (21, 23) where only No. 23 exhibited elevated concentrations of all NMHCs. Nevertheless, by examining the correlation of Hg^0 to carbon monoxide for the plume 3 of the flight # 166 together with the plume 6 of the return flight (leg # 169), and analogically plume 4 together with plume 5 of the return flight (leg # 169), we derive a slope of 0.0039 ± 0.0009 (R = 0.72) and 0.0069 ± 0.0017 (R = 0.67) ng/m^3/ppbv respectively. Thus both episodes can be said to be influenced by industrial emission, especially the plume 2 of flight #166.

The plumes were assessed to biomass burning as well. Biomass burning has been identified to be by far the dominant source of CH_3CN and has therefore been proposed as a tracer for biomass burning emissions (Holzinger et al., 1999). Biomass burning emissions of CH_3CN coincide with substantial emissions of CO and a correlation between the two gases can be expected. Figure 51 shows data series of CH_3CN and CO

during flights #166 and #169. The CO plume 3 of the flight #166 and CO plume 6 of the flight #169 are coincident in their CH$_3$CN values. Generally, both species have elevated concentrations during the first two hours (shown flight phase) period of the flight #169. Maximum concentration of CH$_3$CN in plumes is around 300 ppt. As in case of TGM, plumes 3 and 6 were considered together when making correlation of CH$_3$CN to CO. The molar enhancement ratio of CH$_3$CN is then the slope of linear regression. Correlation plot for CH$_3$CN vs. CO is shown in Figure 52.
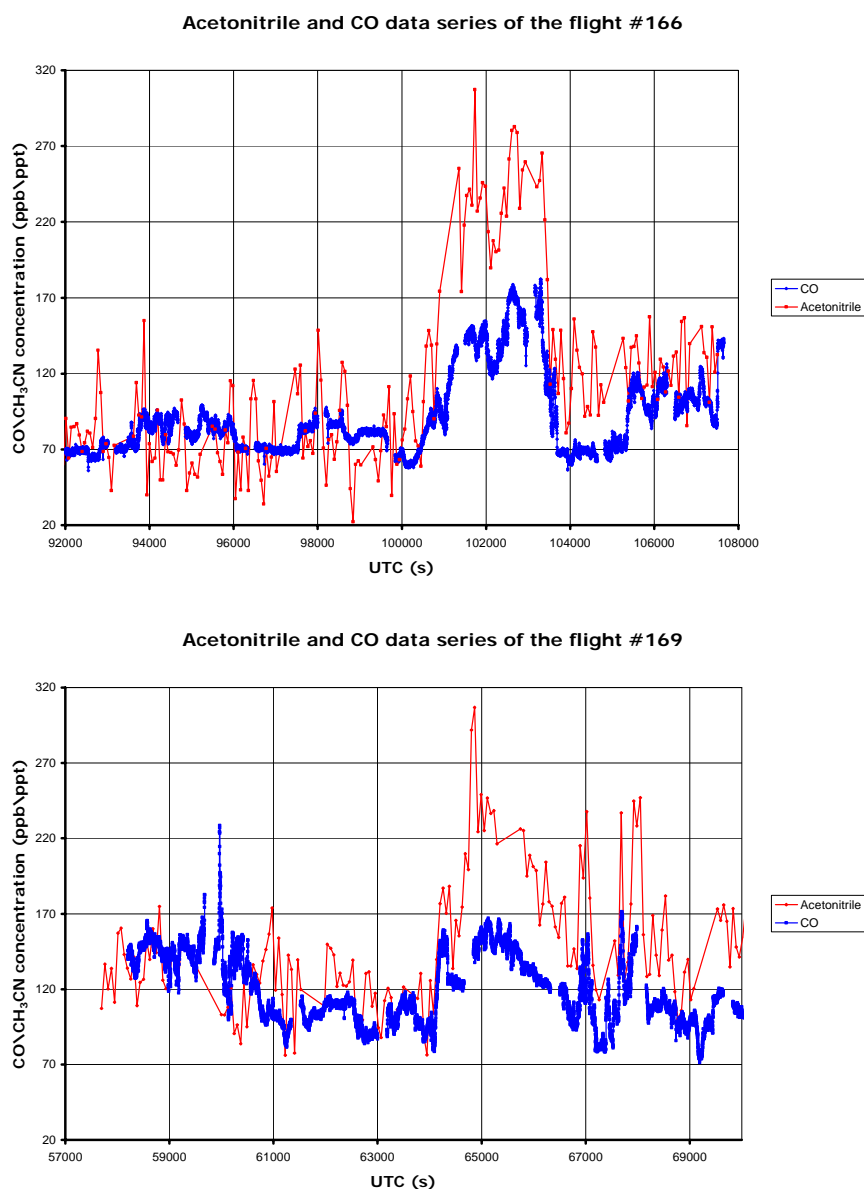
Figure 51: CH$_3$CN and CO data series. The CO plume3 of the flight #166 (at 28:00-29:00 UTC) and CO plume 6 of the flight #169 (at 18:00-19:00 UTC) were coincident with the enhanced concentrations of CH$_3$CN.

ER of CH$_3$CN/CO is dependent on the nitrogen content of the fuel and is therefore quite variable (Andreae et al., 1996; Holzinger et al., 1999). From published ERs for

CH_3CN/CO it is fact that higher values have been measured in laboratory experiments or in a young plume than in aged plumes. This cannot be explained with the known lifetimes of CH_3CN and CO against reaction with HO. From linear regression we derive slope 1.68 ± 0.09 (ppt/ppb) with the squared correlation coefficient $R^2 = 0.78$.
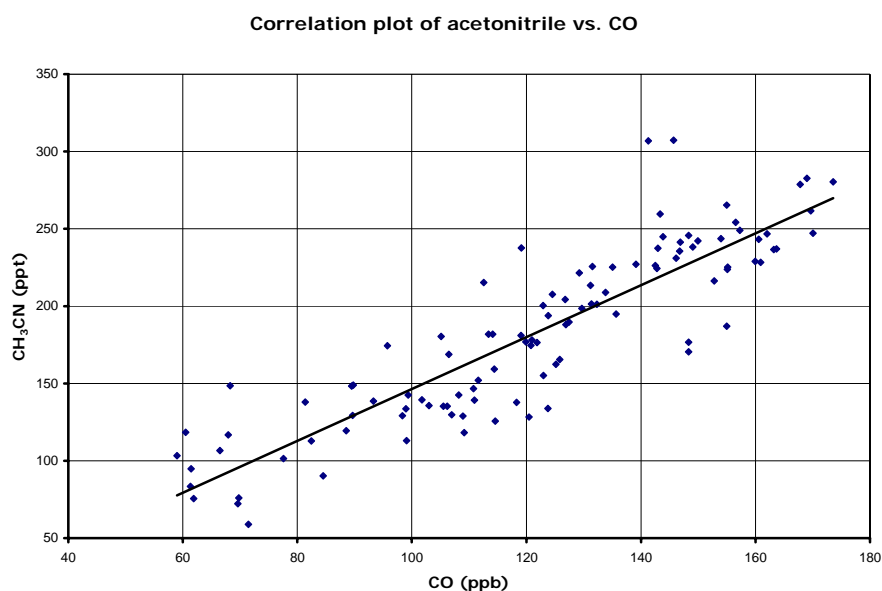
Figure 52: Correlation plot of CH_3CN *vs. CO for the plumes 3, 6 of the flights #166, #169 respectively.*

The correlation coefficient implies very well correlated data. Enhancement ratio of 1.68 is in a very good agreement with the values determined by (Jost et al., 2002; Holzinger et al., 1999). Jost et al.(2002) values represent aged (1-10 days) biomass burning plumes over southern Africa. Thus there is a solid evidence for biomass origin in case of the samples No. (11, 12) and No. 23. Together with TGM data, samples No. (11, 12, 13, 14, 21, 23) have their origin in industrial emissions but only samples No. (11, 12, 23) were affected by the biomass burning emissions.

In order to assess chemical fingerprints of detected NMHCs from samples No. (9, 10, 11, 12, 13, 14) the NMHCs concentrations were divided by the corresponding CO mixing ratios and compared to literature results (Andreae and Merlet, 2001), (Guo et al., 2006), (Chan et al., 2006), (Russo et al., 2003). Andreae and Merlet (2001) show emission factors (EFs) from which ERs can be easily obtained. The other three authors are showing average values eventually median concentrations measured at different locations within China. Finally, the NMHCs/CO ratios are shown in Table 21. The principal difference of NMHCs/CO ratio to ER is that the latter is more sensitive to background concentrations thus calculated enhancement ratios can be associated with published ones more easily. Direct NMHCs/CO ratio can, on the other side, serve as an aid when comparing fingerprints of species because it restrains variability (too much

variance without markers makes matching obscure) in ratios and additionally they do not need to define background concentrations that precisely. Apart from data measured at a single source, data measured at a distance from a source (free troposphere), will always represent mixed data from different sources. Nevertheless, the table presents also results obtained at or close to source to see the differences.

sample\compound		Ethane	Propane	i-Butane	n-Butane	Toluene	Benzene	n-Pentane	i-Pentane
#166	9	9.799	2.676	0.670	1.339	0.017	0.317	0.147	0.192
	10	11.125	3.585	1.007	1.902	0.071	0.499	0.219	0.281
	11	9.095	1.727	0.265	0.389	0.054	0.527	0.091	0.118
	12	7.277	1.097	0.148	0.226		0.501	0.059	0.070
	13	6.561	0.866	0.098	0.159		0.369	0.036	0.032
	14	5.678	0.677	0.093	0.128		0.358	0.053	0.041
#169	21	5.014	0.584	0.052	0.079	0.031	0.352	0.026	0.029
	22	5.707	0.522	0.066	0.094	0.062	0.314	0.030	
	23	14.974	3.554	0.494	0.827	0.090	0.820	0.189	0.194
I[a]		4.586	0.879	0.044	0.141	0.608	1.264	0.030	0.066
II[a]		10.748	0.916	0.070	0.190	0.731	1.374	0.052	0.030
III[a]		5.223	1.484	0.099	0.311	1.136	1.636	0.200	0.100
IV[a]		14.331	4.071	0.185	0.494	4.287	8.703	0.348	0.398
V[a]		2.468	0.588	0.019	0.145	0.524	1.786	0.194	0.136
Pearl River - 1[b]		4.042	3.901	1.531	3.120	10.800	1.655	0.853	1.531
Pearl River - 2[c]		1.643	2.643	1.143	1.857	9.643	2.000	0.929	1.571
Pearl River - 3[c]		2.800	4.200	1.600	2.600	14.600	2.600	0.800	1.800
WSW[d]		6.041	0.636	0.107	0.116		0.248		
SE[d]		5.841	0.375	0.080	0.091		0.125		
Central[d]		9.881	2.067	0.289	0.430		0.459		

Table 21: NMHCs to CO concentration ratios in (pptv/ppbv) calculated for canisters No. 9-14, No. 21-23 and for results reported in literature.
[a] Andreae and Merlet (2001); [b] Guo et al. (2006); [c] Chan et al. (2006); [d] Russo et al. (2003).

The table contains CARIBIC samples No. (9, 10, 11, 12, 13, 14) of flight # 166 and No. (21, 22, 23) of flight #169. EFs given by (Andreae and Merlet, 2001) are separated based on various types of biomass burning I, II, III, IV and V. I stands for savanna and grassland, II is tropical forest, III is extratropical forest, IV is biofuel burning and V stands for charcoal burning. Guo et al. (2006) and Chan et al. (2006) made measurements at Pearl River delta which is a region where Guangzhou belongs to (in the table „Pearl River"). Guo et al. (2006) identified major sources of pollutants and their contributions to pollutant loadings at Tai O location based on comprehensive dataset of NMHCs collected from August 2001 to December 2002. Average concentrations were used in the table. Chan et al. (2006) studied the effect of rapid industrialization in five cities in the Pearl River delta region in a study conducted in late summer 2000. Two categories are shown: industrial („Pearl River-2") and industrial-suburban („Pearl River-3"). Russo et al. (2003) characterized the chemical composition of Asian continental outflow based on five principal Asian source regions (in the table WSW, SE, Central). The TRACE-P airborne mission was conducted during February-

April 2001, it was composed of research flights in the geographic region of west Pacific (0-50 ^{o}N, 110-180 ^{o}E). Russo et al. (2003) used five-day backward trajectories to identify continental source regions of outflow: west-southwest region WSW (0-40 ^{o}N, 0-60 ^{o}E), southeast region SE (0-25 ^{o}N), central region (30-60 ^{o}N, 80-130 ^{o}E). The data present the same altitude range above 7 km except for central region where only data from altitudes 2-7 km were measured.

As mentioned above, samples No. (11, 12, 23) reflect biomass burning where the ratio size was largest for samples No. (23, 11, 12) respectively. Sample No. 23 differs from the other two samples substantially which corresponds to fast changing concentration of CO during the first phase of the flight leg # 169. From published ERs only the first three types of biomass burning I, II, III seem to have influence on samples No. (11, 12) where both samples comply with the tropical and extratropical biomass burning the most. A noticeable feature is benzene whose ratio is for both samples slightly above 0.5 while all biomass burning types exhibit values largely above 1. The best conformity among all results occur between sample No. 11 and „Central" region. Interestingly, although sample No. 11 was collected south from the „Central" region its backtrajectory goes southwestern away from that region. General feature of „Pearl River" datasets is a small ethane ratio and large ratios for i/n-butanes as well as for toluene and benzene. Sample No. 10 exhibits similar ratios for propane and i/n-butanes as the „Pearl River" datasets.

Similar to the short flight legs # 131, 132, the flights # 167 (No. 15, 16, 17) and # 168 (No. 18, 19, 20) were beyond doubt only in the troposphere. Two samples No. (17, 18) were obviously strongly polluted. Samples No. (15, 16, 19, 20) were more or less similar in concentrations of various NMHCs. All samples had depressed concentrations of corresponding CO. On the contrary, both samples No. (18, 17) had coincident large mixing ratios of CO. All NMHCs were enhanced, some like i/n-butanes even several times. Interestingly, benzene was substantially elevated in both samples with markedly depleted toluene. According to propane/ethane ratio both samples were not relatively that well processed compared to the others. Backtrajectories of all samples resemble each other relatively well. They all followed an elbow pathway to the south turning to the right over Philippines and continued ca. 2000 km north-easterly to the Pacific. The noticeable difference is just in case of sample No. 17 which backtrajectory directed more to south where it turned over the north of Borneo Island, i.e. where Brunei is. Thus convective activity is suspected as this is just at the location of oil fields. For sample No. 18 is not clear where its pollution is coming from. Its backtrajectory came close to Borneo but did not lie over.

The first seven samples of the return flight # 169 No. (21-27) were taken in troposphere while the last sample No. 28 has the most stratospheric characteristics from all

measured samples. This sample had the highest levels of ozone and PV from all collected samples. As mentioned, samples detected two plumes V, VI. The most polluted sample of the flight leg # 169 was sample No. 23 which was associated with biomass burning (plume VI). Its backtrajectory went west over northern Pakistan where it had contact with the surface. From there the backtrajectory went further west at very low altitudes over Arabian Peninsula to the eastern coast of Africa around 25 ^{o}N, 30 ^{o}N. CO concentration had two maxima with 150 ppb at sample No. 21 and between samples No. 22 and 23. CO concentration changed fast and was sinking from sample No. 21 to sample No. 24. Moderately polluted were samples No. (24, 25, 26) which had similar fast backtrajectories, not above 300 hPa, over Europe, Atlantic ocean, Greenland and along the eastern coast of the United States of America. The less polluted were samples No. (27, 28), the latter collected purely in stratosphere. Both had very fast backtrajectories going more or less straight west over Europe, the Atlantic Ocean, the United States of America and the Pacific Ocean. Trajectory of sample No. 28 was one of the fastest originating at eastern coast of Russia around 40 ^{o}N, Figure 53.
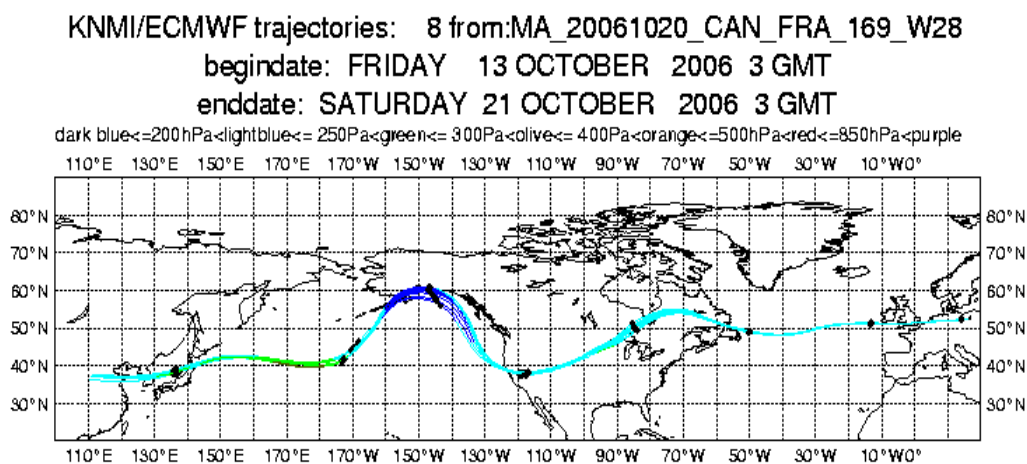
Figure 53: 8-day backtrajectories of sample No. 28 during the flight leg # 169. Backtrajectories of sample No. 28 were one of the fastest originating at eastern coast of Russia. Sample was collected purely in the stratosphere.

4.3 Summary and perspectives

Within the project CARIBIC a GC system with the FID detection for the lab-analyses of NMHCs was developed and applied during the analyses of air samples from the upper troposphere and lower stratosphere. Mutual comparisons with former GC-MS system showed its reliability. Implementing of the V25 system into control over the process of analyses was valid and it made the measurements effective.

As a problematic aspect appeared to be the combination of used PLOT column, Gas-pro, and an insufficient capacity of the CO_2 trap which lead to a suppression of the Gas-pro signal. Altogether five flights were measured: # 114-117, # 118-121, # 122-125, # 130-133 and # 166-169. Plausibility tests for the internal consistency of the given data sets showed that the first three flights did not meet expected pattern. Additionally, alkene artefacts were detected almost during all flights thus potential problems with sampling or storage of a sample are possible.

Flights # 130-133 and # 166-169 were discussed in detail. Samples were analyzed in terms of their origin (troposphere vs. stratosphere, backward trajectories), their aging (NMHCs ratios) and detected plumes were compared to chemical signatures of Asian outflows.

As far as hardware is concerned the future development of system should focus mostly on effective separation of NMHCs. System is using separate enrichment and focusing. Since recently PTV (programmed temperature vaporization) injection (Lewis et al., 1995) has been used in order not to employ focusing by combining both sample conditioning steps in one. Avoided focusing implies a lost of additional separation potential which would, when added up to the column separation, separate many VOC compounds already before injection. Designing the focusing capillary as a real column would bring a quasi second dimension into the separation process thus quasi 2-D chromatography is possible. Such a performance consists of three steps. The first is a redesigned valve-structure due to the reverse focusing contra injection. This is responsible for re-mixing of already separated compounds. In the second step, a temperature programmable ramp during heating must be made to produce one by one evaporation of compounds with different boiling points while they are still kept in narrow zones being carried through the line. In the last step, controlled flows transferring compounds from enrichment trap into the focusing trap would separate species during the process of focusing. Focusing is in respect to temperature like a negative chromatography where at its end substances do not enter the detector but they stay focused in the solid state. The point is, they stay at different locations inside the capillary what makes they are separated. Because the focusing capillary has own stationary phase, the process of separation is strongly dependent on the temperature. A rate of separation increases as the temperature decreases. To take an advantage of this effect a new design of the focusing capillary is needed. A helix form made of the focusing capillary has a lower temperature decrease along its length.

Other steps in future development involve CO_2 management (flushing instead of LiOH), to make measurements of samples with low pressures possible, removing Gas-pro column, alternatively using only one column etc. Building of alkene artefacts as

well as not reliable measurements of ethyne presents problem for the later NMHCs data analysis. Stability of certain NMHCs in the collector needs to be tested.

In general, although the system presented here has had problems with reliability of Gas-pro column its analytical performance is comparable (in some aspects better) to earlier developed systems. The system is able to analyze CARIBIC samples in relatively short time. Discussed flights show that apart from alkenes and ethyne the instrument output can be used in interpretation of NMHCs results.

Bibliography

Ackermann R., Auswirkungen von Kraftfahrzeugsemissionen in der urbanen atmosphäre, *Dissertation, Institute for environmental physics*, University of Heidelberg, 1, 3.2, 3.2.3, 7., 2000.

Ackman R.J., The flame ionization detector: further comments on molecular breakdown and fundamental group response, *J. Gas Chromatog. 6*, 497-501, 1968.

Andreae M. O. and Merlet P., Emission of trace gases and aerosols from biomass burning, *Global Biogeochemical Cycles 15*, 955-966, 2001.

Andreae M. O., et al., Trace gas and aerosol emissions from savanna fires, in Biomass Burning and Global Change, edited by J. S. Levine, 278–295, *MIT Press, Cambridge, Mass.,* 1996.

Apel E.C., Calvert J.G., Fehsenfeld F.C., The Nonmethane Hydrocarbon Intercomparison Experiment (NOMHICE): Tasks 1 and 2, *J. Geophys. Res. 99*, 16651-16664, 1994.

Apel E.C., Calvert J.C., Gilpin T.M., Fehsenfeld F.C., Parrish D.D., Lonneman W.A., The Nonmethane Hydrocarbon Intercomparison Experiment (NOMHICE): Task 3, *J. Geophys. Res. 104*, 26069-26086, 1999.

Apel E.C., Calvert J.G., Gilpin T.M., Fehsenfeld F., Lonneman W.A., Nonmethane Hydrocarbon Intercomparison Experiment (NOMHICE): Task 4, ambient air., *J. Geophys. Res. 108(D9)*, 4300, doi:10.1029/2002JD002936, 2003.

Atkinson R., Gas-phase tropospheric chemistry of organic compounds: A review, *Atmos. Environ. 24A*, 1-41, 1990.

Atkinson R., Gas-phase tropospheric chemistry of organic compounds, *J. Phys. Chem. Ref. Data Monograph 2*, 1-216, 1994.

Atkinson R., Atmospheric chemistry of VOCs and NOx, *Atmos. Environ. 34*, 2063-2101, 2000.

Atkinson R., Arey J., Gas-phase tropospheric chemistry of biogenic volatile organic compounds: A review, *Atmos. Environ. 37*, S197-S219, 2003.

Bhattacharyya G.K., Johnson R.A., Statistical Concepts and Methods, *John Wiley & Sons*, Canada, 1977.

Blake D.R., Smith T.W., Chen T.Y., Whipple W.J., Rowland F.S., Effects of biomass burning on summertime non-methane hydrocarbon concentrations in the Canadian Wetlands, *J. Geophys. Res. 99*, 1699, 1994.

Bluestein H. B., Synoptic Dynamic Meteorology in the Midlatitudes, *New York, New York: Oxford University Press*, Inc., 1993.

Brenninkmeijer C. A. M. and Coauthors, Civil Aircraft for the Regular Investigation of the atmosphere Based on an Instrumented Container: the new CARIBIC system, *Atmos. Chem. Phys. Discuss. 7*, 5277-5339, 2007.

Brunner D., Staehelin J., Jeker D., Wernli H., Schumann U., Nitrogen oxides and ozone in the tropopause region of the Northern Hemisphere Measurements from commercial aircraft in 1995/96 and 1997, *J. Geophys. Res. 106*, 27673-27699, 2001.

Camel V., Caude M., Trace enrichment methods for the determination of organic pollutants in ambient air, *J. Chromatog. A 710*, 3, 1995.

Cao X.L., Hewitt C.N., The sampling and analysis of volatile organic compounds in the atmosphere, in *Reactive Hydrocarbons in the Atmosphere*, Hewitt C.N., Ed., Academic Press, San Diego, 119-157, 1999.

Castello G., Benzo M., Gerbino T.C., Automated gas chromatographic analysis of volatile organic compounds in air, *J. Chromatog. 710*, 61, 1995.

Chan L.-Y., Chu K.-W., Zou S.-C., Chan C.-Y., Wang X.-M., Barletta B., Blake D. R., Guo H., Tsai W.-Y., Characteristics of nonmethane hydrocarbons (NMHCs) in industrial, industrial-urban, and industrial-suburban atmospheres of the Pearl River Delta (PRD) region of south China, *J. Geophys. Res. 111*, D11304, doi: 10.1029/2005JD006481, 2006.

Christian T. J., Kleiss B., Yokelson R. J., Holzinger R., Crutzen P. J., Hao W. M., Shirai T., Blake D. R., Comprehensive laboratory measurements of biomass-burning missions: 2. First intercomparison of open-path FTIR, PTR-MS, and GC-MS//FID//ECD, *J. Geophys. Res. 109,* D02311, doi:10.1029/2003JD003874, 2004.

Colman, J. J., Swanson A. L., Meinardi S., Sive B. C., Blake D. R., Rowland F. S., Description of the analysis of a wide range of volatile organic compounds in whole air samples collected during PEM-Tropics A and B, *Anal. Chem. 73*, 3723–3731, 2001.

Crutzen P.J., Williams J., Pöschl U., Hoor P., Fischer H.,Warneke C., Holzinger R., Hansel A., Lindinger W., Scheeren B., Lelieveld J., High spatial and temporal resolution measurements of primary organics and their oxidation products over the tropical forests of Surinam, *Atmos. Environ. 34*, 1161-1165, 2000.

De Zeeuw J., de Nijs R. C. M., Henrich L. T., Adsorption chromatography on PLOT columns: A new look at the future of capillary GC, *J. Chromatogr. Sci. 25*, 71-83, 1987.

Dollard G.J., Davies T.J., Jones B. M. R., Nason P. D., Chandler J., Dumitrean P., Delaney M., Watkins D., Field R. A., The UK hydrocarbon monitoring network, in *Volatile Organic Compounds in the Atmosphere, Issues in Environmental Science and*

Technology, Hester R.E., Harrison R.M., Eds., The Royal Society of Chemistry, cambridge, 37-50, 1995.

Doskey P. V., The effect of treating air samples with magnesium perchlorate for water removal during analysis for non-methane hydrocarbons, *J. of High. Resol. Chromat. 14*, 724-728, 1991.

Etzkorn T., Klotz B., Sorensen S., Patroescu I. V., Barnes I., Becker K. H., Platt U., Gas-Phase Absorption Cross Sections of 24 Monocyclic Aromatic Hydrocarbons in the UV and IR Spectral Ranges, *Atmos. Environ. 33*, 525-540, 3.2, 3.1, 3.5.2, 4.3.6, 5.1, 5.1.1, 5.1.2, 1999.

EURACHEM/CITAC Guide CG 4, Quantifying Uncertainty in Analytical Measurement, 2000.

Fall R., Biogenic Emissions of Volatile Organic Compounds from Higher Plants. In: Hewitt C.N., Ed., *Reactive Hydrocarbons in the Atmosphere.*, San Diego: Academic Press, 322 , 1999.

Farmer C. T., Milne P. J., Riemer D. D., Zika R.G., Continuous hourly analysis of C_2-C_{10} non-methane hydrocarbon compounds in urban air by GC-FID, *Environ. Sci. Technol. 28*, 238, 1994.

Friedrich R., Obermeier A., Anthropogenic emissions of volatile organic compounds, in *Reactive Hydrocarbons in the Atmosphere*, Hewitt C.N., Ed., Academic Press, San Diego, 1999.

Fuentes J. D., Lerdau M., Atkinson R., Baldocchi D., Bottenheim J. W., Ciccioli P., Lamb B., Geron C., Gu L., Guenther A., Sharkey T.D., Stockwell W., Biogenic hydrocarbons in the atmospheric boundary layer: A review, *Bull. Amer. Met. Soc. 81*, 1537, 2000.

Gholson A. R., Jayanty R. K. M., Storm J. F., Evaluation of aluminum canisters for the collection and storage of air toxics, *Anal. Chem. 62*, 1899, 1990.

Gong Q., Demerjian K.L., Hydrocarbon losses on a regenerated Nafion dryer, *J. Air Waste Mgt. Assoc. 45*, 490, 1995.

Goldan P.D., Kuster W.C., Fehsenfeld F.C., Montzka S.A., Hydrocarbon measurements in the southeastern United States: the Rural Oxidants in the Southern Environment (ROSE) program 1990, *J. Geophys. Res. 100*, 25945-25963, 1995.

Greenberg J. P., Helmig D., Zimmerman P. R., Seasonal measurements of nonmethane hydrocarbons and carbon monooxide at the Mauna loa Observatory during the Mauna Loa Observatory Photochemistry Experiment 2, *J. Geophys Res. 101*, 14581-14598, 1996.

Guenther A. B., Hills A. J., Eddy covariance measurement of isoprene fluxes, *J. Geophys. Res. 103*, 13145-13152, 1998.

Guenther A., Hewitt C. N., Erickson D., Fall R., Geron C., Graedel T., Harley P., Klinger L., Lerdau M., McKay W. A., Pierce T., Scholes B., Steinbrechcer R., Tallamraju R., Taylor J., Zimmerman P., A global-model of natural volatile organic-compound emissions, *J. Geophys. Res.*. 103, 8873-8892, 1995.

Guenther A., Key species in land surface atmospheric interactions: biogenic volatile organic compounds, in: *Report series in aerosol science*, eds: Arneth A., Korhonen H., Kulmala M., Raivonen M., Ruuskanen T. and Suni T., 2003.

Guo H., Wang T., Blake D. R., Simpson I. J., Kwok Y. H., Li Y. S., Regional and local contributions to ambient nonmethane volatile organic compounds at a polluted rural/coastal site in Pearl River Delta, China, *Atmos. Environ. 40*, 2345–2359, 2006.

Habram M., Slemr J., Welsch Th., Development of a dual capillary column GC method for the trace determination of C_2-C_9 hydrocarbons in ambient air, *J. High Resol. Chromatogr. 21*, 209-214, 1998.

Hamilton J. F., Lewis A. C., Monoaromatic complexity in urban air and gasoline assessed using comprehensive GC and fast GC-TOF/MS, *Atmos. Environ. 37*, 589-602, 2003.

Hansel A., Jordon A., Holzinger R., Prazeller P., Vogel W., Lindinger W., Proton transfer reaction mass spectrometry: on-line trace gas analysis at the ppb level, *J. Mass Spectrom. Ion. Proc. 149*, 609-619, 1995.

Hansel A., Jordon A., Warneke C., Holzinger R., Lindinger W., Improved detection limit of the proton-transfer reaction mass spectrometer: On-line monitoring of volatile organic compounds at mixing ratios of a few pptv, *Rapid Commun. Mass Spectrom. 12*, 871-875, 1998.

Helmig D., Air analysis by gas chromatography, *J. Chromatog. A, 843*, 129, 1999.

Helmig D., Greenberg J.P., Automated in-situ gas chromatographic-mass spectrometric analysis of ppt level volatile organic trace gasses using multistage solid-adsorbent trapping, *J. Chromatog. A 677*, 123, 1994.

Helmig D., Ozone removal techniques in sampling of atmospheric volatile organic trace gases, *Atmos. Environ. 31*, 3635, 1997.

Holdren M. W., Westberg H. H., Hill Jr. H. H., Analytic methodology for the identification and quantification of vapor phase organic pollutants, Interim Report No., CRCAPRAC-CAPA-11-71, Coordinating Research Council, Air Pollution Research Advisory Committee, 1979.

Holzinger R., Warneke C., Hansel V., Jordan A., Lindinger W., Scharffe D. H., Schade G, Crutzen P. J., Biomass burning as a source of formaldehyde, acetaldehyde, methanol, acetone, acetonitrile, and hydrogen cyanide, *Geophys. Res. Lett. 26*, 1161-1164, 1999.

Hough A.M., Development of a 2-dimensional global tropospheric model-Model chemistry, *J. Geophys. Res. 96*, 7325-7362, 1991.

IPCC, Intergovernmental Panel on Climate Change, Climate change 1994: Radiative forcing of climate change and an evaluation of the IPCC IS 92 emission scenarios, *Cambridge Univ. Press*, New York, 1995.

ISO/IEC 17025, General Requirements for the Competence of Calibration and Testing Laboratories, Genf, 1999.

Jaenicke R., Tropospheric aerosols, in Aerosol-Cloud-Climate Interactions, edited by P. V. Hobbs, 1-31, Academic Press, 1993.

Jaffe D., Prestbo E., Swartzendruber P., Weiss-Penzias P., Kato S., Takami A., Hatakeyama S., Kajii Y., Export of atmospheric mercury from Asia, *Atmos. Environ. 39*, 3029– 3038, 2005.

Jost C., Trentmann J., Sprung D., Andreae M. O., McQuaid J. B., Barjat H., Trace gas chemistry in a young biomass burning plume over Namibia: Observations and model simulations, *J. Geophys. Res. 108(D13)*, 8482, doi: 10.1029/2002JD002431, 2003.

Kaiser R., Gottschalk G., Elementare Tests zur Beurteilung von Meßdaten, *Bibliographisches Institut AG*, Manheim, 1972.

Kato S., Pochanart P., Kajii Y., Measurements of ozone and nonmethane hydrocarbons at Chichi-jima island, a remote island in the western Pacific: Long-range transport of polluted air from Pacific rim region, *Atmos. Environ. 35*, 6021-6029, 2001.

Konrad S., Volz-Thomas A., Characterization of a commercial gas chromatography-flame ionization detection system for the in situ determination of C_5-C_{10} hydrocarbons in ambient air, *J. Chromatogr. A 878*, 215-234, 2000.

Kurdziel M., The effect of different drying agents on the analytical data for non-methane hydrocarbon concentrations in ambient air samples, *Chem. Anal. (Warsaw) 43*, 387-397, 1998.

Lai J. Y. K., Matisova E., He D., Singer E., Niki H., Evaluation of capillary gas chromatography for the measurement of C_2-C_{10} hydrocarbons in urban air samples for air pollution research, *J. Chromatogr. 643*, 77-90, 1993.

Lewis A. C., Bartle K. D., Heard D. E., McQuaid J. B., Pilling M. J., Seakins P. W., In situ, gas chromatographic measurements of non-methane hydrocarbons and dimethyl sulfide at a remote coastal location (Mace Head, Eire) July-August, *J. Chem. Soc. Faraday Trans. 93, 2921*, 1997.

Lewis A. C., Bartle K. D., McQuaid J. B., Pilling M. J., Seakins P. W., Ridgeon P., Atmospheric monitoring of volatile organic compounds using programmed temperature vaporization injection, *J. High Res. Chrom. 19*, 686, 1996 .

Lewis A. C., Seakins P. W, Denha A. M., Bartle K. D., Pilling M. J., Programmed-temperature vaporization injection (PTV) for in-situ field-measurements of isoprene, and selected oxidation-products in a Eucalyptus forest, *Atmos. Environ. 29*, 1871, 1995.

Lewis A. C., Carslaw N., Marriott P. J., Kinghorn R. M., Morrison P. D., Lee A. L., Bartle K. D., Pilling M. J., A larger pool of ozone-forming carbon compounds in urban atmospheres, *Nature 405*, 778-781, 2000.

Lindinger W., Hansel A., Jordan A., Proton-transfer reaction mass spectrometry (PTR-MS): on-line monitoring of volatile organic compounds at pptv levels, *Chemical Society Reviews 27*, 347-354, 1998.

Logan, J., Tropospheric ozone: seasonal behaviour, trends and anthropogenic influences, *J. Geophys. Res. 90*, 10463–10482, 1985.

Marenko A., and Coauthors, Measurement of ozone and water vapor by Airbus in-service aircraft: The MOZAIC program, an overview, *J. Geophys. Res. 103*, 25 631–25 642, 1998.

Matisová E., Škrabáková S., Carbon sorbents and their utilization for the preconentration of organic pollutants in environmental samples, *J. Chromatogr. A 707*, 145-179, 1995.

Matsueda H. and Inoue H. Y., Measurements of atmospheric CO_2 and CH_4 using a commercial airliner from 1993 to 1994, *Atmos. Environ.* 30, 1647-1655, 1996.

Matuska P., Koval M., Seiler W., A high resolution GC-analysis method for determination of C_2-C_{10} hydrocarbons in air samples, *J. High Resolut. Chromatogr. Chromatogr. Commun. 9*, 577-583, 1986.

Mauzerall D. L., Logan J. A., Jacob D. J., Anderson B. E., Blake D. R., Bradshaw J. D., Sachse G. W., Singh H. B. and Talbot R. W., Photochemistry in Biomass Burning Plumes and Implications for Tropospheric Ozone Over the Tropical South Atlantic, *J. Geophys. Res. 103*, 8401-8423, 1998.

Mayrson H., Crabtree J. H., Source reconciliation of atmospheric hydrocarbons, *Atmos. Environ. 10*, 137-143, 1976.

Miller J.C., Miller J. N., Statistics for analytical chemistry, *Ellis Horwood limited West Sussex*, 1984.

Mitchell G., Mills W. N., Garden J. S., Zdeb M., Multiple-curve procedure for improving precision with calibration-curve-based analyses, *Analytical chemistry 49*, 1655-1660, 1977.

Mowrer J., Lindskog A., Automatic unattended sampling and analysis of background levels of C_2-C_5 hydrocarbons, *Atmos. Environ. 25A*, 1971, 1991.

Mühle J., GC/MS-Meßsystem für Nicht-Methan-Kohlenwasserstoffe, *dissertation MPI*, Mainz, 2002.

Nelson P.F., Squigley S.M., Smith M.Y., Sources of atmospheric hydrocarbons in Sydney: a quantitative determination using a source reconciliation technique, *Atmos. Environ. 17*, 439-449, 1983.

Noxon J.F., Nitrogen Dioxide in the Stratosphere and Troposphere measured by Ground-based Absorption Spectroscopy, *Science 189*, 547-549, 1975.

Noxon, J. F., Whipple E. C., Hyde R. S., Stratospheric NO_2. 1. Observational Method and Behavior at Midlatitudes, *J. Geophys. Res. 84*, 5047-5076, 1979.

Oliver K. D., Adams J. R., Daughtrey Jr. E. H., McClenny W. A., Yoong M. J., Pardee M.A., Technique for monitoring ozone precursor hydrocarbons in air at photochemical assessment monitoring stations: Sorbent preconcentration, closed-cycle cryofocusing, and GC-FID analysis, *Atmos. Environ. 30, 2751*, 1996.

Parrish D. D., Hahn C. J., Williams E. J., Norton R. B., Fehsenfeld F. C., Singh H. B., Shetter J. D., Gandrud B. W., Ridley B. A., Indications of photochemical histories of Pacific air masses from measurements of atmospheric trace species at Point Arena, California, *J. Geophys. Res.* 97, 15883-15901, 1992.

Parrish D. D., Trainer M., Young V., Goldan P. D., Kuster W. C., Jobson B. T., Fehsenfeld F. C., Lonneman W. A., Zika R. D., Farmer C. T., Riemer D. D., Rodgers M. O., Internal consistency tests for evaluation of measurements of anthropogenic hydrocarbons in the troposphere, *J. Geophys. Res. 103*, 22339-22359, 1998.

Piccot, S. D., Watson J. J., Jones J. W., A global inventory of volatile organic compound emissions from anthropogenic sources, *J. Geophys. Res. 97*, 9897-9912, 1992

Platt U., Perner D., Pätz H. W., Simultaneous Measurement of Atmospheric CH_2O, O_3 and NO_2 by Differential Optical Absorption, *J. Geophys. Res. 84*, 6329-6335, 1979.

Plass-Dülmer C., Schmidbauer N., Slemr J., Slemr F., D'Souza H., European hydrocarbon intercomparison experiment AMOHA part 4: Canister sampling of ambient air, *J. Geophys. Res. 111*(D0), 4306, doi:10.1029/2005JD006351, 2006.

Plass-Dülmer C., Michl K., Ruf R., Berresheim H., C_2-C_8 hydrocarbon measurement and quality control procedures at the Global Atmosphere Watch Observatory Hohenpeissenberg, *J. Chromatogr. A 953*, 175-197, 2002.

Prather M. R., Derwent D., Ehhalt P., Fraser E., Sanhueza, Zhou X., Other trace gases and atmospheric chemistry, Chapter 2 in Radiative Forcing of Climate 1994, Intergovernmental Panel on Climate Change, Report to the IPCC from the Scientific Assessment Working Group, 1994.

Rudolph J., The tropospheric distribution and budget of ethane, *J. Geophys. Res. 100,* 11369-11381, 1995.

Russo R. S., et al., Chemical composition of Asian continental outflow over the western Pacific: Results from Transport and Chemical Evolution over the Pacific (TRACE-P), *J. Geophys. Res., 108(D20)*, 8804, doi:10.1029/2002JD003184, 2003.

Salisbury G., Williams J., Holzinger R., Gros V., Mihalopoulos N., Vrekoussis M., Sarda-Esteve R., Berresheim H., von Kuhlmann R., Lawrence M., Lelieveld J., Ground-based PTR-MS measurements of reactive organic compounds during the MINOS campaign in Crete, Juli-August 2001, *Atmos. Phys. Chem. 3*, 925-940, 2003.

Scheele, M.P., P.C. Siegmund, and P.F.J. van Velthoven, Sensitivity of trajectories to data resolution and its dependence on the starting point: In or outside a tropopause fold, *Meteorol. Appl. 3*, 267-273, 1996.

Seinfeld J.H., Pandis S.N., Atmospheric chemistry and physics: From air pollution to climate change, John Wiley & Sons, New York, 1997.

Singh H. B., Viezee W., Salas L. J., Measurements of selected C_2-C_5 hydrocarbons in the troposphere: latitudinal, vertical and temporal variations, *J. Geophys. Res. 93*, 15861-15878, 1988.

Singh H. B. and Zimmerman P. B., Atmospheric distribution and sources of nonmethane hydrocarbons, Advances in Environmental Science & Technology, Wiley, *Burlington, Ontario*, 1992.

Singh H. B. and Zimmerman P. B., Atmospheric distribution and sources of nonmethane hydrocarbons, in Gaseous Pollutants: Characterization and Cycling, J.O. Nriagu, Ed., *John Wiley and Sons*, 177-235, 1992.

Skogerboe R. K. and Grant C. L., Comments on the definitions of the terms sensitivity and detection limit, *Spectroscopic Letters 3*, nos. 8 and 9, 215-220, 1970.

Slemr J., Slemr F., Partridge R., D'Souza H., Schmidbauer N., Accurate Measurements of Hydrocarbons in the Atmosphere (AMOHA): Three European intercomparisons, *J. Geophys. Res. 107(D19)*, 4409, doi:10.1029/2001JD001357, 2002.

Smith R. K., Potential vorticity: A brief survey for forecasters. Notes based on workshop on potential vorticity organized by the Bureau of Meteorology Training Centre, 1-37, 1993.

Taylor J. R., An introduction to Error Analysis, University Science Books, Sausalito, California, 1997.

Trost B., UV-Absorption Cross Sections of a Series of Monocyclic Aromatic Compounds, *Atmos. Environ. 31*, No. 23, 3999-4008, 3.2, 4.3.6, 5.1., 1997.

Volkamer R., Etzkorn T., Geyer A., Platt U., Correction of the oxygen interference with UV spectroscopic (DOAS) measurements of monocyclic aromatic hydrocarbons in the Atmosphere, *Atmos. Environ. 32*, 3731-3747, 1998.

Volz-Thomas A., Slemr J., Konrad S., Schmitz T. H., Apel E. C., Mohnen V. A., Quality assurance of hydrocarbon measurements in the German Tropospheric Research Focus (TFS), *J. Atmos. Chem. 42*, 255 – 279, 2002.

Wang T., Raihala T. S., Jackman A. P., St. John R., Use of tedlar bags in VOC testing and storage: Evidence of significant VOC losses, *Environ. Sci. Technol. 30*, 3115, 1996.

Warneck P., Chemistry of the Natural Atmosphere, *Academic Press*, San Diego, CA, US, 2000.

Warnecke C., van der Veen C., Luxembourg S., de Gouw J. A., Kok A., Measurements of benzene and toluene in ambient air using proton-transfer-reaction mass spectrometry: calibration, humidity dependence, and field intercomparison, *Int. J. Mass Spec. 207*, 167, 2001.

Westberg H., Zimmerman P., Analytical methods used to identify non-methane organic compounds in ambient atmospheres, *Adv. Chem. Series 232*, 275, 1993.

Williams J., Pöschl U., Crutzen P. J., Hansel A., Holzinger R., Warneke C., Lindinger W., Lelieveld J., An atmospheric chemistry interpretation of mass scans obtained from a Proton Transfer Mass Spectrometer flown over the tropical rainforest of Surinam*, J. Atmos. Chem 38*, 133-166, 2001.

Xu X., Williams J., Plass-Dülmer C., Berresheim H., Salisbury G., Lange L., Lelieveld J., GCxGC measurements of C_7-C_{11} aromatic and n-alkane hydrocarbons on Crete, in air from Eastern Europe during the Minos campaign, *Atmos. Chem. Phys. 3*, 1461-1475, 2003.

York D., Least-squares fitting of a straight line, *Canadian Journal of Physics 44.*, 1079-1086, 1966.

Young V. L., Kieser B. N., Chen S. P., Niki H., Seasonal trends and local influences on nonmethane hydrocarbon concentrations in the Canadian boreal forest, *J. Geophys. Res. 102*, 5913-5918, 1997.

Zahn A. and Brenninkmeijer C. A. M., New directions: a chemical tropopause defined. *Atmos. Environ.* 37, 439-440, 2003.

Zielinska B. J., Sagebiel J. C., Harshfeld G., Gertler A. W., Pierson W. R., Volatile organic compounds up to C_{20} emitted from motor vehicles: Measurements methods, *Atmos. Environ. 30*, 2269, 1996.

Appendix

Trace Constituent	Where	Measurement principle
O_3 fast	In-flight	Chemiluminescence on an organic dye
O_3 precise	In-flight	UV absorption
CO	In-flight	VUV fluorescence
H_2O total, and gaseous	In-flight	Laser photo acoustic and chilled mirror
H_2O total, and gaseous	In-flight	Laser photo acoustic and chilled mirror
NO	In-flight	Chemiluminescence with O_3
NOy	In-flight	Chemiluminescence after conversion to NO
Hg	In-flight	Enrichment and atomic fluorescence
CO_2	In-flight	Non-Dispersive Infrared Absorption (NDIR)
O_2 ultra, high precision	In-flight	Electrochemical cells with ultimate temperature and pressure stabilization
Methanol, acetone, acetaldehyde, e.o.	In-flight	Proton transfer mass spectrometer (PTR-MS)
Aerosol concentration, diameter > 4 nm	In-flight	Condensation particle counter (CPC)
Aerosol concentration, diameter >12 nm	In-flight	Condensation particle counter (CPC)
Aerosol concentration, diameter >18 nm	In-flight	Condensation particle counter (CPC)
Aerosol size distribution, 150 – 5000 nm	In-flight	Optical particle counter (OPC)
Aerosol elemental composition	Lab	Impactor collection, analysis by PIXE
Particle morphology	Lab	Impactor collection, analysis by electron microscope
VOC	Lab	Enrichment and analysis by GC-MS
Hydrocarbons, halocarbons, CO_2, CH_4, N_2O, SF_6	Lab	Whole air sampler with glass flasks, analysis by GC and GC-MS
BrO, HCHO, OClO, O_4	In-flight Remote sensing	Differential optical absorption spectroscopy (DOAS)
Cirrus clouds, (under certain conditions)	In-flight	Video Camera
Physical data		Aircraft data

A1: List of scientific equipment on Airbus A340-600 for the CARIBIC project. The measurements consist of in-flight and post-flight analyses. Over 50 trace gases, water vapor and aerosols are measured with a high degree of accuracy on regular base.

Compound	10^{-12} k_{OH}	10^{-17} k_{O3}	10^{-6} R_{OH}	10^{-6} R_{O3}	T
	(cm^3 molecule^{-1} s^{-1})		(s^{-1})	(s^{-1})	(days)
Alkanes					
Ethane, C_2H_6	0.26	c	0.2		56
Propane, C_3H_8	1.15	c	0.9		12
n-Butane, C_4H_{10}	2.54	c	2		5.7
Isobutane, C_4H_{10}	2.33	c	1.9		6.2
n-Pentane, C_5H_{12}	3.94	c	3.1		3.7
Isopentane, C_5H_{12}	3.9	c	3.1		3.7
n-Octane, C_8H_{18}	8.68	c	6.9		1.7
Alkenes, alkadienes, alkynes					
Ethene, C_2H_4	8.52	0.16	6.8	1.2	1.4
Propene, C_3H_6	26.3	1	21	6.5	0.4
I-Butene, C_4H_8	31.4	0.96	25.1	6.2	0.4
cis/trans-2-Butene, C_4H_8	60.2	15.7	48.1	102	0.08
I-Pentene, C_5H_{10}	31.4	1	25.1	6.5	0.4
2-Methyl-2-Butene, C_5H_{10}	86.9	40	69.5	260	0.04
1,3-Butadiene, C_4H_6	66.6	0.63	53.3	4.1	0.2
Isoprene, C_5H_8	101	1.28	80.8	8.3	0.1
Acetylene, C_2H_2	0.8	0.0008	0.65	0.005	18
Aromatic compounds					
Benzene, C_6H_6	1.23	c	1		12
Toluene, $C_6H_5CH_3$	6	c	4.8		2.4
o-Xylene, $C_6H_4(CH_3)_2$	13.7	c	11		1
m-Xylene, $C_6H_4(CH_3)_2$	23.6	c	18.9		0.6
p-Xylene, $C_6H_4(CH_3)_2$	14.3	c	11.4		1
Ethylbenzene, $C_6H_5C_2H_5$	7.1	c	5.7		2
Monoterpenes, $C_{10}H_{16}$					
α-Pinene	53.7	8.7	42.9	56.5	0.1
ß-Pinene	78.9	1.5	63.1	9.7	0.16
Limonene	171	20	137	130	0.04
Myrcene	215	47	172	305	0.02
3-Carene	80	3.7	64	24	0.13

A2: Hydrocarbon Reactivities - rate coefficients (at 298 K) and pseudo rate coefficients for reactions with OH radicals and O_3 (Atkinson 1994), and the corresponding lifetimes in days in the troposphere (assuming n(OH) = 8 x 10^5, n(O_3) = 6.5 x 10^{11} molecule cm^{-3}). "c" - rate coefficients for these reactions are less than ~ 1 x 10^{-22} cm^3 molecule^{-1} s^{-1}.

Type of Source	Emission Rate (Tg year^{-1})	Remarks
Anthropogenic sources		
Petroleum-related sources and chemical industry	36 ~ 62	Mainly alkanes, alkenes and aromatic compounds
Natural gas	2 ~ 14	Mainly light alkanes
Organic solvent use	8 ~ 20	Higher alkanes and aromatic compounds
Biomass burning	25 ~ 80	Mainly light alkanes and alkenes
Total anthropogenic sources	71 ~ 175	
Biogenic sources		
Isoprene[f]	175 ~ 503	
Monoterpenes[f]	127 ~ 480	
Other organic compounds[f]	510	Higher alkanes, alkenes, alcohols, aldehydes, ketones, esters
Grasslands	< 26	
Soils	< 3	
Ocean waters	2.5 ~ 6	Light alkanes and alkenes
	< 26	C_9-C_{28} alkanes
Total biogenic sources	815-1530	

A3: Summary of global emissions of hydrocarbons and other organic volatiles from various sources (Warneck, 2000). Isoprene, monoterpenes and other organic compounds were considered to be produced from foliage, "f" - emissions from foliage.

| Compound	Location	Car exhaust	Gasoline spillage	Gasoline evaporation	Natural gas	Industrial processes	Solvents
Alkanes							
Ethane	a	7.9	-	-	90.9"	-	-
Ethane	b	18.2	-	-	82.2	-	-
Propane	a	-	-	3.6	96.4"	-	-
Propane	b	1.2	-	7.9	26.6	64.4	-
n-Butane	a	24	7	40.5	28.2"	-	-
n-Butane	b	14.6	9.3	59.3	4	12.8	-
Isobutane	a	16.3	3.5	33.3	46.9"	-	-
Isobutane	b	11.4	6.1	56.2	4.3	22	-
n-Pentane	a	47.5	13.3	23.3	15.9"	-	-
n-Pentane	b	26.6	24.2	43.7	1.7	-	2.9
Isopentane	a	37.5	14	37.3	10.7"	-	-
Isopentane	b	22.6	22.3	53.6	0.9	-	0.9
2-Methylpentane	b	31.3	29.8	21.8	0.8	-	15.7
3-Methylpentane	b	33.1	30.4	20.4	0.8	-	17.3
n-Hexane	b	32.9	28.3	15	1.3	-	22.6
n-Nonane	b	7.6	6.5	-	-	-	85.1
n-Decane	b	18.1	8.7	-	-	-	73.1
Alkenes							
Ethene	b	98.9	-	-	1.4	-	-
Propene	b	49.9	-	-	0.3	49.8	-
I-Butene	b	67.3	3.3	29.4	-	-	-
Isobutene	b	77.4	2.6	17.7	-	-	-
trans-2-Butene	b	23.3	10.6	65.8	-	-	-
cis-z-Butene	b	22.7	11.3	63.9	-	-	-
Alkynes							
Acetylene	a	100	-	-	-	-	-
Acetylene	b	100	-	-	-	-	-
Aromatics							
Benzene	b	77	17.8	6	-	-	-
Toluene	b	38.7	16.3	1.7	-	-	43
Ethylbenzene	b	45.4	17.5	1.1	-	-	33.7

A4: Percentage contribution of various sources to hydrocarbons in (a) Los Angeles, Califomia (Mayrson and Crabtree, 1976) and (b) Sidney Australia (Nelson et al., 1983). " %" " - Includes both natural gas emanating from the ground before processing and commercial natural gas.

| TimeDate	ProcTime	TmpSCR	TmpDWR	TmpVol	TmpCO2	TmpPF	TmpKF	TmpKFMod	Flow0	RawFlow0	Flow1	RawFlow1	Flow2	RawFlow2	Flow3	RawFlow3	Vol	mol	Volth	Pressure	PressVol	PressVol1
06.10.05 18:33:29	0:00:01	40.64	-197.1	25.32	59.96	14.3	26.8	79.92	2.02	808	2.02	1006	0.09	1	9.26	953	97.309	0.10383	2330.96	1600	100902	100894
06.10.05 18:33:29	0:00:02	40.59	-197.1	25.28	59.96	14.3	26.9	79.92	2.02	808	2.02	1006	0.1	2	9.26	953	97.309	0.10383	2330.96	1599	100902	100894
06.10.05 18:33:29	0:00:02	40.59	-197.1	25.32	59.96	14.4	26.9	79.92	2.02	808	2.02	1006	0.09	1	9.33	960	97.311	0.10383	2330.96	1600	100902	100894
06.10.05 18:33:30	0:00:03	40.55	-197.1	25.32	60	14.4	26.6	79.92	2.02	808	2.02	1006	0.09	1	9.33	960	97.311	0.10383	2330.96	1600	100902	100894
06.10.05 18:33:30	0:00:03	40.55	-197.1	25.28	59.96	14.4	26.6	79.92	2.02	808	2.02	1006	0.09	1	9.51	979	97.312	0.10383	2330.96	1600	100902	100894
06.10.05 18:33:31	0:00:03	40.51	-197.1	25.32	60.08	14.4	26.8	79.92	2.02	808	2.02	1005	0.09	1	9.51	979	97.313	0.10385	2330.96	1599	100890	100894
06.10.05 18:33:31	0:00:04	40.51	-197.1	25.32	60.08	14.5	26.9	79.92	2.02	808	2.02	1006	0.09	1	9.36	963	97.313	0.10385	2330.96	1599	100890	100894
06.10.05 18:33:31	0:00:04	40.51	-197.1	25.28	60.04	14.5	26.8	79.92	2.02	808	2.02	1006	0.09	1	9.36	963	97.314	0.10383	2330.96	1600	100902	100894
06.10.05 18:33:32	0:00:05	40.47	-197.1	25.32	60	14.5	26.8	79.92	2.02	808	2.02	1006	0.09	1	9.44	971	97.314	0.10383	2330.96	1600	100902	100894
06.10.05 18:33:32	0:00:05	40.47	-197.1	25.32	60	14.5	26.8	79.92	2.02	808	2.02	1006	0.09	1	9.44	971	97.315	0.10385	2330.96	1600	100902	100894
06.10.05 18:33:33	0:00:05	40.47	-197.1	25.32	60	14.5	26.9	79.92	2.02	808	2.02	1006	0.12	3	9.5	978	97.316	0.10383	2330.96	1601	100902	100894
06.10.05 18:33:33	0:00:06	40.39	-197.1	25.28	60	14.6	26.6	79.92	2.02	808	2.02	1005	0.1	2	9.47	975	97.316	0.10383	2330.96	1599	100890	100894
06.10.05 18:33:33	0:00:06	40.39	-197.1	25.32	60	14.6	26.9	79.92	2.02	808	2.02	1006	0.09	1	9.36	963	97.316	0.10385	2330.96	1600	100902	100894
06.10.05 18:33:33	0:00:06	40.35	-197.1	25.32	60	14.7	26.8	79.92	2.02	808	2.02	1006	0.09	1	9.36	963	97.317	0.10385	2330.96	1599	100902	100894
06.10.05 18:33:34	0:00:07	40.35	-197.1	25.32	60	14.7	26.6	79.92	2.02	808	2.02	1005	0.1	2	9.56	984	97.317	0.10385	2330.96	1599	100902	100894
06.10.05 18:33:34	0:00:07	40.35	-197.1	25.32	60	14.7	26.6	72.1	2.02	732	2.64	1317	0.14	4	9.56	984	97.318	0.10385	2330.96	1599	100902	100894
06.10.05 18:33:35	0:00:07	40.31	-197.1	25.32	60	14.7	26.6	71.9	2.02	730	3.02	1508	0.09	1	9.56	984	97.318	0.10385	2330.96	1600	100902	100894
06.10.05 18:33:35	0:00:08	40.27	-197.1	25.28	60	14.7	26.6	71.9	2.02	730	3.02	1508	0.12	3	9.58	986	97.319	0.10385	2330.96	1601	100902	100894
06.10.05 18:33:35	0:00:08	40.27	-197.1	25.32	60	14.7	26.6	71.9	2.02	730	3.02	1507	0.14	4	9.68	996	97.32	0.10385	2330.96	1601	100902	100894
06.10.05 18:33:36	0:00:09	40.23	-197.1	25.32	60	14.8	26.4	71.9	2.02	730	3.02	1508	0.12	3	9.65	993	97.321	0.10385	2330.96	1599	100890	100894
06.10.05 18:33:36	0:00:09	40.23	-197.1	25.32	60	14.8	26.4	71.9	2.02	730	3.02	1509	0.09	1	9.65	993	97.321	0.10385	2330.96	1600	100902	100894
06.10.05 18:33:36	0:00:09	40.23	-197.1	25.28	60	14.8	26.4	71.9	2.02	730	3.02	1509	0.09	1	9.58	986	97.321	0.10385	2330.96	1600	100902	100894
06.10.05 18:33:37	0:00:09	40.23	-197.14	25.32	60	14.8	26.4	71.9	2.02	730	3.02	1508	0.12	3	9.65	993	97.322	0.10385	2330.96	1600	100902	100894
06.10.05 18:33:37	0:00:10	40.23	-197.14	25.32	60	14.8	26.4	71.9	2.02	730	3.02	1507	0.14	4	9.68	996	97.323	0.10385	2330.96	1599	100902	100894
06.10.05 18:33:37	0:00:10	40.14	-197.1	25.28	60	14.8	26.4	71.9	2.02	729	3.02	1508	0.1	2	9.72	1000	97.324	0.10385	2330.96	1600	100902	100894
06.10.05 18:33:38	0:00:11	40.14	-197.1	25.28	60.04	14.9	26.4	71.9	2.02	729	3.02	1508	0.12	3	9.87	1015	97.324	0.10386	2330.96	1600	100902	100894
06.10.05 18:33:38	0:00:11	40.14	-197.1	25.28	60	14.9	26.4	71.9	2.02	730	3.02	1507	0.09	1	9.72	1000	97.325	0.10386	2330.96	1600	100902	100894
06.10.05 18:33:38	0:00:11	40.1	-197.1	25.32	59.96	14.9	26.3	71.9	2.02	729	3.02	1508	0.1	3	9.76	1004	97.326	0.10386	2330.96	1600	100902	100894
06.10.05 18:33:39	0:00:12	40.1	-197.1	25.28	59.96	14.9	26.3	71.9	2.02	729	3.02	1509	0.14	4	9.76	1004	97.327	0.10385	2330.96	1600	100890	100894
06.10.05 18:33:39	0:00:12	40.1	-197.1	25.28	60	14.9	26.3	71.9	2.02	729	3.02	1509	0.12	3	9.85	1013	97.327	0.10385	2330.96	1600	100902	100894
06.10.05 18:33:39	0:00:12	40.1	-197.14	25.28	60	14.9	26.6	71.8	2.02	729	3.02	1508	0.12	3	9.85	1013	97.328	0.10385	2330.96	1600	100902	100894
06.10.05 18:33:40	0:00:13	40.02	-197.14	25.28	60	14.9	26.3	71.8	2.02	729	3.02	1507	0.12	3	9.82	1010	97.329	0.10385	2330.96	1600	100890	100894
06.10.05 18:33:40	0:00:13	40.02	-197.14	25.28	60.08	15	26.3	71.8	2.02	729	3.02	1508	0.12	3	9.85	1013	97.33	0.10385	2330.96	1600	100890	100894
06.10.05 18:33:41	0:00:13	40.02	-197.14	25.32	60.08	15	26.8	71.8	2.02	729	3.02	1508	0.12	3	9.82	1010	97.33	0.10385	2330.96	1601	100902	100894
06.10.05 18:33:41	0:00:14	40.02	-197.1	25.32	60.08	15	26.2	71.8	2.02	729	3.02	1508	0.12	3	9.87	1015	97.331	0.10385	2330.96	1601	100902	100894
06.10.05 18:33:41	0:00:14	39.98	-197.1	25.32	59.92	15	26.2	71.8	2.02	729	3.02	1508	0.14	4	9.87	1015	97.332	0.10385	2330.96	1600	100902	100914

A5: Data-record of the first 14 seconds of the calibration procedure. The Data-record was stored with 2.5 Hz which means 2 and 3 values per second alternately.

| time	procedure variable	set-status	setvalue	description
0:00:05	MuPo1	on	3	multi-position valve to position 3
0:00:06	Flow3	on	40	flow3 setting-40 ml/min
0:00:07	Flow0	on	96	flow0 setting-96 ml/min
0:00:08	Flow1	on	4	flow1 setting-4 ml/min
0:00:10	Valco5	off		valve 5 to position B
0:00:15	MV4	on		piston KF up-on
0:00:15	Heater3	on	140	heating KF on 140 °C
0:00:30	Heater3	on	60	heating KF on 60 °C
0:00:35	MV4	off		piston KF up-off
0:02:00	Heater3	off		heating KF off
0:02:20	Valco4	on		valve 4 to position A
0:02:30	Heater1	on	130	heating PF on 130 °C
0:02:35	Heater2	on	100	heating SCR on 100 °C
0:20:00	Heater1	off		heating PF off
0:20:05	Heater2	on	60	heating SCR on 60 °C
0:25:00	Valco2	on		valve 2 to position B
0:28:00	MV1	on		piston PF down-on
0:28:10	MV1	off		piston PF down-off
0:29:00	Valco3	on		valve 3 to position A
0:29:30	Heater1	on	-100	heating PF on -100 °C
0:29:31	p24_5	on	255	3-way valve open
0:30:00	Volume	on	1000	overall volume setting-1000 ml
0:30:01	Flow2	on	50	flow2 setting-50 ml/min
0:30:29	p24_4	on	255	3-way valve open
0:31:00	Valco4	off		valve 4 to position B
0:31:00	p24_5	on	0	3-way valve closed
0:51:05	Valco2	off		valve 2 to position A
0:51:06	Valco4	on		valve 4 to position A
0:52:40	MV3	on		piston KF down-on
0:52:45	MV3	off		piston KF down-off
0:52:59	Heater1	off		heating PF off
0:53:00	MV2	on		piston PF up-on
0:53:05	MV2	off		piston PF up-off
0:53:15	Valco5	on		valve 5 to position A
0:54:05	Heater1	on	120	heating PF on 120 °C
0:54:10	Valco3	off		valve 3 to position B
0:54:20	Heater2	on	80	heating SCR on 80 °C
1:00:00	CTRL2	on		start-command for GC on
1:00:05	CTRL2	off		start-command for GC off

A6: Calibration procedure as a list of commands. It represents one point on the calibration curve. As it may be seen the whole procedure takes 1 hour and 5 seconds. Not all procedure variables admit setvalue. Short description of each step is in the last column.
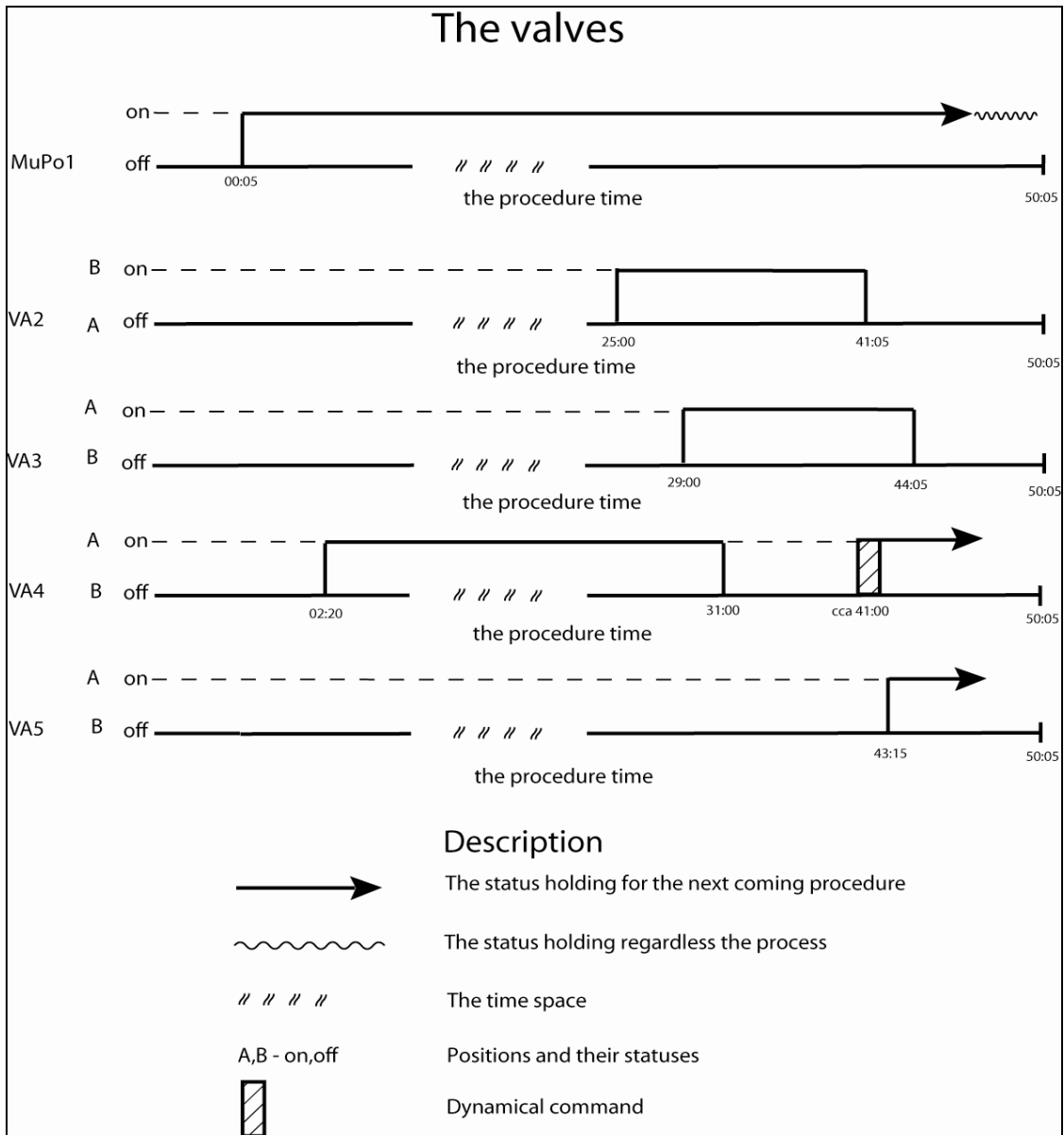
A7: Time space diagram of the Valco-Vici valves for shorter version of procedure (50:05). MuPo1, VA4 and VA5 stay in their positions for next coming procedure. MuPo1 stays in its position even after the main process is switched off. Switching of VA4 is a dynamic event depending on volume integration.
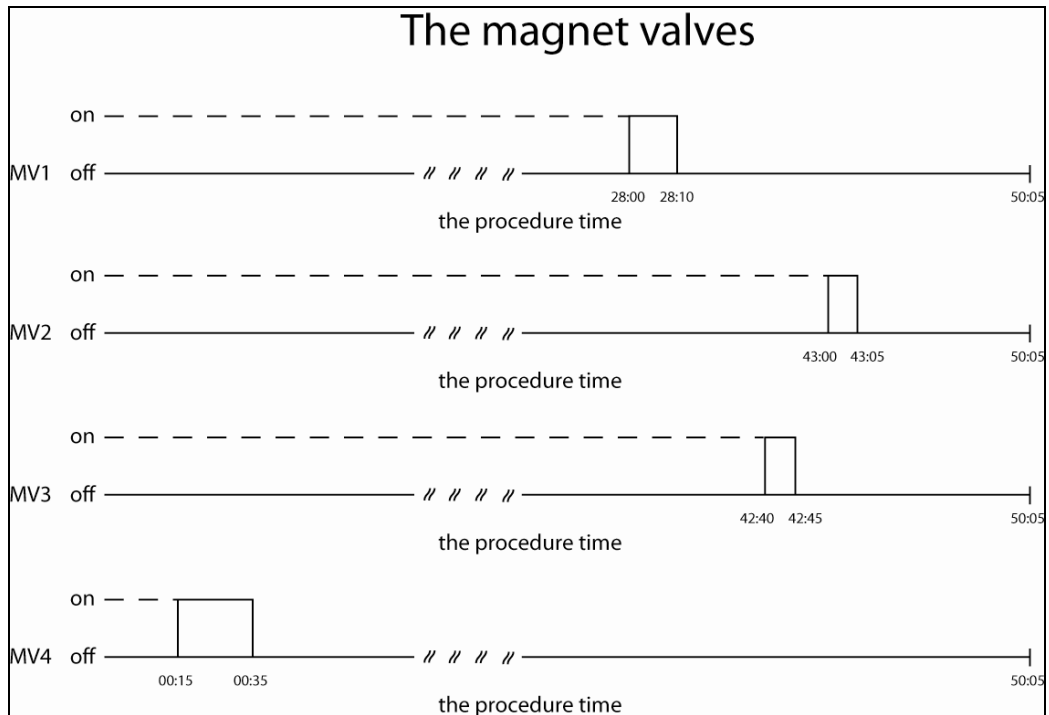
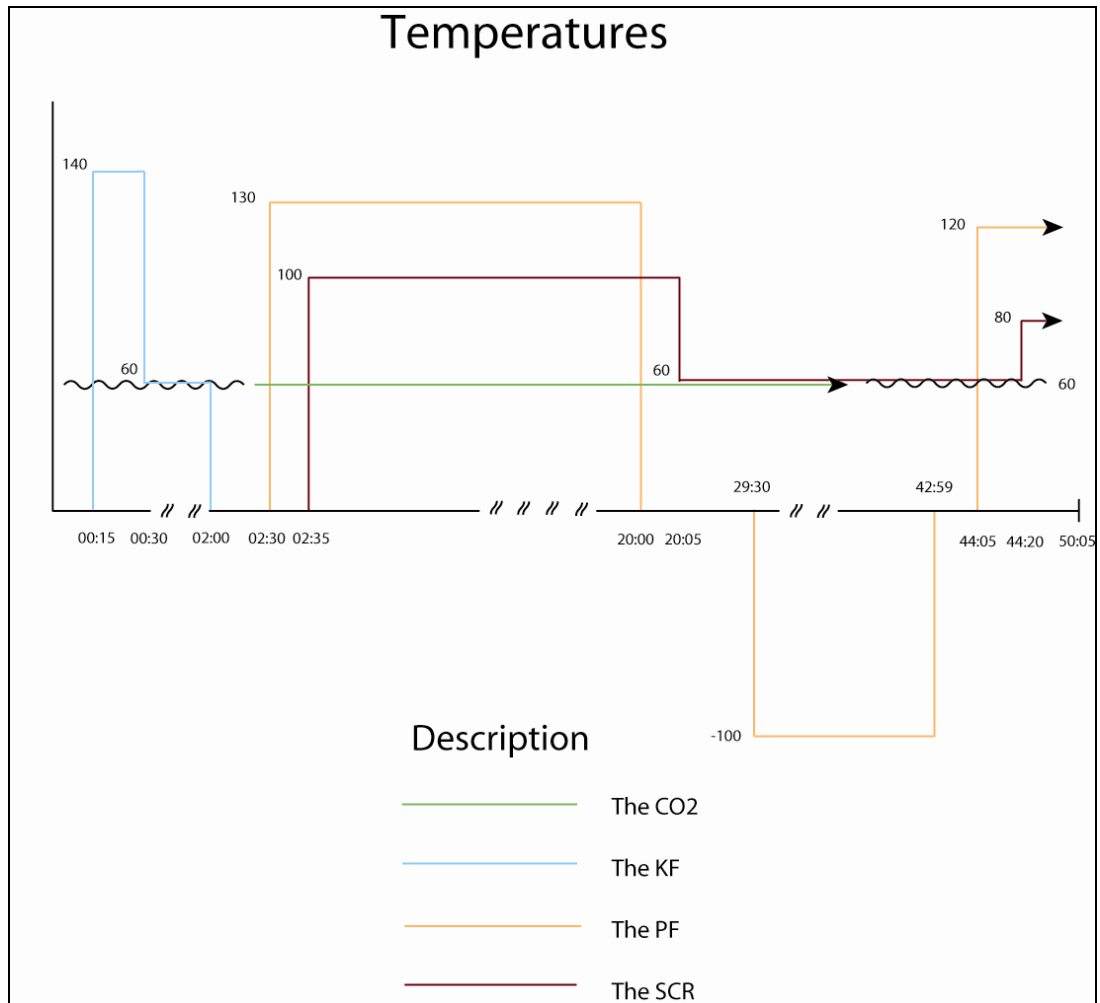*A8: Time space diagram of the magnet valves for shorter version of procedure (50:05). MV1 and MV2 actuate PF, MV3 and MV4 actuate KF.*
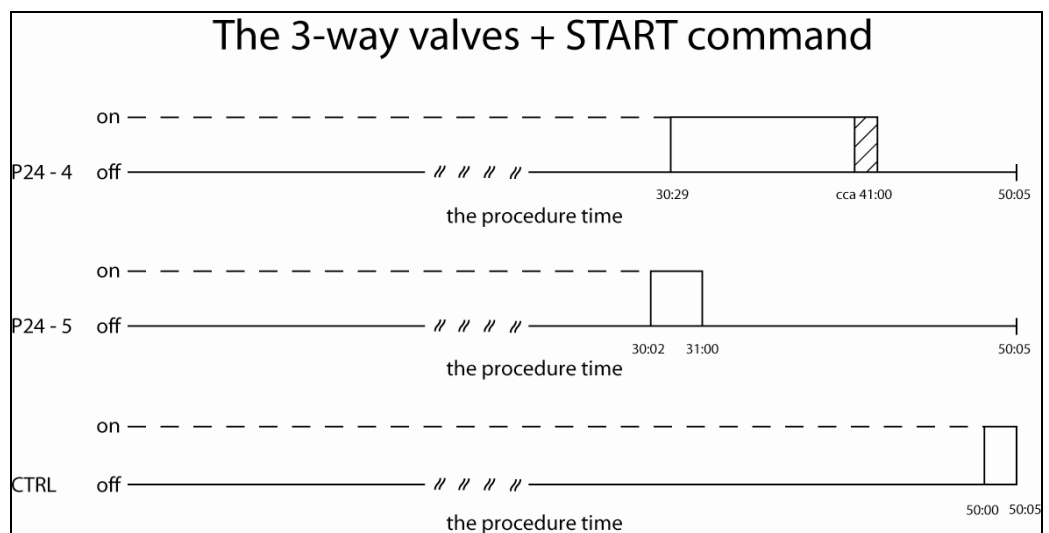
A9: Time space diagram of the 3-way valves and START command for shorter version of procedure (50:05). The p24_4 let sample stream to flow through FC2. The p24_5 is the outlet on expansion volume. The p24_4 switching is a dynamic event depending on volume integration.
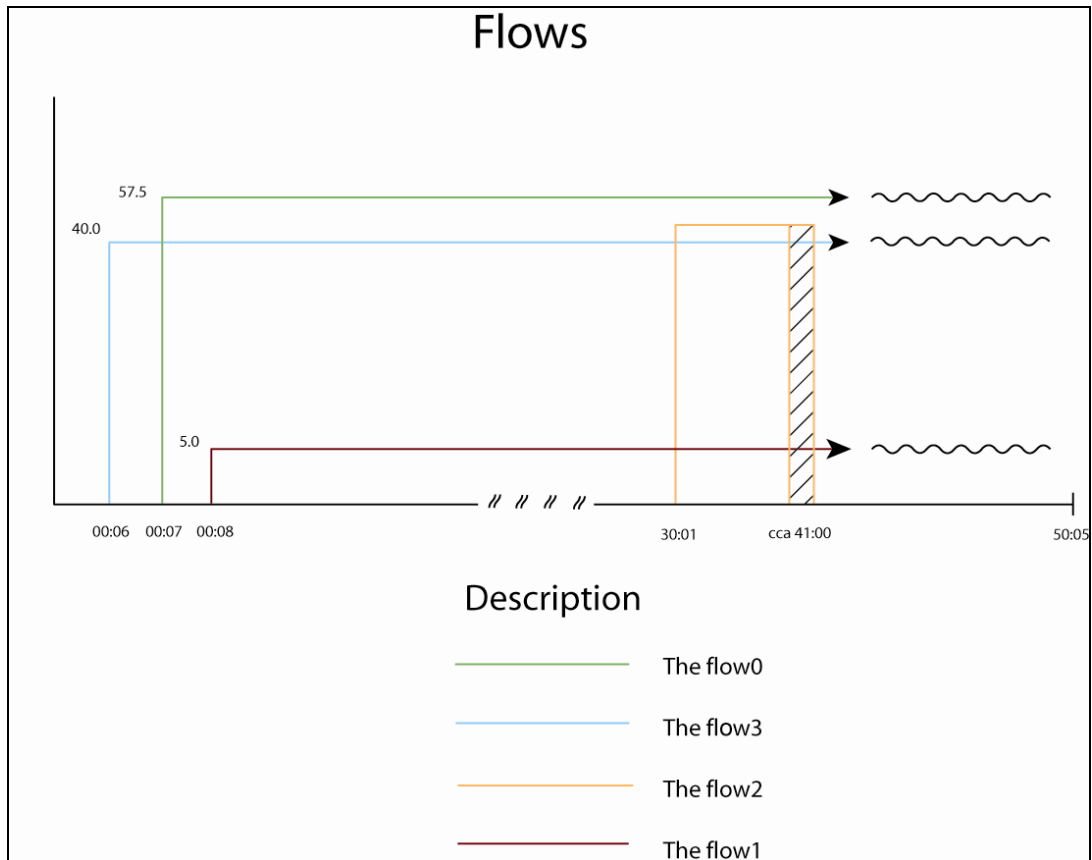
A10: Time space diagram of the used flow controllers for shorter version of procedure (50:05). Except for the flow2 flows stay regardless the main process. Flow2 depends on volume integration.

A11: Time space diagram of the used temperatures for shorter version of procedure (50:05). The CO₂ temperature is not handled from the procedure therefore it stays regardless the main process. The KF temperature is controlled only during the heating phase and not during the focusing.

Compound	concentration (ppb)	uncertainty (ppb)
Ethane	8.17	0.16
Ethene	4.27	0.09
Ethyne	9.06	0.18
Propane	3.63	0.07
Propene	4.10	0.08
Propyne	2.53	0.05
n-Butane	1.90	0.04
iso-Butane	1.20	0.02
iso-Butene	4.04	0.08
But-1-ene	4.01	0.08
trans-2-Butene	1.36	0.03
cis-2-Butene	2.69	0.05
1,3-Butadiene	5.44	0.11
n-Pentane	1.11	0.02
iso-Pentane	1.39	0.03
trans-2-Pentene	4.67	0.09
cis-2-Pentene	2.40	0.05
Isoprene	2.92	0.06
2-MethylPentane	1.79	0.04
3-MethylPentane	2.77	0.06
Cyclohexane	4.76	0.10
n-Hexane	3.15	0.06
Benzene	5.39	0.11
n-Heptane	2.42	0.05
Toluene	4.16	0.08
Ethylbenzene	1.70	0.03
o-Xylene	1.39	0.03
m-Xylene	2.11	0.04
1,2,3-Trimethylbenzene	1.07	0.04
1,3,5-Trimethylbenzene	1.25	0.06

A12: NPL standard gas mixture, cylinder APE 289347, from 10th March 2004. Cylinder has geometrical volume of 10L. Table lists all hydrocarbon concentrations with their uncertainties (all in ppb).
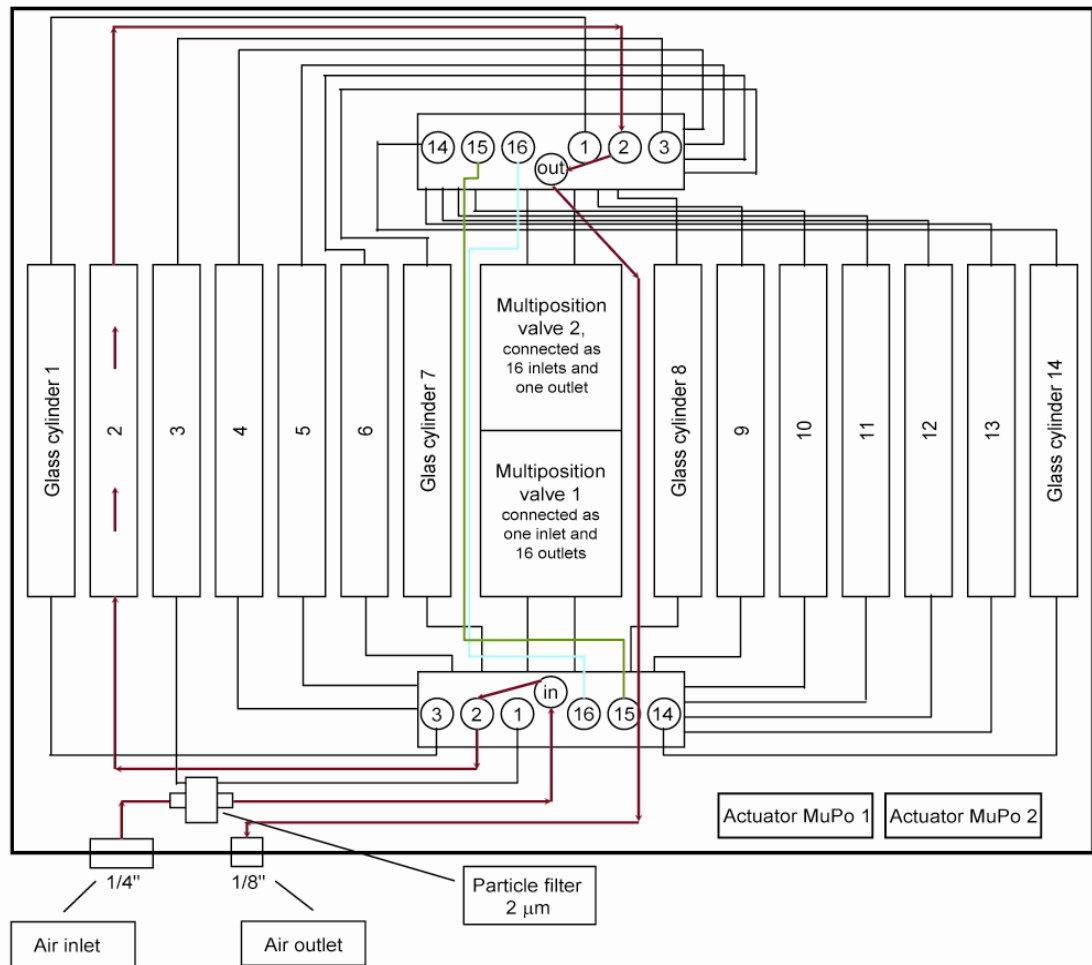
A13: Detailed scheme of the TRAC input-output connections. Each multi-position 16-way valve (MuPo) possesses one inlet and 16 circular arranged outlets (not all shown). The red line stands for the sample way from air inlet to the air outlet. Ports # 15,16 of both valves are connected together, green and blue line respectively. The valves are controlled by actuators mounted inside the collector.

signal	Name/positions	Absolute difference of duplicate measurements (ppt)											
		2	3	4	5	6	7	8	9	10	11	12	13
1	Ethane	5.93	19.97	6.99	14.53	14.91	20.10	12.31	16.47	25.00	3.19	37.57	19.09
1	Ethene	0.45	4.79	2.13	7.18	1.36	2.30	1.91	2.79	0.21	2.62	1.95	4.72
1	Ethyne	2.83	1.64	2.06	0.36	3.16	1.24	0.30	3.42	1.14	1.74	2.01	1.37
1	Propane	3.81	4.92	0.48	1.23	0.13	6.83	1.08	0.17	0.90			6.22
1	Propene	0.91	0.39	1.01	1.84	0.06	1.36	2.28	13.92	2.63	0.62	2.54	2.36
1	i-Butane							1.96				2.50	0.09
1	n-Butane	1.91	0.21	0.51	1.13	1.96	1.57	1.53	0.83	0.37	0.98	2.72	1.57
1	1-Butene	2.53	0.79	0.60	0.28	1.14	1.31	0.99	0.56	1.15	0.70		1.90
1	n-Pentane	0.30	0.45	0.31	0.90	1.01	1.99	0.07	0.50	0.38	1.36	1.05	1.63
2	Ethane	17.34	17.48	1.62	0.84	3.24	19.16	17.06	30.12	17.17	18.78	41.41	45.12
2	Propene	2.18	2.22	2.03	3.25	1.85	0.43	1.88	11.64	0.52	4.46	2.28	0.05
2	Propane	0.93	1.10	0.15	0.39	0.12	0.43	0.50	3.51	2.77	0.36	2.13	5.19
2	i-Butane							0.08				1.47	0.94
2	n-Butane	0.71	0.28	2.17	0.81	0.56	0.84	0.81	0.44	0.26	0.53	1.52	0.25
2	n-Pentane	1.67	0.06	1.01	1.06	0.27	1.13	0.44	0.71	2.86	0.72	0.32	0.83
2	Hexane	0.45	2.02			0.54	0.40	0.26	0.24	0.49	1.36		
2	Benzene	1.33	0.34	0.27	0.20	0.43	0.01	0.68	0.24	2.48	1.66	0.88	0.45
2	Heptane	0.71	0.33										
2	Toluene	0.27	0.35		0.54		0.04	0.18	0.80	0.01	0.16		
2	Ethylbenzene	1.72	0.21					0.97					
2	m-Xylene	1.45	0.87										
2	o-Xylene	2.00	0.38		0.23		0.80				0.43		

A14: Absolute differences of all duplicate measurements in ppt of the flight #114-117, TRAC2. Values calculated separately for both columns and each cylinder in the TRAC. Signal 1 is the Gas-pro, signal 2 is the Petrocol capillary column. Blank space indicates concentration below the detection limit.

| signal	Name/positions	Relative difference of duplicat measurements											
		2	3	4	5	6	7	8	9	10	11	12	13
1	Ethane	0.015	0.057	0.031	0.041	0.039	0.057	0.029	0.033	0.046	0.006	0.042	0.023
1	Ethene	0.007	0.085	0.066	0.140	0.034	0.050	0.040	0.047	0.006	0.064	0.075	0.103
1	Ethyne	0.144	0.066	0.178	0.018	0.182	0.065	0.010	0.158	0.045	0.083	0.063	0.036
1	Propane	0.082	0.121	0.024	0.033	0.004	0.165	0.004	0.013	0.002	0.016	0.008	0.027
1	Propene	0.022	0.008	0.069	0.039	0.002	0.017	0.089	0.394	0.076	0.015	0.174	0.089
1	i-Butane							0.286				0.178	0.003
1	n-Butane	0.218	0.022	0.066	0.147	0.253	0.296	0.173	0.083	0.045	0.116	0.084	0.024
1	1-Butene	0.204	0.047	0.130	0.024	0.237	0.109	0.137	0.107	0.120	0.055		0.277
1	n-Pentane	0.060	0.081	0.040	0.110	0.118	0.132	0.005	0.044	0.036	0.135	0.106	0.211
2	Ethane	0.041	0.044	0.006	0.002	0.008	0.046	0.033	0.051	0.027	0.032	0.038	0.043
2	Propene	0.027	0.025	0.040	0.036	0.025	0.003	0.028	0.149	0.007	0.051	0.040	0.001
2	Propane	0.019	0.025	0.006	0.009	0.003	0.010	0.007	0.037	0.033	0.006	0.007	0.018
2	i-Butane							0.014				0.096	0.027
2	n-Butane	0.067	0.023	0.242	0.085	0.071	0.113	0.070	0.037	0.025	0.057	0.039	0.003
2	n-Pentane	0.267	0.012	0.114	0.115	0.030	0.070	0.029	0.052	0.242	0.064	0.030	0.100
2	Hexane	0.071	0.388			0.113	0.101	0.070	0.058	0.130	0.319		
2	Benzene	0.080	0.016	0.026	0.014	0.042	0.000	0.030	0.014	0.115	0.073	0.046	0.019
2	Heptane	0.157	0.092										
2	Toluene	0.042	0.053		0.152		0.007	0.027	0.135	0.002	0.021		
2	Ethylbenzene	0.246	0.037					0.246					
2	m-Xylene	0.253	0.187										
2	o-Xylene	0.265	0.052		0.049			0.154			0.032		

A15: Relative differences of all duplicate measurements (no unit) of the flight #114-117, TRAC2. Values calculated separately for both columns and each cylinder in the TRAC. Signal 1 is the Gas-pro, signal 2 is the Petrocol capillary column. Blank space indicates concentration below the detection limit.

| signal	Name	a_H	A_{HS}	da_H	dA_{HS}	$(dx_{HS}/x_{HS})^2$	dx_{HSGM}	x_{HSGM}	$(dx_{HSGM}/x_{HSGM})^2$	$(dx_{HoV}/x_{HoV})^2$	dx_{HoV}/x_{HoV}	x_{HS}	dx_{HoV}
					$\delta X_{MES} + \delta X_{FUN}$			δX_{HSGM}			δX_{HoV}		
1	Ethane	0.000700	4.32	0.000003	0.142811	0.001112	0.16	8.17	0.000384	0.001496	0.038675	477.57	18.47
1	Ethene	0.000612	0.35	0.000011	0.020560	0.003786	0.09	4.27	0.000444	0.004231	0.065043	45.16	2.94
1	Ethyne	0.000724	0.22	0.000006	0.016080	0.005635	0.18	9.06	0.000395	0.006030	0.077653	23.30	1.81
1	Propane	0.000940	1.03	0.000005	0.027665	0.000752	0.07	3.63	0.000372	0.001124	0.033528	82.68	2.77
1	Propene	0.001057	0.55	0.000003	0.032932	0.003545	0.08	4.1	0.000381	0.003926	0.062656	37.20	2.33
1	i-Butane	0.001169	0.26	0.000012	0.022168	0.007263	0.02	1.2	0.000278	0.007540	0.086835	16.56	1.44
1	n-Butane	0.001175	0.28	0.000006	0.018723	0.004486	0.04	1.9	0.000443	0.004929	0.070210	15.09	1.06
1	1-Butene	0.001181	0.33	0.000003	0.016046	0.002355	0.08	4.01	0.000398	0.002753	0.052473	9.43	0.49
1	n-Pentane	0.001414	0.31	0.000008	0.014652	0.002298	0.02	1.11	0.000325	0.002622	0.051207	9.42	0.48
2	Ethane	0.000552	4.02	0.000006	0.131508	0.001190	0.16	8.17	0.000384	0.001574	0.039670	569.47	22.59
2	Propene	0.000830	0.85	0.000008	0.028286	0.001202	0.08	4.1	0.000381	0.001583	0.039783	80.01	3.18
2	Propane	0.000758	0.93	0.000006	0.013867	0.000285	0.07	3.63	0.000372	0.000657	0.025634	97.32	2.49
2	i-Butane	0.001027	0.47	0.000008	0.010612	0.000574	0.02	1.2	0.000278	0.000851	0.029180	18.41	0.54
2	n-Butane	0.001018	0.33	0.000007	0.009732	0.000916	0.04	1.9	0.000443	0.001359	0.036868	18.33	0.68
2	n-Pentane	0.001272	0.31	0.000010	0.014658	0.002327	0.06	3.15	0.000363	0.002652	0.051497	10.48	0.54
2	Hexane	0.001547	0.63	0.000006	0.013913	0.000500	0.11	5.39	0.000416	0.000862	0.029367	4.52	0.13
2	Benzene	0.001612	0.37	0.000007	0.015034	0.001654	0.05	2.42	0.000427	0.002070	0.045500	17.96	0.82
2	Heptane	0.001839	0.49	0.000003	0.011950	0.000606	0.08	4.16	0.000370	0.001033	0.032143	4.06	0.13
2	Toluene	0.001758	0.22	0.000004	0.006471	0.000847	0.03	1.7	0.000311	0.001217	0.034884	6.06	0.21
2	Ethylbenzene	0.001731	0.38	0.000007	0.020938	0.003114	0.03	1.7	0.000311	0.003425	0.058524	5.57	0.33
2	m-Xylene	0.001300	0.84	0.000005	0.018860	0.000515	0.04	2.11	0.000359	0.000874	0.029569	5.19	0.15
2	o-Xylene	0.001234	0.41	0.000004	0.011860	0.000839	0.03	1.39	0.000466	0.001305	0.036126	7.59	0.27

A16: Uncertainty overview for the detected compounds of the flight # 114-117. Signals were taken into an account separately. Signal 1 is the Gas-pro, signal 2 is the Petrocol capillary column. Data columns are ordered into three groups: uncertainty of measurements together with uncertainty from calibration function, uncertainty of standard gas mixture NPL and finally the overall uncertainty.

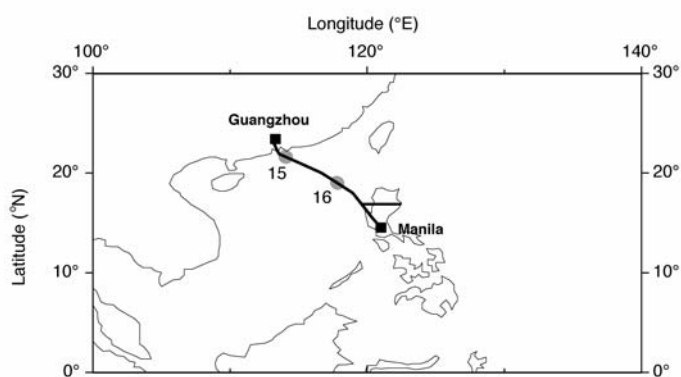| signal	Name	Areas for different enriched NPL volumes (ml)						$10^{-3}a_H$	$10^{-5}da_H$	x_{HS}	$u_c(y)$	dx_{Hov}
		10	20	30	40	50	60					
1	Ethane	0.84	1.66	2.48	3.18	3.99	4.72	0.38	0.42	477.57	3.84	10.11
1	Ethene	0.97	1.62	2.26	2.78	3.40	3.99	0.56	0.81	45.16	3.07	3.22
1	Ethyne	0.24	0.80	1.70	2.74	3.68	4.68	0.40	1.65	23.30	15.28	15.28
1	Propane	0.81	1.55	2.38	3.07	3.88	4.64	0.85	0.77	82.68	1.40	2.12
1	Propene	0.95	1.83	2.73	3.59	4.48	5.30	0.85	0.58	37.20	1.27	1.47
1	i-Butane	0.36	0.67	1.03	1.34	1.64	1.93	1.05	1.71	16.56	0.95	0.99
1	n-Butane	0.52	1.07	1.58	2.07	2.65	3.14	1.10	1.21	15.09	0.96	1.01
1	1-Butene	1.15	2.26	3.42	4.51	5.59	6.69	1.10	0.60	9.43	1.05	1.06
1	n-Pentane	0.39	0.77	1.12	1.50	1.84	2.25	1.33	1.43	9.42	0.55	0.58
2	Ethane	0.86	1.67	2.46	3.35	4.16	5.03	0.41	0.35	569.47	2.78	11.49
2	Propene	0.97	1.86	2.77	3.66	4.53	5.51	0.88	0.59	80.01	1.19	1.96
2	Propane	0.85	1.64	2.47	3.28	3.99	4.93	0.89	1.35	97.32	2.38	3.03
2	i-Butane	0.38	0.74	1.09	1.49	1.85	2.19	1.21	1.32	18.41	0.63	0.70
2	n-Butane	0.62	1.16	1.71	2.28	2.84	3.40	1.17	0.50	18.33	0.38	0.54
2	n-Pentane	0.44	0.84	1.28	1.68	2.10	2.54	1.51	1.17	10.48	0.40	0.44
2	Hexane	1.44	2.85	4.18	5.57	6.96	8.34	1.75	0.57	4.52	0.51	0.51
2	Benzene	2.41	4.70	7.07	9.43	11.77	14.07	1.74	0.39	17.96	0.58	0.68
2	Heptane	1.27	2.52	3.71	4.97	6.18	7.41	2.03	0.46	4.06	0.27	0.29
2	Toluene	2.15	4.27	6.38	8.50	10.63	12.72	2.03	0.25	6.06	0.24	0.27
2	Ethylbenzene	0.94	1.97	2.97	3.99	4.95	5.98	2.36	0.94	5.57	0.33	0.34
2	m-Xylene	1.12	2.39	3.66	4.89	6.14	7.39	2.38	0.65	5.19	0.28	0.30
2	o-Xylene	0.75	1.59	2.40	3.24	4.02	4.83	2.35	1.10	7.59	0.31	0.35

A17: The combined standard uncertainty $u_c(y)$ calculated from the 6 point calibration curve. Signals were taken into an account separately. Signal 1 is the Gas-pro, signal 2 is the Petrocol capillary column. Table shows measured peak areas (pA.s) and corresponding slopes with their uncertainties. The last column dx_{Hov} stands for the combined standard overall uncertainty.
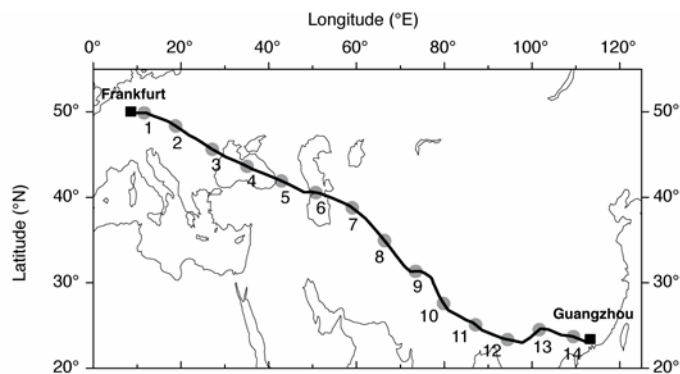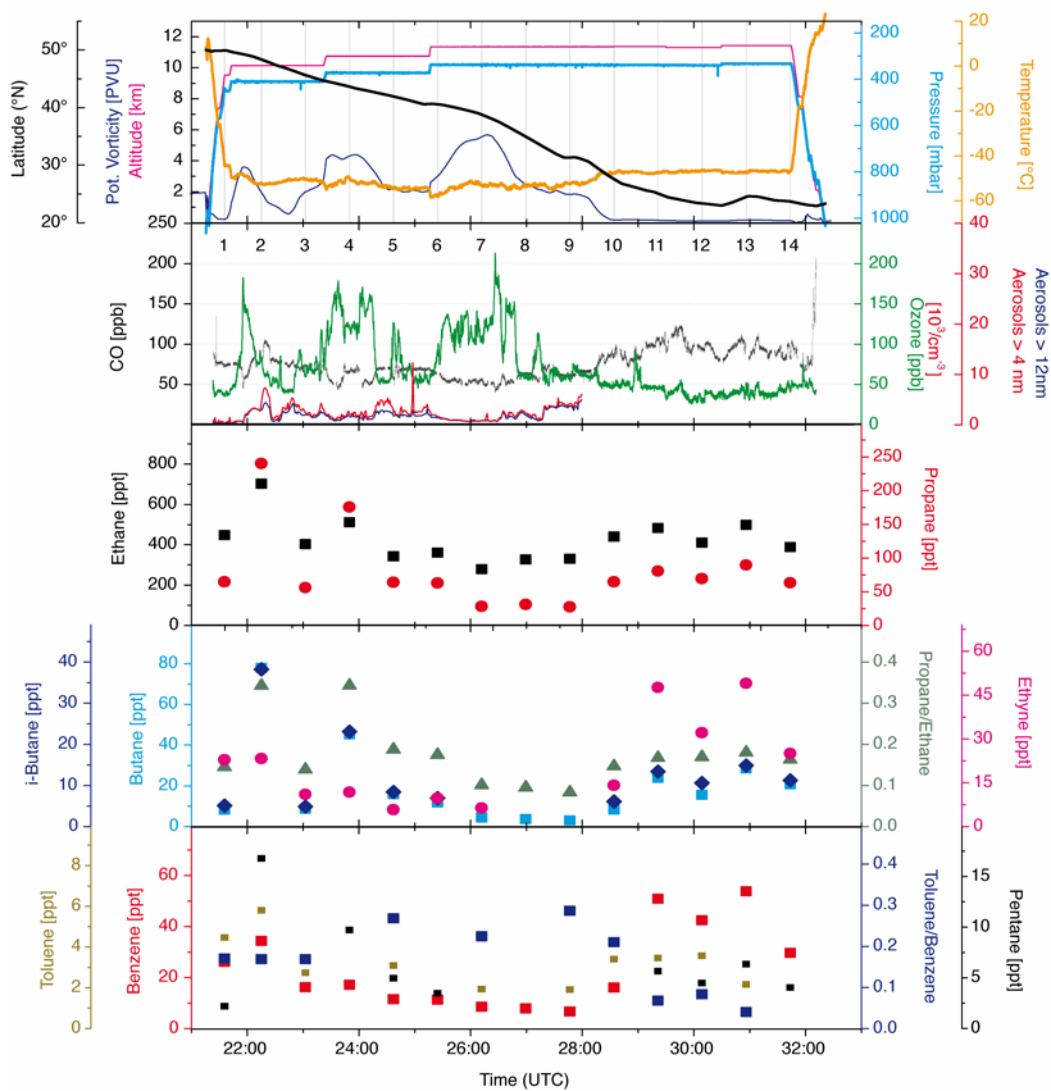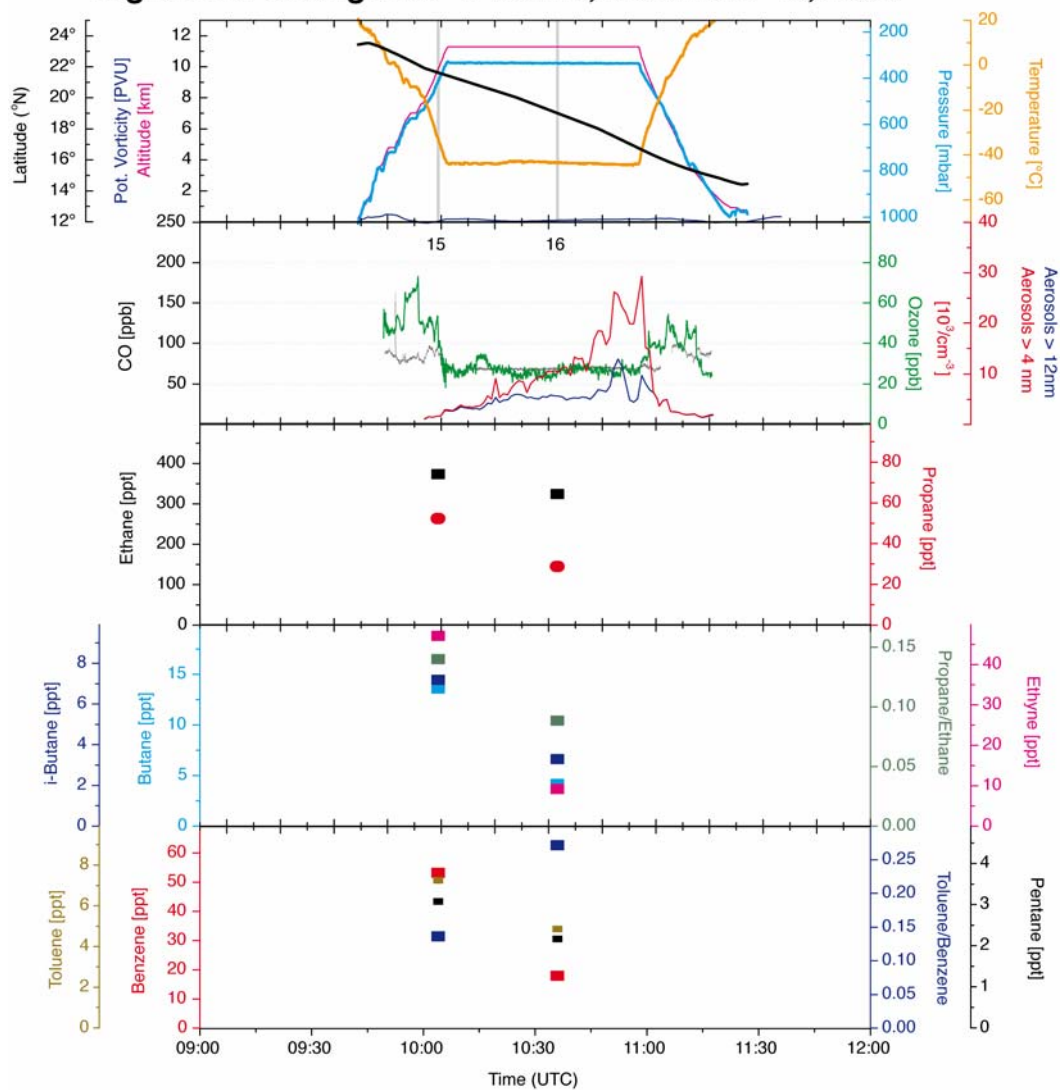
A18: CARIBIC flight # 130 from Frankfurt to Guangzhou on November 14, 2005.
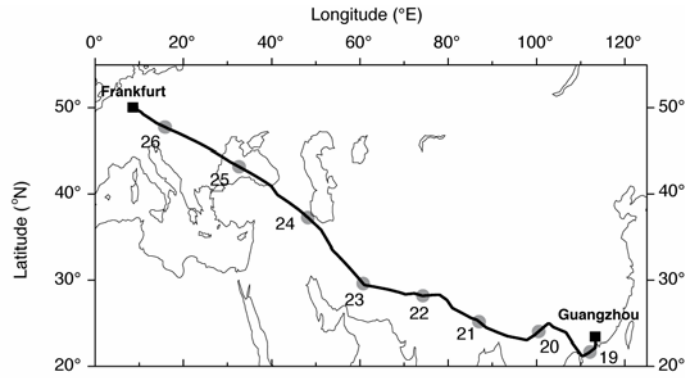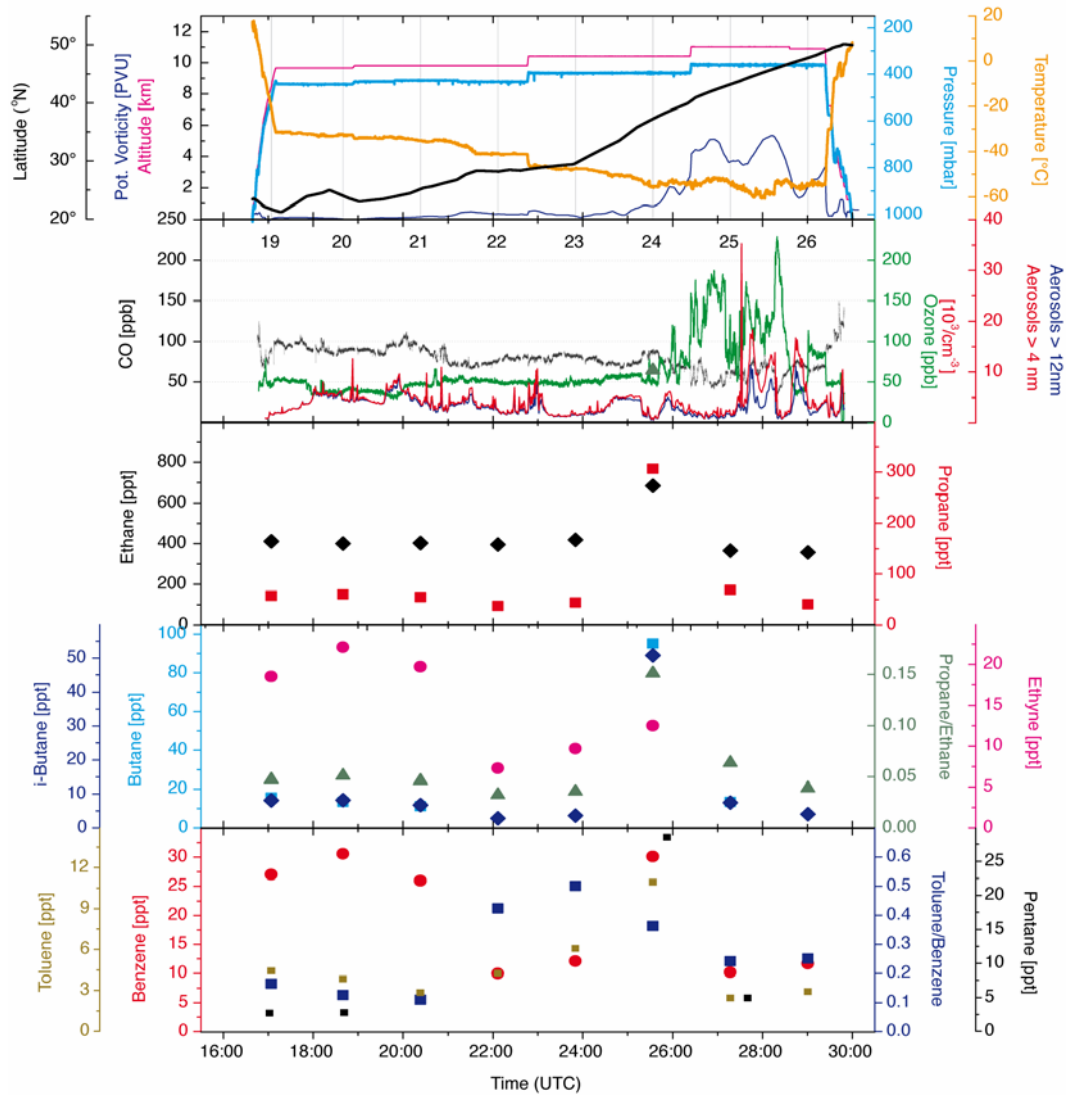
A19: CARIBIC flight # 131 from Guangzhou to Manila on November 15, 2005.
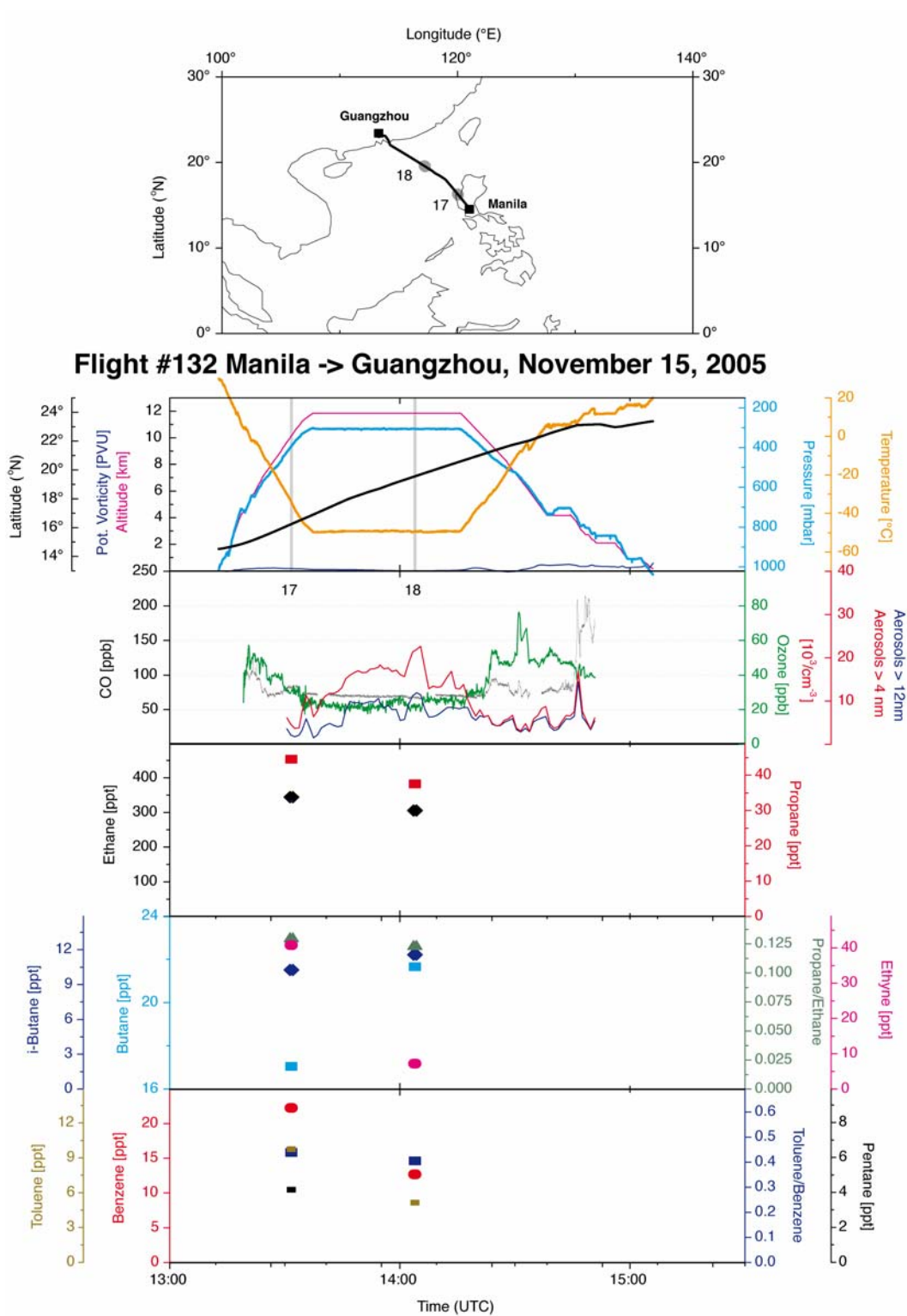
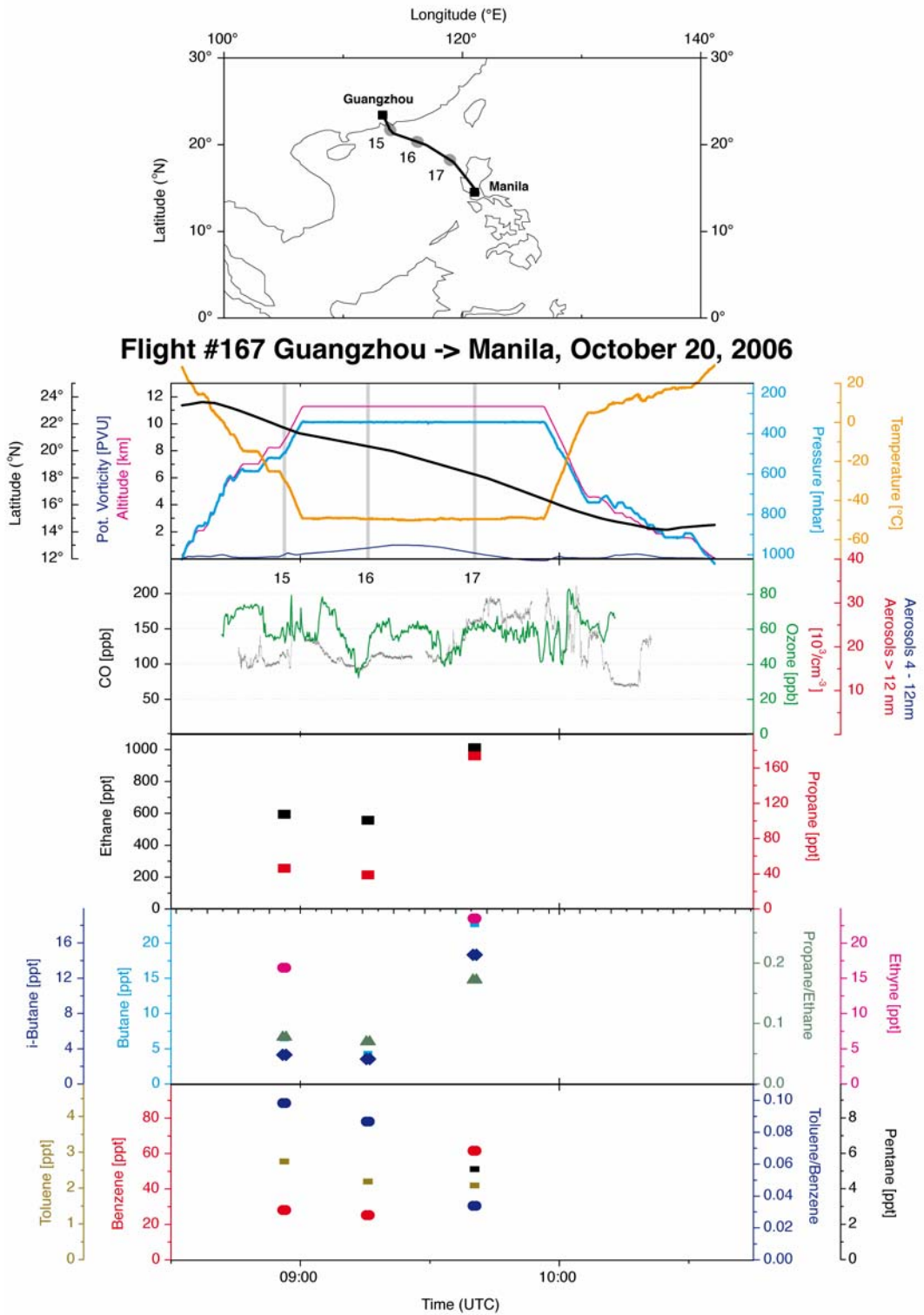*A20: CARIBIC flight # 132 from Manila to Guangzhou on November 15, 2005.*
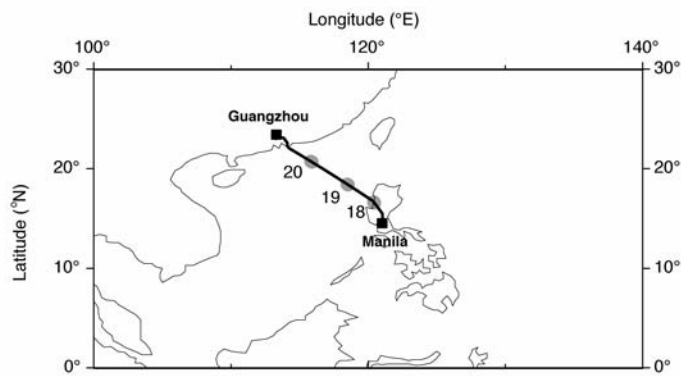
A21: CARIBIC flight # 133 from Guangzhou to Frankfurt on November 15, 2005.
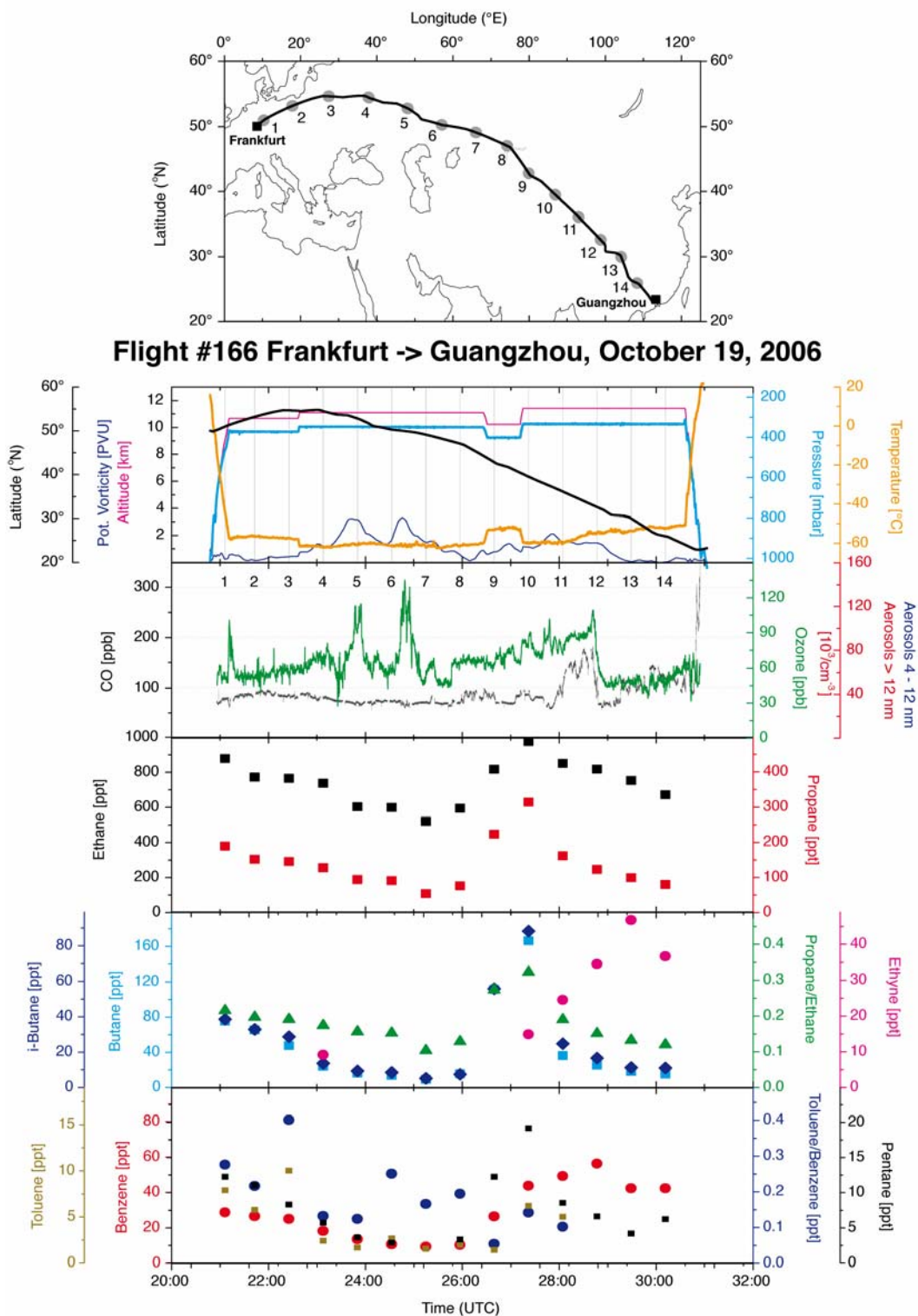
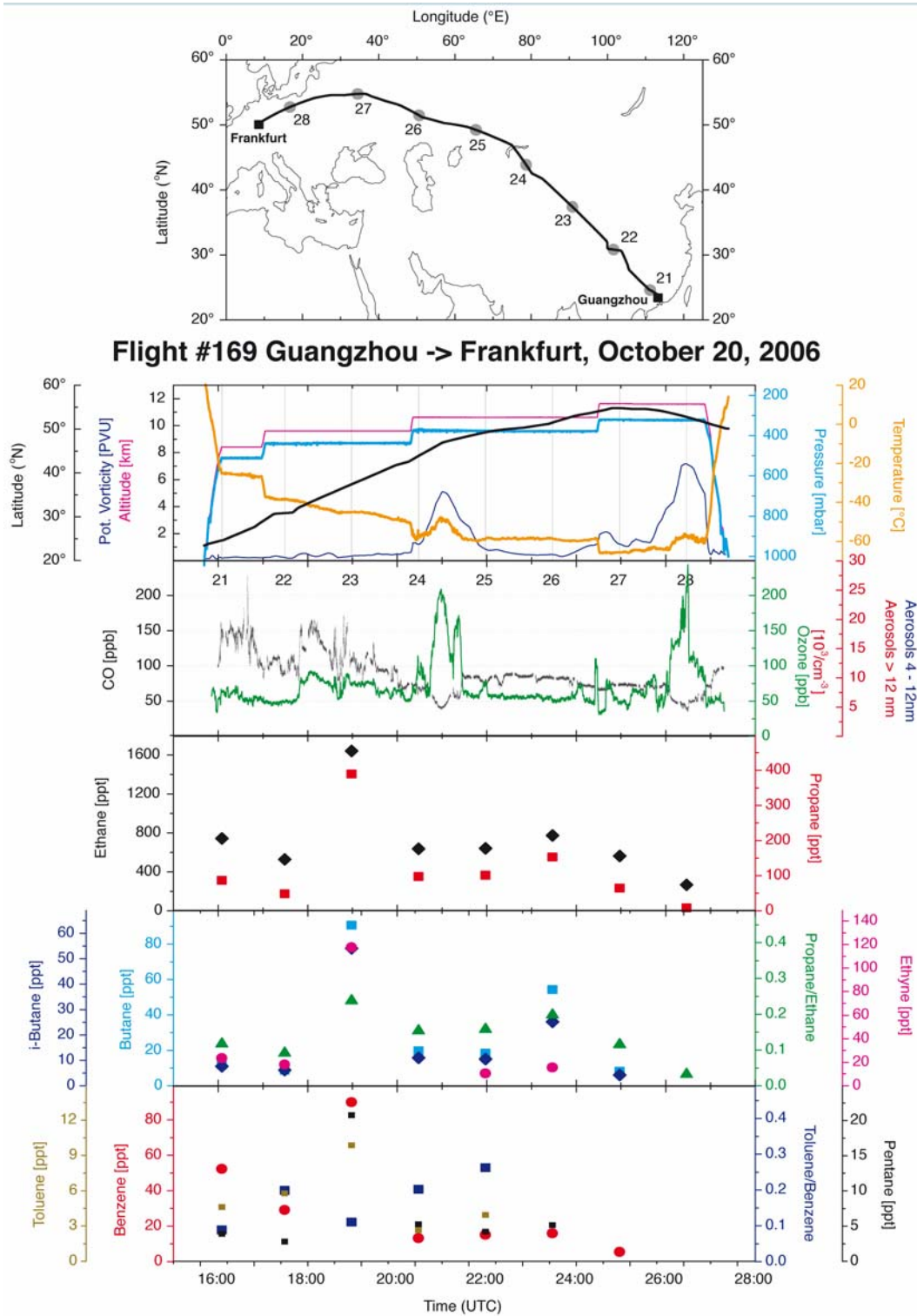*A22: CARIBIC flight # 166 from Frankfurt to Guangzhou on October 19, 2006.*

A23: CARIBIC flight # 167 from Guangzhou to Manila on October 20, 2006.
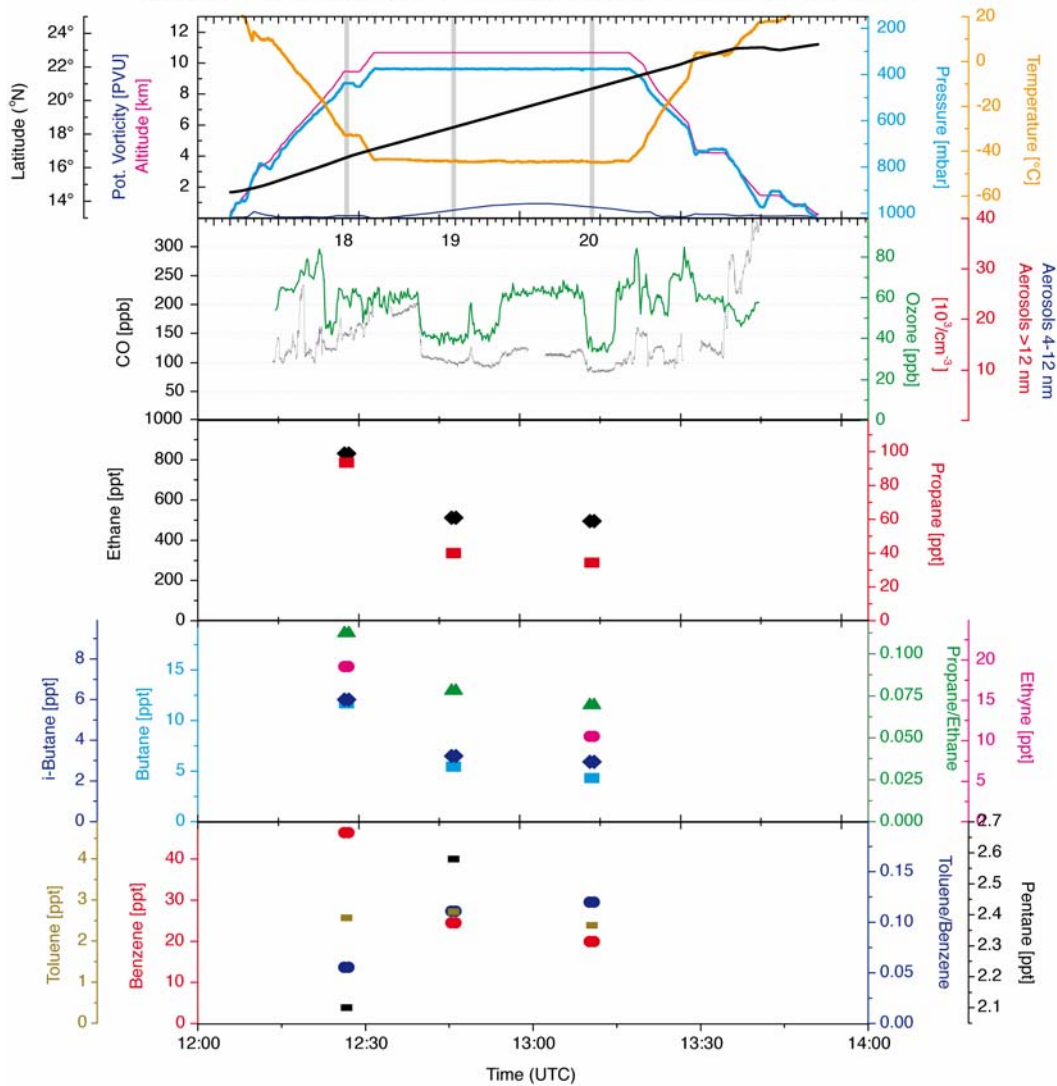
A24: CARIBIC flight # 168 from Manila to Guangzhou on October 20, 2006.

A25: CARIBIC flight # 169 from Guangzhou to Frankfurt on October 20, 2006.